The Potential of Chiral Solvents in Enantioselective Crystallization

Dissertation

zur Erlangung des akademischen Grades

Doktoringenieur

(Dr.-Ing.)

von: M.Sc. Samuel Kofi Tulashie

geboren am: 17. Januar 1971

in: Sekondi-Ghana

genehmigt durch die Fakultät für Verfahrens- und Systemtechnik
der Otto-von-Guericke Universität Magdeburg.

Gutachter: Prof. Dr.-Ing. habil. Andreas Seidel-Morgenstern
                              Prof. Roger Davey

eingereicht am: 01. April 2010

Promotionkolloquium am 27. Juli 2010.

<u>Acknowledgements</u>

Abstract

The objective of this thesis is to evaluate the potential of applying chiral solvents for crystallization-based resolution of racemates. In general, it can be expected that a chiral solvent can discriminate two enantiomers by creating some weak interactions between the solvent and the substrate molecules forming diastereomeric complexes with different physical properties. This may lead to either asymmetry in the solubility phase diagrams or selective kinetic effects which can be employed for resolution purposes. To evaluate the prospect of using chiral solvents for crystallization based enantioseparation and to evaluate the potential of this approach, systematic experimental work is required.

The chosen model systems studied experimentally in this work are two pharmaceutically interesting substances (mandelic acid and N-methylephedrine) which belong to the compound and conglomerate forming systems, respectively. Three different types of chiral solvents were studied: (a) a "classical" chiral solvents, (b) a chiral ionic liquids and (c) a tailor-made chiral solvents.

Three different tests have been investigated; (i) the determination of the ternary solubility phase diagrams for the selected model compounds, (ii) the determination of "nucleation points", i.e. metastable zone widths with regard to primary nucleation and induction time, and (iii) the design of suitable crystallization processes.

In the experimental work, preliminary investigations were performed to identify appropriate "classical" chiral solvents for the discrimination of enantiomers with the aid of nuclear magnetic resonance (NMR) spectroscopy. The screening of the "classical" chiral solvents was particularly performed with mandelic acid, since this component belongs to the class of compound forming systems which are particularly difficult to be resolved. ^{1}H NMR screening measurements and Raman spectra showed that the chosen nine "classical" chiral solvents had no measurable selective influence on the chiral system studied. Since the results obtained from screening were similar, the selection of the chiral solvents for subsequent work was mainly based on the availability and the price.

The ternary solubility phase diagrams determined for the "classical" chiral solvents and the chosen model systems were found to be symmetrical. However, in the case of the chiral ionic liquid (*1R, 2S*)-(-)-dimethylephedrinium bis (trifluoromethylsulfonyl) amide with N-methylephedrine there was asymmetry found in the ternary solubility

phase diagram. Furthermore, in the case of mandelic acid and the tailor-made chiral solvents (*S*)-propyl mandelate and (*S*)-isopropyl mandelate systems, there was also an asymmetry in the phase diagram observed.

Although most of the chiral solvents did not show any quantifiable chiral recognition in terms of solution thermodynamics, regarding kinetics pronounced selective effects were observed as indicated by differences in metastable zone widths and induction times. These important observations made in this thesis work were supported also by the results of molecular modeling calculations and solvation enthalpies evaluations performed in parallel. Thus, the determination of the solvation enthalpies and molecular modeling calculations could be also employed as a useful "screening tool" to estimate the degree of interaction between the solvent and the solute molecules and, thus, to screen for appropriate chiral solvents.

On the basis of the observed pronounced kinetic effects and the chiral recognition in solution thermodynamics, successful enantioselective crystallization processes were finally demonstrated in this work.

Contents

List of Figures

List of Tables

List of Symbols

Symbols

T, t	Temperature, [K] or [°C]
T_m	Melting temperature, [°C]
R	Universal gas constant, 8.314 [J/mol K]
ΔH_{diss}	Dissolution enthalpy, [kJ/mol]
ΔH_{solv}	Solvation enthalpy, [kJ/mol]
ΔH_{fus}	Fusion enthalpy, [kJ/mol]
ΔH_{fus}^{enan}	Fusion enthalpy of the single enantiomers, [kJ/mol]
$T_{m, enan}$	Melting temperature for the single enantiomers, [K]
ΔH_{fus}^{rac}	Fusion enthalpy of the racemic compound, [kJ/mol]
$T_{m, rac}$	Melting temperature for the racemic compound, [K]
ΔT_{max}	Maximum possible subcooling , [K]
ΔC_{max}	Maximum possible supersaturation, [K]
C_p^L	Heat capacity of the liquid, [J/KgK]
C_p^S	Heat capacity of the solid, [J/KgK]
δ	Chemical shift, [ppm]
SD	Standard deviation of the solubilities, [-]
n	Number of experiments
w	Mass fraction solubility, [-]
$\overline{w}$	Mean solubility, [-]
m	Mass, [g]
$\Delta H_{form}^{Stabilization}$	Stabilization enthalpy, [kcal/mol]
$\Delta H_{form}^{Solute/Solvent}$	Heat of formation for solute/solvent, [kcal/mol]
ΔH_{form}^{Dimer}	Heat of formation of dimer, [kcal/mol]
t_{ind}	Induction time, [seconds]
t_r	Relaxation time, [seconds]
t_n	Nucleation time, [seconds]
t_g	Growth time, [seconds]
ΔH_{dec}	Decomposition enthalpy, [kJ/mol]

Chapter 1. Introduction

Chapter 1

1. Introduction

1.1 Project background

Separation technologies such as crystallization processes are very important to chemical and pharmaceutical industries. Crystallization is a separation and purification technique used to generate a broad collection of chemicals for examples pharmaceuticals, agricultural products, flavors, fragrances and other chiral products. Manufacturing of high-value products (fine chemicals and pharmaceuticals) are mostly performed by crystallization processes. Other separation processes are normally more expensive compared with crystallization.[1] This has increased the use of crystallization as one of the major separation processes in the resolution of pharmaceutical products such as enantiomers.

Enantiomers exist in two different forms. These two forms are structured like non-superimposable mirror images of each other. They have identical physical and chemical properties such as solubilities and viscosities, but these compounds can also have very different properties, for example smell, taste, and efficacy. In the extreme case, one enantiomer can be a potent drug and the other a poisonous substance. A case in point is the notorious drug Thalidomide, which was prescribed worldwide in the late 1950s to stop symptoms associated with morning sickness of pregnant women. While the (*R*)-enantiomer has safe sleep-inducing effects, the coexisting (*S*)-enantiomer is believed to be responsible for thousands of cases of birth defects. The majority of the drugs synthesized in the pharmaceutical industry are in the form of racemate, i.e. 50:50 mixtures of both enantiomers.[2]

With such pronounced differences in biological activities, it is not surprising that the demand of single enantiomers is on the rise[2]. Moreover, Food and Drug Administration (FDA) demands for enantiopure substances rather than racemates.[3] This has necessitated the resolution of racemic mixtures and compounds into single enantiomers, since often only one enantiomer exhibits the desired physiological effect. Enantioselective crystallization is considered to be an appropriate move towards separation of enantiomers. In view of this, crystallization from chiral solvents[4,5] is an attractive technique in enantioselective crystallization processes, based on the expectation that the solvent can create selective interactions to the chiral molecules leading to differences in solubilities or rates of crystallization. These differences might be employed for resolution purposes.

A literature search shows that there are a few studies in this area of research.[6-10] Moreover, available solubility data of chiral substances in chiral solvents are limited to distinct measurements with the pure enantiomers. Also there is a deficit in systematic experimental work evaluating the application of chiral solvents and quantifying the corresponding solubility data. For example, Yamamoto et al.[6] reported pure enantiomer solubilities for a chiral cobalt salt in (*2R,3R*)-(+)-diethyl tartrate and described measurable differences between them. Furthermore, Bosnich et al[7] and Mizumachi[8] reported that the solubilities of the pair of enantiomers of cis [Co(en)$_2$Cl$_2$]Cl0$_4$ in l-2,3-butanediol and Tri-α-diimine Ruthenium (II) complexes respectively, were different. However, in all cases no systematic experimental support was presented. Amaya[9] provided a theoretical framework to account for the differences in solubility between *D*- and *L*-optical isomers in a chiral solvent, without presenting any experimental evidence.

Therefore, to evaluate the prospect of the concept of applying chiral solvents for crystallization based enantioseparation and to evaluate the generality of this approach, a comprehensive methodical experimental work is required, which is the focus of this work.

1.2 Project objectives and thesis structure

The goal of this project is to evaluate the potential of applying chiral solvents for crystallization-based resolution of racemates. Generally, it is expected that a chiral solvent can create selective interactions to a chiral solute, which facilitates discrimination between two single enantiomers. This discrimination can provide selective kinetic or thermodynamic effects which can be useful for the separation of racemates. A literature search for crystallization processes using chiral solvents shows that there is a deficiency of systematic experimental work for evaluating the application of chiral solvents and also for quantifying the corresponding solubility data. The chosen systems to be studied experimentally in this work are two pharmaceutical interesting substances which belong to the compound and conglomerate forming systems. Three different possible ways have been employed to achieve this aim; (i) determination of the ternary solubility phase diagrams for the selected model compounds, (ii) determination of "nucleation points" i.e., metastable

zone widths with regard to primary nucleation and induction time, and (iii) suggestion and design of suitable crystallization processes.

Therefore, the present work is concerned with systematic experimental investigations on three different types of chiral solvents, namely "classical" chiral solvents, chiral ionic liquids, and tailor-made chiral solvents, with some chosen as model chiral solvents. Based on the acquired ternary solubility phase diagrams and the metastable zone widths or induction times, racemate resolutions via crystallization processes will be suggested and conducted. Finally, generalized conclusions regarding the potential of chiral solvents for crystallization-based racemate resolution are derived and will be discussed.

Chapter 2 gives details about the background, a literature review and some theoretical aspects of the thesis. Preliminary investigations were carried out to identify appropriate chiral solvents for the discrimination of enantiomers with the aid of nuclear magnetic resonance (NMR) spectroscopy (see chapter 3). Afterward, two fundamental experiments, of data were determined, i.e. solubility and kinetic measurements were conducted to support the design of the enantioselective crystallization experiments (see chapter 3). Fundamental experiments were performed by applying the two chosen chiral substances and the three main chiral solvents ("classical" chiral solvents), chiral ionic liquids, and specially synthesized "tailor-made" chiral solvents. Based on the attained solubility and kinetic data preferential nucleation, preferential crystallization and selective crystallization processes were designed and performed (see chapter 3 and 4).

Molecular modeling and calorimetric measurements (dissolution enthalpies) were conducted to get a deeper understanding of the solvent-solute interactions in the system (see 3 and 4). Molecular modeling was realized with the commercial MATERIALS STUDIO® software to derived enthalpy of formation for the various dimers (solute and solvent dimers) systems studied.

The solid and liquid phases during measurements were characterized with many techniques (see chapter 3 and Appendix section): Raman spectroscopy, FT-IR spectroscopy, X-ray powder diffraction (XRPD) and HPLC.

Chapter 5 gives a summary of the whole work and also enumerates some suggestions for future work, i.e. how a certain solvents such as tailor-made chiral solvents and chiral ionic liquids could be applied more efficiently for chiral discrimination.

Chapter 2. Background and Literature Survey

Chapter 2

2. Background and Literature Survey

2.1 What is chirality and what is its biological and economic significance

The term chirality is derived from the Greek word for hand, χειρ (cheir), as the right and left hand can not be superimposed on each other. A chiral molecule is a type of molecule that lacks an internal plane of symmetry and has a non-superimposable mirror image. The human hands are possibly the most commonly known example of chirality: The left hand is a non-superimposable mirror image of the right hand; no matter how the two hands are oriented, it is impossible for all the major features of both hands to coincide. So, enantiomers are defined as a pair of chiral isomers that are absolute mirror images of each other and are not superimposable on one another. Normally object that has no inverse symmetry, or object that are non-superimposed on their mirror images are termed chiral.[11]
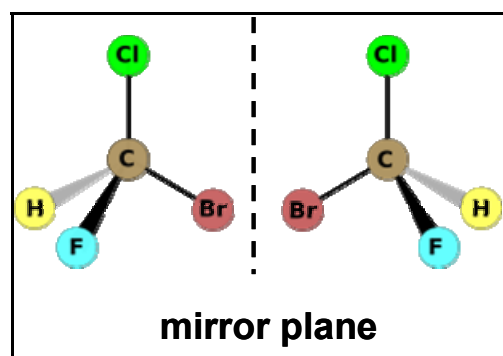
Figure 1: Typical example of chirality of two enantiomers of bromochlorofluoromethane (a tetrahedral arrangement of four substituents bonded to the stereocentre atom.

Figure 1 illustrates a tetrahedral arrangement as a consequence of the central carbon atom (stereocentre or chiral centre) is saturated with four different functional groups. This tetrahedral arrangement was proposed by both Van't Hoff[12,13] and Le Bel[14]. The concept of chirality was established long ago when Pasteur in 1848 [15] through his effort by using manual hand sorting to separate conglomerate crystals of sodium ammonium tartrate and in the process brought to light the fundamentals of stereochemistry. Based on the fact that enantiomers have structural similarity, they have identical physical and chemical properties such as solubility, viscosity etc. The only observable differences between enantiomers are chiraloptical properties such as circular dichroism, optical rotation and optical rotation dispersion.[16]

Based on the specific optical rotation, a classification of chiral species into (+)- and (-)-enantiomers is made. The (+)- sign is denoted for the chiral species when it rotates the polarized light in the positive direction (clockwise direction), and the contrary is the case for (-)- sign. There exists another method of assigning a configuration classification which is commonly used to distinguish between optical isomers for sugars and amino acid. This is the distinction between *L*- and *D*-isomers which was proposed by Emil Fischer[17]. Both of these methods mentioned are sometimes confusing, so a much simpler and explicit method was devised by Cahn-Ingold-Prelog (CIP).[18] Here, assigning the absolute configuration is solely based on the order in which the substituents are arranged around the stereo-centre. It differentiates between (*S*)- and (*R*)-enantiomers. The procedure is that the substituents bonded to the chiral centre atom are given priorities according to their atomic numbers in such a way that the highest atomic number is assigned the highest priority while the lowest atomic number is assigned the lowest priority. Afterward to assign the absolute configuration to the chiral molecule the orientation of the molecule should be placed such that the lowest priority substituents point away from the viewer. The final assignment is made by considering the order for the remaining three substituents. If the priority increases in the clockwise direction then the molecule is assigned (*R*)-configuration, and (*S*)-configuration if the priority increases in anticlockwise route.

Diastereoisomers are stereoisomers with more than one chiral centre, and they are not related through reflection operation.[19] Diastereomers have different chemical and physical properties, for instance melting point, boiling point, absolute optical rotation and spectra. Hence they behave in all aspects as different compounds. If the number of stereocentres increases in the molecules, the number of possible stereoisomers also increases. For example, (*2R, 3R*)-diethyl tartrate has two such centres. There are $2^n = 4$ different stereoisomers, with n representing the number of stereocentres.

Biological significance

Biological system chirality is not only natural, but necessary for life. Generally, DNA and RNA and most carbohydrates exist as a *D*-type. Consequently, essential physiological processes employ exclusively only one of the possible stereoisomers of each substance concerned. Therefore proteins, sugars, and other biological target

receptors of most drugs are chiral. The two enantiomers of a drug thus bind differently to these receptors, which often causes them to have different biological effects.

For instance, of an enzyme made up of a 99 amino acid polypeptides chain, HIV-1 protease, synthesized from *D*-amino acids only, has been illustrated to cleave only *D*-amino acid peptides. On the other hand the same type of enzyme synthesized from *L*-amino acids cleaves only *L*-amino acid peptides.[16,20] This two enantiomers of chiral inhibitor show similar stereospecific behavior toward the subsequent enzyme forms.

Generally, one of the enantiomers represents the more active isomer (eutomer), whereas the other one might give side-effects, display toxicity or act as antagonist.[3,21] On the molecular level, it also illustrates that the chirality of amino acid and sugars are stereospecific in terms of enzymatic reactions and drug. receptor interactions. This also holds for various types of messenger molecules such as neurotransmitters, hormones, allosteric modulators of enzyme activity as well as for xenobiotic, exogenous, messenger molecules such as drugs, insecticides and weedicides. This transfer of stereo-specific information is chemically coded in appropriate molecular carriers into biological systems.[22] Furthermore, stereoisomer discriminate in odor perception is well known[23,24]. For instance it is evident that chirality plays a major role in the olfactory properties of perfumes and fragrance; there are cases where two enantiomers of a pair have significantly different olfactory properties[25]. Moreover, there are some interesting practical examples of carvone and limonene enantiomers showing differences in odor[26]. (*S*)-(+)-carvone possesses the odor of caraway and the counter enantiomer (*R*)-(-)-carvone has spearmint odor. Same is true for (*R*)-(+)-limonene has an orange odor whilst the other enantiomer (*S*)-(-)-limonene has that of lemon. Additional specific case is that only (-)-menthol enantiomer used in tobacco gives a cooling effect during smoking and also provides a lower concentration at which the effect is perceived.[27] An important consequence of the above is that biological systems show stereospecificity toward stereoisomers (enantiomers and diastereomers), which means that it is very necessary for drugs made to be in enantiopure form.

The next section will describe how the high demand for a single enantiomer has increased revenues for pharmaceutical companies.

Economic significance

The fact that biological systems are stereospecific towards chiral substances and also coupled with US Food and Drug Administration (FDA) regulatory demand for single enantiomers has resulted in the high demand for enantiopure drugs from the pharmaceutical companies. So, FDA has demanded a stringent prerequisite to patent new racemic drugs, demanding a full documentation of separate pharmacological and pharmacokinetic profiles of the individual enantiomers as well as their combination.[28] Single enantiomers drug sales increment from 1997 and many top-selling drugs are marketed as single enantiomer (269 out of top 500 drugs)[29]. Since the focus of pharmaceutical companies are to produce drugs for chronic disease such as Alzheimer, Cancer, Obesity, AIDS, Asthma etc. most of this drugs contact one or more chiral centres. There is the need to obtain an enantiomerically pure drug by the means of enantioseparation. Economic interests are obvious and important driving forces in the development of single enantiomers.

Table 1 depicts a detailed summary of annual distribution of worldwide approved drugs in the period of 1990-2002 and of the FDA approved drugs New Molecular Entity (NMEs), i.e. an active ingredient that has never been sold in US.

Table 1: Summary of the annual distribution of worldwide and FDA approved drugs (NMEs) according to chirality character in the period 1990-2002. Data from[2]

Year	Racemates		Single enantiomers		Achiral	
	Worldwide (%)	FDA (%)	Worldwide (%)	FDA (%)	Worldwide (%)	FDA (%)
1990	33	na	35	na	32	na
1992	21	33	44	42	35	25
1994	38	5	38	57	24	38
1998	15	9	50	41	35	50
2000	9	19	62	37	29	44
2002	6	0	55	53	39	47

[a]Including of diastereomeric mixtures; Abbreviations: na, not applicable.

According to Table 1, the trends of the annual distribution of single enantiomer drugs increase along the years against that of the racemic drugs.

There is an outstanding world drug (proportion of single enantiomeric drugs among the top-selling drugs) sales of about $300 billion in 1997. This value increased over the years steadily till 2000 as reported by Maier et al.[3] According to this high demand and good sales for single enantiomers, has triggered in 'racemic switch' a new market strategy of the pharmaceutical companies to change racemic drugs (already approved patent) into single enantiomers ones. In this case the companies can patent also the enantiopure form of the drug, creating more revenues for them.

2.2 Crystal science

2.2.1 What is crystallization?

Crystallization is widely used for manufacturing drug substances and for purification and separation. [1,30] Crystallization is a potent separation technique due to the highly selective nature of crystal surfaces, creating a reproducibility of the assembly of molecules possible. For instance only same growth units are allowed to join the growing crystal lattice, making crystals exceptionally successful in their separating ability. This is why crystallization is such a popular separation method. Crystallization is essential to the resolution of enantiomers, as it is one of the most cost-effective methods, where high enantiomeric excesses can be obtained. In this region other methods fail to deliver. Crystallization can occurs in several ways such as; from melt, from solution, from the gaseous phase or from a supercritical fluid. The most common and useful method for chiral compounds is the crystallization from solution, and so we will concentrate below on this particular method.

In order to understand the crystallization process and the formation of different crystalline phases, one must understand the thermodynamics linked to the fundamental phase equilibrium. For a case in point, a saturated aqueous solution of mandelic acid has *3* different phases; crystal, solution and vapour, and *2* components for the system (the number of constituents required to describe any phase), namely mandelic acid and water. In 1876 J. W. Gibbs[31] derived a famous relationship between the number of phases *P*, the degrees of freedom *F* and the number of components *C* and formulated the phase rule as:

$$F = C + 2 - P$$

<div align="right">Equation 1</div>

Applying the phase rule to the mandelic acid and water system, shows that a system with *2* components and *3* phases (crystal, liquid and vapour), has *1* degree of freedom: *F = 2 + 2 – 3 = 1*. This phase rule permits the computation of the number of variables (*T*, *p* or *x*) that must be fixed in order to define an equilibrium state. Hence, the correlation between the variables and the crystalline solid phase is usually characterized using a phase diagram. This information about the phase diagram is obtained by preliminary measurement of solubility, together with thermal data such as melting temperature and enthalpy of fusion measurable for example by DSC. However, it is necessary to gain an understanding of the crystallizing system under consideration. In crystallization the concentration range over which the process can occur is limited by the solubility isotherm of the phase diagram.

2.2.2 Supersaturation

A prime requirement for crystallization from solution is that the concentration of the solute in the solvent exceeds its equilibrium solubility to provide a driving force. The driving force for crystallization is supersaturation, which is possibly the most important quantity in crystal nucleation and growth processes. Supersaturation can be generated in several ways, for example by cooling a saturated solution, by evaporation of the solvent from a saturated solution. Other less common methods are; by addition of miscible non-solvent to a saturated solution, by the use of common ion effect (for ionic salts), by salting out and by reaction to form the solute *in situ.*

Supersaturation is frequently expressed as the difference between concentrations, and has therefore the same unit as used for concentrations. Supersaturation can be defined as

$$\Delta C = C - C^*$$

<div align="right">Equation 2</div>

where ΔC is the supersaturation in concentration units, C^* is the saturation concentration and C is the actual concentration. A common way to express supersaturation is also the supersaturation ratio defined as

$$S = \frac{C}{C^*}$$

<div align="right">Equation 3</div>

The supersaturation ratio, σ is expressed as;

$$\sigma = \frac{C - C^*}{C^*}$$

Equation 4

is for all times > 1 for a supersaturated solution. It is essential to note that these definitions of supersaturation assume ideal solution activity coefficients of 1.

2.2.3 Kinetics

The spontaneous crystallization of a supersaturated solution comprises of two main steps: (a) the appearance of crystalline seeds (nucleation), and (b) the development of crystals from these seeds. Thus, nucleation is a process of making a new solid phase from a supersaturated homogeneous mother phase. It is fundamental to all types of crystallizations. Once nucleation has taken place to form nuclei which act as surfaces for crystal growth, these grow into macroscopic crystals. Nucleation is divided into two main types; primary and secondary. Primary nucleation occurs in the absence of crystalline surfaces, and can be homogeneous or heterogeneous.[32]

2.2.3.1 Primary and secondary nucleation

Homogeneous nucleation seldom does happen in practice, but it forms the basis for nucleation theories. Heterogeneous nucleation is usually caused by the presence of dissolved impurities. In general the birth of new crystals is called nucleation. Before real nucleation is observed, clusters (embryos) are formed in solution.[33]
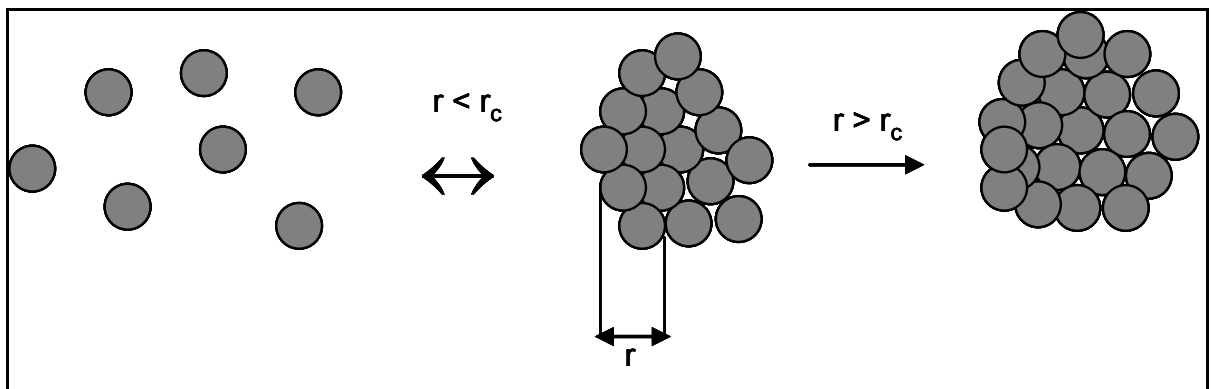
Figure 2: Illustration of the process of nucleation.[33]

Therefore Figure 2 shows the mechanism involves in the process of nucleation. According to the classical theory of nucleation the molecules first undergoes collision to form very small clusters of several molecules (embryos) via a reversible process (see Figure 2). In Figure 3 gives an illustration of the free energy versus size of nucleus (cluster size). The change in free energy associated with the formation of these clusters increases with size, and reaches a maximum at a critical radius, r_c, and then diminishes or decreases.
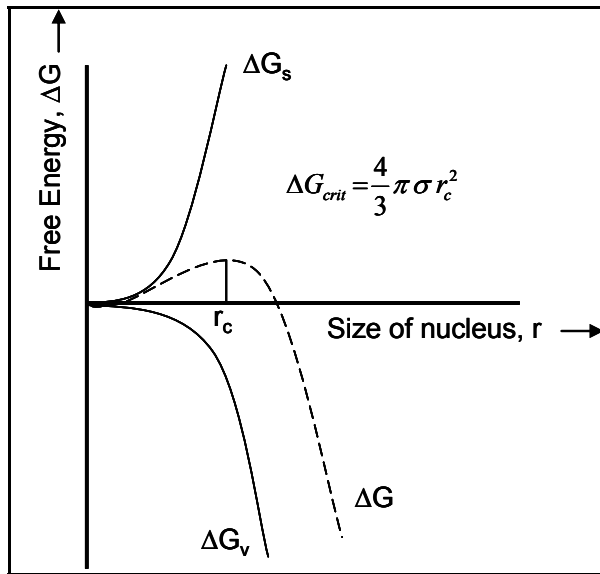
Figure 3: Free energy of nucleation as a function of size of nucleus. [34]

This implies that the clusters smaller than r_c, would eventually fall apart rather than growing, whereas the clusters whose radius are bigger than the critical radius will grow to become nuclei. The free energy change for the formation of the nucleus surface (positive quantity) and the free energy change for the phase transformation (a negative quantity) are expressed as;[34]

$$\Delta G = \Delta G_s + \Delta G_v = \beta L^2 \sigma + \alpha L^3 \Delta G_v \qquad\qquad \text{Equation 5}$$

where σ is the surface tension, and β and α are the area and volume shape factors (based on the characteristic length L), respectively. In the case of spherical nuclei, the area factor $\beta = \pi$, and the volume factor is $\alpha = \pi/6$ based on the diameter, d, of the nuclei. Then Equation 5 becomes;

$$\Delta G = 4\pi r^2 \sigma + \frac{4}{3}\pi r^3 \Delta G_v \qquad\qquad \text{Equation 6}$$

It is obvious from Figure 3 that clusters greater than the critical size result in a decrease in free energy and will take part in the nucleation process. So, the critical size can be obtained by minimizing the free energy function with respect to the radius.

$$\frac{d(\Delta G)}{dr} = 8\pi\, r_c \sigma + 4\pi\, r_c^2 \Delta G_v \qquad\qquad \text{Equation 7}$$

becomes Equation 8;

$$r_c = -\frac{2\sigma}{\Delta G_v} \qquad\qquad \text{Equation 8}$$

Substituting for ΔG_v from Equation 8 into Equation 6 results in

$$\Delta G_{crit} = \frac{4\pi\, r_c^2 \sigma}{3} \qquad\qquad \text{Equation 9}$$

The growth of the clusters is controlled by the Gibbs-Thompson equation[32,34]

$$In\frac{C}{C^*} = In\,S = 2\sigma v / kTr \qquad\qquad \text{Equation 10}$$

where C is the concentration of the clusters with size r. Consequently, the smaller clusters dissolve, as larger cluster grow until they reach a critical size, r_c, and a new phase is made. Substituting for r_c in Equation 9 by Equation 10 gives;

$$\Delta G_{crit} = \frac{16\pi \sigma^3 v^2}{3(kT\,In\,S)^2} \qquad\qquad \text{Equation 11}$$

Now considering the fact that the classical nucleation theory assumes that clusters are formed in solution by the addition mechanism which continues until a critical size of nuclei is obtained. In this case the nucleus formation by this mechanism is given by Arrhenius type of expression;

$$B_0 = A\exp\left(-\frac{\Delta G_{crit}}{kT}\right) \qquad\qquad \text{Equation 12}$$

where A is the preexponential factor which typically has a theoretical value of 10^{30} nuclei/cm^3 s.[34]

The nucleation rate (B_0) can be obtained by putting Equation 11 into Equation 12;

$$B_0 = A\exp\left(-\frac{16\pi\sigma^3 v^2}{3k^3 T^3 (In\,S)^2}\right) \qquad\qquad \text{Equation 13}$$

The induction period (t_{ind}) can be considered to be inversely proportional to the rate of nucleation. Thus;

$$t_{ind} \ \alpha \ B_0^{-1} \qquad\qquad \text{Equation 14}$$

so Equation 13 eventually becomes;

$$t_{ind} \; \alpha \left(\frac{\sigma^3}{T^3 (In\,S)^2} \right)$$

Equation 15

Secondary nucleation results from the presence of crystals in the supersaturated solution. These parent crystals have a catalyzing effect on the nucleation phenomena, and hence, nucleation happens at a lower supersaturation than required for spontaneous nucleation. Shear nucleation can be sufficient to produce secondary nuclei from the crystal surface by the shear force inflicted on a crystal face due to solution flowing past it. The appearance of crystals may be as a result of one or a permutation of crystal-crystal, crystal-impeller or crystal-crystallizer collisions.

2.2.3.2 Crystal growth

Crystal growth involves the integration of growth units into the crystal lattice, once the lattice has developed from a nucleus. These growth units can be molecules, atoms or ions, based on the type of substance. The crystal growth rate is dependent on the supersaturation and the area of the crystal exposed to growth. There are several projected mechanisms of crystal growth.[31,32] The diffusion theory, presumes that matter is placed incessantly on a crystal face at a rate proportional to the difference in concentration between deposition surface and the bulk solution. While the 'adsorption-layer' theory assumes that growth takes place in a layer-wise manner and that molecules arrive at the layer by diffusion through the bulk. This can be understood by viewing Figure 4. A molecule in a supersaturated solution must de-solvate to be absorbed on the crystal surface. In Figure 4 there are three possible sites for the molecule to incorporate into the crystal surface; sites *A*, *B,* and *C*.
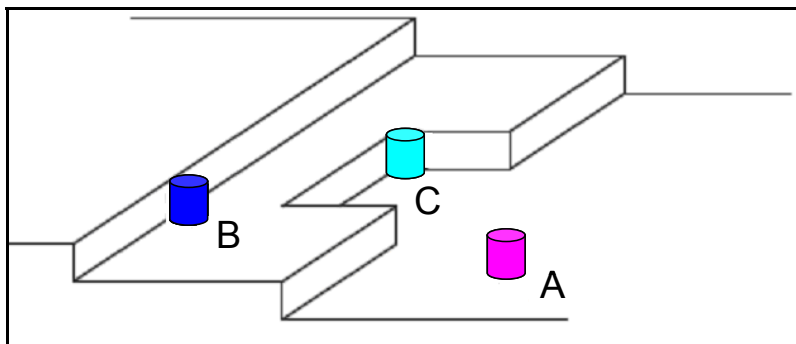
Figure 4: Surface structure of a growth crystal, where A, B and C are the impurities.

These sites are distinguished by the number of bonds the molecule will form with the crystal surface on which it incorporates. At site *A*, the molecule will be attached only to the surface of a growing layer (flat site) while at site *B*, the molecule is attached to both the surface and to a growing step (step site). At site *C*, the molecule is attached at three surfaces, known as a kink site. The mechanism for the incorporation of a molecule into a crystal face is adsorption onto the surface, followed by its diffusion along the surface *(A-type)* to a step *(B-type)* or kink *(C-type)* site for integration.[32] Considering the energetic for this process, *C* is more preferable than *B*, as it makes more interactions, and *B* is more favorable than *A* as molecules have a propensity to bond at locations where they have the maximum number of nearest neighbors to exploit their interaction potential. Also, molecules prefer to bond to an accessible step that is spreading over a surface than to create a new one. In this case it is clear why crystals grow in a layer by layer manner. The pace at which these different crystal faces grow will affect the crystal morphology. This gives the overall shape of a crystal, illustrated as plate-like, needle-like, or prismatic etc. A difference between the equilibrium and growth morphologies needs to be made. The previous is the shape taken up by a crystal when permitted to equilibrate with its surroundings and match up with the minimization of the surface free energy of the crystal, at the same time as the latter is the shape that the crystal generates during the growth when kinetics may control the process. Morphology is decided based on two factors, the relative growths of the faces adjoining the crystal, and the symmetry of the internal crystal structure, evident in the point group symmetry of the crystal form.[31] This is linked to the energetics of the molecule attachment to the crystal surfaces. The surface specific nature of this attachment process means that the morphology of a crystal can be affected by external factors, such as the level of supersaturation, growth solvent, temperature, and solution purity (additives can dramatically affect the morphology, section 2.5.2.2 and section 2.6.2).

2.2.4 Induction period for crystallization

The time period usually elapsing between the attainment of supersaturation and the appearance of the first crystals is called the induction time. The induction time can be considered to be inversely proportional to the nucleation rate (relationship between

induction time and nucleation rate, section 2.2.3.1, Equation 14). The first changes in the system's physical properties due to the formation of the solid phase may be followed by the appearance of the first visible crystals. The measured induction time is generally a complex quantity made up of several components. It is often measured by visual observation or by particle size analyzer. In reality, the induction time consists of three components: the transient period, which is the relaxation time (t_r) needed to achieve a quasi-steady-state distribution of molecular clusters; the period for the formation of the stable nuclei (t_n, i.e. the nucleation/induction time); and the time needed for these critical nuclei to grow to a macroscopic size where they can be detected (i.e. the growth time, t_g). The induction time then can be expressed as:

$$t_{ind} = t_r + t_n + t_g \hspace{4cm} \text{Equation 16}$$

However, in reality, it is impracticable to detach these separate terms. The nucleation time depends on supersaturation which affects the size of the critical nuclei, but its evaluation is a subject of speculation. The growth time is dependent on the size at which nuclei are detectable and the growth rate applicable to this early stage of development. This latter stage is difficult to forecast as the growth rate of a nucleus cannot be assumed to be in the same order of magnitude as the macro-crystal; the mechanism and rates of which may be different. As a result of this the induction time is normally taken as the time at which nuclei are noticed, and as these are often visually observed, measurement of t_{ind} by sensitive methods such as laser light scattering, can result in a different induction time being recorded. This inconsistency highlights that experimentally determined t_{ind} is not, alone, a fundamental characteristic of a crystallizing system.

2.2.5 Metastable zone width

The metastable zone width (MSZW) is extremely important in understanding the kinetic aspects in crystallization processes and in particular of enantioselective crystallization processes.[35] The MSZW with respect to primary nucleation is the region where no significant nucleation occurs after a saturated solution is subjected to cooling, and is given as a maximum possible subcooling (ΔT_{max}) or maximum possible supersaturation (ΔC_{max}). Consider a case where solution at the concentration and temperature represented by point *A* in Figure 5. This point lies beneath the

solubility curve and so represents an undersaturated solution. If this solution is now cooled, the system will travel along a horizontal line on the diagram until at point B, the system becomes just saturated. Further cooling causes the system to become supersaturated, but nucleation to form crystals does not usually occur immediately the system becomes supersaturated. Only when cooling is continued to some point C does ample supersaturation exist for the nucleation to occur. The gap between B and C is designated as the MSZW.
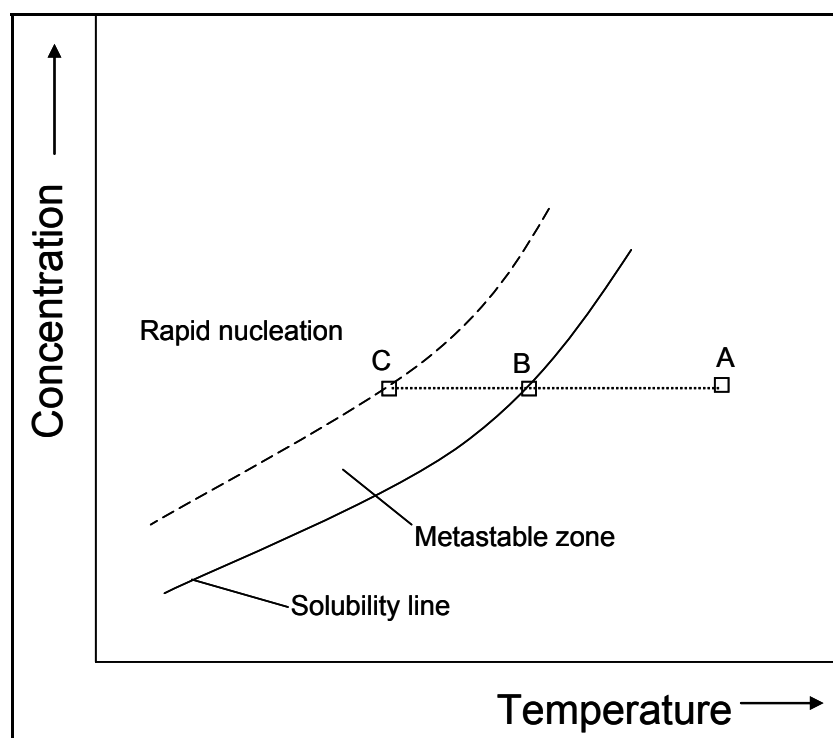
Figure 5: Solubility curve and metastable zone.

2.3 Basic types of racemates

The distinction of the different types of racemates remained controversial as long as it was based only on visual or microscopic comparison of crystal forms or the densities of racemates with those of the single enantiomers.[5] The easiest way of determining the racemate type is by examining the binary phase diagram. This was only realized when it became clear that enantiomers mixtures were specific type of binary phase or ternary system when the solvent is included, and its properties can be described by the phase rule which was initially proposed by J. W. Gibbs in 1876.[31] A phase diagram is used to represent the relationship between temperature, pressure and concentration

and the crystal structure of solid phases. Roozeboom[36] characterized in 1899 three types of enantiomers mixtures by their melting point (fusion) diagrams, which are depicted in Figure 6.
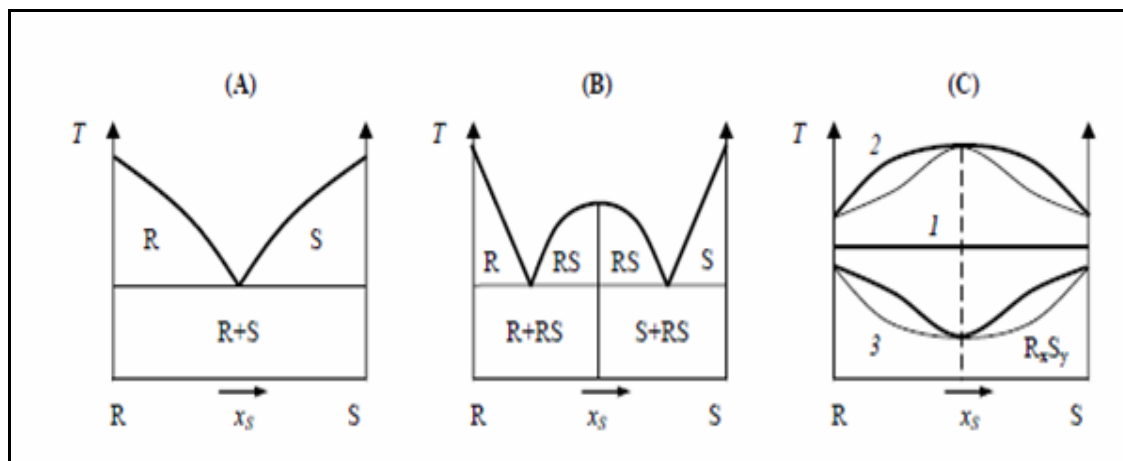
Figure 6: Binary phase diagrams illustrating the three fundamental types of crystalline racemates; (A) conglomerate system, (B) racemic compound, (C) solid solution; (1) ideal, (2) with a maximum, (3) with a minimum. Taking from Anett Perlberg[37]

There are three main types of enantiomers mixtures that have been recognized and characterized well by their binary fusion diagram. The melting phase diagram of the mixtures of enantiomers (*S*) and (*R*) is illustrated in Figure 6. Figure 6(A) shows a binary phase diagram where the racemates crystallizes as a homochiral mixture of the two enantiomers.
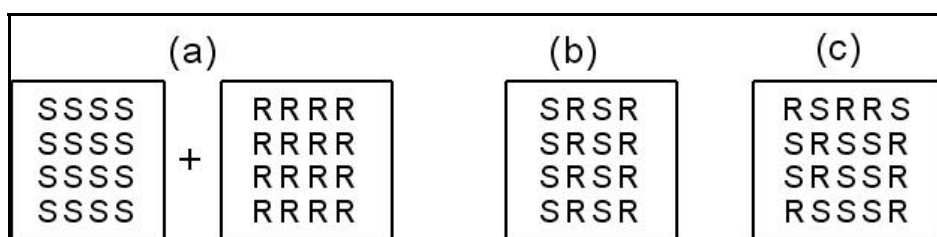
Figure 7: Solid-state racemate types; (a) conglomerates, (b) racemic compound, (c) solid solution

Figure 7 shows how the single enantiomers of (*S*) and (*R*) are arranged in the solid state of the various racemates types, i.e. (a) conglomerate, (b) racemic compound and (c) solid solution, respectively. A conglomerate is an equimolar mixture of two crystalline enantiomers that are in principle, mechanically separable[5] (see Figure 7(a)). The binary phase diagram in this case depicts a simple common eutectic at ($x = 0.5$), since the mixture melts just like a pure substance and this fit the classification of

eutectic. Conglomerate systems can be resolved easily by spontaneous crystallization based on the fact that the racemates crystallized in homochiral form. Unfortunately, only approximately 5-10% of the enantiomeric systems exhibit this behaviour[5]. Actually, the racemate and the enantiomers have most of their chemical and physical properties as the same, for instance the XRPD pattern, infra-red and Raman spectra of the enantiomers and the racemate are identical. The most obvious differences that exist between the enantiomers and racemates of a conglomerate system are the melting point and their solubility. According to Meyerhoffer's 'double solubility rule'[38] the conglomerate solubility is in an ideal case the sum of the corresponding enantiomers solubility. The liquidus line in Figure 6(A) can be estimated by using the Schröder and van Laar equation[5], if the binary mixtures in the liquid phase act ideally. The equation makes use of the enthalpy of fusion and the specific heat of the two enantiomers both in the liquid and the solid phase, the melting point for two single enantiomers and the universal gas constant. The general Schröder and van Laar equation of the liquidus is given by;[5]

$$\ln x\gamma = \frac{\Delta H_{fus}}{R}\left(\frac{1}{T_m} - \frac{1}{T}\right) - \frac{C_p^{\,L} - C_p^{\,S}}{R}\left(\ln\frac{T_m}{T} + 1 - \frac{T_m}{T}\right)$$

<div align="right">Equation 17</div>

where ΔH_{fus} is the enthalpy of fusion at a melting temperature T_m, R is the universal gas constant (8.314 J mol^{-1} K^{-1}), C_p^L and C_p^S, are the heat capacities of the enantiomers at liquid and the solid state and x represents the mole fraction in excess ($0.5 \leq x \leq 1$) of the mixture where melting ends at T. A simplified form of the Schröder and van Laar equation without the contribution of the heat capacity terms is often applied since the heat capacities for the liquid and the solid often compensate each other. For an ideal mixture the activity coefficient is unity. In this case the Schröder and van Laar equation becomes;

$$\ln x = \frac{\Delta H_{fus}^{enan}}{R}\left(\frac{1}{T_{m,enan}} - \frac{1}{T}\right)$$

<div align="right">Equation 18</div>

where ΔH_{fus}^{enan}, $T_{m,\,enan}$, are the enthalpy of fusion and the melting point of the single enantiomers, respectively.

The second type of racemate is the racemic compound which is the most abundant occurring type of racemate, constituting about 90-95% of racemates. These racemates are characterized by a crystal form in which the two enantiomers coexist in the same unit. The (*S*) and (*R*) crystallize in the same crystal (heterochiral) forming a defined 50:50 compound. Mixtures of enantiomers crystallizing as racemic compounds result in a phase diagram which was envisaged by Roozeboom[36]. A typical example of this phase diagram is illustrated in Figure 6(B). A clear description of its arrangement in the solid state is given in Figure 7(b). Normally, the solid state XRPD patterns, of the enantiomers are different from that of the racemic compound. The melting point of the enantiomers can be lower or higher compared to that of the racemic compound. The difference between the two temperature seldomly exceeds ±20 °C[1] As mentioned earlier on that, the Schröder van Laar equation allows the calculation of the liquidus curve from the enthalpy of fusion and the melting point of the single enantiomers. In the case of racemic compound, the same equation can be used to calculate the liquidus line found between the single enantiomers and their corresponding eutectic, while the racemic compound curve (part of the curve below which the solid phase is pure racemic compound; $0.5 \leq x \leq x_{eu}$) can be calculated using a comparable Equation known as Progogine-Defay equation[5,39].

$$\ln 4x(1-x) = \frac{\Delta H_{fus}^{rac}}{R}\left(\frac{1}{T_{m,rac}} - \frac{1}{T}\right)$$

Equation 19

Equation 19 is similar to Equation 18, the only difference is that Equation 19 takes the stoichiometric considerations into account, ΔH_{fus}^{rac} and $T_{m,\,rac}$ are the enthalpy of fusion and the melting temperature, respectively, of the racemic compound.

The third class of racemates is known as solid solution (mixed crystals). An equimolar mixture of the enantiomers in the solid state is called a pseudo-racemate. In this case (*S*) and (*R*) enantiomers co-crystallize arbitrarily. In both Figures 6(C) and 7(c) is shown a typical binary phase diagram and the solid state arrangement for this system. Figure 6(C) is classified into three different types which were identified by Roozeboom[36]. In type *1* (ideal solid solution) indicated in Figure 6(C) as *1*, is made up of mixture of (*S*) and (*R*) enantiomers in all proportions melt at the same temperature as the single enantiomer . In the second type (with maximum melting point), shown in

Figure 6(C) as 2, the phase diagram exhibits a maximum melting point for the racemate and in the third case (with minimum melting point) is the contrary.

The next section will discuss various techniques capable to separate enantiomers.

2.4 Chiral separation techniques

Basically, techniques for acquiring chiral compounds can be classified into three main areas: generating chiral substances from starting material via the "chiral pool" of nature, asymmetric synthesis (making chiral substances from achiral starting material), and resolution of racemates. On the industrial scale, enantiomers are produced mainly by enantioselective synthesis or from the resolution of racemates. In the first case substances are synthesized by using biological and chemical catalysis to make desired molecules from pure chiral building blocks that are already accessible. The second category is also classified as asymmetric synthesis. Herein, the desired enantiomer is synthesized by a selective synthesis with achiral starting material. In most cases an asymmetrical mixture of both enantiomers is obtained. The third category involves first the unselective production of the racemate followed by the resolution process. The third class is frequently employed on commercial level in the industry. A comprehensive description of enantioselective syntheses has been reported in.[40] Most of the production of enantiomers in the industry involves racemate synthesis and subsequent resolution processes.

In the next section, the various resolution methods that are commonly used in the industry are discussed.

Chromatographic techniques. Chromatographic separation involves different distribution of the compounds to be separated between a mobile phase (eluent) and a stationary phase (adsorbent). In the case of enantioselective chromatography, chiral selectors are attached to the surface of the stationary phase (chiral stationary phase, CSP) so as to offer a chiral milieu necessary for selective interactions. Currently there are several types of CSPs in use, for instance cyclodextrins, proteins and polysaccharides. There are a couple of reasons for the growing number of applications of chromatography, for example the relatively short time necessary to develop a chromatographic method, simplicity in scale up and the availability of several

possible CSPs for many separation systems. There are different types of chromatographic techniques, based on its mobile and stationary phases applied for interaction e.g. Liquid chromatography, Subcritical or Supercritical fluid chromatography and Gas chromatography. High-pressure liquid chromatography (HPLC) separation in one of the most essential fields in the preparative resolution of enantiomers [41] Herein, enantiomers are discriminated with the aid of different molecular interactions with the chiral stationary phase, which separate the two enantiomers by employing the chirality of the stationary phase. However, this method applies typically a large amount of solvent and requires sufficient capital investment in the form of expensive stationary phases and high pressure equipments.[42] In the last years, the execution of the Simulated Moving Bed (SMB) expertise proved to reduce separation costs.

Kinetic resolution. Generally, a chemical material capable of enantiomeric discrimination is used to catalyze a chemical transformation of the two enantiomers at substantially different rates. Preferably, the rate of conversion is zero for one of the enantiomers whilst its counter enantiomer is readily converted. This concept is based on chemical reactions of various types, and mainly divided into two sections: enzymatic and inorganic catalyzed systems. Though, it gives very high selectivity, usually in practice a compromise needs to be made between conversion and enantiomeric purity. It has been reported that enzymatic reagents often deliver higher optical purities.[43] Although it is effective, powerful and capable of producing in some cases very high enantiomeric excesses, application is limited due to lengthy development times and limited availability of enantio-discriminating substances.[42]

Reaction/resolution combinations.[42] This involves reactions to form a diastereomeric salt which is subsequently introduced into classical resolutions. Diastereomeric salt resolutions are widely employed in chemistry and are often considered as the most cost effective technique. However, racemization of the separated enantiomers can frequently occur during the elimination of the salt, rendering this method then ineffective for chiral separation. Another, new technique applied here is the usage of enzymes to catalyze the reaction of one enantiomer into different chemical species. For instance pig liver esterase is used to catalyze the esterification of an undesired enantiomer, followed by the application of standard physical techniques such as crystallization, evaporation, etc. Though, this gives a suitable separation there are a couple of limitations such as inability of the enzymes to

survive typical organic solvents which are being used in pharmaceutical processing. Also, high cost and lengthy development time limit the application of this method.

Membrane-based separations. There are two main kinds of membrane processes for enantioseparation; either by direct separation using an enantioselective membrane, or separation in which a non-selective membrane aids an enantioselective process. Enantioselective membranes offer barriers, allowing selective transport of one of the enantiomers of a racemic mixture. There are two types of such membranes; dense polymers or liquid membranes. In the latter case a selective carrier is usually added to the liquid membrane. Therefore liquid membranes have been considered promising for the selective transport of enantiomeric solutes across membrane. Larger scale application has been very restricted due to the extreme poor stability of the supported liquid membranes. If the liquid membrane is suitably developed then would require lowest capital and lowest operating cost process to realize chiral purity via separation.[41,42,44] . Recently, Seebach et al.[45] also reported the application of molecularly imprinted polymeric membranes as an alternative way of chiral separation.

Crystallization. This is often the preferred method due to its easiness of operation, minimal cost of manufacture and its effectiveness. Crystallization methods are extensively used by large industrial scales for the separation of chiral substances and diastereomeric salts, since they are more straightforward and more economical relative to the other methods.[1] A chiral compound can be obtained directly via crystallization of the desired enantiomer from the racemic mixture. Generally, enantioselective crystallization occurs by adding seed crystals of the preferred enantiomer to a supersaturated solution of racemic mixture. Moreover, enantioselective crystallization can also occur by using a chiral environment to carry out the crystallization. A chiral environment can be produced by using a chiral solvent or a chiral additive. These ingredients might create selective interactions with the chiral solutes, which can facilitate differentiation between the two single enantiomers.[4,5,46] Unfortunately, most of the enantioselective crystallization processes are only suitable for conglomerate systems, which are not so common. Racemic compounds are more frequently encountered in nature[1]. Based on this fact, efforts are currently focused on developing resolution processes capable to resolve compound forming systems.

The next section will discuss options for racemate resolution by various enantioselective crystallization processes.

2.5 Separation of racemates by enantioselective crystallization

The following sections summarize different enantioselective crystallization techniques capable to provide pure enantiomers. The possibility of enantioselective crystallization strongly depends on the whims of nature, generating the shapes of the solubility isotherms in the ternary solubility phase diagram. Since this type of resolution method is effectively used for conglomerate systems, there had been the need to find out other ways for applying it also to racemic compound. Herein, this technique can also be employed to compound forming systems by starting with a solution having (almost) eutectic composition of the racemic compound and one of the pure enantiomers.[47,48]

2.5.1 Classical resolution

Actually, this technique was discovered by Pasteur in 1853. This is a method which entails the combination of a racemate with one enantiomers of another chiral substance (resolving agent) to give a 50:50 mixture of (p, n)-diastereomeric salts. The diastereomers have different properties, aiding a physical separation. Thus, separations of the diastereomeric salts are feasible. A schematic example of this method is illustrated in Figure 8.
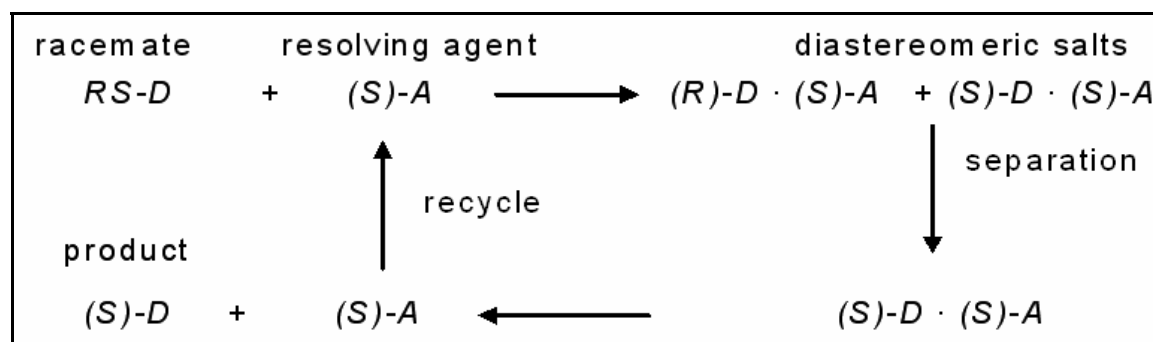
Figure 8: Classical resolution of diastereomeric salts. The racemic mixture RS-D is converted into two diastereomeric salts applying the homochiral resolving agent (S)-A. The diastereomers are separated, and the single enantiomer, (S)-D is released. The resolving agent is regenerated via recycle.

Diastereomeric salt crystallization is widely used industrially. Approximately 65% of the enantiomeric drugs are obtained in this way, and hence it plays a major role in the industrial production of enantiomers.[49] Collet[1] reported that DSM Company has resolved *DL*-phenylglycine by crystallization of its diastereoisomeric salts with (+)-10-camphorsulphonic acid, to produce at a scale of more than 1000 tonnes per year. The *D*-enantiomer is applied in the manufacture of antibiotic ampicillin. Moreover, thousands of tonnes per year of (S)-naproxen[50], are produced by diastereomeric salt resolution, rather than other methods such as asymmetric synthesis. The reasons of this preference are that crystallization is a more straightforward and economical method compared to other techniques.

However, this technique has some limitations regarding the availability of resolving agent and the yield. For instance, decision on what is cheap to be used, available, optically active and chemically and optically stable along with many other restrictions. Another shortcoming of this method is that the maximum yield that can be realized is only 50%. Mostly only 33% yield[1] is achieved. However, unless racemization is localized into the process so that complete conversion to the desired enantiomers is attained.

In 1998 Vries et al.[51] reported an improved way of dealing with this technique. These authors employed a smart combinatorial approach to ease the cumbersome selection of the appropriate resolving agent. This method is known as "Dutch Resolution". They observed that the simultaneous addition of several resolving agents of the identical family (normally three) to a racemate led to a fast precipitation of the crystalline diastereomeric salt; moreover, the diastereomeric salts obtained had high enantiomeric purities. Furthermore, the use of multiple resolving agents speeded up the process of finding the best resolving agent. The use of a family of resolving agents rendered in the last years trial-and-error method of resolution into an acceptable practice. Leusen et al.[52] presented a thermodynamic approach which shows that the resolution efficiency is related to the lattice energy differences of the pair of diastereomeric salts.

2.5.2 Resolution by direct crystallization

The precondition of enantioseparations by direct crystallization is that the racemate of the respective enantiomers crystallizes as conglomerate form (see Figure 6(A)). Direct crystallization which is an economical resolution technique has been discussed comprehensively by Jacques et al.[5] In the case of racemic compound system, the method can only apply when the racemic compound is converted into conglomerate, and this can be made through changing it to derivative.[16] Thus, when the two enantiomers crystallize as a conglomerate, then two resolution methods (preferential nucleation/crystallization) are feasible. Before these resolutions methods may be applied it is obviously necessary to establish the existence of the conglomerate; this may be done in a number of ways: (i) determination of binary (Figure 6(A)), or ternary phase diagrams, (ii) effecting resolution by direct crystallization (confirmatory test); (iii) powder X-ray or solid state IR spectra (enantiomers give spectra indistinguishable with those of racemic conglomerate but differ for racemic compounds)[49].

Direct crystallization can be performed in two main ways, i.e. simultaneous and preferential crystallization.

2.5.2.1 Resolution by simultaneous crystallization

The process consists of seeding the racemic supersaturated solution with comparatively large seeds of one of the enantiomers which eventually grows larger. At the same time, the spontaneous crystallization of the counter enantiomers by the small seeds will create small crystals which can be separated from the larger enantiomeric crystal by sieving.[5]

In 1848, Louis Pasteur successfully performed enantioseparation of racemic sodium ammonium tartrate by visually distinguishing between the levorotatory and dextrorotatory crystals and manually sorted them out.[15] This manual crystal sorting approach of Pasteur's by utilizing the hemihedral faces is laborious and not commercially or industrially appropriate. Since only well-defined morphological characteristics that can distinguish between the left and right crystals, a situation that does not always attain constant if large crystals is present. On the other hand, an alternative technique (schematically shown in Figure 9) uses two crystallizers which

are seeded with the corresponding enantiomer. Herein, the crystallization proceeds with a supersaturated solution, and after the crystals are collected the solution is resaturated and this cycle continues.
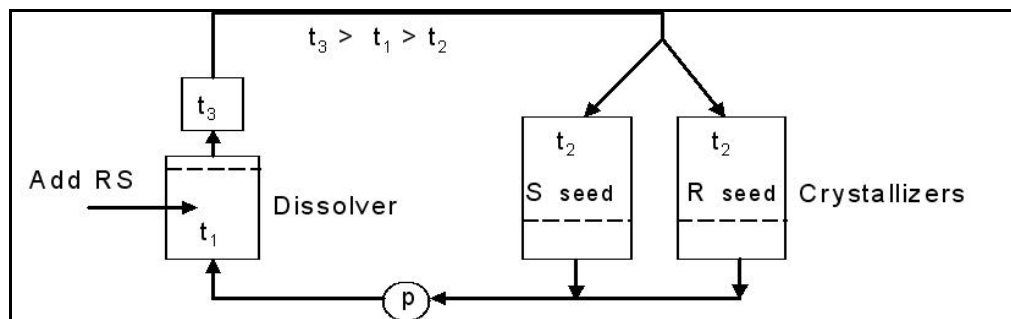
Figure 9: Schematic diagram showing process for the resolution of α-methyldopa by seeding with individual enantiomers within metastable zone width. t_1, t_2 and t_3 represents the temperatures[44]

The principle used here is that a supersaturated solution is created within the metastable zone width and then seeded with the single enantiomers. This method has been used commercially by Merck to produce tonnes of antihypertensive drug methyldopa.[44,49] For instance, Doki et al.[53] used preferential crystallization in the presence of a "tailor-made" additive to resolve *DL*-asparagine. They applied a novel combined natural cooling and pulse heating technique where both enantiomers crystallized simultaneously but could be separated by their different sizes.

2.5.2.2 Resolution by preferential crystallization

The resolution of enantiomers by preferential crystallization is a kinetically controlled separation process that is terminated before thermodynamic equilibrium is attained. This technique is also known as resolution by entrainment.[5] Crystals of the desired enantiomer are obtained from a supersaturated solution enriched in example one-enantiomer by seeding with this enantiomers, say the (*S)*-enantiomer when enriched with the (*S*)-enantiomer. Crystals of (*S*)-enantiomer are crystallized and the solution is now enriched in the (*R*)-enantiomer, to which equal amount of racemate is added, i.e. equal to the mass of the (*S*)-enantiomer that crystallized. Afterward supersaturation is restored with the solution now further enriched in the (*R*)-enantiomer and crystals of (*R)*-enantiomer are collected. This process can be carried out repeatedly by crystallizing both enantiomers alternatively.

The application of a cyclic mode of preferential crystallization for a conglomerate system is illustrated in Figure 10. At the start, the solution is saturated at temperature T_{start}, with an enantiomeric composition of point *A* (enriched in (*S*)-enantiomer). Afterward the solution is cooled down to T_{end} and the solution then becomes supersaturated.
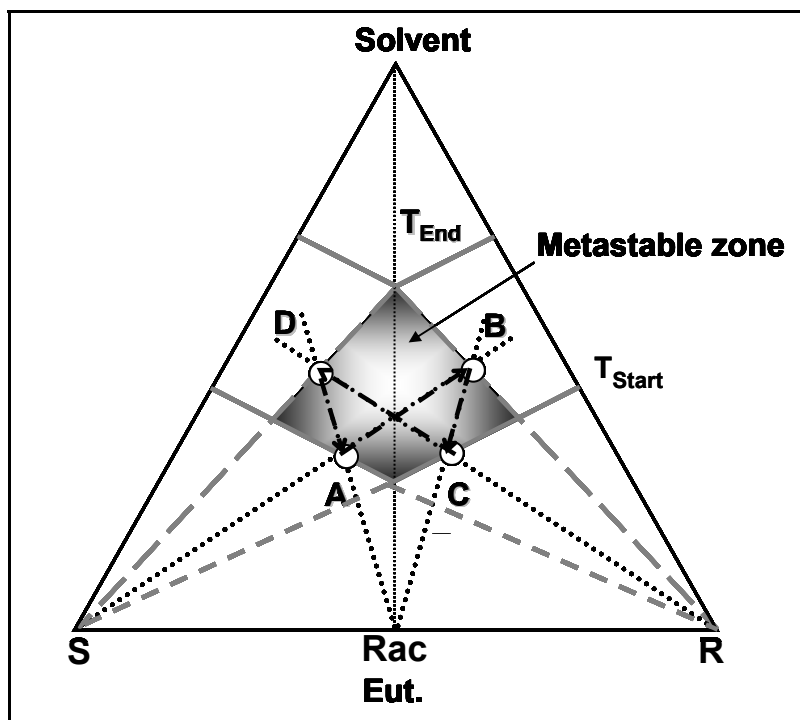
Figure 10: Preferential crystallization conducted in a cyclic operation mode for a conglomerate system.

The clear solution (free from any particles of crystals) is seeded with crystals of the enantiomer *S*. As a consequence, the pure enantiomer *S* crystallizes along the trajectory *A* to *B*. At the point *B*, the process is stopped; the solid enantiomer *S* is cropped and predetermined amount of the racemic mixture is added to the remaining mother liquor. After complete dissolution of the solid feed, the solution has a new composition which is represented by point *C*. Here, solution is cooled down to temperature T_{end} and subsequently seeded with crystals of enantiomer *R*, so pure enantiomer *R* crystallizes along the trajectory *C* to *D*. After reaching the point *D* the process is interrupted once again to be able to harvest the pure enantiomer *R*. All seeding processes are done only in the metastable zone width (see section 2.2.5, Figure 5), which is demarcated in Figure 10 in grey color.

Although most of preferential crystallization process can be applied conveniently to conglomerate system, there are few cases where it has been used for racemic compound systems. Recently, Lorenz el al.[47] have illustrated the possibility of preferential crystallization for such systems starting with a solution having approximately eutectic composition (made up of the racemic compound and one of the pure enantiomers). Figure 11 shows the application of a cyclic operation mode for preferential crystallization of a racemic compound system.[47]
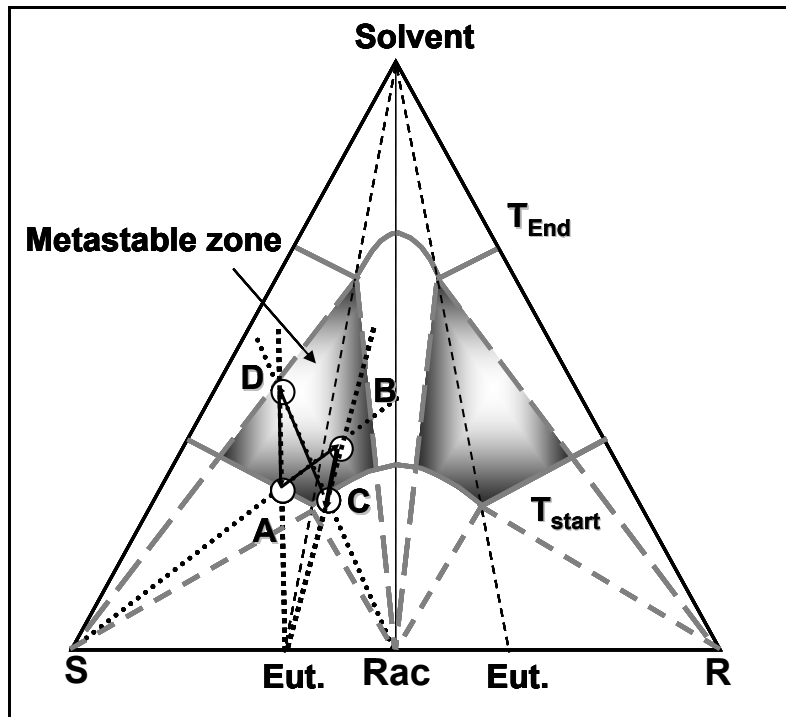
Figure 11: Preferential crystallization conducted in a cyclic operation mode for a racemic compound.[47]

Analogously to conglomerates, preferential crystallization is performed in the *3*-phase region of the conglomerate forming system. The same concept of preferential crystallization for racemic compounds can be described by Figure 11. The same procedure and techniques as in the case of Figure 10 is employed, except that after seeding the supersaturated solution at point *A* crystals of pure enantiomer *S*. The composition of the solution shifts from point *A* to *B* as (*S)*-enantiomer crystallizes from the solution. At point B, the process is stopped, and the (*S)*-enantiomer crystals are filtered off. Later, a predetermined amount of, eutectic mixture (*Eut)* is added to the remaining mother liquor. After dissolving entirely the solid feed, the solution assumes a new composition represented by point C. When reaching *T_end* and seeding

with crystals of the racemic compound (*Rac),* then the racemic compound starts to crystallize along the trajectory *C* to *D*. At point *D* the process is interrupted and the crystallized racemic compound is filtered off. Subsequently, new *Eut* is added into the crystallizer to provide a solution having the start composition A to do again the whole cycle illustrated.

Preferential crystallization can be also carried out in the presence of additives. A stereochemical way has been applied which involves the growth and dissolution of molecular crystals in the presence of tailor made additives.[54,55] An additive can be adsorbed stereoselectively on the enantiomer of the same absolute configuration. This inhibits the growth of the enantiomer and preferential crystallization of the unaffected enantiomer (of the opposite chirality, which implies the well known "rule of reversal") Hence the existence of the incorporated additive differentially affects growth directions.

Additives are used for the control of nucleation and growth of molecular crystals and are classified broadly as inhibitors and promoters.[56] Tailor made inhibitors which are used for crystal growth can be applied for a number of functions such as morphological engineering[57] and also etching, reduction of crystal symmetry (from the occlusion of additive into the crystal)[58], explaining the effects of solvents on crystal growth, crystallization of the preferred polymorph and assignment of absolute configuration of chiral molecules and polar crystals.[59] Figure 12 illustrate the influence of additive on the morphology of crystal during crystal growth process.
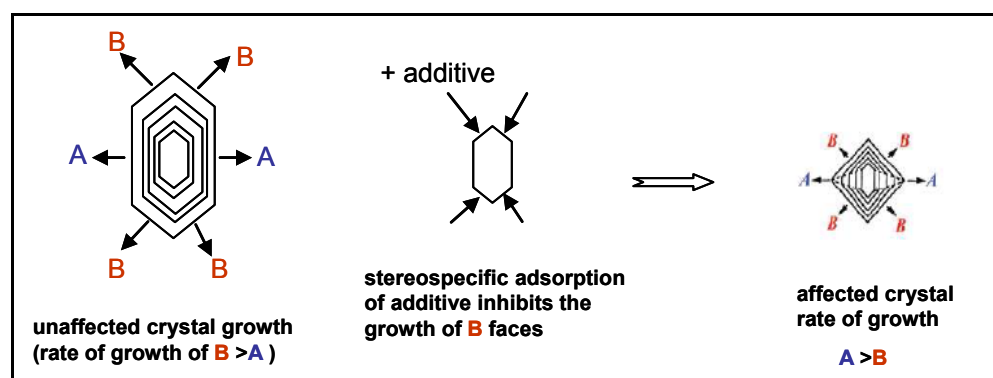
Figure 12: Influence of additive on the morphology of crystal during crystal growth.[54]

Tailor made additives have been used at length to control crystal polymorphism by selectively hindering the nucleation of the undesired polymorph by the selective

adsorption of the additive on certain surfaces of the growing crystal.[54,56,60] This is due to the hypothesis that in supersaturated solutions, some molecular clusters are present which bear a resemblance to the structure of the macroscopic crystals into which they eventually grow. There are many instances where additives have been successfully been used to crystallize one of the enantiomers from a conglomerate solution.[55,60-64]

The method of inhibition requires no resolving agents and is conducted under explicit conditions designed such that the undesired enantiomer does not suddenly crystallize out. In a strict thermodynamic sense, preferential crystallization can be attained only for substances that are conglomerates. But, it might be possible with compound existing either as conglomerates or racemic compounds within available temperature range under kinetic control, stirring, variable temperature and seeding. Resolution by entrainment is based on the differences in solubility of the racemate and the pure enantiomers.[65] Resolution of racemic conglomerates by preferential crystallization is the easiest and cheapest method available for the generation of enantiomerically pure products.[1,5] The preferential crystallization process as a method for commercial resolution of racemates has great potential and real economic importance in both pharmaceutical and chemical industries. However, understanding of the underlying fundamentals processes such as thermodynamics and kinetics of this technique in the crystallization process is rather restricted. To optimize the resolution technique, the behavior of chiral crystals under varied conditions must be understood.[65]

2.5.3 Resolution by preferential nucleation

In preferential nucleation[66,67] the nucleation rates of both enantiomers are different. This behavior can be attained by e.g. addition of a suitable additive that selectively inhibits nucleation of one of the enantiomers. This promotes the other enantiomer to nucleate. The nucleation rates of the two enantiomers can be sometimes altered even with addition of small amount of a suitable additives ($<< 1\%$). The method is illustrated on Figure 13. Figure 13 shows the principle of preferential nucleation in; (a) without chiral tailor-made additive, where the enantiomers of *R* and *S* have the same nucleation and crystal growth rates, (b) after adding chiral tailor-made additive such as example *R**, the crystallization of *R* in this case is more strongly inhibited than for its counter enantiomer *S*.

$$(R)_{Solvent} - (S)_{solvent} \qquad (R)_{Solvent} + (R^*_{solvent}) - (S)_{solvent}$$

<R>   <S>   ‹R›   <S>

(a)   (b)
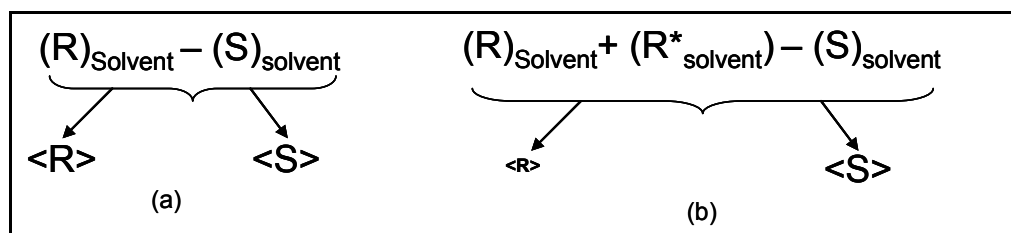
Figure 13: Principle of S preferential nucleation. (a) Without chiral tailor-made additive, *R* and *S* nucleation rate and crystal growth rate are equal. (b) After addition of the chiral tailor-made additive *R** the crystallization of R is more strongly inhibited than that of ‹S›.[67]

Thus, the "rule of reversal"[55,68,69] applies in this case. It means the additive is stereoselectively adsorbed at the surface of growing nuclei of the enantiomer of the same absolute configuration, resulting in a strong reduction in their growth rate and thus allowing for preferential crystallization of the counter-enantiomer. Herein, the solute with identical absolute configuration as that of the chiral tailor-made additive experiences the strongest disrupting effect (inhibition) of the nucleation rate. In this situation "similar or identical molecules" means species which are able to contribute in the same strong bond network in the crystal lattice (ionic bonds if they exist, H-bonds) but differ by organic substituents involved in the van der Waals interactions.[67] Ndzié et al.[66] demonstrated a successful enantiomeric resolution of (±)-5-Ethyl-5-Methylhydantoin by means of preferential nucleation. Barton and Kirby[70] also conducted resolution of (±)-narwedine in the presence of (-)-galanthamine with the aid of preferential nucleation to isolate (+)-narwedine. According to Jacques et al.[5] chiral solvents can also play a useful role in modifying the rate of growth of enantiomeric crystals, and can be exploited for preferential nucleation/crystallization.

2.5.4 Chiral solvents

Chiral solvents (optically active organic solvents), consisting of chiral molecules which rotate the plane of linearly polarized light.[71] Generally, diastereomeric solvates (complexes) could be formed when a mixture of enantiomers is dissolved in a chiral solvent. Consequently, these complexes should possess slightly different physical and chemical properties.[4]

According to a letter Van't Hoff wrote to Meyerhoffer in 1893 in which he stated that there should be the possibility to find differences in the solubility of enantiomers in optical active solvent (chiral solvent)[72], predicted the use of this property as a new

resolution method. Basically, in the kinetic sense the chiral solvent can modify the rate of growth of enantiomeric crystals. More precisely, it probably influences both the nucleation/crystal growth rate of the chiral substrate in different ways, depending on the nature, stereospecificity, and the effectiveness of solvent-substrate interaction.[5] On the other hand, thermodynamically, the chiral solvent possesses a certain potential to discriminate between two enantiomers by creating specific weak interactions and forming diastereomeric complexes which gives different physical properties such as solubility differences.[4] This discrimination can provide selective kinetic or solution thermodynamic effects which can be useful for the separation of enantiomers as suggested by Van't Hoff.

The next section will present a discussion on role of solvent in selective crystallization.

2.6 Role of solvent in selective crystallization

Solvents play a major role in crystallization. Generally, solvents are selected based on the resulting solubilities, the mode of crystallization and the type of crystals. The main point that should be considered in the process of selecting a solvent for crystallization is that the solute which has be crystallized must readily be soluble in the solvent. The solute used should form desired as a solute crystalline form after cooling, evaporating or salting out with an additive. The solvent applied can also have a major influence on crystallization, for instance capacity of solute-solvent reactivity, solvate formation, the viscosity of solvent, recovery of solvent, and how the freezing point of the solvent is related to the operation window and hazardous nature of the solvent.[31]

However, in the case of selective crystallization, the kind of solvent applied can influence the shape of the solubility isotherms which eventually allow high entrainment in a preferential crystallization. This is so because, it might provide a wide area for entrainment, i.e. it might be possible to obtain high yields in resolution or it may be possible even to enter the two phase region of the phase diagram, which would be more lucrative for obtaining enantiopure crystals.[5,33] Recently, Kaemmerer et al.[73] performed experimental studies on two chiral systems (malic acid and methionine) and reported that the eutectic composition of the two enantiomers can be altered by temperature and choice of solvent.

The following section will give a comprehensive discussion on state of research on chiral solvent/chiral media being used as means for chiral separation.

2.6.1 State of research

Since a chiral solvent has the potential to discriminate between two enantiomers, asymmetry could be induced in a solubility phase diagram. Based on this asymmetry, the resolution of a racemate should be feasible by direct crystallization.[4,5] On the basis of this expectations, several resolution work involving chiral solvents and other chiral media have been discussed comprehensively in this section. Literature survey on chiral solvent/chiral medium has revealed couple of successful chiral resolutions by employing enantioselective crystallization with the help of chiral solvents or chiral medium. For instance, Buhse et al.[46] demonstrated a successful kinetic resolution of racemic glutamic acid by using a chiral solvent derived from lysine and water. Small amounts of *L*- or *D*-Lysine were used to retard the crystallization rate of the corresponding enantiomer of glutamic acid in a stereospecific way, which resulted in transient optical resolution of racemic glutamic acid during crystallization. Moreover, Lüttringhaus et al.[74] and Groen et al.[75] reported successful chiral resolutions of some racemic conglomerates by crystallization using *D*-isopropyl tartrate and (-)-α-pinene respectively, as chiral solvents. This direct crystallization was feasible due to the different rates of nucleation and/or growth of one enantiomer comparative to the other. On the other hand, Groen et al. further illustrated that the resolution of a racemic compound in (-)-α-pinene was not feasible [75]. All the authors observed a certain enantiomeric excess. Further work has been done by applying "tailor-made" additives in kinetic resolution. For example, Addadi et al.[55] conducted efficient resolutions of a couple of conglomerates by preferential crystallization with the help of "tailor-made" additives. More recently, also Doki et al.[53] used preferential crystallization in the presence of a "tailor-made" additive to resolve *DL*-asparagine. They applied a novel combined natural cooling and pulse heating technique where both enantiomers crystallized simultaneously but could be separated by their different sizes. However, the examples given only apply to conglomerate systems.

Moreover, Mughal et al[48] conducted similar work on primary nucleation in the mandelic acid/water system by starting with eutectic composition of the mandelic acid

enantiomers in water ((S)-enantiomer in excess) using an additive. Additive is used to further inhibit the racemate, i.e. delayed the rate of equilibration. The authors could demonstrate an enantiomeric enrichment of the (*S*)-MA in the crystallized material for a certain period of time. This is expected since the MSZW (see section 2.2.5) of the mandelic acid enantiomers in water is explicitly lower than that of the racemic compound in the temperature range studied[47]. However, this enantioselective crystallization process needs to start with a solution containing the enantiomers (more or less) in the domain of eutectic composition. Barton and Kirby also conducted resolution of (±)-narwedine in the presence of (-)-galanthamine with the aid of preferential nucleation to isolate (+)-narwedine.[70]

Furthermore, new approaches of chiral resolution based on enantioselective separations aided by chiral surfaces are reported. For example , Medina et al.[76] published a new way of chiral separation based on enantioselective crystallization on chiral polymeric microspheres. Chiral resolution of *DL*-valine a racemic compound system was carried out and with the help of chiral polymeric micropsheres an enantiomeric excess of 25% for *L*-valine in the chiral microspheres were realized during crystallization. Here, basic principle of chiral discrimination aided by enantioselective crystallization on chiral mocrospheres is performed. Gabashvili et al.[77] demonstrated quite similar work by using chiral mesoporous silica based on chiral block copolymers of poly (ethylene oxide) and of *D*-phenylalanine (PEO-*b*-D-Phe) as a surfactant template for racemic valine, and preferential chiral selective adsorption of D-valine enantiomer was observed. Also, Fireman-Shoresh et al.[78] reported possible discrimination between pairs of enantiomers ((R)- and (S)-propranolol, and (R)- and (S)-2,2,2-trifluoro-1-(9-anthryl)ethanol, respectively) by employing chirally templated sol-gel thin films. In both pairs of enantiomers, the chiral templated sol-gel thin films could preferentially adsorb the (R)-enantiomer.

Moreover, novel methods of chiral resolution based on enantioseparations with the help of chiral extraction are demonstrated in some recent publications. Tang et al.[79] reported on a feasible novel method for the separation of mandelic acid enantiomers by applying biphasic recognition chiral extraction. Also, Dzygiel et al.[80] reported on successful resolution of racemic N-Benzyl α-amino acid by liquid-liquid extraction with a practical method using lipophilic chiral cobalt (III) salen complex and mechanistic studies.

Recently, Hüttenhain and Dickerhof reported a comprehensive work on the asymmetric induction by means of chiral solvents "Asymmetrische Induktion durch Lösungsmittel" to realize enantioselectivity.[81] In this work, acetophenone was successfully converted to 33% ee of (R)-phenyl ethanol in the liquid phase with the aid of the chiral solvent (S)-ethyl lactate at 0 °C. Also, the authors demonstrated that a unique reaction pathway at lower temperature -78 °C with a quantifiable conversion of acetophenone and (S)-methyl lactate into 60% ee of (R)-phenyl ethanol is possible with triple the amount of boron hydride in excess. The authors further investigated the theoretical computations in cooperation with professors Schmidt and Rueping of the Universitat Frankfurt for the possible transition states and product distributions for the reactions with acetophenone occurring at room temperature were calculated by means of computer simulation. Initial computational works have shown that there is an intensive dependence between the structures of the solvent and the enantioselectivity. Hence, molecules with similar structure should better fit the solvent cage and attain higher enantiomeric excess (ee). Based on entropy principles, it would be favorable for the (*S*) solvent and its corresponding (*R*) form of the transition state molecule. Additionally, they revealed that the surrounding solvent and its chiral cage have little influence on the advancement of the reaction, and only a direct interaction on the hydrogen bonds impacts the enantioselectivity.

2.6.2 Effect of additives on crystallization

In this thesis work tailor-made chiral solvents are employed as one of the chiral solvents for enantioselective crystallization. So, this section will be used to describe how tailor-made additives inhibit crystal growth.

Tailor-made additives are specially designed to interact in a precise way with selected faces of crystalline materials. The molecules of tailor-made additives are composed in two parts. One section which belong to for instance the chemical group or moieties, and is identical with that of the substrate molecules undergoing crystallization. When such molecules are added to a solution undergoing crystallization, by nature of their moieties identical to the substrate these segments of the additive imitate the solute molecules and are, hence, readily adsorbed at growth sites of the crystal surface. The second part of the additives is designed in such a way that the ends of these parts are

chemically or structurally different from the host molecules, thus disrupting subsequent attachment of the solute molecules. This effect is realized by tailoring the additive molecules to introduce steric hindrance. The largest morphological changes occur in crystals grown in the presence of additives that interact strongly and selectively to one or a few crystal surfaces.[57] Figure 14 depicts schematic representation of inhibition of growth of benzamide crystals along the b direction by adsorption of benzoic acid molecules of the additive. For example, in the presence of benzoic acid the morphology of benzamide crystals is altered.[56] Hence, the benzamide forms plate-like crystals and consists of hydrogen bonded cyclic dimers interlinked by NH---O bonds along the *b*-axis. Since in the presence of benzoic acid, competitive binding occurs between the stereochemically identical benzamide and benzoic acid along the *b*-axis. This results in an enhanced surface area of the faces which cut the *b*-axis, and leads to wider plate-like crystals compared to the narrow plate-like crystals grown in the absence of benzoic acid.[82] Hence, additives designed to adsorb onto crystal faces can retard the growth of that face to which they bind; whilst crystal faces unaffected by the additive continue to grow[57] (as also shown in Figure 12).
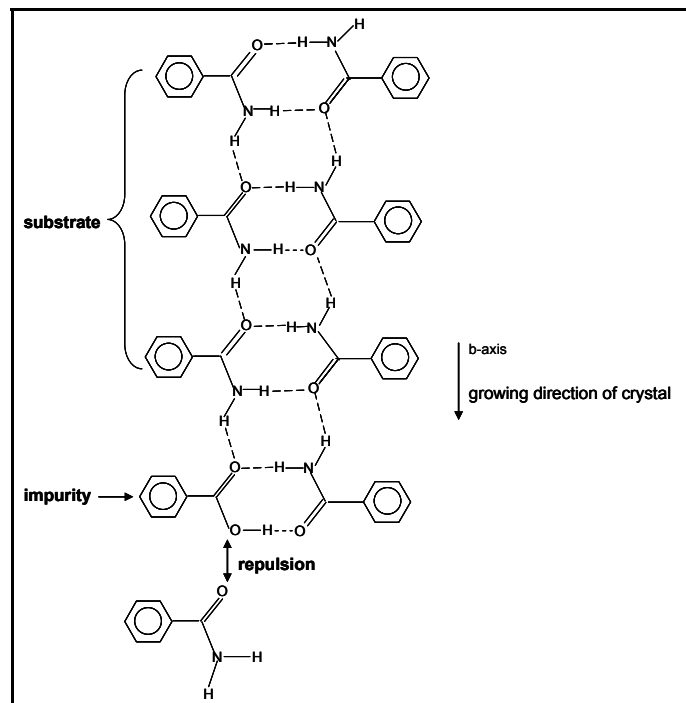
Figure 14: Schematic representation of inhibition of growth of benzamide crystals along the b direction by adsorption of benzoic acid molecules of the additive.[56]

2.7 Molecular modeling for solvent-solute interactions

Molecular modeling studies are required to get a deeper understanding of the solute-solvent interactions in the system studied in this thesis work. Molecular modeling techniques are widely used in pharmaceutical research. Crystal structure data such as unit cell parameters, solute-solvent interaction, fractional atomic coordinates and space group can either be imported as a Crystallographic Information File (CIF file) from experimentally solved structures, or extracted from the ConQuest (CCDC) or mercury Cambridge Structural Database (CSD)[83], where a large number of crystal structure solutions are available and imported into MATERIALS STUDIO 4.3 as data file, which can be then used for the visualization of hydrogen bonding motifs and for various calculations. For the molecular modeling work carried out in this thesis, MAETERIALS STUDIO 4.3[84] (VAMP model) was applied to calculate single energy point calculations for solute-solvent interactions.

In the following sections, specific details on the different molecular modeling studies that can be carried out using these applications are summarized.

2.7.1 Hydrogen bonding

One of the strongest of the non-bonded interactions that organize molecules into superstructures and hold them together is hydrogen bonds. According to L. Pauling[85] a hydrogen bond is defined as "an interaction that directs the association of a covalently bound hydrogen atom with one or more other atoms, groups of atoms, or molecules into an aggregate structure that is sufficiently stable to make it convenient for a chemist to consider it as an independent chemical species" A hydrogen bond is a donor *(B)* and acceptor *(A)* interaction exclusively, involving hydrogen atoms. It is formed between electronegative atoms such as *O* and *N* and electropositive atoms such as *H* atoms. Three parameters (d, θ and r) are employed to illustrate a hydrogen bond (see Figure 15). Hydrogen bonds are categorized by using the rule that the distance d between the *2* atoms involved is less than or equal to the sum of the van der Waals radii for the 2 atoms.
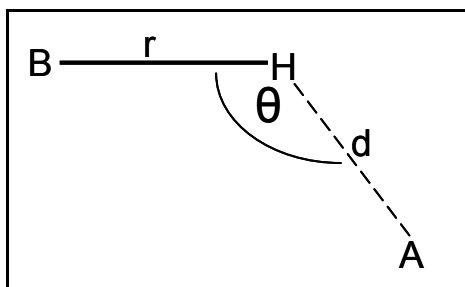
Figure 15: Hydrogen bond parameters (where *r* is the bond length, *d* is the hydrogen bond length and θ is the angle between the bond and the hydrogen bond)[85]

Hydrogen bonds can be intramolecular, where the donor and acceptor atoms are on the same molecule or intermolecular when they are on different molecules. There are three main types of intermolecular hydrogen bonds; (i) the simple linear, *1* donor *1* acceptor hydrogen bond, where the angle (θ) is approximately 180° (characteristic of strong hydrogen bonds); (ii) bifurcated also referred to as three centred hydrogen bond, involving *2* acceptors and *1* donor atom; (iii) trifurcated hydrogen bond with *3* acceptor groups and *1* donor atom, which are relatively rare. Figure 16 shows these three types of hydrogen bonds.[86]
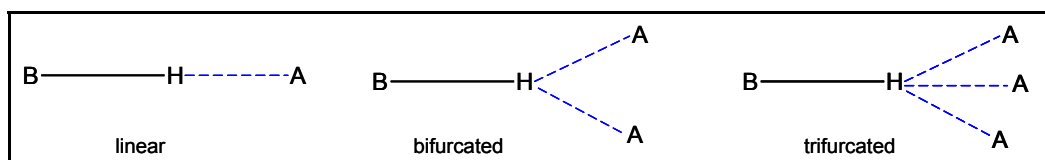
Figure 16: The three main hydrogen bond types.

In the case of this work hydrogen bond dimers bond distances (1.8-2.5 Å)[87] are very necessary as one of the criteria set to perform structural optimizations.

2.7.2 Enthalpy of formation calculations

In this thesis, the enthalpy of formation (ΔH_{form}, is the energy released when individual atoms are brought together to form a molecule of a specific conformation) calculations have been performed for only mandelic acid, since this component belongs to the class of compound forming systems which are particularly difficult to be resolved. The calculations of the enthalpy of formation were performed by employing the VAMP model in MATERIALS STUDIO from software package

Accelrys Materials Studio 4.3. VAMP uses semi-empirical calculations to determine a molecular wave function. This wave function can then be applied to evaluate molecular properties such as energy, dipole moment.[88]

In this work the molecular modeling calculations have been performed for the solute-solvent dimers. Recently, Davey et al.[89] demonstrated that mandelic acid in only chloroform solutions exhibit self assembly dimers, but in all other solvents mandelic acid is strongly solvated. Based on this outcome, all the molecular modeling calculations were conducted on solvated dimer systems. The enthalpy of formation (ΔH_{form}) was obtained by first performing a geometry optimization of the molecules (optimized structures) by setting the charge on each molecule to zero. In order to realize global minima or the most optimized structures, it is necessary to obtain structures which have hydrogen bonds between the ranges of 1.8-2.5 Å and are coupled with more negative enthalpy of formation value. The geometry optimization was carried out with the VAMP model together with the Austin model 1 (AM1), and also the Neglect of Diatomic Differential Overlap (NDDO). The VAMP model is used together with the AM1, which gives good estimation for hydrogen bonding calculations. The AM1 was designed to eliminate the problems from MNDO caused by the tendency to overestimate repulsion between atoms separated by the sum of their van der Waals radii.[90] Whiles, the NDDO is a basic approximation for neglecting less important integrals. When VAMP model is used from the Materials Studio interface, then AM1 is the default NDDO Hamiltonian.[91] From the obtained optimized structures, the heat of formation is calculated by also using the same procedure as explained earlier on. The stability of a conformation is quantified by the stabilization enthalpy ($\Delta H_{form}^{Stabilization}$), where the most stable dimer possesses the largest most negative value for the stabilization enthalpy and vice versa. More information with regard to the approach used is given in[92,93] and the Accelrys software manual.[84]

The whole procedure used for the solvent-solute dimer single energy point calculations for the enthalpy of formation has been explained in detailed in the flow chart in Figure 17.
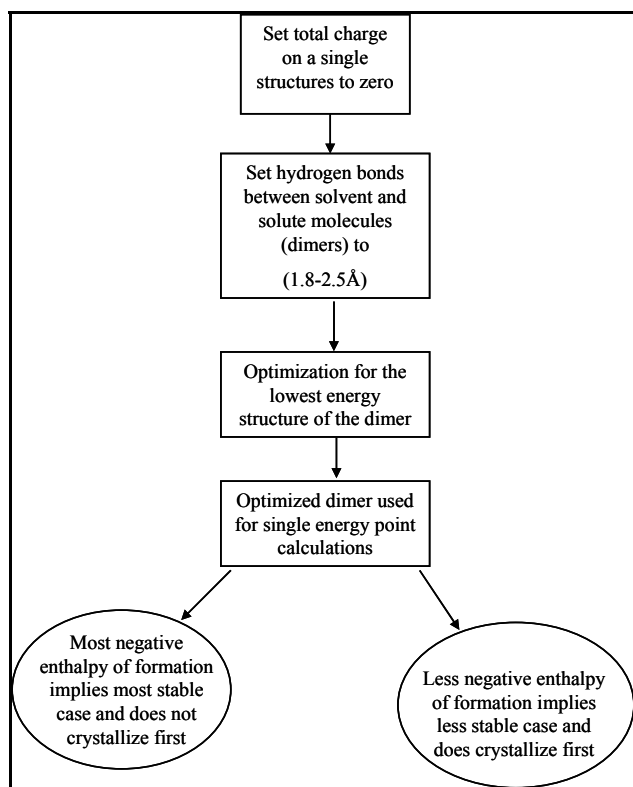
Figure 17: Flow chart for single energy point calculations (at specific molecular geometry) for enthalpy of formation by using MATERIALS STUDIO 4.3 (VAMP model).

2.8 Summary

In this chapter basics of the theory of crystallization were summarized, and concepts how chiral substances can be resolved. For resolution, crystallization is the most economical and easy to use techniques and hence very attractive. In addition, crystallization techniques are not only applicable to racemates (50:50 mixtures of both enantiomers) but pure enantiomers crystals can be obtained from non-racemic, i.e. asymmetric mixtures. However, it is vital to establish whether a substance forms a racemic compound, a conglomerate or a solid solution before a resolution crystallization based process can be selected.

For racemic compounds, the separation of the two enantiomers requires the utilization of diastereomeric interactions, including the formation of diastereomeric salts with a chiral resolving agent, or chromatography using optically active stationary phases or possibly by applying chiral solvents which might create diastereomeric interactions (complexes)[4,5] and can be exploited for enantioselective crystallization. Contrary to this, the resolution of conglomerate systems does not require optically active

resolving agents as in preferential crystallization the resolution occurs spontaneously for the period of crystallization.

The role of additives and solvents in crystallization processes was discussed in this chapter; studies to help elucidate basic scientific questions, such as the molecular interactions at interfaces, the role of solvent on the crystal growth. Also, details on crystal science have been discussed. Moreover, the current state of research using chiral solvent/chiral media to effect enantioselective crystallization has been reviewed. Principles of the metastable zone width and induction time have been highlighted in this chapter.

Molecular modeling studies concerning solvent-solute interactions were used to gain a deeper understanding into certain interesting experimental observation. The procedure applied has been detailed out in this chapter.

The next chapter will give an in-depth discussion on the experimental techniques and two systematic fundamental experiments for solubility and metastable zone width. Also, successfully designed resolution experiments will be presented.

Chapter 3. Experimental techniques and procedures

Chapter 3

3. Experimental Techniques and Procedures

3.1 Introduction

This chapter will give a description of the fundamental principles of the analytical techniques employed for the characterization of liquids and solids phases obtained. A study of the fundamental solubility and metastable zone width data (primary nucleation) has been performed in order to realize enantioselective crystallization from chiral solvents The following analytical techniques have been used; Fourier transform infra-red (FTIR) spectroscopy, Raman spectroscopy, Calorimetry (C80 Calvet Calorimeter), Nuclear magnetic resonance (NMR) spectroscopy, HPLC, Refractometer, X-ray powder diffraction (XRPD), Polarimeter, Density meter, DV-III ultra rheometer for viscosity measurement, Turbidity sensor, Crystal16[TM]. A description of the different enantioselective crystallization techniques (preferential nucleation, preferential crystallization and selective crystallization) applied in this work is presented.

3.2 Chiral solutes (mandelic acid and N-methylephedrine)

The pharmaceutical chiral systems chosen are the compound forming system mandelic acid (MA) and the conglomerate forming system N-methylephedrine (NME). Mandelic acid is common and easily accessible as a chiral resolving agent used in classical resolution for wide viariety of racemates. For instance, (S)- and (R)-enantiomers of MA have been used as resolving reagents in classical resolution for a wide variety of racemates.[94] Additionally, they are applied as a chiral products intermediate for the production of optically active drugs and agricultural based chemicals such as crop protectants. (R)-mandelic acid and (R)-ortho-mandelic acid (mandelic acid derivative) belong to BASF's portfolio for chiral intermediates, trademarked as ChiPros[®] for pharmaceuticals and crop protection agents like herbicides, fungicides and insecticides. Presently, BASF is applying in a stereospecific biocatalyst to synthesize MA.

NME belongs to the class of ephedrines, which are possible stimulants drugs for the central nervous system.[95] In recent times, there has been an increasing interest in drugs that include ephedrine alkaloids because these compounds are known to have weak amphetamine-like effect on the central nervous system (energy booster) and enhance calorie-burning activity when taken together with aspirin and caffeine. It is also commonly used as decongestant (relieve nasal congestion) and against hypotension (low blood pressure).[96]

Screening experiments were carried out to be able to select appropriate chiral solvents which have the potential to create chiral recognition in the chiral system. As the result of this

screening of various chiral solvents showed no discrimination for the chiral system (mandelic acid) applied. Therefore, selection of the chiral solvents for this project was solely based on the availability and the price. In addition tailor-made chiral solvents and chiral ionic liquids were specifically synthesized to fit target chiral molecules in order to provide stronger chiral interactions.

Mandelic acid

(S)- and (R)-enantiomers of mandelic acid have been used as resolving reagents in classical resolution for a wide variety of racemates.[94] Furthermore, the pure (R)-mandelic acid is used as a precursor for the synthesis of cephalosporin and penicillin.[97] Mandelic acid has bacteriostatic properties and it is administered for the treatment of urinary tract infections, i.e. from either calcium or ammonium salt.[98] The racemic form of mandelic acid is also utilized in the mandelate (ester) form as a relevant pharmaceutical constituent due to its analgesic, antirheumatic and spasmolytic effects (Mandrophine and Spasmocyclon).[99] Another feature of mandelic acid is that there is a broad data basis available for this compound. Lorenz et al.[100] determined the ratio of the mandelic acid enantiomers in water at the symmetric eutectic compositions to be 0.69 and 0.31. Figure 18 shows the molecular structures of (*RS*)-MA and (S)-MA and give some background information.

Empirical formula: $C_8H_8O_3$ Molecular weight: 152.15 g/mol

(RS)-Mandelic Acid   (S)-Mandelic Acid

Melting Point: Form I: 119 – 121 °C   Melting Point: 131 – 134 °C
Form II: 107–108 °C
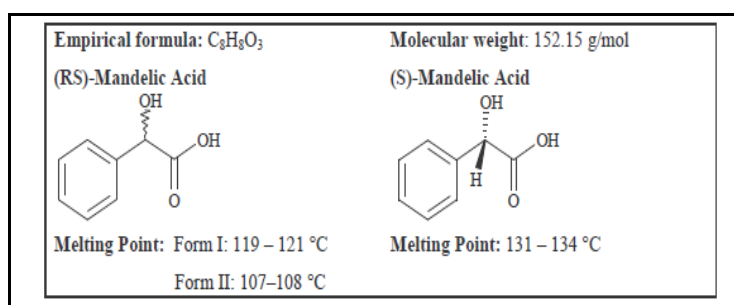
Figure 18: (RS)-MA and (S)-MA data.[87]

N-methylephedrine

N-methylephedrine belongs to the class of ephedrines, which are possible stimulant drugs for the central nervous system.[95] In recent times, there has been an increasing interest in drugs that include ephedrine alkaloids because these compounds are known to have a weak amphetamine-like effect on the central nervous system (energy booster) and enhance calorie-burning activity when taken together with aspirin and caffeine. It is also commonly used as decongestant (relieve nasal congestion) and against hypotension (low blood pressure).[96]

Moreover, N-methylephedrine is extensively applied as a chiral resolving precursor to chiral supporting electrolytes, a catalyst for phase transfer and a reducing agent.[101]

The physicochemical properties and the crystallization thermodynamics of the pure enantiomers and the racemate for N-methylephedrine have been studied intensively by Wang et al.[102] On the other hand, there exist quiet a number of literature on ephedrine.[95,96] The chemical structures of both (a) (*1S,2R*)-(+)-N-methylephedrine, (b) (*1R,2S*)-(-)-N-methylephedrine is shown in Figure 19.
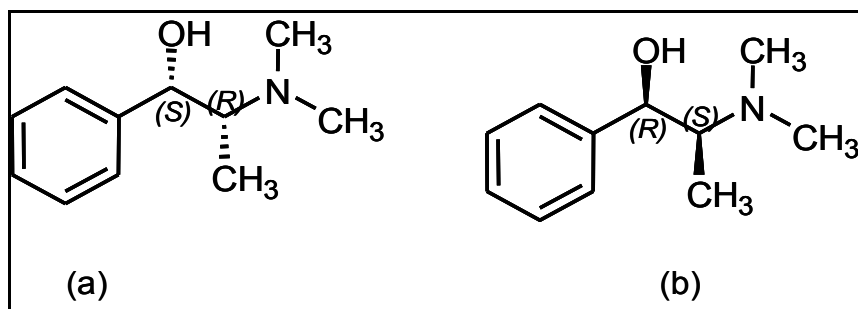
Figure 19: Chemical structures of: (a) (*1S, 2R*)-(+)-N-methylephedrine, (b) (*1R, 2S*)-(-)-N-methylephedrine.

Table 2 gives a summary of some properties and specifications of N-methylephedrine.

Table 2: Properties and specifications of N-methylephedrine [Sigma-Aldrich]

Name	(1S,2R)-(+)-N-methylephedrine	(1R, 2S)-(-)-N-methylephedrine
Molecular Formula	$C_{11}H_{17}NO$	$C_{11}H_{17}NO$
Molecular Weight	179.3 g/mol	179.3 g/mol
Melting point	87-90 °C	86-88 °C
Optical rotation	$[\alpha]_D^{20} = +29°\ (C = 5\, in\ CH_3OH)$	$[\alpha]_D^{21} = -29.2°\ (C = 5\, in\ CH_3OH)$

3.3 Materials

Chemical and reagents used in this thesis together with their purities and sources are complied in Table 3.

Table 3: Chemicals used with their purities.

Material	Purity %	Source
(*S*)-(+)-mandelic acid	≥99	Aldrich/Sigma Merck, Germany.
(*R*)-(-)-mandelic acid	≥99	Sigma-Aldrich
(*RS*)-mandelic acid	≥99	Sigma-Aldrich
(*1S,2R*)-(+)-N-methylephedrine	≥99	Sigma-Aldrich
(*1R,2S*)-(-)-N-methylephedrine	≥99	Sigma-Aldrich
(*S*)-2-butanol	98	BASF
(*S*)-2-pentanol	97-98	BASF
(*S*)-2-hexanol	98	BASF
(*S*)-1-phenylethanol	≥99	BASF
(*R*)-1-phenylethanol	≥99	BASF
(*R*)-2-chloro-1-phenylethanol	98.5	BASF
(*R*)-2-chloro-1-(3-chlorophenyl)ethanol	98	BASF
(*S*)-methyl lactate	97	PURAC
(*S*)-ethyl lactate	≥99	Sigma-Aldrich/Fluka
(*S*)-propyl lactate	97	PURAC
(*S*)-butyl lactate	97	PURAC
(*2R,3R*)-diethyl tartrate	≥99	Sigma-Aldrich/Fluka
Methanol-d_4	≥98	Deutero GmbH
(*S*)-propyl mandelate	≥98	Our lab
(*S*)-isopropyl mandelate	97	Our lab

Continuation of Table 3		
(*S*)-2-(methoxycarbonyl) pyrrolidinium bis(trifluoromethylsulfonyl) amide	99	Aachen RWTH (ITMC, Aachen, Germany.)
(*1R,2S*)-(-)-Ephedrinium bis (trifluoromethylsulfonyl) amide	99	Erlangen Universität
2-propanol	99	Sigma-Aldrich
methanol	99	Sigma-Aldrich

3.4 Chiral solvents

Optically active organic solvents, consisting of chiral molecules (chiral solvents), which rotate the plane of linearly polarized light, have become increasingly important. In principle, diastereomeric solvates might form when a mixture of enantiomers is dissolved in an optically active solvent.[4,5] Consequently, these solvates should possess slightly different physical and chemical properties. In principle, it is expected that a chiral solvent can create selective interactions to a chiral solute, which facilitates differentiation between the two single enantiomers. This discrimination can provide selective kinetic or solution thermodynamic effects which can be useful for the separation of enantiomers.[4] This idea was proposed in 1893 by Van't Hoff in a letter he wrote to Meyerhoffer expressing the possibility to find a difference in the solubility of enantiomers in an optically active solvent.[5]

In fact, optically active solvents have already found it use in stereospecific syntheses, as NMR shift reagents, HPLC analysis, in the evaluation of the optical purity of enantiomers, and in the gas chromatographic separation of enantiomers on chiral phases.

Chiral solvents used in this work are basically classified into "classical" chiral solvents, chiral ionic liquid and tailor-made chiral solvents. Additionally, liquid crystals are also considered to have similar effects as proposed for chiral solvents. Liquid crystals are known to form partially ordered structures. Small anisotropic solute molecules dissolved in liquid-crystalline solvents experience partial orientation. Thus rapid tumbling of the solute molecules about only two of the three axes is possible. This results in some averaging but still allows coupling between the magnetic dipoles of the nuclei as well as chemical shift anisotropies. Though liquid crystal might also have the ability to create discrimination between two enantiomers it has not been considered in this thesis work.

3.4.1 Characterization of various types of chiral solvents

3.4.1.1 "Classical" chiral solvents

"Classical" chiral solvent in this work refers to the normal chiral solvents which are listed in Table 4. The "classical" chiral solvents were characterized under several physical measurements such as boiling point, melting point, and viscosity. Moreover, the FTIR is used to characterized the various chiral solvent used. Figure 20 depicts the chemical structures for both (S)-alkyl lactate and (2R, 3R)-diethyl tartrate.
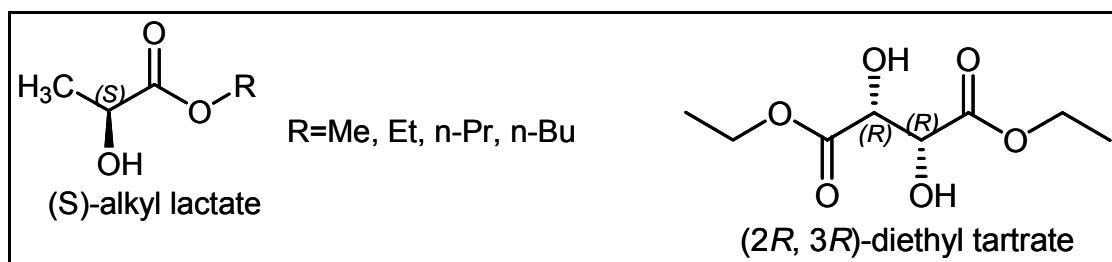
Figure 20: Chemical structures of the solvents ((*S*)-alkyl lactate and (*2R, 3R*)-diethyl tartrate).

The chemical structures for the other lactates are not given since they would have almost similar structures with differences originating from differences in chain length. Table 4 gives a summary of selected physical properties of all the "classical" chiral solvent used in this work.

Table 4: "Classical" chiral solvents and some physical properties.

Chiral solvents	Boiling point (°C)	Melting point (°C)	Viscosity mPa s
(*S*)-methyl lactate	144	-44	3.1 (25°C)
(*S*)-ethyl lactate	154	-25	3.6 (23°C)
(*S*)-propyl lactate	170	-14	3.3 (20°C)
(*S*)-butyl lactate	187	-	3.9 (25°C)
(*2R,3R*)-diethyl tartrate	280	18	354.4 (25°C)

Nuclear magnetic resonance (NMR), Fourier transform infra-red (FTIR) and Raman spectroscopies studies were carried out to investigate interactions which can be exploited in

thermodynamically based discriminations of the two enantiomers. The chiral solvents were characterized with respect to selected several physical properties such as boiling point, melting point, and viscosity.

3.4.1.2 Chiral ionic liquids

Ionic liquids are described as organic salts with melting point below 100 °C. They possess characteristics which have recently given much attention in the scientific community. As ionic liquids have attracted a lot of attention as a new class of solvents, they have successfully been used as solvent for enantioselective asymmetric synthesis.[103] Moreover, Reichert et al.[104] reviewed and discussed the possibility of using complex solvents like ionic liquids for crystallization. However, this application is still in its infancy. Chiral ionic liquid were studied in this work to exploit their potential in enantioselective crystallization. Chemical reaction scheme of synthesis of (*S*)-2-(methoxycarbonyl) pyrrolidinium bis (trifluoromethylsulfonyl) amide is shown in Figure 21.
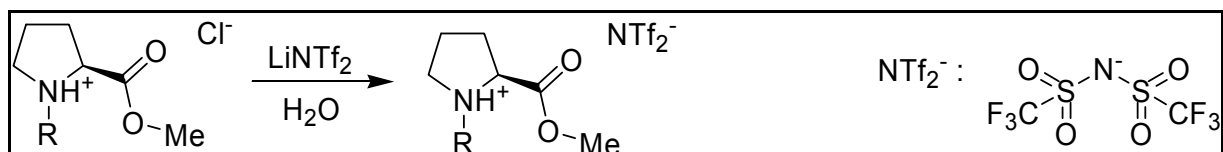
Figure 21: Chemical reaction scheme for synthesis of (S)-2-(methoxycarbonyl) pyrrolidinium bis(trifluoromethylsulfonyl) amide.

The chemical structure of the other chiral ionic liquid, (*1R, 2S*)-(-)-Dimethylephedrinium bis (trifluoromethylsulfonyl) amide applied in this work is shown in Figure 22.
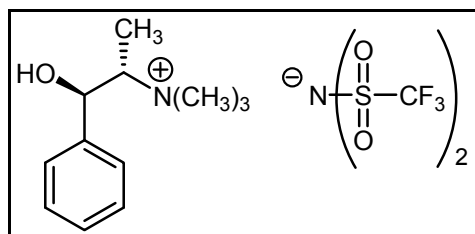
Figure 22: Chemical structure for (1R, 2S)-(-)-dimethylephedrinium bis (trifluoromethylsulfonyl) amide.

Table 5 gives a summary of selected physical properties of the two chiral ionic liquids used in this work.

Table .5: Chiral ionic liquids and their physical properties.

Chiral solvents	Boiling point (°C)	Melting point (°C)	Viscosity mPa s
(*S*)-2-(methoxycarbonyl)pyrrolidinium bis(trifluoromethylsulfonyl) amide	305	-	324.5 (25.05°C)
(*1R,2S*)-(-)-Dimethylephedrinium bis(trifluoromethylsulfonyl) amide	-	-	481.6 (23.10°C)

3.4.1.3 Tailor-made chiral solvents

The synthesis of the mandelic acid esters (Mandelates) was adopted from Basavaiah et al.[105] and was slightly modified. Figure 23 illustrates as an example the reaction scheme for the synthesis of (S)-isopropyl mandelate.
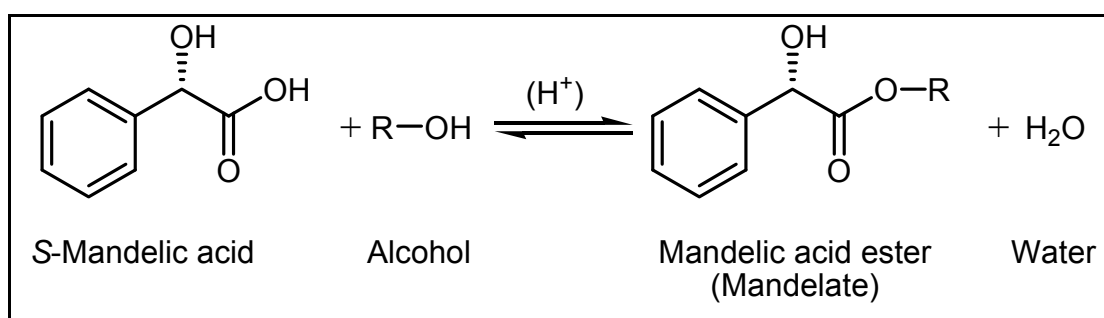
Figure 23: Typical reaction scheme of Mandelic acid ester (Mandelate) synthesis.

The procedure applied for the synthesis is as follows:

50 g (*S*)-mandelic acid was dissolved in a 25-fold excess of the corresponding alcohol, 25 drops of concentrated sulphuric acid were added and the mixture refluxed for 4 hours. Afterwards the remaining isopropanol was removed under reduced pressure. The resulting crude ester was taken into 275 mL diethyl ether, washed with aqueous K_2CO_3, followed by saturated aqueous NaCl and finally dried over Na_2SO_4. After removal of the diethyl ether the crude ester was distilled under high vacuum for purification. Yield: 60-65%. The purity was determined via DSC and NMR.

(*S*)-Mandelic acid n-propyl ester ((*S*)-propyl mandelate)
^{1}H NMR (400 Mhz, CDCl$_3$): δ 0.8 (t, 3H), 1.59 (p, 2H), 4.11 (m, 2H), 5.17 (s, 1H), 7.25-7.51 (m, 5H)

(*S*)-Mandelic acid isopropyl ester ((*S*)-isopropyl mandelate)

^{1}H NMR (400 Mhz, CDCl$_3$): δ 1.13 (d, 3H), 1.30 (d, 3H), 5.06-5.12 (p, 1H), 5.14 (s. 1H), 7.33-7.44 (m, 5H)

In the case of the other forms of the mandelate they were also synthesized based on the same reaction scheme except that the alcohol used change to suit the particular mandelate wanted, to synthesize (S)-propyl mandelate the alcohol should be propanol. Compilations of selected physical properties of the two synthesized tailor-made chiral solvents employed in the thesis are listed in Table 6.

Table 6: "Tailor-made chiral solvents" and their physical properties data

Chiral solvents	Boiling point (°C)	Melting point (°C)	Viscosity mPa s
(*S*)-propyl mandelate	214.6	20.5	99.2 (24°C)
(*S*)-isopropyl mandelate	223.6	43.0	solid at R.T

The next section will describe the screening of the "classical" chiral solvents with the aid of NMR spectroscopy. In order to study systematically the feasibility of chiral resolution with the help of chiral solvents, first investigations have been devoted to screen a variety of "classical" chiral solvents eventually suitable for chiral discrimination. Also, mandelic acid was selected for the screening of appropriate "classical" chiral solvent for chiral recognition because it is a compound forming system which is normally difficult to be resolved.

3.5 Nuclear magnetic resonance spectroscopy-screening of "classical" chiral solvents

Nuclear magnetic resonance (NMR) is a technique employed to determine the structure of organic and non organic compounds. The nuclei of all elements possess a charge. When the spins of the protons and neutrons comprising these nuclei are not paired, the overall spin of the charged nucleus generates a magnetic dipole along the spin axis. NMR is based on the atomic nuclei having a nuclear spin (I) which makes these nuclei behave like small magnets, which when no magnetic field is present are aligned randomly. When a magnetic field (Bo) is

used, these nuclear magnets orientate themselves in 2I+1 ways. 1H and 13C have both a spin of (-½) and therefore can orientate themselves in two ways, a low energy (N_1) orientation aligned with the applied magnetic field (spin +½) and a high energy (N_2) orientation opposed to the applied field (spin -½) (Figure 24).
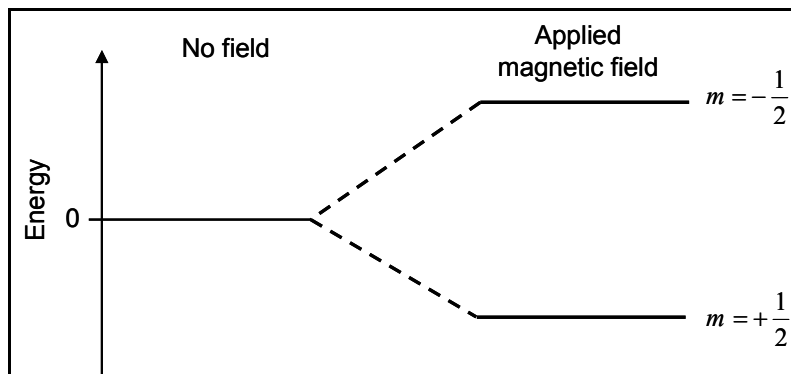
Figure 24: Energy level diagram of a one spin ½ nucleus in the presence and absence of Bo.

The number of nuclei in the low energy state and the number in the high energy state will differ by an amount given by the Boltzmann distribution:[106]

$$\frac{N_2}{N_1} = \exp\left(-\Delta E / kT\right)$$

Equation 20

3.5.1 Principle of NMR spectrometer and spectra acquisition

Samples for NMR studies are made from deuterated solvents, providing in deuterium and hydrogen in the same sample. Hydrogen has one proton in its nucleus while deuterium has a proton and a neutron in its nucleus. This is necessary to "lock" the NMR on a specific frequency so that the spectrum will not drift around during acquisition. The sample is then place into the spectrometer, where an air jet spins the sample tube to give a more uniform sample to scan. In order to acquire spectra, first a radio frequency generator "pulses" the sample with a short burst of radio waves. These waves are absorbed and transmitted through the sample to the receiver which detects the signal from the sample. This information is then transmitted to the computer linked to the spectrometer, where it is translated and analyzed. Figure 25 shows a schematic of a NMR spectrometer.
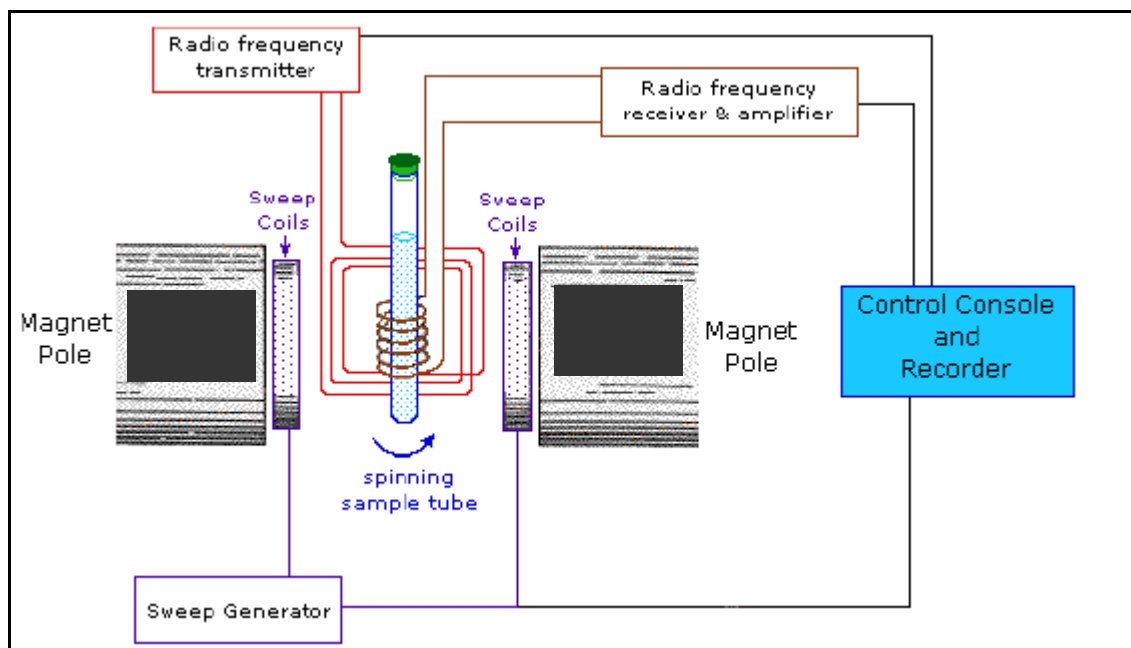
Figure 25: Schematic of continuous wave NMR spectrometer.[87,106]

3.5.2 Apparatus and experimental procedure

In order to study systematically the feasibility of chiral resolution with the help of chiral solvents, we first screened a variety of chiral solvents which would be suitable for chiral discrimination. (S)- and (R)-mandelic acid were used for the screening experiments.

^{1}H NMR spectra were recorded on a Bruker AVANCE 600 spectrometer at 600.13 MHz. The measurements were done at the Institute of Chemistry, Otto-von-Guericke Universität Magdeburg, Germany. The AVANCE 600 is fitted with a 5mm CPTXI-1H-13C/15N/2H probe head with z-gradients. The samples were measured in Methanol-d_4 deuterated solvent as internal lock. Spectra were recorded at T = 293 K with a pulse width of 7.8 µs for 90° pulse. The ^{1}H NMR chemical shifts (δ) were reported in ppm downfield from TMS (internal).[106,107]

The following samples were prepared in NMR tubes:

Test samples: (a) (S)-mandelic acid (10mM) + (S)-ethyl lactate (50mM) + CD_3OD (600µl)

(b) (R)-mandelic acid (10mM) + (S)-ethyl lactate (50mM) + CD_3OD (600µl)

Reference sample: (R)-mandelic acid (10mM) + CD_3OD (600µl).

The same procedure was repeated for the other chiral solvents studied.

3.5.3 Chemical shift and spectra interpretation

The electrons which surround the spinning nuclei are also charged and spin and hence the spinning charge makes a magnetic field. The magnetic field at the nucleus is not equal to the

applied magnetic field; electrons around the nucleus shield it from the applied field. The distinction between the applied magnetic field and the field at the nucleus is termed the nuclear shielding. The *s*-electrons in a molecule possess spherical symmetry and travel in the applied field, creating a magnetic field which opposes the applied field. This means that the applied field strength must be increased for the nucleus to absorb at its transition frequency. This upfield shift is also termed diamagnetic shift. Electrons in *p*-orbitals do not have spherical symmetry. They produce comparatively large magnetic fields at the nucleus, giving a low field shift (increasing chemical shift, dH values). This "deshielding" is termed paramagnetic shift.

Chemical shift (δ) is defined as nuclear shielding/applied magnetic field and refers to the position of a peak on the spectrum. Chemical shift is a function of the nucleus and its environment. It is measured relative to a reference compound. For ^{1}H NMR, the reference is usually tetramethylsilane, $Si(CH_3)_4$ (TMS) because it is the most shielded molecule and all its protons are equivalent. Consequently, gives one peak which can be used to set the zero mark on the spectrum. Moreover, single peaks, double peaks, and even larger groups of peaks are seen on the sample spectrum; these groups of peaks are each due to one type of nucleus. The reason there are a group of peaks instead of just one is that hydrogen on one carbon are tied to, or influenced by, the magnetic fields of H's on adjacent nuclei. This coupling "splits" the signal into the multiple or numerous peaks. This splitting follows what is know as the "n+1 rule", which states that the number of peaks observed for each and every type of hydrogen is equal to the number of H's on adjacent nuclei (n) plus one in consecutive terms.

In this work chemical shift was used as a means to discriminate the chiral molecules. A methodology was designed to achieve this goal. The screening experiment was devised based on discrimination definition of the alpha hydrogen of the reference sample and that of the test sample in the chiral solvent, and which is expressed as the difference in alpha hydrogen chemical shift ($\Delta\delta$)[107,108] in Equation 21 below. The criteria set for the ^{1}H NMR screening measurement was $\Delta\delta > 0.02$,[107] thus when a chiral solvent meets this requirement then there might be some chiral recognition.

$$\Delta\delta = \delta_{reference} - \delta_{sample}$$

Equation 21

In the screening process twelve chiral solvents were used. The screening experiments were carried out to be able to identify chiral solvents which eventually have the potential to create chiral recognition.[108,109] Figures 26 and 27 show exemplarily the ^{1}H NMR spectra for mandelic acid in (S)-ethyl lactate and (2R, 3R)-diethyl tartrate, respectively. It can be seen in

both Figures that there are no differences in the chemical shifts between the alpha hydrogen (5.134 ppm) of the reference and that of the test samples.
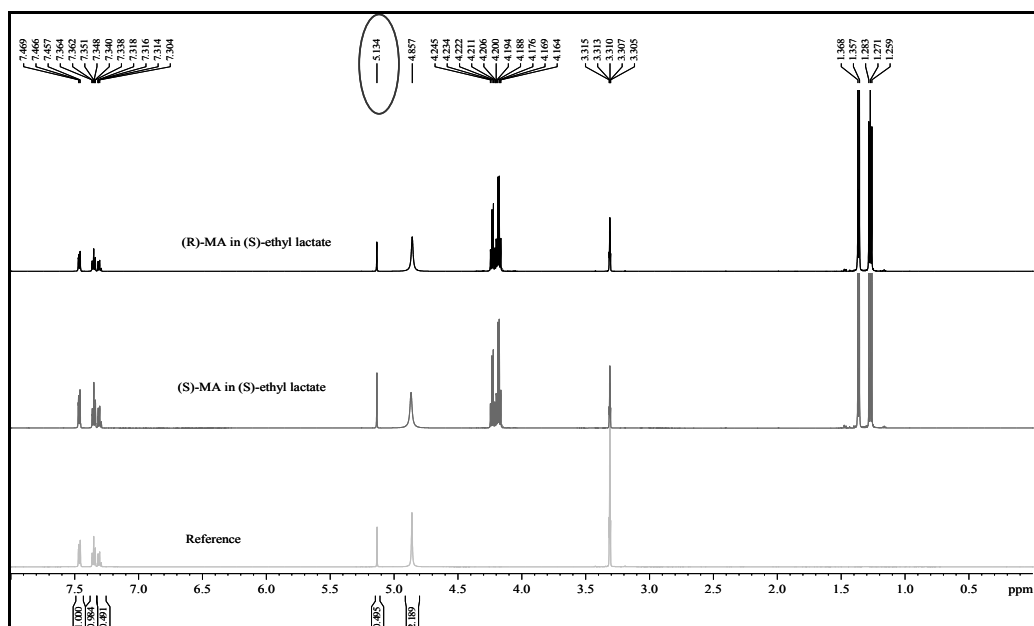
Figure 26: ^{1}H NMR spectra for mandelic acid in (S)-ethyl lactate
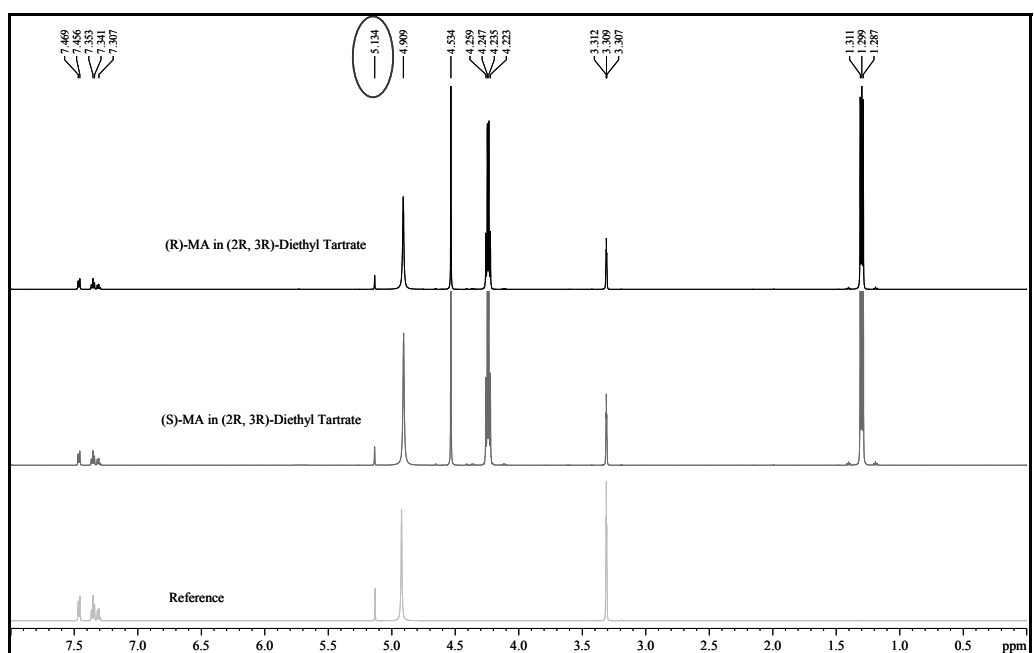
Figure 27: ^{1}H NMR spectra for mandelic acid in (2R, 3R)-diethyl tartrate.

Table 7 summarizes the experimental results of mandelic acid in the various screened solvents and their respective chemical shifts in ppm. Unfortunately, none of the twelve chiral solvents fulfilled the criterion set ($\Delta\delta > 0.02$). This reveals that the chiral solvents investigated had no significant interactions on the chiral system studied in terms of solution thermodynamics.

Table 7: Screened chiral solvents and the resulting chemical shifts.

Chiral solvents	(*S*)-MA alpha hydrogen peak (ppm)	(*R*)-MA alpha hydrogen peak (ppm)	(*S*)-MA Δδ-values (ppm)	(*R*)-MA Δδ-values (ppm)	Reference sample alpha hydrogen peak (ppm)
(*S*)-methyl lactate (*)	5.13	5.13	0.00	0.00	5.13
(*S*)-ethyl lactate (*)	5.13	5.13	0.00	0.00	5.13
(*S*)-propyl lactate (*)	5.13	5.13	0.00	0.00	5.13
(*S*)-butyl lactate (*)	5.13	5.13	0.00	0.00	5.13
(*S*)-2-butanol	5.05	5.05	0.00	0.00	5.05
(*S*)-2-pentanol	5.07	5.06	0.00	0.01	5.07
(*S*)-2-hexanol	5.13	5.13	0.00	0.00	5.13
(*S*)-1-phenylethanol	5.14	5.14	0.01	0.01	5.13
(*R*)-1-phenylethanol	5.14	5.14	0.01	0.01	5.13
(*R*)-2-chloro-1-(3-chlorophenyl)ethanol	5.14	5.14	0.01	0.01	5.13
(*2R,3R*)-diethyl tartrate (*)	5.13	5.13	0.00	0.00	5.13
(*R*)-2-chloro-1-phenylethanol	5.14	5.14	0.01	0.01	5.13

MA, Mandelic acid.   (*) selected for further studies

Since the results obtained from screening the various chiral solvents were similar, selection of the chiral solvents for further work was solely based on the availability and the price. The following five "classical" chiral solvents were selected: (*S*)-methyl lactate, (*S*)-ethyl lactate, (*S*)-propyl lactate, (*S*)-butyl lactate and (*2R, 3R*)-diethyl tartrate.

3.6 Experimental procedures

This section would present all the experiments that were performed in this thesis work. Basically, three types of experimental measurements were conducted, namely solubility determination (solution thermodynamic measurement), nucleation points determination, (i.e. MSZW and induction time determination) and enantioselective crystallization experiments.

3.6.1 Solubility measurements

In general solubility measurements[110] serve as a fundamental prerequisite which is required before designing enantioselective crystallization processes. So, in this work reliable solubility data have been generated from the solubility experiments. Solubility measurements were carried out in different systems;

1. Mandelic acid and N-methylephedrine in (*S*)-methyl lactate, (*S*)-ethyl lactate, (*S*)-propyl lactate and (*S*)-butyl lactate).

2. Mandelic acid and N-methylephedrine in (*2R,3R*)-diethyl tartrate.

3. N-methylephedrine in the two chiral ionic liquids ((*S*)-2-(methoxycarbonyl) pyrrolidinium bis (trifluoromethylsulfonyl) amide and (*1R,2S*)-(-)-Dimethylephedrinium bis (trifluoromethylsulfonyl) amide).

4. Mandelic acid and in the tailor-made chiral solvent ((*S*)-ethyl mandelate, (*S*)-propyl mandelate and (*S*)-isopropanol mandalate).

The next section will discuss how the solubilities were measured in a first step with the successive solute addition method.

Successive solute addition method

Initially, the solubility experiments were done by the successive solute addition method at isothermal conditions (temperature of 25 °C). In this technique small amounts of solute are added to the solvent in some time intervals until some non-dissolved crystals remain in the solution for a long time until equilibrium is attained in the solution. The samples (solute in solvent) were prepared in a small glass vessel with a defined composition and concentration of solute or mixtures of solutes in the solvent. A magnetic stirrer was used inside at 500 rpm for effective mixing. This glass vessel was immersed in a double or triple walled thermostatted apparatus. Defined quantities of solutes were added to the system until equilibrium concentration was attained (undissolved solute). The sample was maintained at the same conditions for 24 hours for the equilibrium confirmation and then the sample was filtered to get the liquid and solid phases for further analysis. A defined amount of liquid phase was taken in a 25 mL flat bottom conical flask and was diluted with isopropanol. The collected liquid phase sample was analyzed with HPLC. In this way solubility experiments were conducted for; (*S*)-, (*R*)- and *RS*-MA and (*2R,3R*)-diethyl tartrate. The outline is shown in the Table 8.

Table 8: Pre-experiments for initial solubility determination of solute in solvent at 25°C by using successive solute addition method.

Experiment number	Mass of (*S*)-solute (g)	Total mass of Solute (g)	Mass of Solvent (g)	Mass of Solution (g)	Initial Concentration (wt %)	Solubility (wt %)
1	0.5000 0.2501 0.7500	1.5001	5.0539	6.554	22.88	14.42
	Mass of (*R*)-solute (g)	Total mass of Solute (g)	Mass of Solvent (g)	Mass of Solution (g)	Initial Concentration (wt %)	Solubility (wt %)
2	0.5002 0.2501 0.7502	1.5005	5.0098	6.5103	23.04	14.62
	Mass of *RS*-solute (g)	Total mass of Solute (g)	Mass of Solvent (g)	Mass of Solution (g)	Initial Concentration (wt %)	Solubility (wt%)
3	0.5001 0.2503 1.0002	1.7506	5.0893	6.8399	25.59	18.36

Classical isothermal method

In order to evaluate the minimum time required to establish thermodynamic equilibrium. At first a few dissolution kinetics experiments were performed before the solubility measurements were carried out for all the systems investigated in this work for the racemate and the enantiomers, Liquid phase samples were taken at specific time intervals from the suspension, and the concentrations were analyzed by HPLC. In all the systems equilibrium was reached after less than 24 hrs. Accordingly, the experimental time was set to be at least 24 hrs.

After approximated solubility data were obtained from the successive solute addition method, classical isothermal solubility measurements were employed for refined solubility measurements. In this method the temperature, pressure and composition (when equilibrium is reached) of the system are kept constant. If the solubility of the substance is approximately available, the exact value can be obtained by taking an excess of solute in the solution (Isothermal excess method). The sample present in the solution is dissolved completely at a higher temperature and allowed to recrystallize at the desired solubility temperature. The

process is continued until equilibrium is attained. Solubility measurements for enantiomeric compositions of mandelic acid and N-methylephedrine were performed in various chiral solvents at temperatures ranges depending on the system.

1. Mandelic acid in (*S*)-methyl lactate, (*S*)-ethyl lactate, (*S*)-propyl lactate and (*S*)-butyl lactate, temperature range from (0 to 35) °C.

2. N-methylephedrine in (*S*)-methyl lactate, (*S*)-ethyl lactate, (*S*)-propyl lactate and (*S*)-butyl lactate, temperatures range from (0 to 25) °C.

3. Mandelic acid in (*2R,3R*)-diethyl tartrate, temperature range from (25 to 60) °C

4. N-methylephedrine in (2R, 3R)-diethyl tartrate, temperature range from (25 to 40) °C

5. N-methylephedrine in (*S*)-2-(methoxycarbonyl) pyrrolidinium bis (trifluoromethylsulfonyl) amide and (*1R,2S*)-(-)-Dimethylephedrinium bis (trifluoromethylsulfonyl) amide, temperature range from (5 to 35) °C.

6. Mandelic acid in (*S*)-ethyl mandelate, (*S*)-propyl mandelate and (*S*)-isopropyl mandelate, temperature at 50 °C.

The method involved preparing a solvent and solute mixture of known composition with solid in excess in a 10 mL glass vessel, which was put into a thermostatted apparatus (RC6 CP Lauda, Germany), and magnetically stirred at a constant temperature (within ± 0.01 K) until equilibrium was attained. Subsequently, the liquid and solid phases were separated and analyzed. For analysis the saturated solution was filtered with a glass filter (pore size, 10 μm), and samples of (1-3) mL were withdrawn from the filtrate for double analysis. The concentrations and the enantiomeric excess were determined by means of chiral HPLC after dilution with 2-propanol. In sections 3.6.4, 3.6.5 and 3.6.9 the analytical devices and methods used to analyze the liquid and solid phases will be discussed in detailed. Figure 28 depicts a classical solubility measurement apparatus.
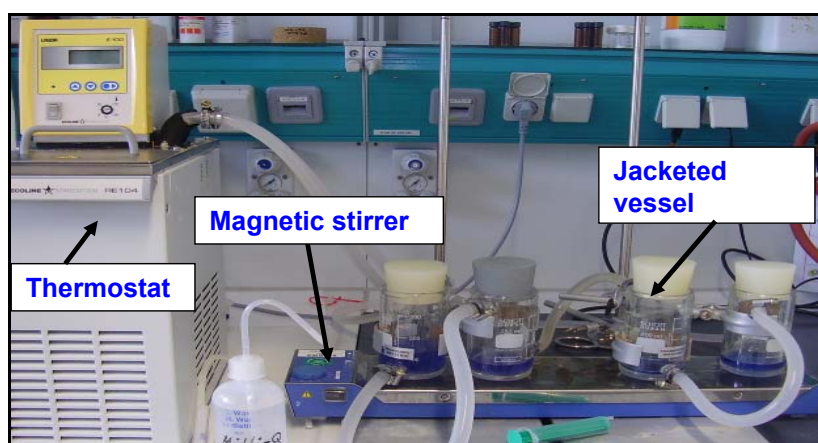
Figure 28: Solubility measurement apparatus.

An evaluation of the reproducibility solubility measurements was restricted to mandelic acid and N-methylephedrine systems in all the lactates used in this work and (*2R,3R*)-diethyl tartrate. In the other solvents, for instance chiral ionic liquids and the tailor-made chiral solvents, it is so expensive that two time measurements were done and the mean solubility values were used.

The reproducibility of the solubility measurements was studied for several repeated experiments under the same conditions. The measurements were conducted with racemic mandelic acid, (*S*)-mandelic acid and (*R*)-mandelic acid in all the lactates and (*2R,3R*)-diethyl tartrate at the lowest and the highest temperatures considered by executing between 3 and 4 experiments under the same conditions. Also, reproducibility of the solubility measurements was studied for N-methylephedrine in all the lactates and (*2R,3R*)-diethyl tartrate at the lowest and the highest temperatures considered by executing between 3 and 6 experiments under the same conditions. The standard deviations of the solubilities (*SD*) were calculated by Equation 22.

$$SD = \sqrt{\frac{1}{n-1} \sum_{k=1}^{n} \left(w_k - \overline{w} \right)^2}$$

Equation 22

with n being the number of experiments and w_k and $\overline{w}$ being the mass fraction solubility and the mean solubility, respectively. Hereby holds:

$$w_i = \frac{m_i}{\sum_{i=1}^{z} m_i}$$

Equation 23

The summation covered always the two enantiomers for both mandelic acid and N-methylephedrine and the solvent used. In addition, mass fraction solubilities w_i according to Equation 23 were used in this work, since this simplifies process design based on graphical representations of e.g. a ternary solubility phase diagrams. Herein, m_i represents the mass of the constituent i.

In order to assess the solid liquid equilibria comprehensively, we determined the ternary solubility phase diagram. Thorough solubility measurements were carried out for different temperatures for the single enantiomers, the eutectic and the racemic compositions. Moreover, in order to check for asymmetry in the phase diagram various compositions were measured along particular isotherms, ranging from the racemic compositions to the single enantiomers.

Polythermal method

To apply this method the Crystal16^{TM} equipment from Avantium Research and Technology was employed for the solubility measurements of certain systems where small amount was available for the experiments. Figure 29 illustrates the Crystal16 ^{TM}, it shows the multiple-reactor system which can hold 16 (4 x 4) standard HPLC glass vials (11.5 mm diameter, flat bottomed, 1.8 mL volume). A unit consists of four independently heated aluminum reactor blocks encased in a robust bench top setup. The crystal16^{TM} setup is connected to a thermostat.

Figure 29: Crystal16^{TM} equipment (16 multiple-reactor system).[111]

These blocks are electrically heated and cooled by a combination of Peltier elements and a cryostat. In order to prevent condensation of water on the reactor blocks and electronics during runs at temperatures below 10 °C, the Crystal16™ system provides an inlet for a dry purge gas (typically nitrogen).

The polythermal method was applied with charging into the reactors known concentrations of the substance. Then an increasing temperature programme was planned for the experiments. The setup was heated until the charged known concentration substance is completely dissolved. Subsequently different concentrations were also subjected to the same temperature program and it was also identified at which temperatures the solid dissolved completely. Afterward, the evaluated temperatures for corresponding concentrations were plotted. A linear correlation is then extracted from the linear plot and could be used to determine subsequent solubilities.

3.6.2 Nucleation points determination

Basically, two nucleation points determination techniques were applied in this work: the metastable zone width measurements and induction time measurements.

In the next section description of both measurements techniques is given.

3.6.2.1 Metastable zone width measurements (MSZW)

Estimates for the widths of metastable zones with regard to primary nucleation were determined for the various systems as follows;

1. Mandelic acid in (*S*)-methyl lactate, (*S*)-ethyl lactate, (*S*)-propyl lactate and (*S*)-butyl lactate.

2. N-methylephedrine in (*S*)-methyl lactate, (*S*)-ethyl lactate, (*S*)-propyl lactate and (*S*)-butyl lactate.

3. Mandelic acid in (*2R,3R*)-diethyl tartrate.

4. Mandelic acid in (*S*)-propyl mandelate.

The experiments and the analysis were conducted using the polythermal method as described by Nyvlt et al.[112] Saturated solutions of ~ 20g were used. The solutions were subjected to heating and cooling programs based on the saturation temperature (T_{sat}) of the system. The initial concentrations were adjusted based on the solubility data. Desired solutions were prepared and placed into a batch crystallizer of 60 mL volume. Nucleation and dissolution were observed by means of an inline-turbidity sensor (QR-System; BASF AG, Ludwigshafen, Germany) and a Pt-100 temperature sensor. The metastable zone width for primary nucleation is expressed as the maximum possible subcooling:

$$\Delta T_{max} = T_{sat} - T_{nucleation}$$

<div align="right">Equation 24</div>

where T_{sat} is the saturation temperature and $T_{nucleation}$ the nucleation temperature. The latter was measured at different cooling rates. Finally the values were extrapolated to a cooling rate of zero to obtain $T_{nucleation}$ for a given solution composition. The obtained ΔT_{max} data are valid for the experimental set up used and depend on, e.g. reactor size and geometry, stirrer type and stirring rate. The schematic representation of the experiment is shown in Figure 30.
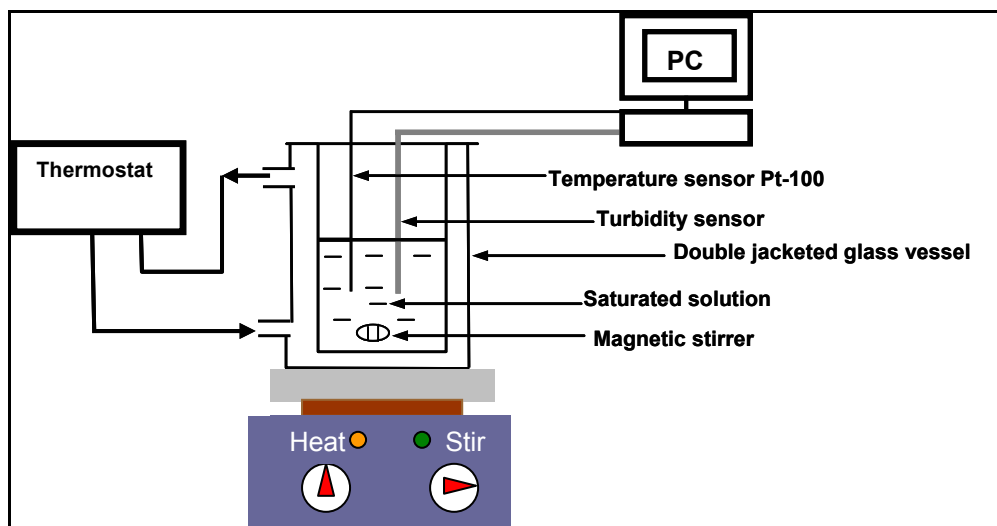
Figure 30: Schematic setup of metastable zone width experimental setup.

3.6.2.2 Induction time measurements

In this method a saturated solution is prepared and the temperature of the solution is quickly reduced to a chosen value and maintained. At this point the time taken for first nuclei to appear is noted. In this work, the induction time measurements were solely applied to situations where it became impossible to carry out the MSZW experiments. The MSZW experiments were not possible in a condition where there is either not sufficient temperature range or less solvent available (due to the fact that it is very expensive).

So, in the case of the N-methylephedrine in (*S*)-2-(methoxycarbonyl) pyrrolidinium bis (trifluoromethylsulfonyl) amide system the induction time method was applied because the solvent is extremely expensive. The method was applied to N-methylephedrine in (*2R,3R*)-Diethyl tartrate system since the solutions were very viscous in nature.

Primary nucleation (induction time) experiments were performed for racemic-NME, (+)-NME and (-)-NME in [(*S*)-2-Pro-Me] [NTF_2] / methanol 70/30 v/v at 35 °C using an isothermal method. The experiments were conducted in a magnetically stirred double jacketed glass vessel of 50 mL. Saturated solutions of about 10 g (35 °C) were prepared for all the samples. The various saturated solutions were crash-cooled to 1.0 °C, and the induction time (t_{ind}) at this temperature for appearance of first crystals was determined by visual observation. The solubility measurement apparatus which is already illustrated in Figure 28 was also employed for this measurement. The same experimental procedure was used for N-methylephedrine in (2R, 3R)-diethyl tartrate.

3.6.3 Enantioselective crystallization experiments

Three different types of enantioselective crystallization experiments were applied in this work. These three experiments are preferential nucleation, preferential crystallization and selective crystallization experiments. They were chosen based on the acquired fundamental solubility and MSZW results. The next section of this thesis will elaborate on how these three enantioselective crystallization experiments were conducted.

3.6.3.1 Preferential nucleation experiments

(a) Preferential nucleation experiments have been performed for racemic-MA in (2R, 3R)-diethyl tartrate using a 350 mL stirred batch crystallizer (stirring speed: 400 rpm). Figure 31 depicts the experimental setup used for preferential nucleation.
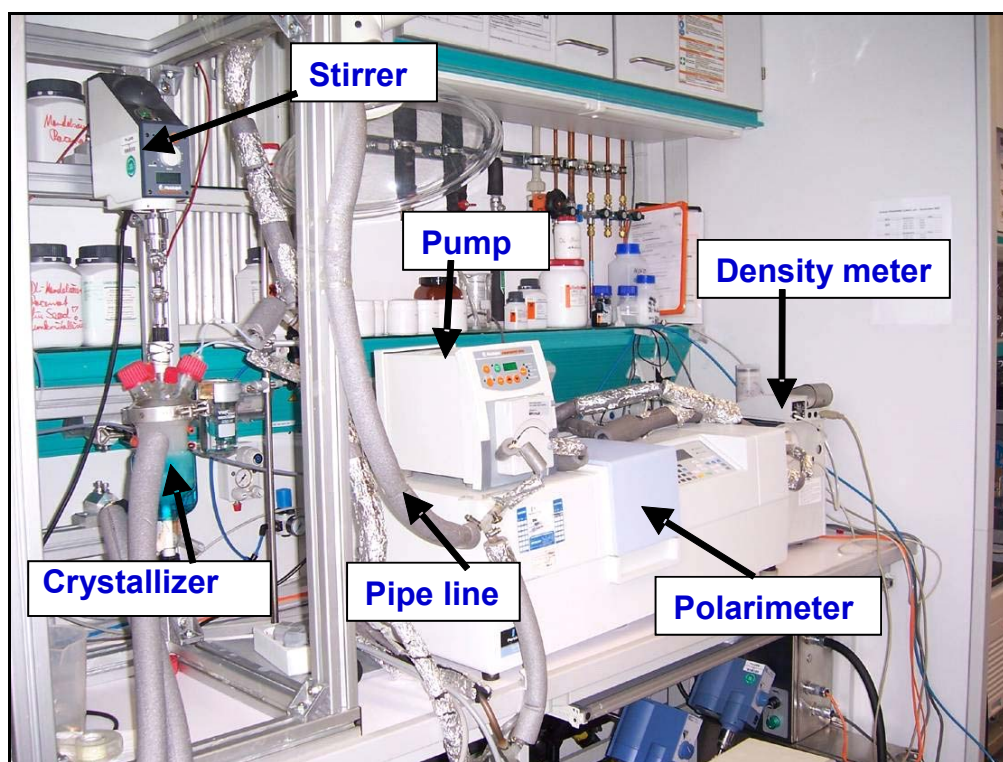
Figure 31: Experimental setup (online measurements) for preferential nucleation.

For an experiment, 250 g initial solutions was prepared according to solubility data at T_{sat} = 55 °C, i.e. the concentration was w_{sat} = 31.66 wt %. The prepared initial solutions were heated to 60 °C to ensure that even the smallest crystals were fully dissolved. Then, the temperature was decreased to a crystallization temperature of T_c = 25 °C with a cooling rate of 0.5 K/min. The liquid phase concentrations and composition were measured continuously using online

polarimetry and densitometry. For this, crystal free solution was conveyed from the crystallizer and thermostatted during the transfer to the online polarimeter (PerkinElmer, Model 341, Beaconsfield/UK; optical path length of the flow cell: 100 mm; wavelength: 589 nm; temperature at the cell 62.50 °C) and the density measurement device (Density Meter DE40, Mettler Toledo, Giessen/Germany; measurement temperature 60 °C). After the measurements, the liquid phase was pumped back into the crystallizer through an insulated line (flow rate: 10.8 mL/min). For comparison, samples were collected during the experiment for offline HPLC analysis. The HPLC analysis will be described in the analytical techniques section.

Further experiments were conducted using the same method described above with water as solvent at a temperature T_{sat} = 33 °C. These experiments were aimed at comparing the solvent influence and finally evaluating the effect of the chiral solvent on preferential nucleation.

(b) Preferential nucleation experiments have been performed also for racemic mixture of N-methylephedrine in (2R, 3R)-diethyl tartrate. 50 g initial solutions were prepared according to solubility data at T_{sat} = 35 °C, i.e. concentration was w_{sat} = 49.20 wt %. The prepared initial solutions were heated to 38 °C to ensure that even the smallest crystals were fully dissolved. Then, the temperature was decreased to a crystallization temperature of T_c = 25 °C with a cooling rate of 0.16 K/min. Liquid phase samples were collected for offline HPLC analysis. An experimental offline setup for both preferential nucleation/crystallization is illustrated in Figure 32.
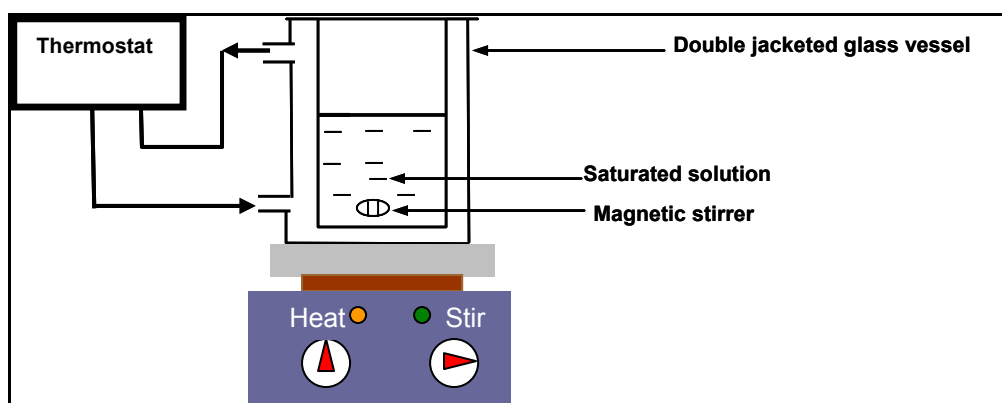
Figure 32: Experimental setup (offline measurements) for preferential nucleation/crystallization.

3.6.3.2 Preferential crystallization experiments

An initial solution of 50 mL racemic-MA in (*S*)-ethyl lactate was prepared according to the solubility data at T_{sat} = 15 °C, i.e. concentration was w_{sat} = 25.10 wt %. This solution was

heated up and kept at 25 °C to ensure that all solid material was dissolved. Afterward, the sample was cooled down with a cooling rate of 0.3 K/min to the crystallization temperature (T_c = -5 °C). At this temperature, 21 mg of (*S*)-MA seed crystals (purity > 99%) were added. Immediately, as crystallization started liquid samples were collected at definite intervals and analyzed by HPLC. The HPLC analysis details will be presented in the analytical section. The same experimental offline setup for both preferential nucleation/crystallization shown in Figure 32 was also applied here.

3.6.3.3 Preliminary preferential crystallization experiments

Firstly, a saturated solution of racemic-MA in (*S*)-propyl mandelate was prepared according to the classical solubility measurement already described in the above section 3.6.1 at T_{sat} = 50 °C. Saturated solution of 40 mL was obtained from the solubility experiment. This solution was heated up and kept at 52 °C to ensure that all solid material was dissolved. Then, the sample was cooled down with a cooling rate of 0.2 K/min to the crystallization temperature (T_c = 43 °C). At the T_c, a defined amount of seed crystals 86 mg of (*S*)-MA seed crystals (purity > 99%) were added. After the supersaturated solution was seeded, it took 4 hrs before crystallization started. Later on the crystallization product was separated (filter pore size, 10 μm) and washed with 20 mL of cooled methanol to remove the adhering mother liquor. X-ray powder diffraction was used to identify the solid phase present, and HPLC was applied to determine the product purity. The HPLC analysis details will be presented in the analytical section. The same experimental setup for solubility measurements shown in Figure 28 was also applied here.

In the following section all the various analytical techniques employed in this thesis work are elaborated in detailed.

3.6.4 Chiral HPLC analysis

High Pressure Liquid Chromatography (HPLC) is a very good analytical technique for the separation of components of a mixture which is diluted with a solvent or mixture of solvents (analyte) by using a variety of chemical interactions with the Chromatographic column. When a small amount of analyte (mobile phase) is forced through a column packed with micro spherical particles (stationary phase) with certain surface chemistry it is retarded by specific chemical interactions with the stationary phase. The time taken by the analyte to travel in the column is called retention time, and mobile phase plus the analyte comes out as elute. Better separation in HPLC analysis is achieved by increasing the pressure which subsequently

reduces the retention time. In the case of chiral compounds separations by the HPLC requires special column such as Chiralcel OD-H, Eurocel OD and chirobiotic T. In this thesis both Chiralcel OD-H and Eurocel OD were used. The fundamental schematic representation of separation in chromatographic column is shown in Figure 33.
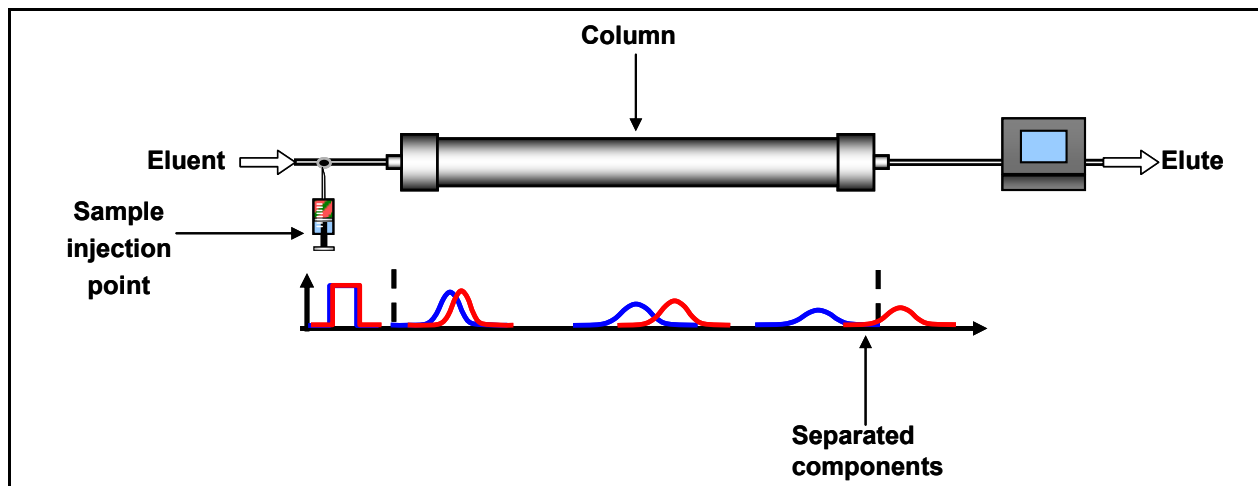
Figure 33: Schematic setup of separation in chromatographic column.

3.6.4.1 Apparatus and analytical method

Liquid phase analysis

The liquid samples collected from the solubility experiments were diluted with 2-propanol. The concentration of the solution and the enantiomeric excess were determined with HPLC:

An Agilent HP 1100 unit with a Chiralcel OD-H column (Astec, 250x4.6mm/5μm) for mandelic acid analyses and a Eurocel OD column (Knauer, 250x4.6mm/5μm) for N-methylephedrine analyses was used. The column temperature was 25 °C and the flow rate 1.0mL/min. A UV diode array detector was used for peak detection at a wavelength of 254nm. The eluent compositions were as follows:

(a).Mandelic acid in (*S*)-ethyl lactate: 84% n-hexane, 16% 2-propanol and 0.1% trifluoroacetic acid.

(b).Mandelic acid in (*2R,3R*)-diethyl tartrate: 90% n-hexane, 10% 2-propanol and 0.1% trifluoroacetic acid.

(c).N-methylephedrine in (*S*)-ethyl lactate and (*2R,3R*)-diethyl tartrate: 85% n-hexane, 15% 2-propanol and 0.1% diethylamine.

(d).N-methylephedrine in (*S*)-2-(methoxycarbonyl) pyrrolidinium bis (trifluoromethylsulfonyl) amide and (*1R,2S*)-(-)-Dimethylephedrinium: 85% n-hexane, 15% 2-propanol and 0.1% diethylamine.

The same eluent compositions used for mandelic acid and (S)-ethyl lactate, was also employed for the other lactates.

3.6.5 Refractometer

A refractometer was employed in rapid measurements of solution concentration (solubility concentration) in terms of Refractive Index (*n*). Basically, the liquid samples concentration can be obtained by the refractometer by initially preparing a calibration curve which is later used to evaluate the concentration. Refractive Index of a substance is the ratio of the velocity of a ray of light in vacuum to its velocity in a medium. When a ray of light passes from one medium to another less dense medium, for instance water to air illustrated in Figure 34 at an angle other than vertical, it changes its angle. This can be explained by using Snell's law;
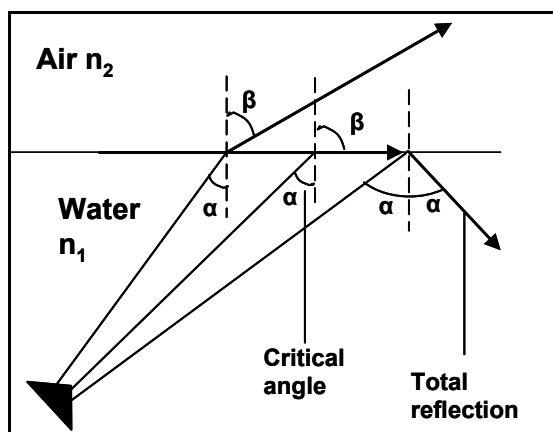
Figure 34: Systematic setup of critical angle and total reflection for medium of Air and Water.

$$Sin\,\beta = \frac{n_1}{n_2} Sin\,\alpha \qquad\qquad \text{Equation 25}$$

If a ray of light passes into an optically less dense medium from an optically denser medium, then it changes its direction. If the incidence ray α is increased, it later reaches a critical value (angle of refraction $\beta = 90°$) at which the ray of light no longer passes into optically less dense medium. Subsequently, the critical angle α is used to calculate the refractive index from the Equation 25 resulting in Equation 26.

$$\beta = 90° \Rightarrow Sin\,\beta = 1 \Rightarrow n_1 = \frac{n_2}{Sin\,\alpha}$$

Equation 26

3.6.5.1 Apparatus and analytical method

In the thesis a refractometer Mettler-Toledo RE40 was used. The solubility concentrations were determined also with the refractometer. The data obtained from the evaluation of the solubility concentrations with the refractometer compared well with HPLC.

The measuring principle is based on light from the source passes through the prism and reaches the sample. Then this light partially refracts and reflects. This reflected light is recorded by an optical sensor (CCD). The dark and light areas are divided by a boundary which gives the critical angle, which is required to calculate the refractive index (n_1) as expressed in Equation 26. The setup of the refractometer system RE40 describing the measurement principle is shown below in Figure 35(a).

The reflection is dependent on the wavelength of the light and temperature of the medium. Here sodium light of constant wavelength 589.3 was used and a constant temperature was maintained while measuring. Figure 35(b) depicts the setup of the measurement system with light source from a light emitting diode (LED).
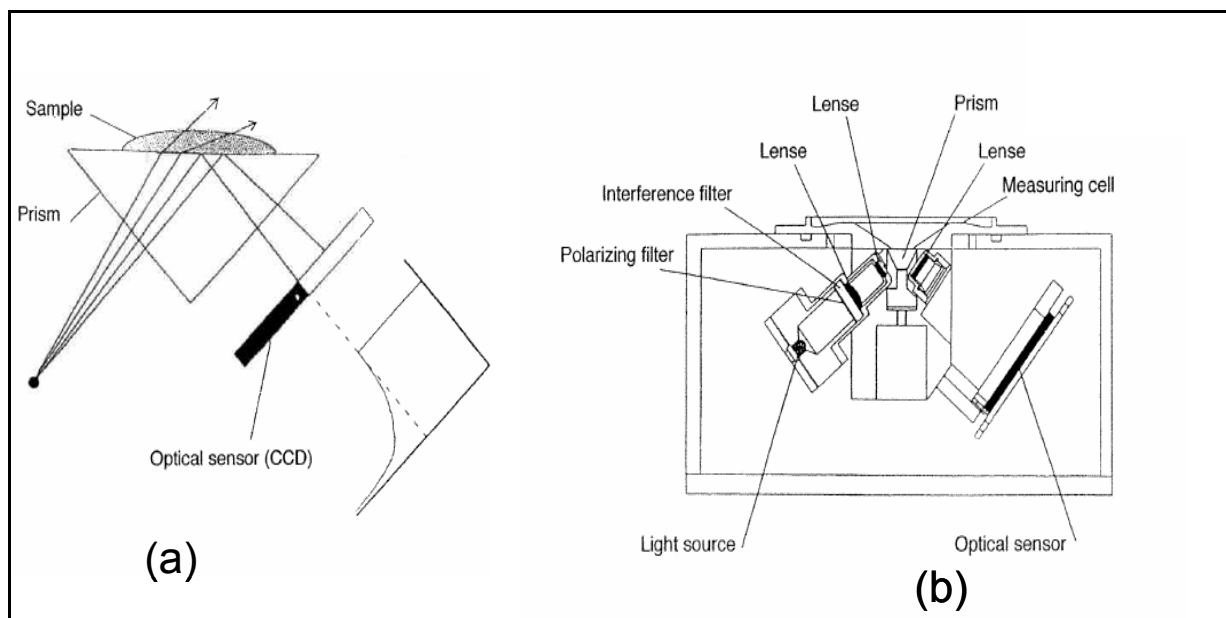
Figure 35: Schematic setup of the refractometer setup of the measurement system.[113]

3.6.6 Density meter

In this thesis the density meter DE40 from Mettler Toledo, Germany was applied in the online preferential nucleation experiments to quantify concentration. The density (ρ) of a solution is the mass (m) of the solution per unit volume (V) at constant temperature because the density of a substance is dependent on temperature.

3.6.6.1 Apparatus and analytical method

This density meter works based on the principle of electromagnetically induced oscillations of a glass tube. A magnet is attached to the U-tube and the transmitter subsequently induces the oscillation. The period of oscillation is measured by a sensor. Generally, period is seen as one complete back and forth motion of a vibration. Its duration is the period of oscillation T. Moreover, the number of periods per second is the frequency f. Each glass tube vibrates at its characteristic or natural frequency. There are changes that occur when the tube is filled with gas or liquid. Then the oscillation frequency (f) would depend on the mass of the gas/liquid which is introduced in it. Thus the density of the required gas/liquid can be calculated by using the formula.

$$f = \frac{1}{T}$$
<div align="right">Equation 27</div>

The period of oscillation T is obtained from the Equation 28.

$$T = 2\pi \sqrt{\frac{\rho V_c + m_c}{K}}$$
<div align="right">Equation 28</div>

where ρ = Density of the sample in measurement tube [g/cm^3], V_c= Volume of the sample (capacity of the tube) [cm^3], m_c= Mass of measurement tube [g], and K= Measurement tube constant [g/s^2].

It follows that,

$$\rho = \frac{KT^2}{4\pi^2 V_c} - \frac{m_c}{V_c}$$
<div align="right">Equation 29</div>

The density and the period of oscillation T are related as follows:

$$\rho = AT^2 + B$$
<div align="right">Equation 30</div>

A and B are constants which are determined by the elasticity, structure and mass of the measurement tube. Since the mass varies from tube to tube, it must be determined by measurement (factor determination). The factor of determination of the measurement tube is

calculated by measuring the period of oscillation T of two standard substances of known density, for instance water and air.

$$F = \frac{K}{4\pi^2 V_c} = \frac{\rho_A - \rho_w}{T_A^2 - T_w^2}$$

Equation 31

where ρ_A= Density of air [g/cm^3], ρ_w= Density of water [g/cm^3], T_A= Period of oscillation of the air measurement [s], and T_w= Period of oscillation of the water measurement [s].

Therefore the density can be measured based on Equation 31, and water can be substituted by other substances in the equation. Figure 36 illustrates the schematic representation of the measuring cell showing the U-tube and temperature control of the density meter.
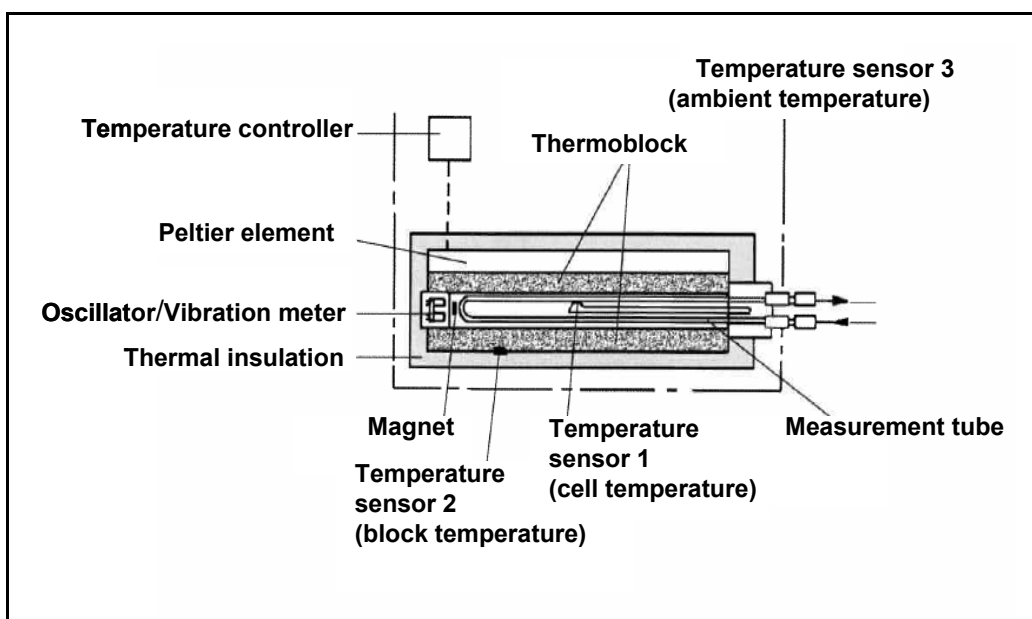
Figure 36: Schematic setup of the measuring cell and temperature control for a density meter.[114]

3.6.7 Turbidity sensor

Turbidity is defined as an expression of the optical property that causes light to be scattered and absorbed rather than transmitted in straight lines through the sample. Also turbidity can be seen as measure of relative sample clarity. The turbidity sensor used in this thesis is a fiber optic QR-sensor is a system received from the BASF Company in Germany. In this a mono- or polychromatic light is projected into the solution. The LED is built in continuous operation with 150 mA maximum load. A part of light may reflect or scatter to other directions due to the presence of solids, which reduce the reflection quantity of the light. The reflected light is received from another glass fiber cable connected to the detector. The detector is a Photomultiplier which converts the received light quantity into a voltage signal. Figure 37 shows the interaction of a light beam and finely distributed nuclei around the sensor
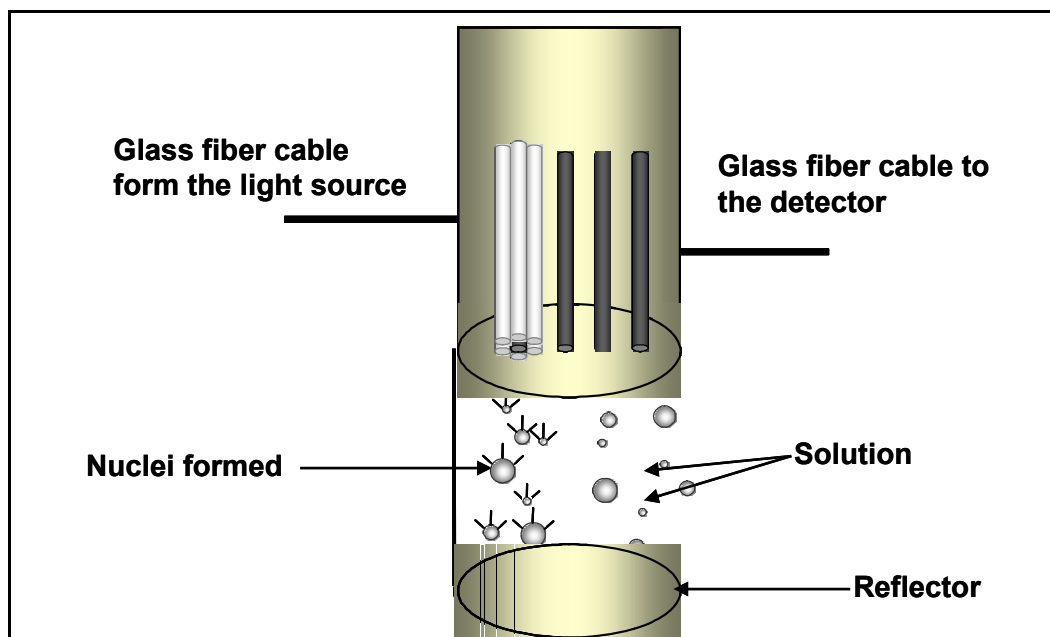
Figure 37: Schematic setup of turbidity measuring sensor.

3.6.8 Polarimeter

The polarimeter used in the present work was a PerkinElmer, Model 341, Beaconsfield/UK (optical path length of the flow cell: 100 mm). The polarimeter was employed in online preferential nucleation experiments. It is very effective and sensitive equipment for analyzing the rotation magnitude and sign of optically active substances. In a polarimeter a monochromatic light passes through a polarizer, the sample cell and the analyzer to a photomultiplier. When the polarized light beam passes through the optically active sample (placed in the sample cell), it changes the analyzer position which is perpendicular to the direction of polarization. By the principle of null position this analyzer automatically rotates to its original position. The schematic setup of the Polarimeter is shown in the Figure 38.
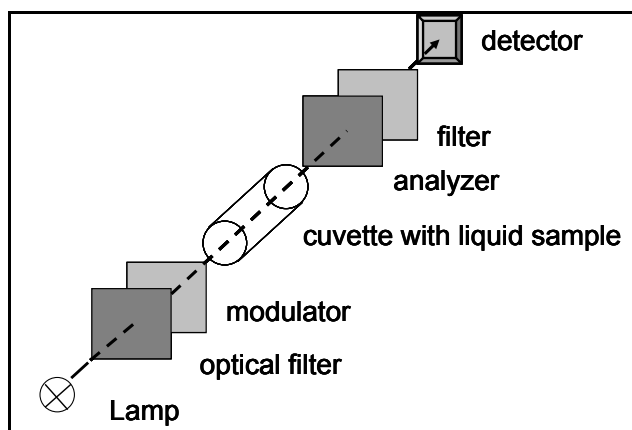
Figure 38: Schematic setup of the polarimeter.

3.6.9 X-ray powder diffraction (XRPD) methods

X-ray powder diffraction (XRPD) analysis[106,115,116] is used increasingly in the pharmaceutical and other chemical industry for a wide range of applications, ranging from polymorph screening to analysis and optimization of final dosage forms. X-ray powder diffraction methods are extensively employed for the identification of solid phases, and in cases where single crystals cannot be grown or the bulk identity of a powder, i.e. a polycrystalline substance, has to be confirmed. XRPD is a fingerprint technique, as every compound has a unique powder pattern permitting polymorphs, solvates, racemates and enantiomers to be identified decisively. Powder patterns or reflexes can also be matched with the calculated patterns from single crystal data. XRPD studies are normally carried out at room temperatures under ambient conditions, although it is possible to carry out analysis under variable temperature, wherein powder patterns are acquired whilst the sample is heated or cooled. Such studies are very useful for identifying thermally induced or sub-ambient phase transitions.

Theory

Generally, a single crystal gives a diffraction pattern with discrete diffracted beams, each in a definite direction relative to the orientation of the crystal and the incident beam, according to the Bragg's law (Equation 32).

$$n\lambda = 2d\sin\theta$$

<div align="right">Equation 32</div>

where n is the refractive index; λ represents wavelength; d is the lattice distance represent the diffraction angle. If the diffraction reflection of several single crystals is taken, each crystal would give its own diffraction pattern, superimposed on one another. Reflections generated by the rotation of the composite sample, would all satisfy the Bragg's equation with the reflections occurring along the single *2θ* axis. The angle and intensity of the reflection would be the same for each reflection produced as a result of the individual single crystals. On the detector this set of corresponding reflections from multiple crystals appear as identical spots on a circle. As the number of randomly orientated crystals is increased more such spots appear, all lying on the same circle, where a cone of diffracted radiation hits the detector. A microcrystalline powder consists of essentially an infinite number of tiny crystals and this produces a complete circle for a particular reflection. The same occurs for every Bragg reflection, each one giving a cone of radiation with angle *2θ*, and the overall result being a set of many concentric circles, with the radii governed by the Bragg's equation.

3.6.9.1 Apparatus and experimental procedure

Solid phase analysis

A possible formation of solvates and/or polymorphs in the chiral systems studied was verified analyzing the solid phases by X-Ray Powder Diffraction (XRPD). Crystalline materials were characterized on a PANalytical X`Pert Pro diffractometer (PANalytical GmbH) with Cu Kα radiation and compared with reference patterns. The samples were measured on Si sample holders and scanned from a diffraction angle of 3 to 40° with step size of 0.017° and counting time of 50s per step.

The powder was ground so that there is uniform or evenly spread orientation of the crystallographic planes and all planes have an equal chance of being detected. If a particular plane is detected more often than the others, for example because of exact crystal morphology, the intensity of that peak is abnormally huge and "floods" the rest of the pattern. A schematic representation of the instrumentation required for XRPD is shown in Figure 39.
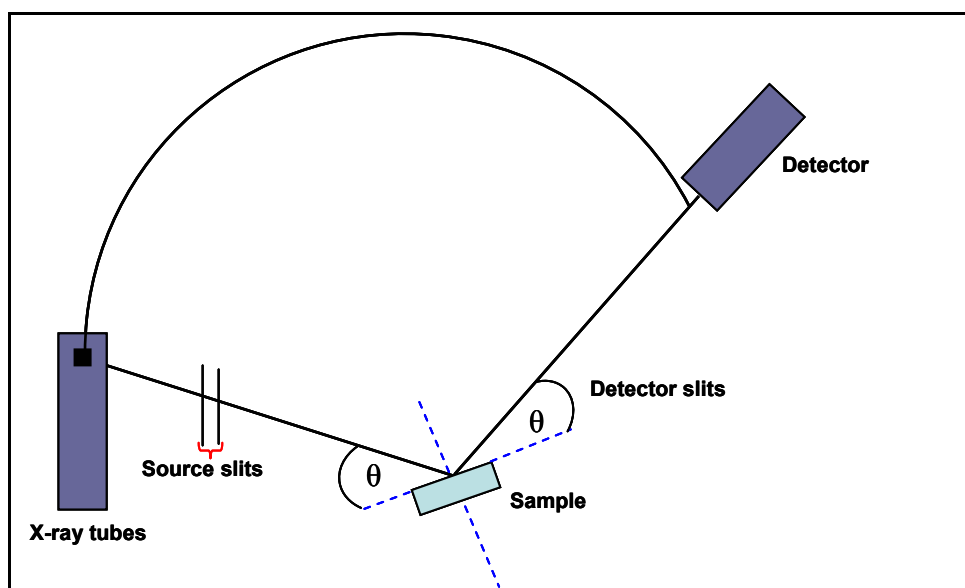
Figure 39: A schematic setup of X-ray powder diffractometer.

3.6.10 C80 calvet calorimeter for dissolution enthalpy measurement

To study the enthalpy of solvation (ΔH_{solv}; solvent-solute interaction), first of all it is required to measure the enthalpy of dissolution (ΔH_{diss}). Therefore C80 calvet calorimeter from Setaram, Germany was employed to measure the dissolution enthalpy. The enthalpies of dissolution (ΔH_{diss}) of the mandelic acid enantiomers in both chiral solvents (*S*)-ethyl lactate

and (*2R,3R*)-diethyl tartrate and also for N-methylephedrine enantiomers in (*2R,3R*)-diethyl tartrate were determined at ambient temperature (298.15 K). These systems were chosen based on the fact that resolution was possible here and it was worthwhile to study the solvent-solute interaction.

3.6.10.1 Apparatus and experimental procedure

In the C80 calvet calorimeter is made up of two compartment separated by a PTFE membrane. The solute is placed in the lower compartment (2.5 mL), and the solvent is charged in the upper compartment (2.9 mL). Figure 40 shows the schematic setup of the C80 calvet calorimeter with the sample chamber and the reference chamber specifically elaborated.
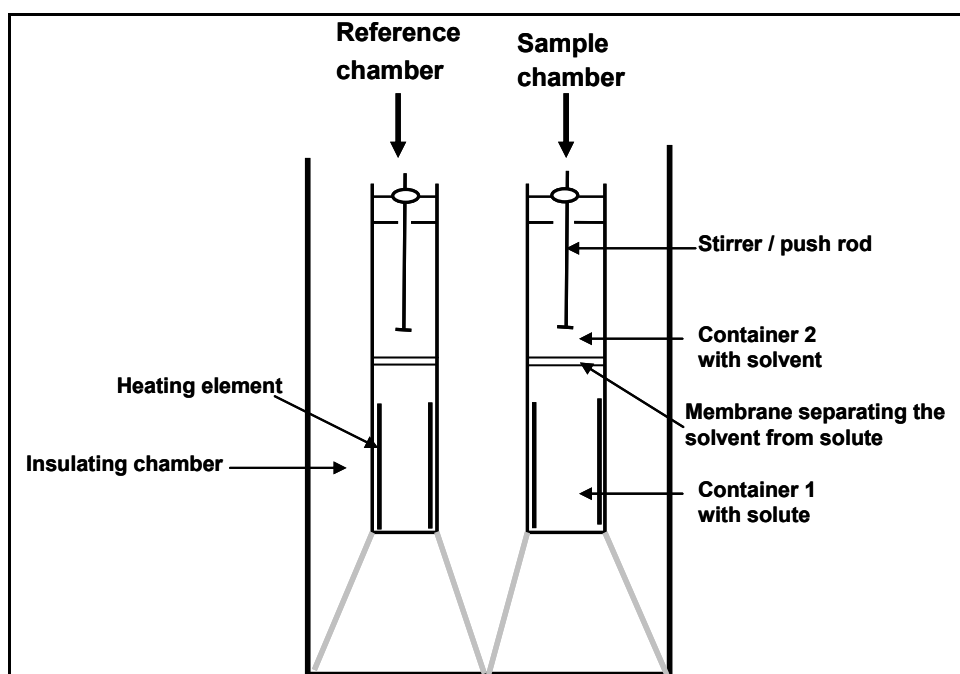
Figure 40: Schematic setup of C80 calvet calorimeter.

The setup of C80 calvet calorimeter is arranged such that the sample chamber is in the front side of the equipment whiles the reference chamber is at the rear. For the experiment, a defined solute amount of 0.065 g, which would dissolve completely in the solvent, was charged in the lower compartment of the sample chamber while the solvent of 2.5 g is placed in the upper chamber. The reference chamber upper compartment contained same amount of solvent as reference sample. However, care must be taken to ensure that equal amounts of solute and solvent are applied in both enantiomers experiments. At the beginning of the experiment, all weighing of the solutes and the solvents was made and charged into their right compartment of the calorimeter. The system was then programmed to the set temperature and

allowed to equilibrate. After equilibration of the set temperature, the experiment was started by perforating the two membranes simultaneously with the stirrer/push rod. The perforation of the membrane allowed the two substances to be brought together for mixing. Afterwards both stirrer/push rods were stirred continuously and rapidly until the solid dissolve in the solvent completely. The instrument measures the differences in temperature between the sample and reference pans for the period of heating or cooling, recording the amounts of heat added to or removed from the sample at a particular temperature, the sample pan requires more heat to keep inline with the reference pan. The area under the peak provided enthalpy changes associated with thermal event, as these are directly proportional to the heat absorbed by any thermal event or enthalpy of dissolution.

3.6.11 DV-III ultra rheometer for viscosity measurement

DV-III ultra rheometer from Brookfield Company, U.S.A with cone spindle CPE 40 was used to measures the viscosity of the chiral solvent applied in this thesis work. Basically, the internal friction of the fluid is measured. The greater the friction, the enormous the amount of force required to cause this movement, which is designated as shear. Highly viscous fluids, therefore, require more force to move than less viscous materials. So, viscosity can be expressed mathematically as;

$$\eta = \frac{\tau}{\gamma}$$

Equation 33

where η represents the viscosity, τ is the shear stress and γ represents the shear rate. The viscosity of the solvents was measured in (mPa.s) units.

3.6.12 Fourier transform infra-red spectroscopy

Infra-red (IR) energy is a small portion of the electromagnetic spectrum; typically divided into three segments, the near-, mid-, and far- IR regions, and with their individual energy/frequency limits. The infrared spectrum is highly sensitive to the structure, conformation and environment of molecules, and hence is a powerful tool for the analysis and characterization of organic compounds. Enantiomers and racemates can be identified using IR spectroscopy by comparing the spectrum of an unknown with that of a known sample.

Theory

When a beam of infra-red radiation[106,117] is incident on a sample, then absorption of different frequencies of the incident radiation occurs, at the same time as some frequencies passes through the sample without being absorbed. The molecule absorbs $E = hv$ from the IR radiation source at each vibrational transition, resulting in the excitation of the molecule from its lowest, or ground vibrational state to a higher one. Since the molecules are highly selective with reference to the frequencies of radiation they absorb, resulting in their characteristic range of absorption allows for their identification. The energy absorbed by a sample at a specific frequency is measured by the detector. This is mostly illustrated as a transmission compared to a blank background. A transmission of 10% means most of a particular frequency has been absorbed by the sample. Frequency is measured in wavenumbers is expressed as follows;

$$wavenumber = \frac{1}{\lambda}$$

Equation 34

However, it is necessary to introduce the quantum aspect for species at the atomic level. Then the bonds holding the atoms together in a molecule vibrate with a particular vibrational energy E_{vib} (Equation 35) owing to the attractive bonding forces and the repulsive non-bonded electron interactions.

$$E_{vib} = hv(V + 1/2)$$

Equation 35

where V= 0, 1, 2....which is known as the vibrational quantum number, v represents the vibrational frequency and h is the Planck's constant.

Moreover, the vibrations of individual bonds of functional groups (localized vibrations) take place in the region between (1500 – 4000) cm^{-1} and are applied for the identification of functional groups. Figure 41 depicts the various vibrations of the individual bonds; stretching, bending, rocking, twisting and wagging modes, as illustrated by a methylene (CH$_2$) group.
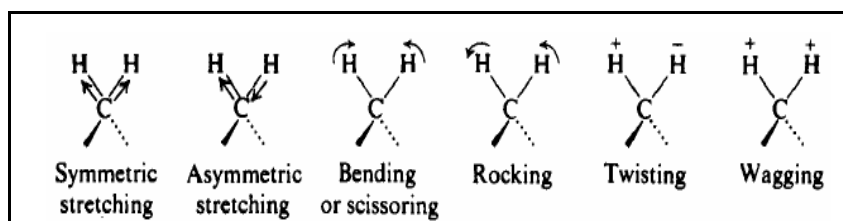
Figure 41: Molecular vibrations in methylene. A characteristic stretching and bending vibrations in plane and out of plane.[106]

Often, bands that do not correspond to any of the fundamental vibrations of the molecule are observed in the region below 1500 cm^{-1}, which is due to combination bands that result from interactions between two or more vibrations. The fingerprint region (625 – 1500 cm^{-1}) is the highly sensitive section of the spectrum, where the pattern differs most from compound to compound. Assessment of the fingerprint area allows the identification of very comparable molecules as they may be characteristic of molecular symmetry or combination bands arising from simultaneous multiple bond deformations.

The IR spectroscopic methods have considerably been enhanced using Fourier transform methods[106,117], which permit measurement of all the frequencies at the same time, rather than successively recording individual frequencies, as is the case in dispersive spectrometers. In addition, spectra are recorded much more quickly, with less noise and therefore a better signal to noise ratio. A schematic setup of a Fourier transform spectrometer is shown in Figure 42.

The infra-red radiation from the source goes through a beam splitter, which divides the planes of the fixed and moving mirrors and sends the light in two directions at right angles. Half of the light goes to the moving mirror and 50% reflected onto the fixed mirror. The motion of the moving mirror, versus that taken by the stationary-mirror beam, makes the total path length variable. Both beams are reflected back to the beam splitter, but the difference in path lengths creates constructive and destructive interference: an interferogram. The recombined beam is now passed through the sample, which absorbs specific frequencies of radiation, and the resultant beam transmitted to the detector. A reference for the instrument operation is provided by superimposing a laser beam. Fourier transformation by the computer converts the final interferogram into a single beam spectrum. A background corrected spectrum is usually displayed or printed.
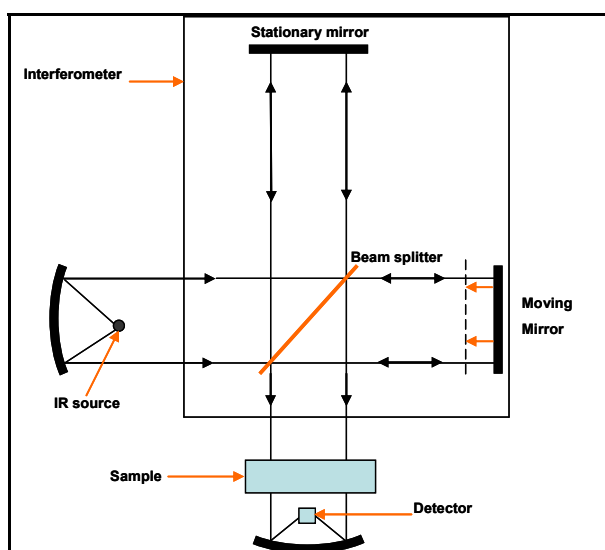
Figure 42: Schematic setup of Fourier transform infra-red spectrometer.

3.6.12.1 Apparatus and experimental procedure

A NICOLET 6700 FTIR spectrometer from Thermo Electron Corporation was used in conjunction with Nicolets OMNIC software v.5.1b, for data collection. An Attenuated Total Reflectance (ATR) accessory employing a germanium (Ge) crystal was used (Figure 43). This makes data collection easy, with little sample preparation required. Liquid samples were prepared at the same concentrations and placed directly on the crystal and spectra acquired, which is an average of 32 or 64 spectral acquisition and 4 cm^{-1} resolution. The passing wave penetrates the sample to an average depth of about 20 µm. A background spectrum of the crystal substrate is run prior to running the IR of the sample, and this is then automatically subtracted from subsequent spectra.

Figure 43: NICOLET 6700 FTIR spectrometer.

3.6.13 Raman spectrometer

Raman spectroscopy[106,117,118], the sample is irradiated by an intense monochromatic laser beam in the UV-vis-NIR region (v_o), most of the radiation is transmitted unchanged, with only a small amount scattered by the molecules. The scattered light is usually observed in the direction perpendicular to the incident beam. The scattered light consists of two types: Rayleigh scattering, which is passed into the spectrometer and Raman scattering. Modern Raman instruments are designed to filter out the Rayleigh light as only one in every million photons will be Raman scattered.

However, there is one other condition for a vibration to be Raman active when the molecule vibrates there must be a change in polarizability; a change in the shape, size or orientation of

the electron cloud that surrounds the molecules. The first case is strong and has the equal frequency as the incident beam (v_o), whereas the second case is very feeble (10-5 of the incident beam) and has frequencies $v_o \pm v_m$, where v_m is a vibrational frequency of a molecule, making detection and measurement complicated. These Raman lines are due to absorption and re-emission of light together with vibrational excitation and decay correspondingly. The $v_o - v_m$, (the gain of energy by the irradiated molecule) and $v_o + v_m$ (the loss of energy from the irradiated molecule) lines are the Stokes and anti-Stokes lines, respectively in Figure 44. Hence, Raman spectroscopy has the vibrational frequency (v_m) as a shift from the incident beam frequency (v_o) which is measured. Usually, the anti-Stokes lines are less strong than the Stokes lines because these transitions arise from higher vibrational energy levels with fewer molecules. Hence, the Stokes region of the spectrum is commonly used.
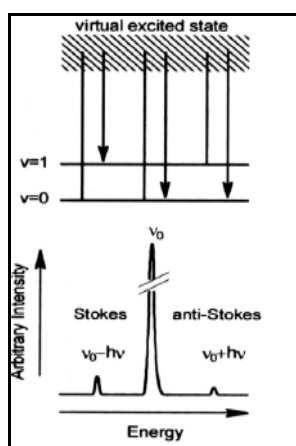
Figure 44: The stokes and anti stokes energy levels in Raman spectroscopy.[87]

Raman spectroscopy provides information about the vibrational frequency of excited molecules in a sample where the vibrational frequency is measured as a Raman shift, relative to the exciting energy source.

3.6.13.1 Apparatus and experimental procedure

In this work Raman spectroscopy is used to study interactions of the chiral molecules and the chiral solvent in the liquid phase. Raman spectra were collected with a MultiRAM spectrometer from Bruker Company, Germany. The system employed a laser beam at 1064 nm operating at 300 mW. The analyses were carried out for liquid phase samples at ambient temperature. Figure 45 shows the MultiRAM spectrometer.

Figure 45: A MultiRAM spectrometer.

The samples were scanned for a period of 10 seconds; the resolution was at 4 cm^{-1}. Liquid phase samples of solute in solvent at a concentration of 8 wt % were used.

3.7 Summary

In this chapter, the various analytical techniques used have been described with details of the apparatus applied. Experimental work was performed for solubility data and nucleation points which were necessary for the enantioselective crystallization to be designed. Prior to the fundamental experiments, the "classical" chiral solvents were initially screened with NMR-spectroscopy to select appropriate "classical" chiral solvents that can create chiral discrimination. The selected "classical" chiral solvents, the tailor-made chiral solvent and the chiral ionic liquids that were used in this thesis were characterized with FTIR spectroscopy and also regarding their physical properties (viscosity, melting point and boiling point). Subsequently, enantioselective crystallization experiments were designed and successfully conducted. Hereby, Raman spectroscopy and calorimetric methods were applied to study the interactions between the solvent and solute molecules.

The next chapter will present the results achieved.

Chapter 4. Results and discussion

84

Chapter 4

4. Results and Discussion

4.1 Introduction

This chapter will give and discuss the results obtained in this work. The outcome of the characterization experiments for the chiral solvents with FTIR will be shown and discussed. Moreover, details on the study of the fundamental solubility and metastable zone width data (primary nucleation) will be presented. A detailed description of the different enantioselective crystallization (preferential nucleation and preferential crystallization) carried out in this work will be discussed. Afterwards, results on the solvent-solute interactions related to the kinetic effect will be shown. Molecular modeling calculations results on solvent-solute interactions study which was carried out to get a deeper understanding of the system will be highlighted here. The FTIR results are included in Appendix A (since the measured FTIR spectra do not give measurable solvent-solute interaction in the liquid phase).

The next section will discuss the results of the binary phase diagrams for the two chiral substances studied: mandelic acid and N-methylephedrine. These data were taken from literature, as these systems have been well studied by various researchers already.

4.2 Binary phase diagrams

It is always useful to characterize first the chiral substances by melting point studies. Melting temperatures and the enthalpies of melting will later be employed for the quantification of the binary phase diagram. The binary phase melting diagram gives an idea about which type of racemate the system studied belongs to. In the previous chapter a description of the various racemate types has been given.

4.2.1 Mandelic acid

A lot of work on the crystallization, stability, thermal analysis, solubility and phase diagram determination has been studied on both, the racemic and the enantiomeric mandelic acid dating as far back as 1899.[119] Mandelic acid as a model system has been studied intensively by four different research groups[48,100,120-123] all working on different aspects of its crystallization and thermodynamics. Through this research work, Mughal[87] reported on the bases of IR that it was a metastable polymorph of (*RS*)-MA (denoted (*RS*)-MA II) that crystallized out from the racemic mandelic acid solution, not the conglomerate as reported by Profir et al.[120] However, the stable racemic compound is denoted by (*RS*)-MA I. The

polymorph had been reported in the past but only from melt crystallizations,[124] with no crystal structures determined. Mughal also observed that soon after her crystallization and successful characterization of (*RS*)-MA II its crystal structure was published.[125] The binary phase diagram of MA has been determined by many authors[100,122,123,126-130] and it is being described in the following sections.

4.2.1.1 (RS)-MA Form I

The melting point phase diagram determined by Brandstätter[126] located the eutectic composition at 114 °C and 70% for (*RS*)-MA I. A more current study,[100,122,123] dedicated to the determination of the mandelic acid binary and ternary phase diagrams (using DSC and classical isothermal method, respectively) specified the x_{eu} at 69%, which is in close agreement with couple of studies done by Fouquey[131] Brandstätter[126] and Nishiguchi[132] eutectic composition of 70%. Figure 46 epitomizes the binary phase diagrams reported since 1899.
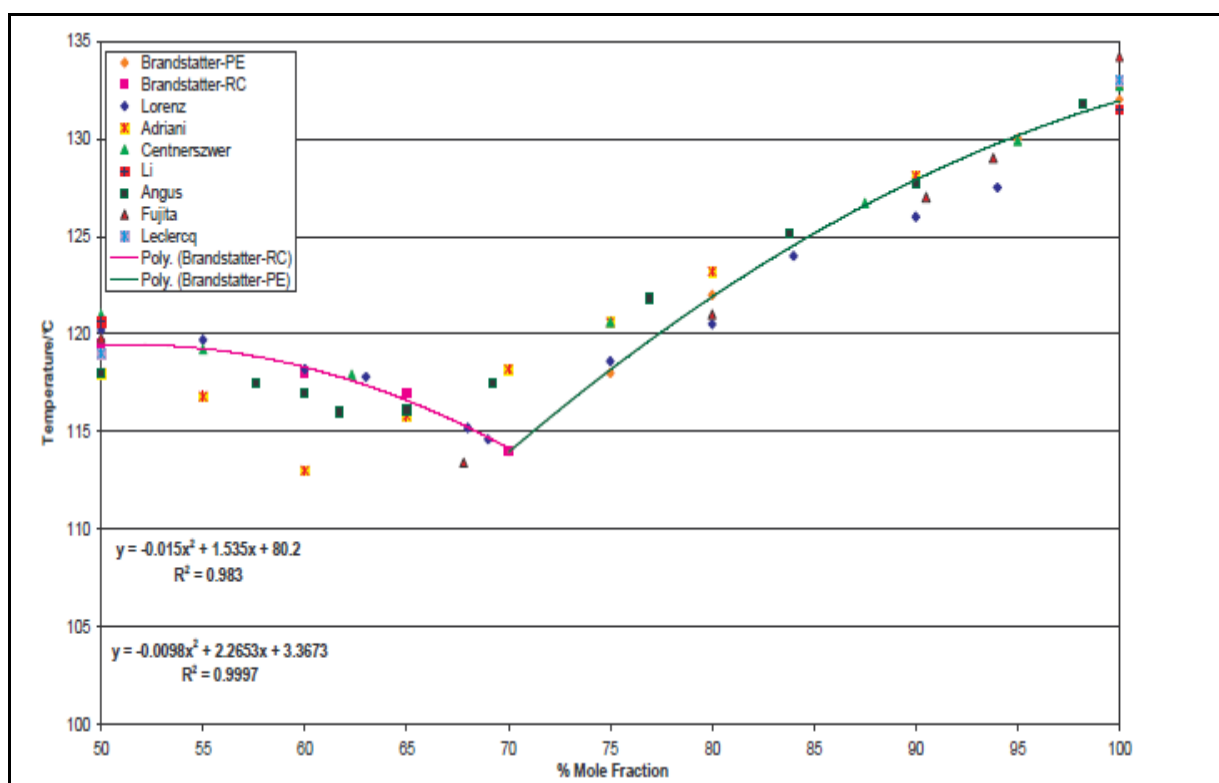
Figure 46: Binary phase diagram of MA enantiomers. Solid lines are 2nd Polynomial fitting to the Brandstätters data. (x and y represents composition and temperature, respectively). Diagram is taken from Mughal.[87]

The experimental binary phase diagram determined by Lorenz[122] was compared to that predicted using the Schröder-van Laar equation[5] (see section 2.3, Equation 18) for the enantiomeric mixture, and the Prigogine-Defay equation[5,39] (see section 2.3, Equation19) for

the racemic compound. This comparison is shown in Figure 47 which depicts accurately data points close to the pure enantiomer sides ($x > 0.605$; $x \geq 0.799$) when fitting the experimental data to the predicted phase diagram. As a result of this the (*RS*)-MA I eutectic composition is specified at 69%. This value for x_{eu} will be applied in this thesis.
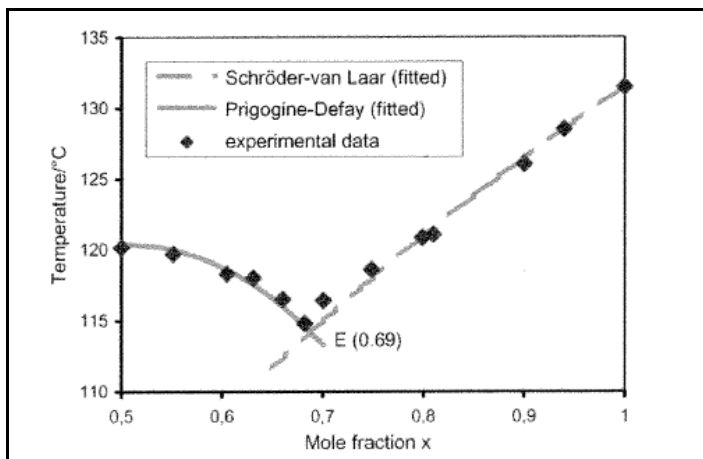
Figure 47: Binary melting phase diagram of (*RS*)-MA Form I. Experimental and fitted values.[122]

4.2.1.2 (RS)-MA Form II

Kuhnert-Brandstätter[126] identified the eutectic temperature of (*RS*)-MA II at 106 °C and $x_{eu} = 63\%$. The results are illustrated in Figure 48.
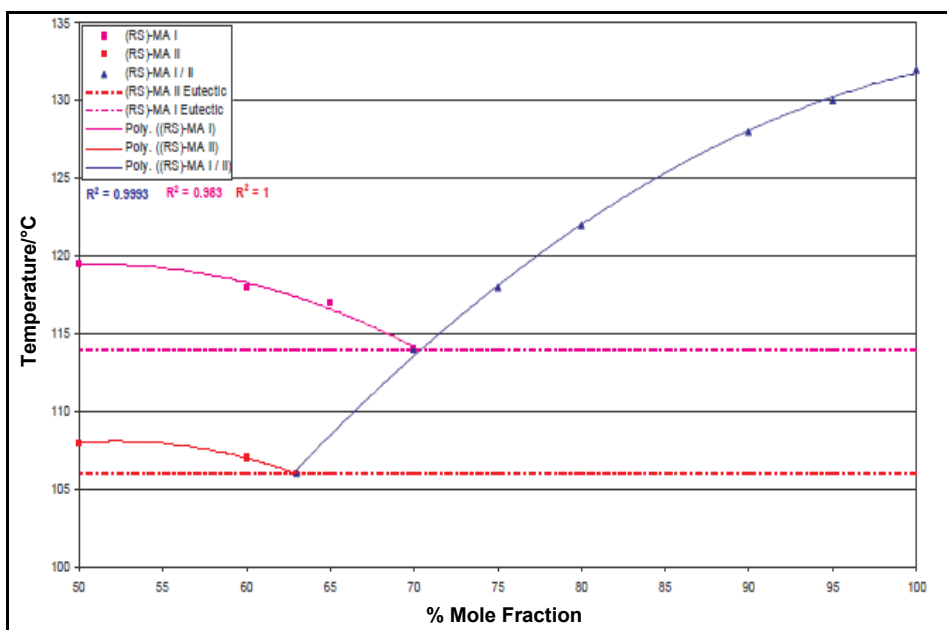
Figure 48: Binary phase diagram of (RS)-MA polymorphs as reported by Brandstätter et al.[126]. Solid lines are 2nd order polynomial fitting is used. Diagram is taken from Mughal.[87]

Profir et al.[120] investigated the crystallization experiments of (*RS*)-MA II in various solvents: (water, a mixture of toluene and methyl isobutyl ketone (TMIK) in weight proportions 3:1, isobutyl acetate and pure acetic acid). Crystallizations experiments were carried out with lower starting solution concentration in acetic acid yield (*RS*)-MA II by nucleating at high cooling rates and at either high or low agitation rates. The metastable racemate ((*RS*)-MA II) has been crystallized from solutions of (*RS*)-MA in water, which were filtered with a 0.2 mm membrane filter. The solution was evaporated slowly at room temperature and after several weeks, crystals of (*RS*)-MA II were collected. Single crystal structure determination was carried out with the identity of the bulk solid verified using XRPD.[125] Similarly, Lorenz et al.[123] crystallized (*RS*)-MA II from water and ethanol by evaporative crystallization at room temperature and at atmospheric pressure. Crystallization from significantly enriched solutions (enantiomeric excess (ee) 0.07 − 0.95%) of 1:1 mixtures of enantiomers have also yielded (*RS*)-MA II, as did for freeze-drying from racemic solutions and sublimation under reduced pressure.

4.2.1.3 Thermal properties and stability of mandelic acid

C. D. Hurd and H. R. Raterink[133] studied the thermal decomposition process of MA up to 250 °C and established carbon monoxide (traces of carbon dioxide), water and benzaldehyde as the decomposition by products. Moreover, MA experiences considerable and irreversible decomposition[134] on heating faintly over its melting point, the degree of decomposition depends on the temperature MA is heated at and the method of heating. This makes identification of the real melting point intricate, as the samples can not be heated twice. The decomposition of the MA is associated with mass loss which has been estimated by using the mass loss due to decomposition, which was estimated by means of TG-DSC coupling to be 2.2 wt.% until the melting starts and 2.8 wt.% at the end of the melting peak.[122] When comparing the melting points and enthalpies of melting reported in literature, great variation is observed. Profir et al[135] reported that the variation in the ΔH_{fus} found in the literature ranges from 25 to 30 kJ/mol for (*RS*)-MA I and from 20 to 31 kJ/mol for the pure enantiomer. Some of the melting points and ΔH_{fus} reported for the (*RS*)-MA I and (*S*)-MA are tabulated below in Table 9.

Table 9: Melting points and melting enthalpies of (RS)-MA Form I and (S)- and (R)-MA reported in the literature

Literature Source	(RS)-MA Form I		(S)-MA/(R)-MA	
	T_m (°C)	ΔH_{fus} (kJ/mol)	T_m (°C)	ΔH_{fus} (kJ/mol)
Centnerszwer[119]	121	-	132.7	-
Adriani[127]	118	-	132.8	-
Angus[128]	118	-	133	-
Fujita[129]	119.8	30	133.8/134.2	31.0/31.1
Leclercq[130]	119	25.1	133	26.4
Patil[136]	-	-	136	-
Jacques[5]	119	25.5	133	26.4
Lorenz[100,122]	120.2	25.6	131.6	24.5
Profir[135]	118.9±0.1	26.1±0.4	130.9±0.4	26.2±0.5
Z. J. Li[137]	120.6	26.8	131.5	25.7
Ullmann's Encyclopedia[99]	118-121	-	132-135	-
Handbook of Chemistry & Physics[138]	118-123	-	134-135/133-135	-
Sigma Aldrich website www.sigma-aldrich.com	119-121	-	131-133/131-134	-

From this compiled physical data, it can be realized that the melting point ranges from 117 to 123 °C and 130.9 to 136 °C with the corresponding ΔH_{fus} also ranging from 24.5 to 30 kJ/mol and 24.5 to 31.1 kJ/mol for (*RS*)-MA Form I and for the single enantiomers, respectively.

Several researchers have reported the melting point of (*RS*)-MA Form II. These results are summarized in Table 10.

Table 10: Published melting and melting enthalpies of (RS)-MA Form II

Literature Source	T_m (°C)	ΔH_{fus} (kJ/mol)
Lorenz[123]	108	-
Brandstätter[126]	108	-
Rose[124]	108.4	24.6
Profir[135]	103.6±2.2	20.7±2.1

Potential energy surface for the decomposition of mandelic acid

The decomposition of mandelic acid has been studied by ab initio calculations MP2/6-31G.with the GAUSSIAN92/DFT program by Domingo et al.[139] The potential energy surface (PES) for the gas phase decomposition of MA has been studied. Benzaldehyde, carbon monoxide and water are the products of the decomposition, which is homogenous, unimolecular and obeys first-order rate law.[140] The PES studies show that there are three competitive reaction pathways associated with the decomposition of MA: pathways *1* and *2* are stepwise processes. Step *1* represents the dehydration process, forming an α-lactone ring, as the second step is the ring opening of the α-lactone yielding benzaldehyde and carbon monoxide. In steps *1* and *2* the dehydration takes place by eliminating the hydroxyl on the chiral carbon atom (C3); the mechanism which yields the lactone intermediate is different. In step *1* the ring closure is from the nucleophilic attack of the carboxylic acid oxygen atom on the C3 centre, in step *2* this is carried out by the hydroxyl oxygen of the carboxyl group. Pathway *3* is a one step process where the decomposition takes place in a concerted manner. The decomposition process[139] can be described schematically as follows in Figure 49:
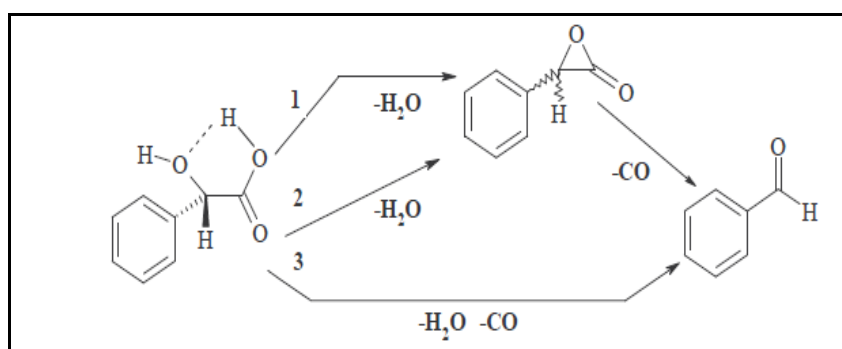
Figure 49: The decomposition process.[139]

So in the study, the conformer of *(RS)-MA* with intramolecular hydrogen bond is the most stable structure, found from the conformational analysis and was used as the starting reactants. The decomposition of MA is an endothermic process with the ΔH_{dec} for the overall process being 73.9 kJ/mol. At 300 °C this overall process is spontaneous, with a Gibbs free energy *(ΔG)* value of –95.8 kJ/mol. The validity of the theoretical work has been confirmed using the experimentally obtained data showing good quantitative agreement.

Furthermore, Chuchani and Martin[140] also did similar work and reported that benzaldehyde; carbon monoxide and water are the molecular elimination products up to 60% of MA decomposition, after which some benzyl alcohol from the decarboxylation process and carbon dioxide are also produced. The reaction was carried out in a hardened static reaction vessel in the temperature ranges from 300.1 to 340 °C and pressure range from 15.2 to 52.1 Torr. The reaction is described in detailed in Figure 50.
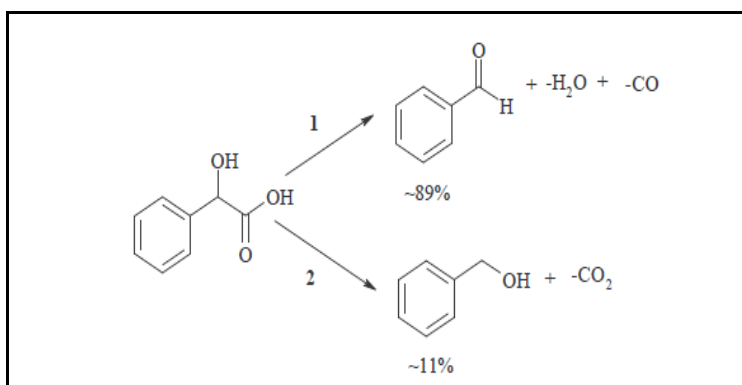
Figure 50: Molecular elimination of products of *(RS)-MA*.[87]

4.2.2 N-methylephedrine

The binary melting phase diagram of (+)-N-methylephedrine ((+)-ME) and (-)-N-methylephedrine is given in the Figure 51, (taken from Wang et al.[102]). Considering the phase diagram the eutectic composition is located at same place as the racemic mixture composition (mole ratio: (+)/(-) = 0.5/0.5). This shows that N-methylephedrine forms a simple eutectic (conglomerate) system. The liquidus line is calculated from the melting point and the melting enthalpy of the single enantiomer (see Table 11), using the Schröder-van Laar equation (see chapter 2 in section 2.3, Equation.18). Table 11 gives details of some melting points (T_m) and enthalpy of fusion (ΔH_{fus}) reported for the (+)-N-methylephedrine and (±)-N-methylephedrine which are tabulated below.
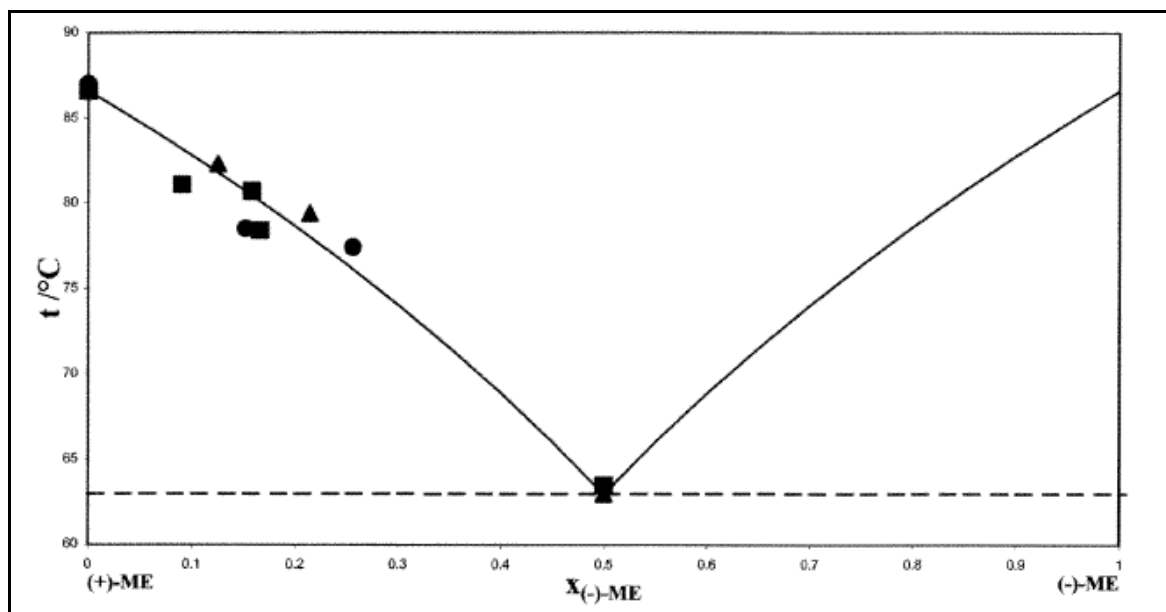
Figure 51: Binary phase diagram (melting point diagram) of N-methylephedrine ▲, heating rate 2 K/min ; ■ heating rate 5 K/min ; ● Heating rate 10 K/min ; ▬, simplified Schröder-van Laar equation (liquidus line) ; - - -, solidus line.[102]

Table 11: Melting points and melting enthalpies of (+)-N-methylephedrine and (±)-N-methylephedrine reported in the literature.

Literature Source	(+)-N-methylephedrine		(±)-N-methylephedrine	
	T_m (°C)	ΔH_{fus} (kJ/mol)	T_m (°C)	ΔH_{fus} (kJ/mol)
Wang[102]	86.6	30.53	63.50	26.57
Sigma Aldrich website www.sigma-aldrich.com	87-90	-	-	-

The following section will present the solid liquid equilibria results, considering the various solute and solvent systems studied in this work.

4.3 Ternary phase diagrams

This section will entail the results of the following solubility measurements that were carried out. The results will be presented in the following order:

Mandelic acid and N-methylephedrine in the various "classical" chiral solvents

1. Mandelic acid in (*S*)-methyl lactate, (*S*)-ethyl lactate, (*S*)-propyl lactate, (*S*)-butyl lactate and (*2R,3R*)-diethyl tartrate.

2. N-methylephedrine in (*S*)-methyl lactate, (*S*)-ethyl lactate, (*S*)-propyl lactate, (*S*)-butyl lactate and (*2R,3R*)-diethyl tartrate.

N-methylephedrine in two chiral ionic liquids

3. N-methylephedrine in the two chiral ionic liquids ((S)-2-(methoxycarbonyl) pyrrolidinium bis (trifluoromethylsulfonyl) amide and (1R, 2S)-(-)- Dimethylephedrinium bis (trifluoromethylsulfonyl) amide).

Mandelic acid in two tailor-made chiral solvents

4. Mandelic acid and in the tailor-made chiral solvents ((*S*)-propyl mandelate and (*S*)-isopropanol mandalate).

4.3.1 Mandelic acid and N-methylephedrine in various "classical" chiral solvents

The different results obtained in the various "classical" chiral solvents will be highlighted in this section. The first part of this section will deal with mandelic acid and the lactates.

4.3.1.1 Mandelic acid in "classical" chiral solvent

The solubility data measured are summarized in Tables 12. Figure 52 illustrates the ternary solubility phase diagrams of the mandelic acid enantiomers in (S)-ethyl lactate for the temperature range from 0 to 25 °C. The liquid phase is in equilibrium with the corresponding solid phase of the crystalline enantiomer (Figure 52, left upper corner, dashed tie lines) for ratios of the enantiomers within 0-31% and 69-100%, while compositions of 31-69 % of the enantiomers in the liquid phase are in equilibrium with the crystalline racemic compound (Figure 52, left upper corner, dotted tie lines). The solubility isotherms confirm the compound forming character of the mandelic acid system. The diagram shows symmetrical mirror image with respect to the racemic axis rather than asymmetry which could be possible in the case of chiral solvents. The symmetry verification was supported by detailed measurement of the solubility isotherm at 15 C. The ratio of the enantiomers at the symmetric eutectic compositions remained unchanged with temperature at 0.69 and 0.31 in this solvent as it was

also reported in earlier results for non-chiral solvents.[47,100,123] The solubilities of the pure enantiomers, the racemate and the eutectic mixture increase with increasing temperature.

Table 12: Mass fraction solubility (w_i) of (*S*)-Mandelic acid (1) and (R)-Mandelic acid (2) in (*S*)-Ethyl Lactate at different enantiomeric excesses (ee) $\left[ee = |w_1 - w_2|/(w_1 + w_2)\right]$ and temperatures.

100 ee	100 (w_1+w_2)	100 w_1	100 w_2	100 $w_{solvent}$
t = 0 °C				
100.00	17.22	17.22	0.00	82.78
37.00	22.20	15.20	7.00	78.80
0.00	21.18	10.59	10.59	78.82
37.36	22.00	6.89	15.11	78.00
100.00	17.20	0.00	17.20	82.80
t = 5 °C				
100.00	18.30	18.30	0.00	81.70
38.32	23.78	16.45	7.33	76.22
0.00	23.07	11.53	11.53	76.94
40.74	24.17	7.16	17.01	75.83
100.00	18.58	0.00	18.58	81.42
t = 15 °C				
100.00	21.50	21.50	0.00	78.50
98.70	21.51	21.37	0.14	78.49
90.34	21.85	20.79	1.06	78.15
72.74	24.99	21.58	3.41	75.01
61.38	24.72	19.95	4.77	75.28
52.68	26.42	20.17	6.25	73.58
42.96	26.78	19.14	7.64	73.22
40.78	28.14	19.81	8.33	71.86
32.16	27.41	18.11	9.30	72.59
22.56	27.72	16.99	10.73	72.28
12.36	25.91	14.56	11.35	74.09
0.00	25.10	12.55	12.55	74.90
2.82	25.17	12.23	12.94	74.83
13.82	25.55	14.54	11.01	74.45
23.96	26.69	16.54	10.15	73.31
35.22	26.50	8.58	17.92	73.50
43.62	27.80	7.84	19.96	72.20
44.20	26.81	7.48	19.33	73.19
55.50	24.95	5.55	19.40	75.05
66.46	24.93	4.18	20.75	75.07
78.08	24.25	2.66	21.59	75.75
87.70	22.21	1.37	20.84	77.79
87.84	22.86	1.39	21.47	77.14

Continuation of Table 12

95.00	21.68	0.54	21.14	78.32
100.00	21.50	0.00	21.50	78.50
		t = 25 °C		
100.00	25.17	25.17	0.00	74.83
38.00	32.27	22.26	10.01	67.73
0.00	30.61	15.34	15.27	69.39
38.00	32.27	10.01	22.26	67.73
100.00	25.02	0.00	25.02	74.98

The ternary solubility phase diagram shown in Figure 52 was evaluated from the solubility data in Table 12.
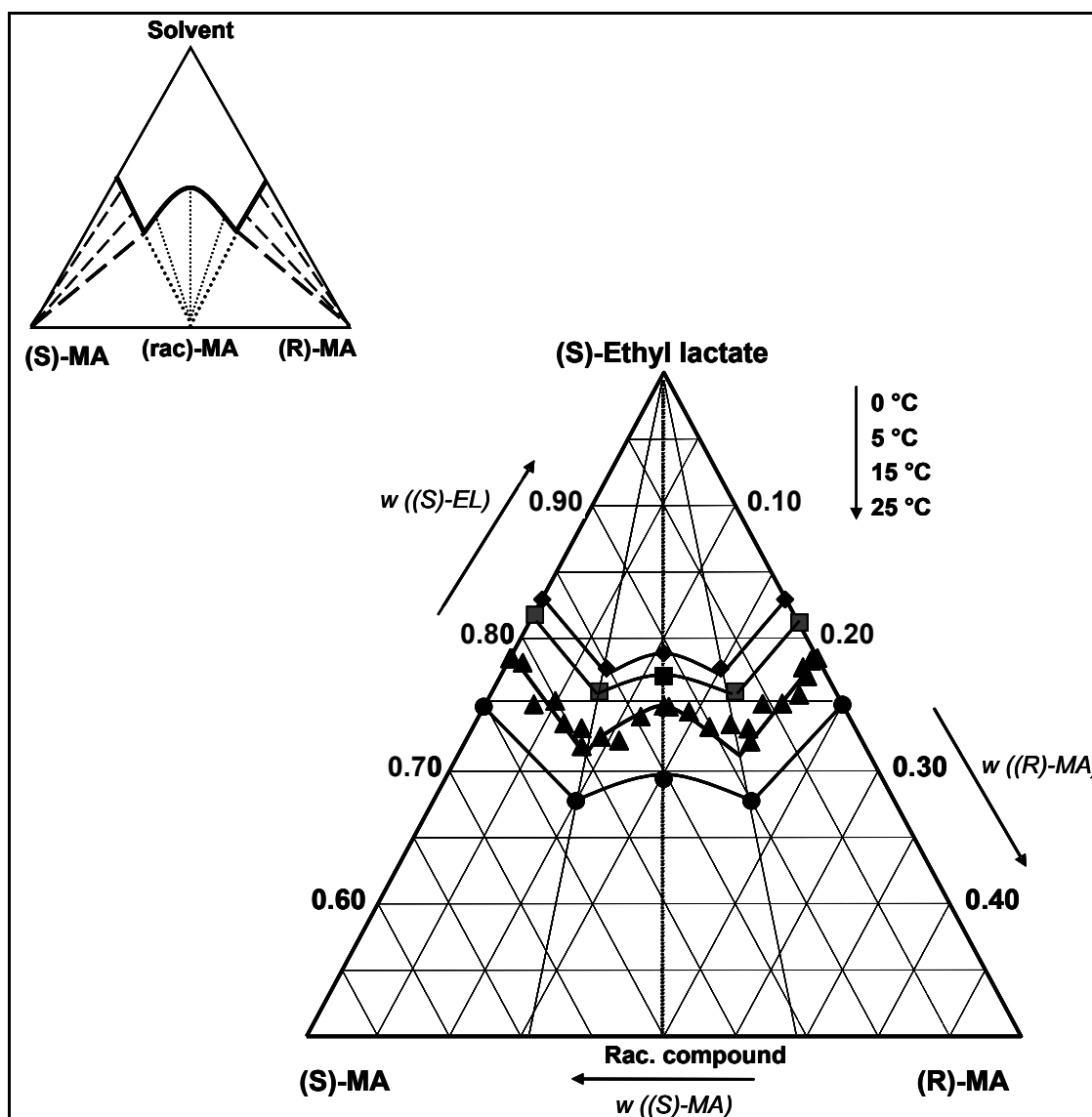
Figure 52: Ternary phase diagram of the mandelic acid enantiomers in (*S*)-ethyl lactate. Axes in weight fractions; $w_{(S)-MA}$ and $w_{(R)-MA} \leq 0.5$ of the phase diagram is shown for four solubility isotherms between 0 and 25 °C. Schematic overview (figure, upper left) with proposed tie lines linking the liquid phases with the corresponding solid phases with dash lines. The isothermal lines have been added as a visualization aid, and only the marked points show measured data.

Investigation into different chain length of the lactates

Investigations were also carried out to verify the effect of chain length of the lactates, (*S*)-methyl lactate, (*S*)-ethyl lactate, (*S*)-propyl lactate and (*S*)-butyl lactate on the ternary solubility phase diagrams. Here four different chiral solvents with varying chain length were employed. Figure 53 shows the ternary solubility phase diagram of mandelic acid in different "classical" chiral solvents at 25 °C. The phase diagram also shows no asymmetry, which implies that no measurable discrimination was observed. It is also evident that solubility increases with decreasing chain length from (*S*)-butyl lactate to methyl lactate. This is attributed to the fact that smaller chain length solvents have higher polarity, and as a consequence would dissolve more solute and vice versa. Moreover, the phase diagram shows again the typical feature of a compound forming system observed for all the lactates studied. The solubility data measured for the various lactates, (*S*)-methyl lactate, (*S*)-ethyl lactate, (*S*)-propyl lactate are summarized in Tables 13. The ternary solubility phase diagram shown in Figure 53 was derived from the solubility data in Table 13.

Table 13: Mass fraction solubility (w_i) of (*S*)-Mandelic acid (1) and (*R*)-Mandelic acid (2) in different "classical" chiral solvents at different enantiomeric excesses (ee) $\left[ee = |w_1 - w_2|/(w_1 + w_2)\right]$ and at temperature 25 °C.

100 ee	100 (w_1+w_2)	100 w_1	100 w_2	100 $w_{solvent}$
		(S)-ML		
100.00	27.49	27.49	0.00	72.51
38.01	35.04	24.18	10.86	64.96
1.55	32.89	16.70	16.19	67.11
37.97	34.89	10.82	24.07	65.11
100.00	27.57	0.00	27.57	72.43
		(S)-EL		
100.00	25.02	25.02	0.00	74.98
38.08	32.27	22.28	9.99	67.73
0.22	30.61	15.34	15.27	68.39
38.20	32.27	9.97	22.30	67.73
100.00	25.17	0.00	25.17	74.83
		(S)-PL		
100.00	20.31	20.31	0.00	79.69
38.20	27.35	18.90	8.45	72.65
1.37	25.51	12.92	12.59	74.49
38.42	27.51	8.47	19.04	72.49
100.00	20.39	0.00	20.39	79.61

		Continuation of Table 13		
		(S)-BL		
100.00	16.90	16.90	0.00	83.1
38.09	23.23	16.04	7.19	76.77
1.71	21.00	10.68	10.32	79.00
38.08	23.00	7.12	15.88	77.00
100.00	16.64	0.00	16.64	83.36

(*S*)-ML, (*S*)-methyl lactate; (*S*)-EL, (*S*)-ethyl lactate; (*S*)-PL, (*S*)-methyl lactate; (*S*)-BL, (*S*)-butyl lactate
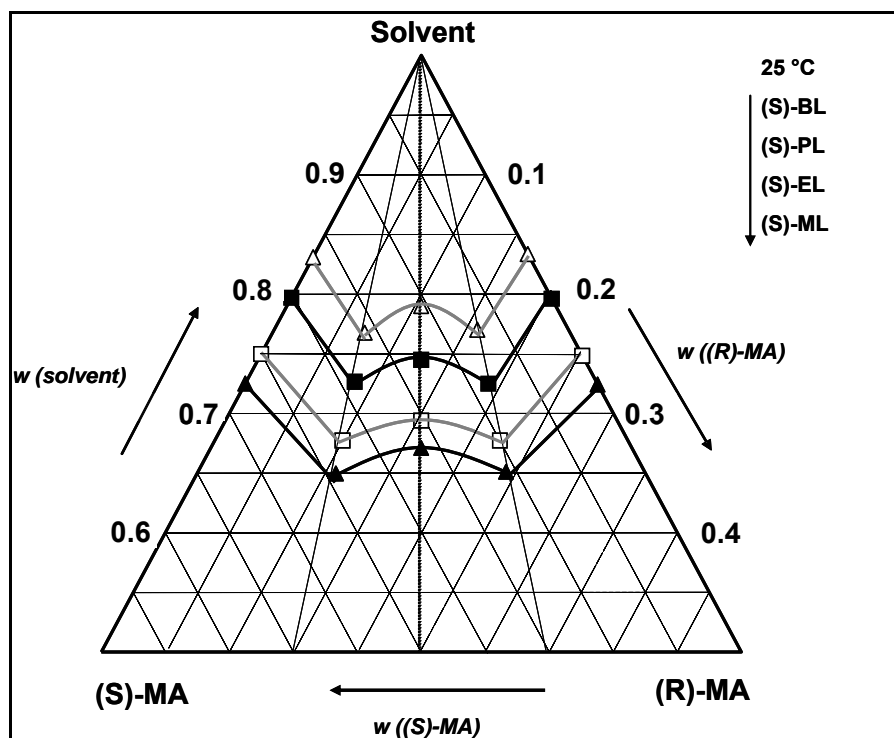
Figure 53: Ternary phase diagram of mandelic acid in different "classical" chiral solvent at 25 °C. Axes in weight fractions*; w_(S)-MA* and w_(R)-MA ≤ 0.5. The isothermal lines have been added as a visualization aid and only the marked points show measured data.

Molecular modeling calculations were performed to understand the effect of chain length of the chiral solvents and how it affects the potential for enantioselective crystallization. The molecular modeling calculations have revealed that the chain length has no influence on the chiral recognition since a change does not offer better interactions. The stabilization enthalpy ($\Delta H_{form}^{Stabilization}$) is derived from the enthalpy of formation of the dimer molecules (ΔH_{form}^{Dimer}) minus the enthalpy of formation of the single molecules of the solute and also solvent ($\Delta H_{form}^{Solute} + \Delta H_{form}^{Solvent}$). The stabilization enthalpy ($\Delta H_{form}^{Stabilization}$) is derived by this means of subtracting the summation of the single molecules ($\Delta H_{form}^{Solute} + \Delta H_{form}^{Solvent}$) from that of the dimer (ΔH_{form}^{Dimer}), since Davey et al.[89] reported that mandelic acid in all other solvents except chloroform in solution is strongly solvated. From thermodynamic point of view the dimer

with more negative $\Delta H_{form}^{Stabilization}$ is suppose to be more stable thermodynamically. Figure 54 illustrates a schematic representation of optimized molecular structures of the dimer of (a) (*S*)-mandelic acid and (*S*)-methyl lactate with lactate part hydrogen interaction, and (b) (*S*)-mandelic acid and (*S*)-methyl lactate with the carbon chain hydrogen interaction, respectively.
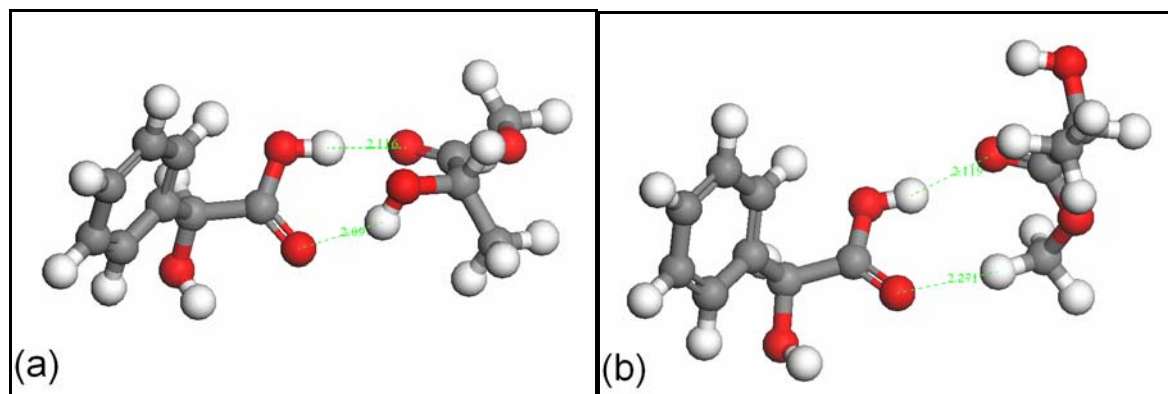
Figure 54: Schematic representation of optimized molecular structures of the dimer of (a) (*S*)-mandelic acid and (S)-methyl lactate with hydrogen bond interactions only at the lactate part of the molecule and (b) (S)-mandelic acid and (S)-methyl lactate with carbon chain hydrogen interactions, respectively.

The expected classical interaction is the one that would take place at the lactate part of the molecule (i.e. C=O….O-H at both points). This case of interaction is the one depicted in Figure 54(a), and should be stronger interactions compared to the (C=O….H-C and C=O….O-H) illustrated in Figure 54(b). Table 14 gives the geometry-optimized energy values for the single and dimer molecules considered.

Table 14: Summary of results of ΔH_{form} of individual molecules and dimers of (*S*)-MA in (*S*)-methyl lactate (lactate base hydrogen interaction) and (*S*)-MA and (*S*)-methyl lactate (carbon chain hydrogen interaction)**.**

Single molecule energies		Dimer energies		Stabilization enthalpy
Single molecules	$\Delta H_{form}^{Solute\,/\,Solvent}$ (kcal/mol)	Dimer types	ΔH_{form}^{Dimer} (kcal/mol)	$\Delta H_{form}^{Stabilization}$ [ΔH_{form}^{Dimer} - ($\Delta H_{form}^{Solute} + \Delta H_{form}^{Solvent}$)] (kcal/mol)
(*S*)-MA	-117.56			
(*S*)-ML	-146.14	(*S*)-MA-(*S*)-ML$_{lactate\ part}$	-270.00	-6.30
(*S*)-MA	-117.56			
(*S*)-ML	-146.14	(*S*)-MA-(*S*)-ML$_{carbon\ chain}$	-268.07	-4.37

MA, mandelic acid; ML, methyl lactate

The results obtained from the molecular modeling summarized in Table 14 indicate that $\Delta H_{form}^{Stabilization}$ of (*S*)-mandelic acid and (*S*)-methyl lactate dimer with hydrogen bond interactions only at the lactate part of the molecule is more negative (-6.3 kcal/mol) compared to that of (*S*)-mandelic acid and (*S*)-methyl lactate which is less negative (-4.37 kcal/mol). This shows that interaction with the lactate part of the molecule would be preferred to the carbon chain one. Therefore these molecular modeling calculations confirm that no asymmetry was observed for different chain lengths of the lactates.

Furthermore, to understand why by increasing the chain length of "classical" chiral solvents (lactates) results in less solubilities and the vice versa, molecular modeling calculations were made between (*S*)-mandelic acid and two lactates, (*S*)-methyl lactate and (*S*)-butyl lactate. Figure 55 depicts a schematic representation of optimized molecular structures of the dimer of (a) (*S*)-mandelic acid and (*S*)-methyl lactate, and (b) (*S*)-mandelic acid and (*S*)-butyl lactate, respectively.
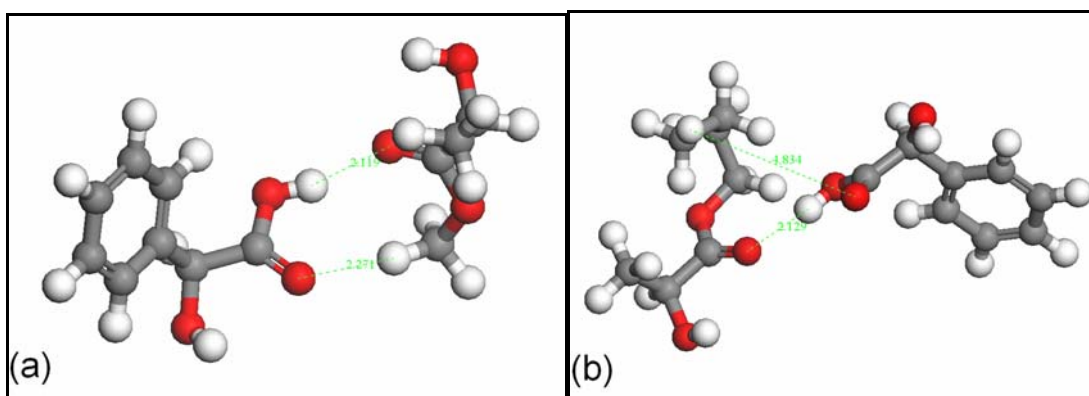
Figure 55: Schematic representation of optimized molecular structures of the dimer of (a) (*S*)-mandelic acid and (*S*)-methyl lactate and (b) (*S*)-mandelic acid and (*S*)-butyl lactate, respectively.

Table 15 gives the geometry-optimized energy values for the single and dimer molecules considered. The $\Delta H_{form}^{Stabilization}$ of (*S*)-mandelic acid and (*S*)-methyl lactate dimer with hydrogen bond interactions at lactate and the carbon chain part of the molecule is more negative (-4.37 kcal/mol) compared to that of (*S*)-mandelic acid and (*S*)-butyl lactate dimer with also hydrogen bond interactions at lactate and the carbon chain part of the molecule which is less negative (-3.27 kcal/mol).

Therefore, according to thermodynamics the (*S*)-mandelic acid in (*S*)-methyl lactate dimer should be more stable and as a consequence should be more soluble compared to the (*S*)-mandelic acid in (*S*)-butyl lactate dimer. So, the results from the molecular modeling support that the (*S*)-methyl lactate dissolves best compared to the other lactates studied (see Figure 53).

Table 15: Summary of results of ΔH_{form} of individual molecules and dimers of (*S*)-MA in (*S*)-methyl lactate (lactate and carbon chain hydrogen interaction) and (*S*)-MA and (*S*)-butyl lactate (lactate and carbon chain hydrogen interaction)**.**

Single molecule energies		Dimer energies		Stabilization enthalpy
Single molecules	ΔH_{form}^{Dimer} (kcal/mol)	Dimer types	ΔH_{form}^{Dimer} (kcal/mol)	$\Delta H_{form}^{Stabilization}$ [ΔH_{form}^{Dimer} - ($\Delta H_{form}^{Solute} + \Delta H_{form}^{Solvent}$)] (kcal/mol)
(*S*)-MA	-117.56			
(*S*)-ML	-146.14	(*S*)-MA-(S)-ML	-268.07	-4.37
(*S*)-MA	-117.56			
(*S*)-BL	-164.17	(*S*)-MA-(S)-BL	-285.00	-3.27

MA, mandelic acid; ML, methyl lactate; BL, butyl lactate

Solid phase analysis

The solubility measurements were accompanied by XRPD solid phase analyses to check for new phases. The solid phase analyses were performed since there is the possibility, for example for mandelic acid to partially decompose at higher temperatures (see chapter 4, section 4.2.1.3).[47,133,139,140] Figure 56 depicts experimental XRPD patterns for solid phases obtained during the solubility measurements of mandelic acid in (*S*)-ethyl lactate at 15 °C. Different compositions of the chiral species are included. In each case the reflexes of the racemic compound and/or the mandelic acid enantiomer are clearly distinguishable. Typical reflexes characterizing the different species are indicated by grey to black colors, e.g. the reflex at 6.0° is typical for the enantiomer, and reflex at 10.84° is typical for the racemic compound. The results for the eutectic compositions (~ 38 % ee) show consistently reflexes of both the enantiomer and the racemate. No new phases were found.

The solid phase analysis was also performed for the mandelic acid/(*S*)-butyl lactate system. Also the other lactates were studied in this thesis. In the solid phase analysis no new phases were observed. This clearly confirms that the entire solid phases had no additional or new phases (neither polymorphs nor solvates) differing from those of the pure enantiomers identified from the results of the crystal lattice analysis by XRPD.
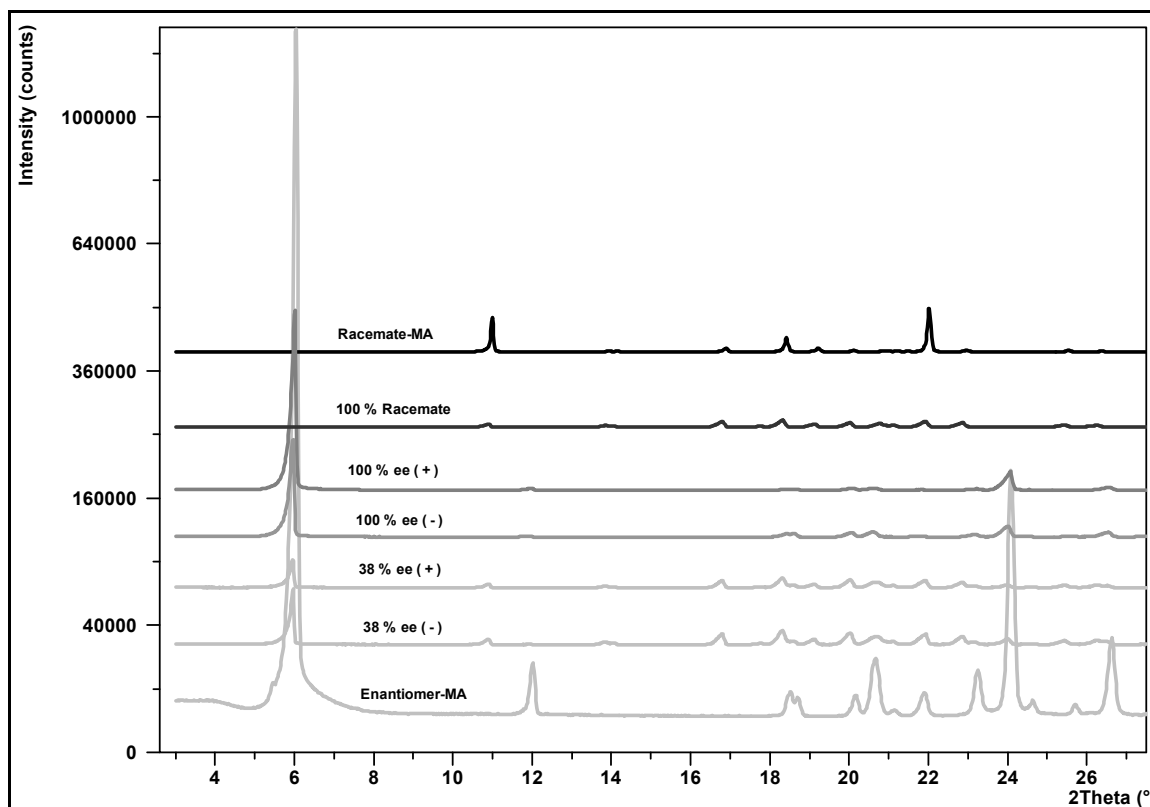
Figure 56: Experimental XRPD patterns for pure enantiomers and the racemate of mandelic acid, and the experimental compositions from (*S*)-ethyl lactate and mandelic acid at 15 °C.

The other "classical" chiral solvent studied in this work is (*2R,3R*)-diethyl tartrate. The solubility data measured are summarized in Tables 16. Figure 57 illustrates the ternary solubility phase diagrams of the mandelic acid enantiomers in (*2R,3R*)-diethyl tartrate at temperature ranging from 25 to 60 °C.

Table 16: Mass fraction solubility (w_i) of (*S*)-Mandelic acid (1) and (*R*)-Mandelic acid (2) in (*2R,3R*)-diethyl tartrate at different enantiomeric excesses (ee) $\left[ee = |w_1 - w_2|/(w_1 + w_2)\right]$ and temperatures.

100 ee	100 (w_1+w_2)	100 w_1	100 w_2	100 $w_{solvent}$
		t = 25 °C		
100.00	13.34	13.34	0.00	86.66
66.84	15.08	12.58	2.50	84.92
55.26	17.03	13.22	3.81	82.97
40.36	19.54	13.71	5.83	80.46
1.32	16.84	8.53	8.31	83.16
41.32	20.05	5.88	14.17	79.95
100.00	13.24	0.00	13.24	86.76
		t = 35 °C		
100.00	17.03	17.03	0.00	82.97
70.00	19.26	16.37	2.89	80.74
54.48	21.58	16.67	4.91	78.42

Continuation of Table 16

38.18	24.93	17.22	7.71	75.07
17.90	23.71	13.98	9.73	76.29
37.02	24.93	7.85	17.08	75.07
0.20	21.36	10.70	10.66	78.64
100.00	17.01	0.00	17.01	82.99
		t = 45 °C		
100.00	20.00	20.00	0.00	80.00
76.86	23.25	20.56	2.69	76.75
55.96	26.99	21.05	5.94	73.01
39.94	31.12	21.77	9.35	68.88
23.50	29.15	18.00	11.15	70.85
37.80	31.15	9.69	21.46	68.85
0.20	25.68	12.87	12.81	74.32
100.00	19.11	0.00	19.11	80.89
		t = 50 °C		
100.00	22.87	22.87	0.00	77.13
36.72	32.49	22.21	10.28	67.51
37.86	32.30	10.04	22.26	67.70
0.54	29.44	14.80	14.64	70.56
100.00	22.28	0.00	22.28	77.72
		t = 55 °C		
100.00	24.15	24.15	0.00	75.85
38.04	36.63	25.28	11.36	63.37
39.02	35.95	10.96	24.99	64.05
0.20	31.66	15.86	15.80	68.34
100.00	24.10	0.00	24.10	75.90
		t = 60 °C		
100.00	26.07	26.07	0.00	73.93
36.82	41.98	28.72	13.26	58.02
37.86	40.50	12.58	27.92	59.50
0.54	36.45	18.32	18.13	63.55
100.00	26.31	0.00	26.31	73.69

The ternary solubility phase diagram (see Figure 57) was derived from the solubility data in Table 16. The solubility isotherms reveal again the compound forming character of the mandelic acid system. The diagram shows symmetry with respect to the racemic axis rather than asymmetry, which could be in principle possible in the case of chiral solvents. The ratio of the enantiomers at the symmetric eutectic compositions remained unchanged with temperature and was found at a fraction of 0.69 and 0.31.
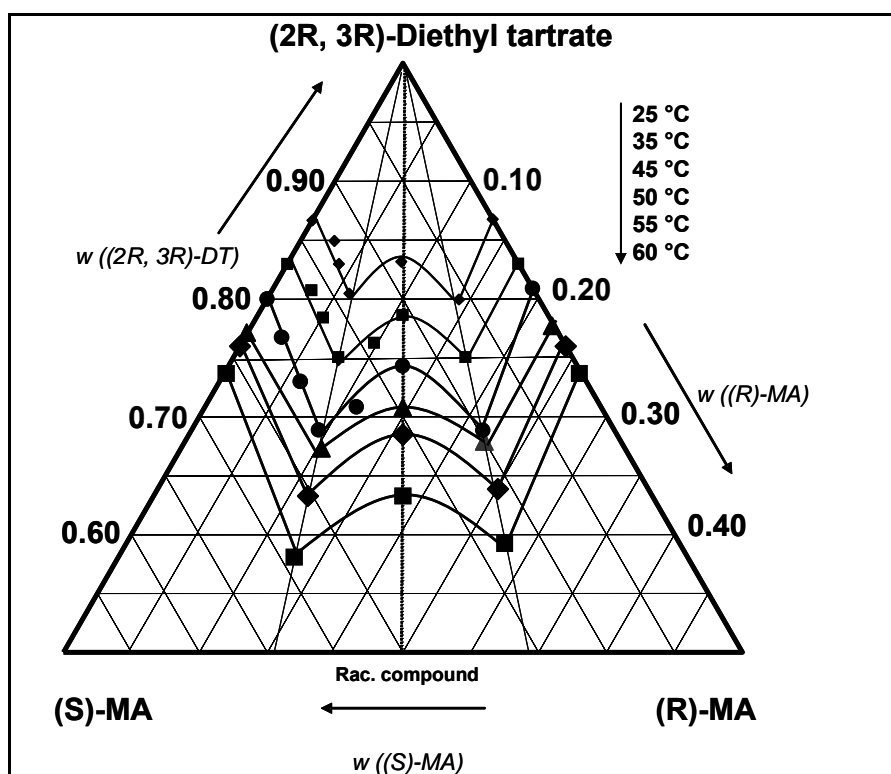
Figure 57: Ternary phase diagram of the mandelic acid enantiomers in (*2R,3R*)-diethyl tartrate (solubility isotherms between 25 and 60 °C). Axes in weight fraction; $w_{(S)\text{-MA}}$ and $w_{(R)\text{-MA}} \leq 0.5$. The isothermal lines have been added as a visualization aid and only the marked points show measured data.

The same general shape of the solubility isotherm was observed in the entire ternary solubility phase diagram as for the "classical" chiral solvents. Also it became obvious that there was no measurable chiral recognition of the mandelic acid and the "classical" chiral solvent studied.

Raman spectra

In this work also Raman spectroscopy was also used to investigate the interaction between the solute and the solvent molecules. The investigations were restricted to mandelic acid and the "classical" chiral solvents, because mandelic acid being a compound forming system is more difficult to resolve, and therefore a good candidate to check for whether there exists measurable chiral interaction between the solute-solvent molecules. Unfortunately, Raman spectra measurements were not feasible for the tailor-made chiral solvents used in this thesis work due to overlapping spectra of the mandelic acid functional groups and the mandelates. Moreover, since there are no differences between the (*S*)- and (*R*)-mandelic acid spectra in all the "classical" chiral solvent studied, only the spectra of (*S*)- and (*R*)-mandelic acid in the two "classical" chiral solvent, (*S*)-ethyl lactate and (*2R,3R*)-diethyl tartrate were measured. The Raman spectra of the other lactates, (S)-methyl lactate, (*S*)-propyl lactate and (*S*)-butyl lactate

are included in the Appendix D. The Raman spectra of (*S*)- and (*R*)-mandelic acid in both (*S*)-ethyl lactate and (*2R,3R*)-diethyl tartrate respectively are shown in Figures 58 and 59.
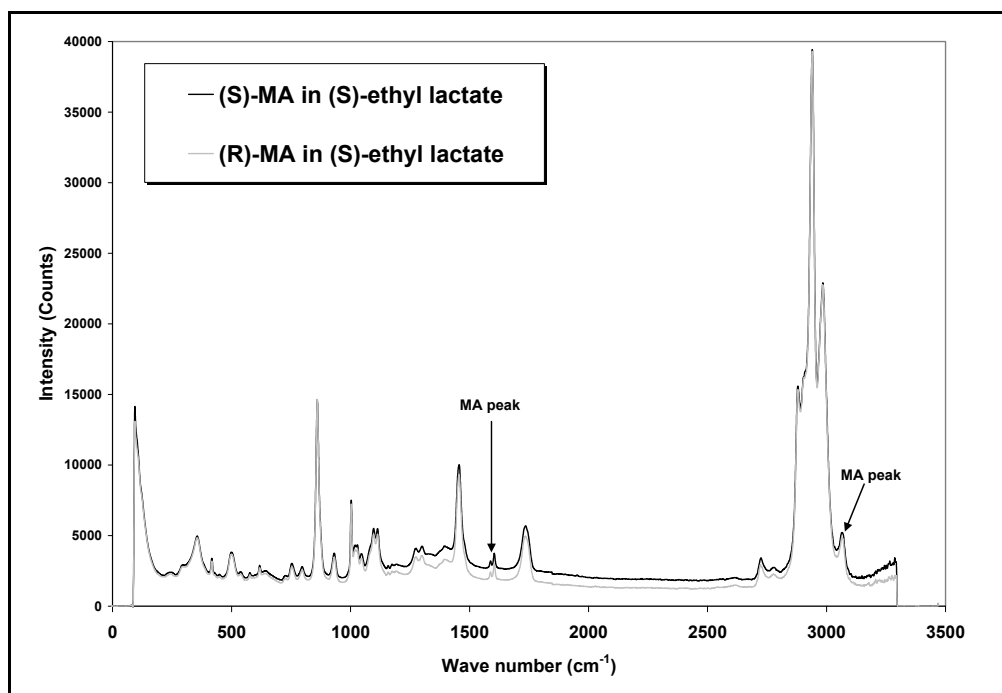
Figure 58: Raman spectra of (*S*)- and (*R*)-mandelic acid in (*S*)-ethyl lactate (liquid phase samples, and concentration of 8 wt %).
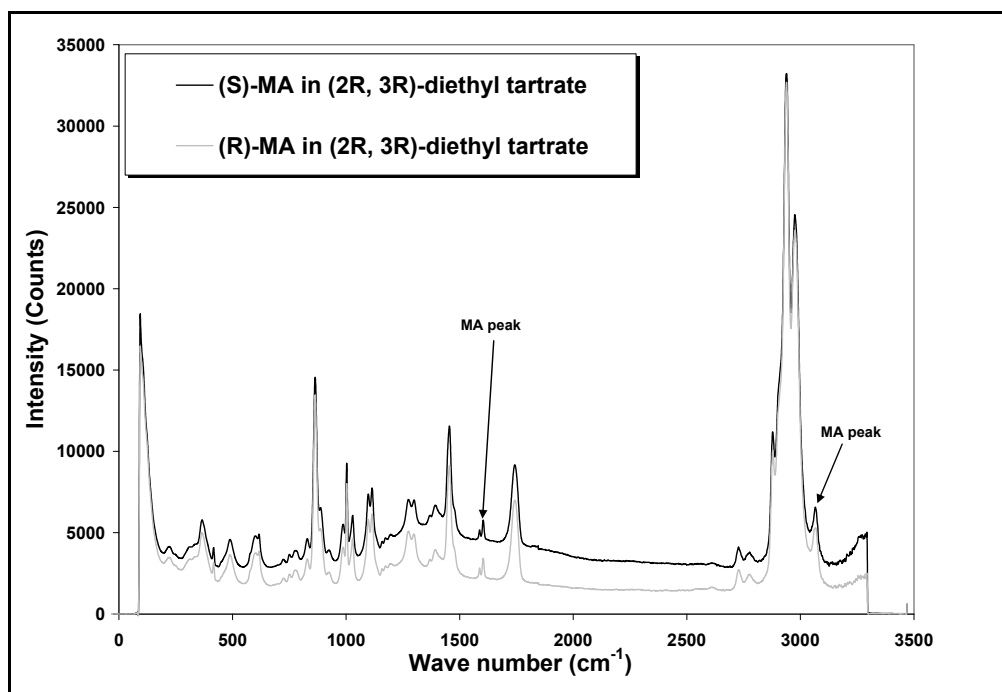
Figure 59: Raman spectra of (*S*)- and (*R*)-mandelic acid in (*2R,3R*)-diethyl tartrate (liquid phase samples, and concentration of 8 wt %).

In both Figures 58 and 59, the Raman spectra of (*S*)- and (*R*)-mandelic acid in both (*S*)-ethyl lactate and (*2R,3R*)-diethyl tartrate are identical to each other. Since there are no differences in the spectra of (*S*)- and (*R*)-mandelic acid in both chiral solvents, the results indicate again the absence of measurable interactions of the chiral molecules and the chiral solvent in the liquid phase.

Solid phase analysis

Solid phase analysis was also conducted for the other "classical" chiral solvent, (*2R,3R*)-diethyl tartrate. Figure 60 depicts experimental XRPD patterns for solid phases obtained from the solubility measurements at higher temperatures for mandelic acid in (*2R,3R*)-diethyl tartrate at 60 °C. The solid phase analyses were performed since there is the possibility for mandelic acid to partially decompose at higher temperatures which has been discussed already. Further, the absence of solvate phases was checked. Different compositions of the chiral species are included. It can be derived that in each case just the reflexes of the racemic compound and/or the mandelic acid enantiomer are clearly evident. Thus the absence of new phases in the working range of the crystallization experiments is confirmed.
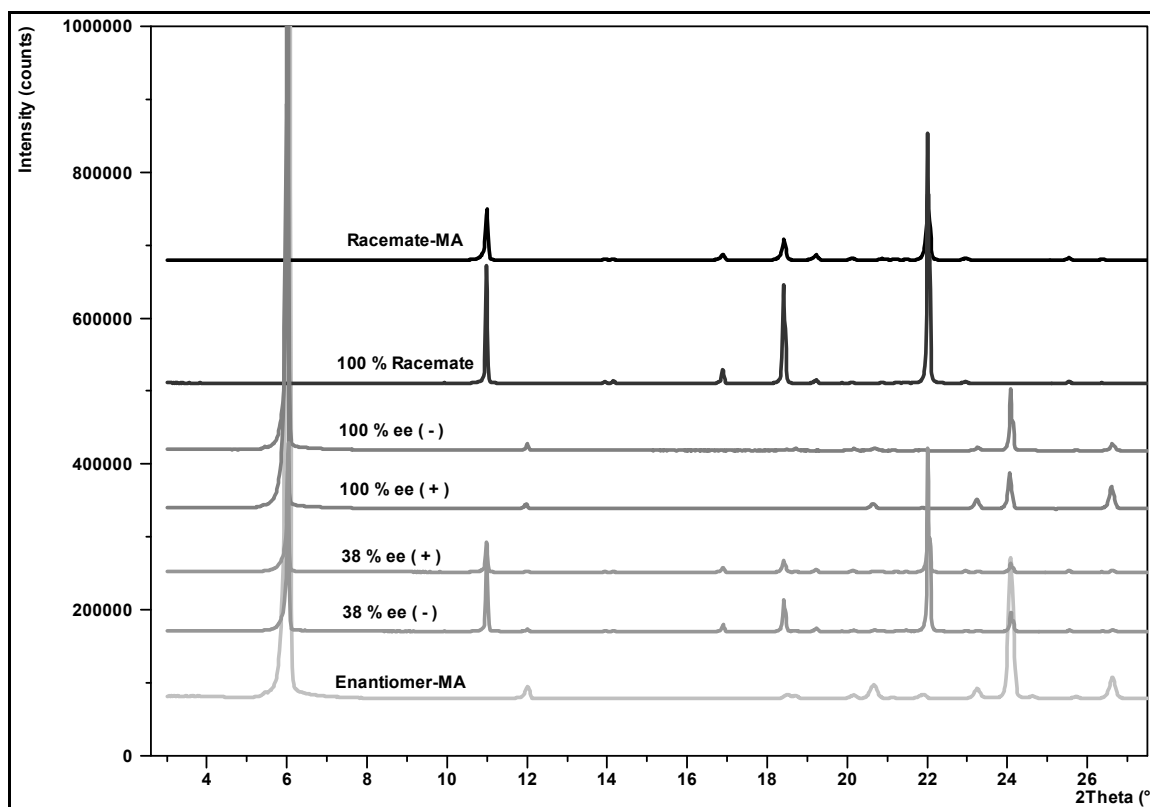
Figure 60: Experimental XRPD patterns for pure enantiomers and the racemate of mandelic acid (MA), and different experimental compositions from (*2R,3R*)-diethyl tartrate and mandelic acid at 60 °C.

The standard deviations for the solubility data measured were calculated by Equation 22 with n being the numbers of experiments. The results of standard deviation of the solubility data for mandelic acid in the "classical" chiral solvents are compiled in Table 17.

Table 17: Error Analysis of Solubility Determination Procedure (standard deviation SD according to Equation 22 in chapter 3, number of experiments *n*).

t / °C	(*S*)- and (*R*)-mandelic acid in (*S*)-methyl lactate	
	n	SD
25	4	0.46
t / °C	(*S*)- and (*R*)-mandelic acid in (*S*)-ethyl lactate	
	n	SD
0	4	0.36
25	4	0.60
t / °C	(*S*)- and (*R*)-mandelic acid in (*S*)-propyl lactate	
	n	SD
25	3	0.03
t / °C	(*S*)- and (*R*)-mandelic acid in (*S*)-butyl lactate	
	n	SD
25	3	0.49
t / °C	(*S*)- and (*R*)-mandelic acid in (*2R,3R*)-diethyl tartrate	
	n	SD
25	4	0.36
60	4	0.51

The standard deviation of the solubility data of the racemic mandelic acid are in the same range as the as the summarized SD in Table 17.

4.3.1.2 N-methylephedrine in "classical" chiral solvent

The solubility data are compiled in Tables 18 and 19 for N-methylephedrine enantiomers in (*S*)-ethyl lactate and (*2R,3R*)-diethyl tartrate, respectively. Whiles Figures 61 and 62 illustrate the resulting ternary solubility phase diagrams of the N-methylephedrine enantiomers in (*S*)-ethyl lactate and (*2R,3R*)-diethyl tartrate, respectively. The diagram reveals symmetry with

respect to the racemic axis, rather than asymmetry which in principle is possible in chiral solvents. As known from the binary phase diagram of the chiral system, N-methylephedrine enantiomers do not form a racemic compound but rather a simple eutectic (conglomerate) system.[101] This was confirmed by the determined ternary solubility phase diagrams. Symmetry verification was carried out by detailed measurement of selected solubility isotherms.

Table 18: Mass fraction solubility (w_i) of (1S,2R)-(+)-N-methylephedrine (3) and (1R,2S)-(-)-N-methylephedrine (4) in (S)-ethyl lactate at different enantiomeric excesses ee $\left[ee = |w_3 - w_4|/(w_3 + w_4)\right]$ in the liquid phase and for different temperatures.

100 ee	100 (w_3+w_4)	100 w_3	100 w_4	100 $w_{solvent}$
		t = 0 C		
100.00	11.68	11.68	0.00	88.32
40.00	17.19	12.03	5.16	82.81
0.00	21.96	10.98	10.98	78.04
40.00	17.09	5.13	11.96	82.91
100.00	11.10	0.00	11.10	88.90
		t = 5 C		
100.00	15.00	15.00	0.00	85.00
40.00	18.20	12.74	5.46	81.80
0.00	27.75	13.88	13.87	72.25
44.00	18.92	5.30	13.62	81.08
100.00	15.10	0.00	15.10	84.90
		t = 15 C		
100.00	18.73	18.73	0.00	81.27
50.00	23.31	17.48	5.83	76.69
0.00	34.50	17.25	17.25	65.50
40.00	23.31	6.99	16.32	76.69
100	19.26	0.00	19.26	80.74
		t = 25 C		
100.00	21.12	21.12	0.00	78.88
40.00	30.18	21.13	9.05	69.82
0.00	41.82	20.91	20.91	58.18

40.00	30.28	9.08	21.20	69.72
100.00	21.29	0.00	21.29	78.71

Table 19: Mass Fraction Solubility (w_i) of (1S, 2R)-(+)-N-methylephedrine (3) and (1R,2S)-(-)-N-methylephedrine (4) in (*2R,3R*)-diethyl tartrate at different enantiomeric excesses ee $\left[ee = \left| w_3 - w_4 \right| / (w_3 + w_4) \right]$ in the liquid phase and for different temperatures.

100 ee	100 (w_3+w_4)	100 w_3	100 w_4	100 $w_{solvent}$
t = 25 C				
100.00	23.67	23.67	0.00	76.33
50.00	29.24	21.93	7.31	70.76
0.00	42.00	21.00	21.00	58.00
50.00	29.24	7.31	21.93	70.76
100.00	23.67	0.00	23.67	76.33
t = 30 C				
100.00	28.00	28.00	00.00	72.00
40.00	33.00	23.10	9.90	67.00
0.00	46.50	23.25	23.25	53.50
40.00	33.00	9.90	23.10	67.00
100.00	29.00	29.00	0.00	71.00
t = 35 C				
100.00	30.29	30.29	0.00	69.71
50.00	35.40	26.55	8.85	64.60
0.00	49.20	24.60	24.60	50.80
50.00	35.40	8.85	26.55	64.60
100	30.29	0.00	30.29	69.71
t = 40 C				
100.00	36.28	36.28	0.00	63.72
30.00	44.75	29.09	15.66	55.25
0.00	55.58	27.79	27.79	44.42
50.00	40.99	10.25	30.74	59.01
100.00	35.63	0.00	35.63	64.37
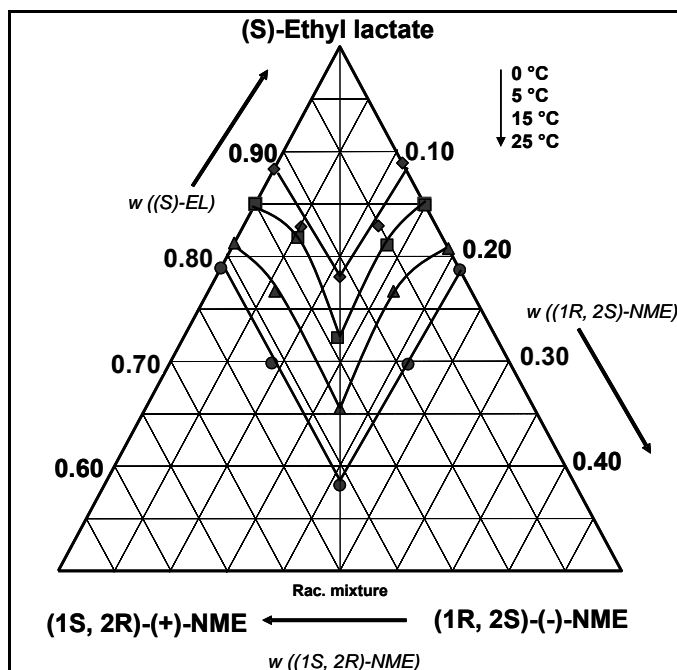
Figure 61: Ternary phase diagram of N-methylephedrine in (*S*)-ethyl lactate at different temperatures. Axes in weight fractions; $w_{(S)-MA}$ and $w_{(R)-MA} \leq 0.5$. The isothermal lines have been added as a visualization aid and only the marked points show measured data.
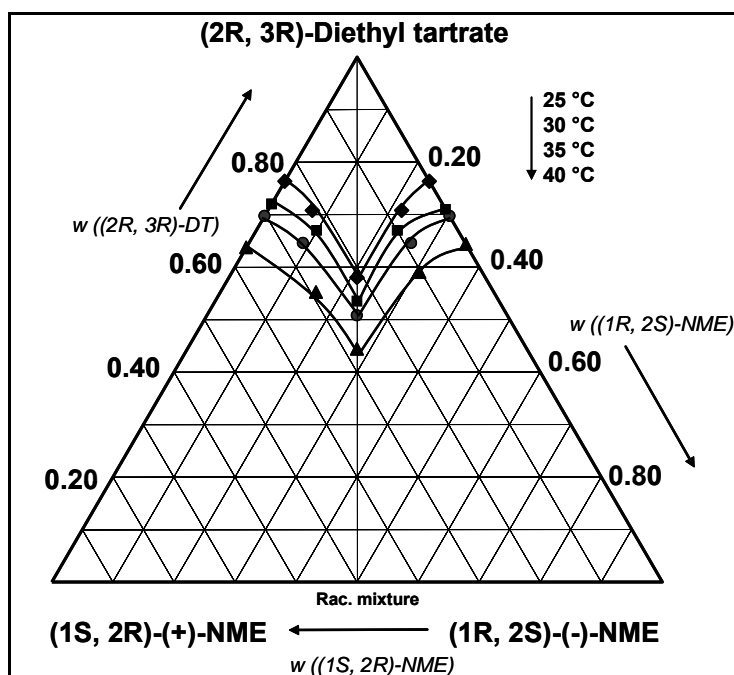
Figure 62: Ternary phase diagram of N-methylephedrine in (*2R,3R*)-diethyl tartrate at different temperatures. Axes in weight fractions; $w_{(+)-NME}$ and $w_{(-)-NME} \leq 1.0$. The isothermal lines have been added as a visualization aid and only the marked points show measured data.

The same general shape was observed in both Figures, while the solubility isotherms are clearly steeper in (*S*)-ethyl lactate than in (*2R,3R*)-diethyl tartrate, which is quantified in the so called solubility ratio (α_{mol}). The α_{mol} is defined as the ratio of the racemate solubility to that of the enantiomers solubility (both evaluated in mole fractions). It has been determined

109

for (S)-ethyl lactate to be about 2 (1.95 and 2.14 at 0 °C and 25 °C, respectively) and for (*2R,3R*)-diethyl tartrate to be smaller than 2 (1.73 and 1.49 at 25 °C and 40 °C, respectively), which shows a clear deviation from ideal behavior. One has to be aware that this statement does hold only in one direction. An ideal systems always exhibits α_{mol}=2 according to the "double solubility" rule by Meyerhoffer[38], while also very nonideal systems like the N-methylephedrine/(*S*)-ethyl lactate can have α_{mol} close to two. A comprehensive discussion on α_{mol} close to two but not ideal will be outlined in the next section which deals with the investigation of effect of chain length of lactates.

The solubility ratio has a large influence on the metastable zone width (MSZW), smaller α_{mol} values ($\alpha_{mol} < 2$) account for possibly larger MSZW[35], which can be exploited for entrainment processes, i.e. preferential crystallization. Figure 63 depicts the different solubility isotherm slope and how they affect the α_{mol} values. The Figure shows two examples, i.e. situation where the isotherm is really bent ($\alpha_{mol} << 2$), or steeper ($\alpha_{mol} > 2$). It is clearly shown in Figure 63(a) that the metastable solubility line allows a wider area for entrainment, as compared to Figure 63(b). The behavior of the ternary solubility phase diagram of N-methylepherdrine in (*2R,3R*)-diethyl tartrate system resembles a situation in between the two cases, i.e. Figures 63(a) and 63(b), N-methylephedrine in (*S*)-ethyl lactate is related to Figure 63(b). Therefore, (*2R,3R*)-diethyl tartrate is considered to be the better "classical" chiral solvent for a chiral separation of the considered pair of enantiomers due to lower corresponding α_{mol} values.
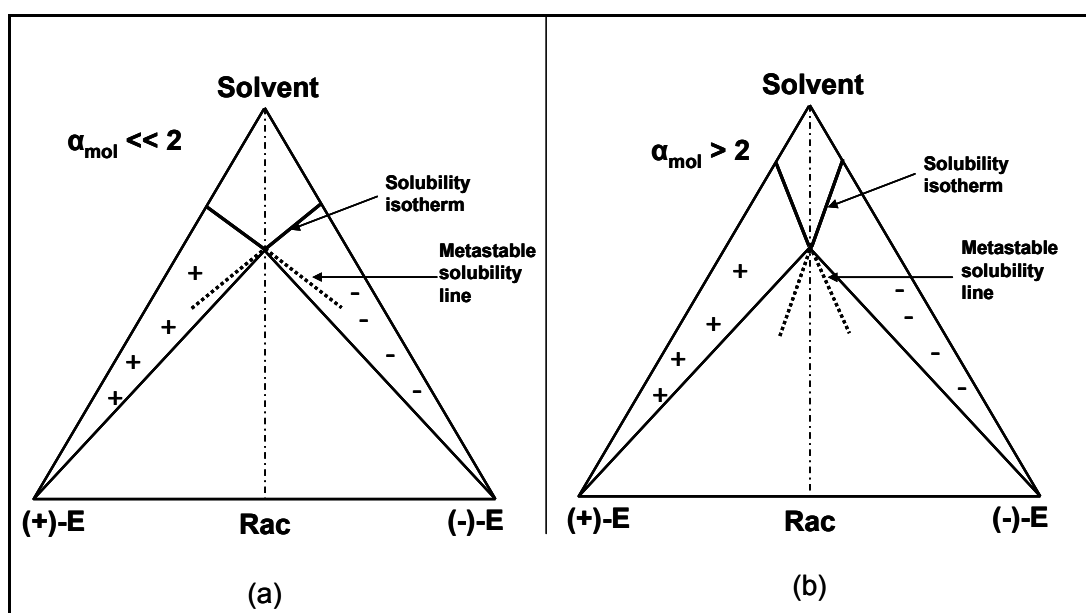
Figure 63: Schematic ternary solubility phase diagram course of showing metastable solubility line for a conglomerate system, with (a) $\alpha_{mol} << 2$ and (b) $\alpha_{mol} > 2$, respectively.

A comprehensive discussion of this aspect can be found by Collet et. al., Levilain et al. and Polenske et.al.[33,141,142] Considering the solubility ratios evaluated from the determined ternary solubility phase diagrams of N-methylephedrine in (*2R,3R*)-diethyl tartrate there is the possibility for a wide area for entrainment, i.e. it should be in same cases possible even to enter the two phase region of the phase diagrams via crystallization, which would be more lucrative for obtaining enantiopure crystals. Thus, in particular (*2R,3R*)-diethyl tartrate seems to be the better solvent due to the lower α_{mol} values. Thus, a well defined exploitation of selective kinetic effects for enantioselective crystallization appears to be promising.

Investigation into different chain length of the lactates

Investigations were also carried out to verify the effect of chain length of lactates on the shape of the isotherm in the ternary phase diagram. As a case study the different lactates, (*S*)-methyl lactate, (*S*)-ethyl lactate, (*S*)-propyl lactate and (*S*)-butyl lactate were studied. Thus, four different "classical" chiral solvents with varying chain length were employed.

Table 20: Solubilities of Enantiomer and Racemate N-methylephedrine and α_{mol} Values for the Different Lactates at 25 °C.

Solvents	Enantiomer solubility (mol %)	Racemate solubility (mol %)	α_{mol} values
(*S*)-methyl lactate	15.791	32.350	2.05
(*S*)-ethyl lactate	14.997	32.142	2.14
(*S*)-propyl lactate	15.709	32.345	2.06
(*S*)-butyl lactate	15.706	32.552	2.07

Table 20 gives a compilation of the solubilities of enantiomer and the racemate and their corresponding α_{mol} values of N-methylephedrine in the different lactates at 25 °C. Though the α_{mol} values are close to 2, and which has been discussed in the previous section, but they do not show ideality. Illustration of the deviation of the (*S*)-butyl lactate with (α_{mol}-value equal to 2 is considered for the plot) from ideal behavior has been shown in Figure 64. The ideal solubilities were derived from the Schröder van Laar equation (Chapter 2, Equation 18), using the enthalpy of fusion ΔH_{fus} and the melting temperatures T_m for the N-methylephedrine enantiomers taken from Wang et al.[102]
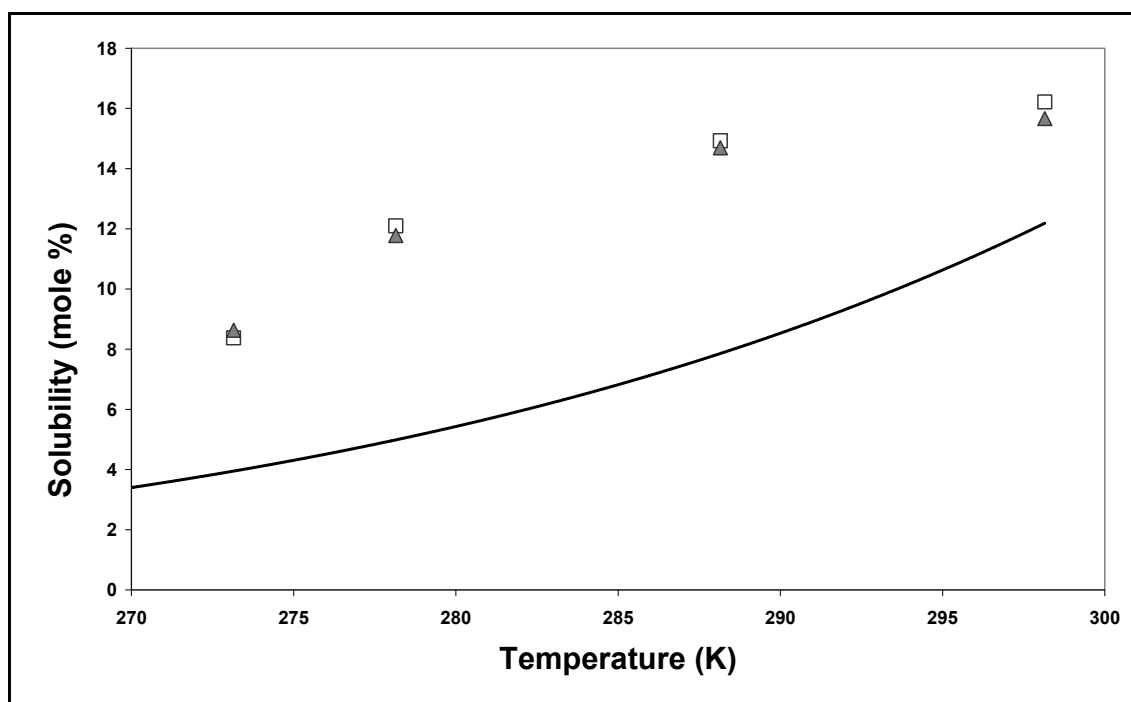
Figure 64: Solubility in mole% of ▲, (*1S,2R*)-(+)-N-methylephedrine and □, (*1R,2S*)-(-)-N-methylephedrine in (*S*)-butyl lactate between 273 K and 298 K. Symbols are measurements, solid line: ideal solubility.

The solvents considered are methyl lactate, ethyl lactate, propyl lactate and butyl lactate. Figure 65 illustrates ternary solubility phase diagram of N-methylephedrine in different classical chiral solvents at 25 °C. The diagrams also show no asymmetry which implies no measurable discrimination was observed. It is evident that solubility increases with decreasing chain length of the chiral solvents, from (*S*)-butyl lactate to methyl lactate, which is attributed to the increase in the polarity of smaller chain length for instance (*S*)-methyl lactate. This effect has also been explained by the molecular modeling calculations in the early discussions for mandelic acid system. A summary of all the entire solubility data obtained from the measurements is compiled in Table 21.

Table 21: Mass Fraction Solubility (w_i) of (1S, 2R)-(+)-N-methylephedrine (3) and (1R, 2S)-(-)-N-methylephedrine (4) in different "classical" chiral solvents at different Enantiomeric Excesses (ee) $\left[ee = |w_3 - w_4|/(w_3 + w_4)\right]$ and at temperature 25 °C.

100 ee	100 ($w_{3+}w_4$)	100 w_3	100 w_4	100 $w_{solvent}$
		(S)-ML		
100.00	24.41	24.41	0.00	75.59
39.09	35.06	24.38	10.68	64.94
0.97	45.16	22.80	22.36	54.84
39.40	35.06	10.62	24.44	64.94
100.00	24.50	0.00	24.50	75.50

(S)-EL

Continuation Table 21

100.00	21.12	21.12	0.00	78.88
42.00	31.00	22.01	8.99	69.00
0.47	41.82	21.01	20.81	58.18
42.00	30.28	8.78	21.50	67.73
100.00	21.29	0.00	21.29	74.83
	(S)-PL			
100.00	20.18	20.18	0.00	79.82
38.85	28.88	20.05	8.83	71.12
0.84	39.34	19.84	19.50	60.66
37.56	29.53	9.22	20.31	70.47
100.00	20.76	0.00	20.76	79.24
	(S)-BL			
100.00	18.60	18.60	0.00	81.40
40.50	27.07	19.02	8.05	72.93
1.43	37.18	18.85	18.33	62.82
37.10	27.85	8.76	19.09	72.15
100.00	18.55	0.00	18.55	81.45

(*S*)-ML, (*S*)-methyl lactate; (*S*)-EL, (*S*)-ethyl lactate; (*S*)-PL, (*S*)-methyl lactate; (*S*)-BL, (*S*)-butyl lactate
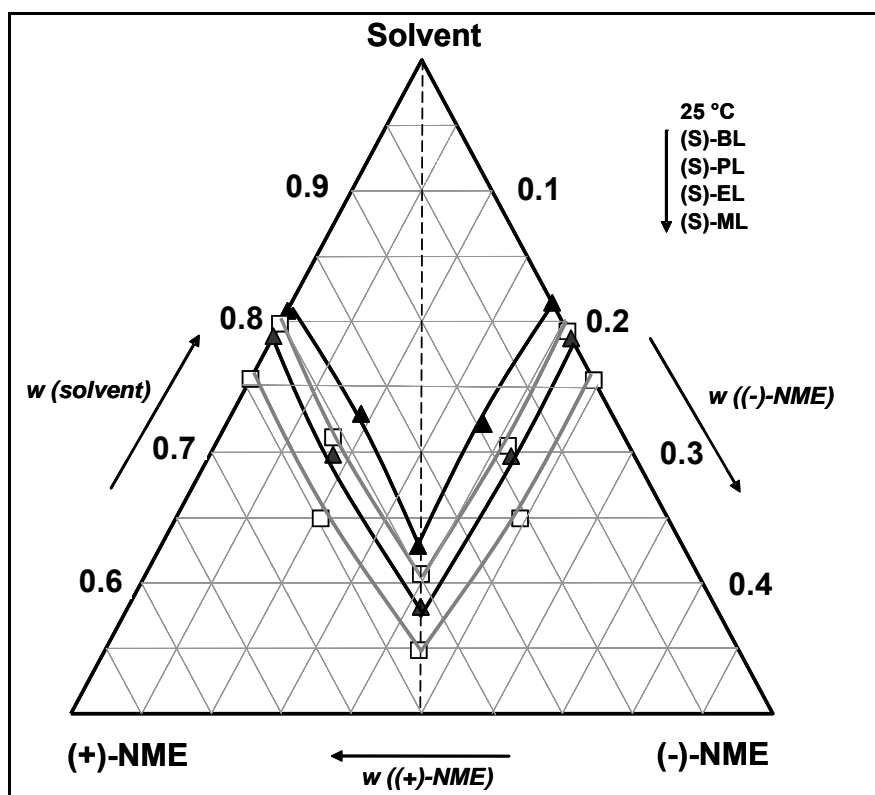
Figure 65: Ternary phase diagram of N-methylephedrine in different "classical" chiral solvent at 25 °C. Axes in weight fractions; $w_{(+)-NME}$ and $w_{(-)-NME}$ ≤ 0.5. The isothermal lines have been added as a visualization aid and only the marked points show measured data.

Here, molecular modeling calculations were not done since already for the mandelic acid system detailed discussion was made and the same trends were expected here.

Solid phase analysis

Figure 66 illustrates experimental XRPD patterns for the solid phases obtained in solubility measurement for N-methylephedrine in (*S*)-ethyl lactate at 15 °C. Since N-methylephedrine in (*S*)-ethyl lactate is clearly a conglomerate forming system (see Figure 65), so the reflexes of the enantiomers and the racemic mixture must be identical. Deviations in the patterns would indicate the presence of different phases like a solvate or a polymorph. The various compositions really mimic the reference reflexes in the XRPD patterns, i.e. no new phases exist. Also the solid phases for N-methylephedrine in (*2R,3R*)-diethyl tartrate were checked. In this case no additional or new phases were formed in the crystal lattice.
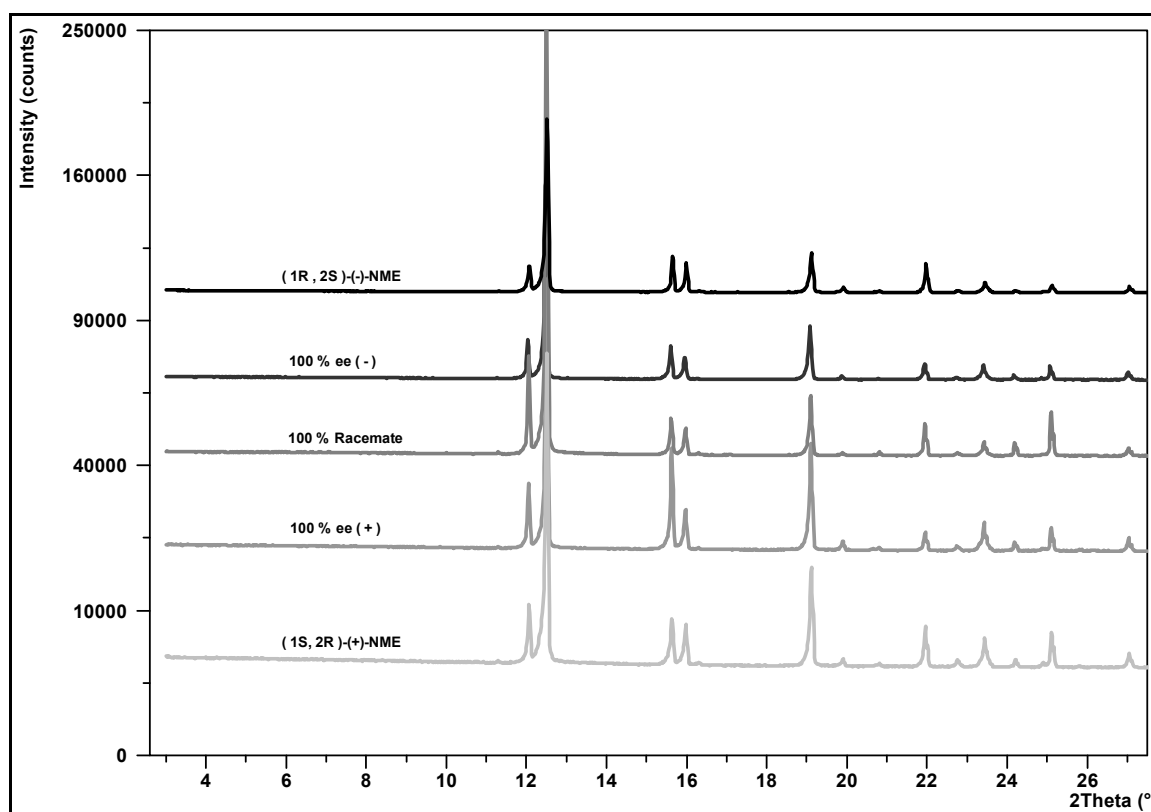
Figure 66: Experimental XRPD patterns for pure enantiomers and the racemate of N-methylephedrine, and the experimental compositions from (*S*)-ethyl lactate and N-methylephedrine at 15 °C.

The solid phase analysis was conducted also for the other lactates, (*S*)-methyl lactate, (*S*)-propyl lactate and (*S*)-butyl lactate studied. The standard deviations for the solubility data measured were calculated by Equation 22 in chapter 3 with n being again the number of experiments are compiled in Table 22.

Table 22: Error Analysis of Solubility Determination Procedure (standard deviation SD according to Equation 22 in chapter 3, number of experiments *n*).

t / °C	(*1S,2R*)-(+)-N-methylephedrine in (*S*)-methyl lactate	
	n	SD
25	3	0.34

t / °C	(*1S,2R*)-(+)-N-methylephedrine in (*S*)-ethyl lactate	
	n	SD
0	6	0.04
25	6	0.14

t / °C	(*1S,2R*)-(+)-N-methylephedrine in (*S*)-propyl lactate	
	n	SD
25	4	0.54

t / °C	(*1S,2R*)-(+)-N-methylephedrine in (*S*)-butyl lactate	
	n	SD
25	4	0.28

t / °C	(*1S,2R*)-(+)-N-methylephedrine in (*2R,3R*)-diethyl tartrate	
	n	SD
25	6	0.24
40	6	0.45

The standard deviations for the counter enantiomers and the racemic mixture of N-methylephedrine solubilities are in the same range.

The subsequent section will deal with the usage of chiral ionic liquids for enantioselective crystallization of N-methylephedrine.

4.3.2 N-methylephedrine in chiral ionic liquids

This study is directed to the use of a chiral ionic liquid for enantioselective crystallization since the structured nature of these solvents might provide more appropriate chiral interactions. Reichert et al.[104] reviewed and discussed the possibility of using complex solvents like ionic liquids for crystallization. Furthermore, lately Gausepohl et al.[103] reported an example of an enantioselective asymmetric synthesis using a chiral ionic liquid as a

reaction medium. On that basis, it appears attractive to apply chiral ionic liquids as solvents in enantioselective crystallization.

4.3.2.1 N-methylephedrine in (*S*)-2-(methoxycarbonyl) pyrrolidinium bis(trifluoromethyl sulfonyl) amide

First, a HPLC method which was used to determine the concentrations and enantiomeric compositions has been elaborated.

Chiral HPLC separation / analysis

The analytical techniques made and applied for determining concentrations and enantiomeric compositions (ee) are described in detail in Figure 67. A typical chromatogram of a racemate of N-methylephedrine dissolved in [(*S*)-2-Pro-Me] [NTF$_2$] / MeOH 70/30 v/v is shown. The separation factor (α) was determined according to Equation 36 which gives a measure of the separation or the selectivity between the enantiomers.

$$\alpha = \frac{t_{R2} - t_0}{t_{R1} - t_0}$$

Equation 36

where t_0 is the dead time, t_{R1} and t_{R2} are the retention times for both components 1 and 2, respectively. The separation factor was determined to be 1.5, almost a baseline separation was obtained. The (-)-enantiomer elutes before the (+)-enantiomer.
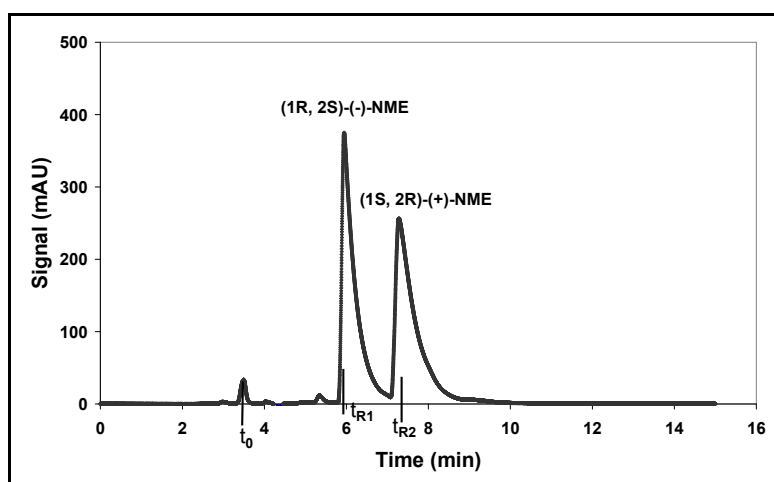
Figure 67: Chromatographic separation of racemic N-methylephedrine (NME) in [(*S*)-2-Pro-Me][NTF$_2$] / MeOH 70/30 v/v. Injection volume, 5μl; flow rate, 1 ml/min; temperature 25 °C; detection, UV at 254 nm. Chiral stationary phase, Eurocel OD (Knauer, 5μm, 250x4.6mm); mobile phase, 85% n-Hexane, 15% isopropanol and 0.1% diethylamine.

Since in the lower temperature ranges the viscosity of the chiral ionic liquid increases, methanol as co-solvent was added in an appropriate ratio. As a result the solubility increased, and the viscosity decreased, allowing a more suitable window for crystallization processes. The obtained solubility data are summarized in Table 23.

Table 23: Mass fraction Solubility (w_i) of (*1S,2R*)-(+)-N-methylephedrine (3) and (*1R,2S*)-(-)-N-methylephedrine (4) in (S)-2-(methoxycarbonyl) pyrrolidinium bis (trifluoromethylsulfonyl) amide / MeOH 70/30 v/v at different enantiomeric excesses (ee) $\left[ee = \left| w_3 - w_4 \right| / (w_3 + w_4) \right]$ and temperatures.

100 ee	100 (w_3+w_4)	100 w_3	100 w_4	100 $w_{solvent}$
		t = 5 °C		
100.00	31.22	31.22	0.00	68.78
49.08	36.00	26.83	9.17	64.00
0.00	42.83	21.42	21.41	57.17
49.74	36.30	27.17	9.13	63.70
100.00	31.37	0.00	31.37	68.63
		t = 15 °C		
100.00	34.00	34.00	00.00	66.00
39.62	38.82	27.10	11.72	61.18
0.00	45.56	22.78	22.78	54.44
43.58	39.00	11.00	28.00	61.00
100.00	33.58	00.00	33.58	66.42
		t = 25 °C		
100.00	39.00	39.00	0.00	61.00
35.80	45.42	30.84	14.58	54.58
0.00	52.61	26.31	26.30	47.39
31.98	43.84	14.91	28.93	56.16
100	38.36	0.00	38.36	61.64
		t = 30 °C		
100.00	41.63	41.63	0.00	58.37
44.98	46.74	33.88	12.86	53.26
0.00	55.58	27.79	27.79	44.42
44.42	46.47	12.91	33.56	53.53
100.00	41.00	0.00	41.00	59.00
		t = 35 °C		
100.00	43.23	43.23	0.00	56.77
50.00	50.00	37.50	12.50	50.00
0.00	59.00	29.50	29.50	41.00
50.00	49.78	12.44	37.34	50.22
100.00	43.19	0.00	43.19	56.81

Figure 68 depicts the phase diagram of N-methylephedrine in [(*S*)-2-Pro-Me][NTF$_2$] / MeOH 70/30 v/v at different temperatures. The ternary solubility phase diagram has been derived from the summarized solubility phase diagram in Table 23. The solubility data measured in

Table 23 were derived from taken the mean values from the two sets of obtained data. It was impossible to calculate the standard deviation due to the fact that experiments were conducted only two times, since the chiral ionic liquid was very expensive.
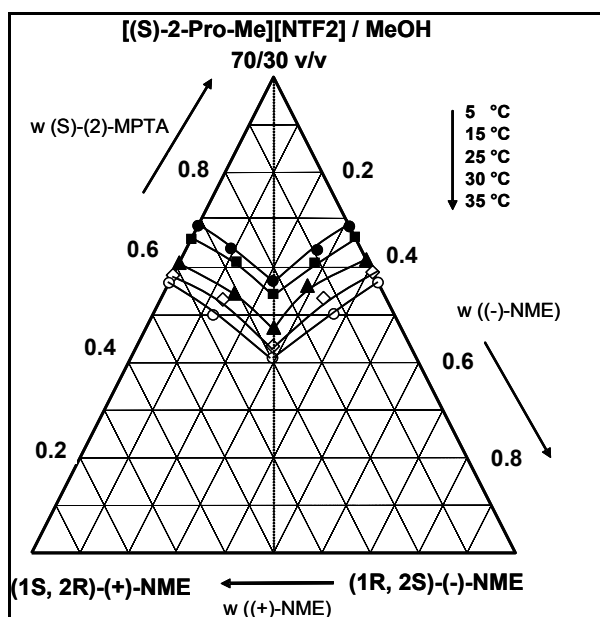
Figure 68: Ternary phase diagram for N-methylephedrine in (*S*)-2-(methoxycarbonyl) pyrrolidinium bis (trifluoromethylsulfonyl) amide / MeOH 70/30 v/v temperatures from 5 °C to 35 °C. Axes in weight fractions; $w_{(+)-NME}$ and $w_{(-)-NME} \leq 1.0$. The isothermal lines have been added as a visualization aid and only the marked points show measured data.

In fact, also this diagram shows symmetry with respect to the racemic axis rather than asymmetry. Also in the ternary system investigated the solubilities of pure enantiomers, racemates and enantiomeric compositions between the pure enantiomers and the racemate increase with increasing temperature. As identified already for the binary chiral system, the N-methylephedrine enantiomers do not form a racemic compound but rather a simple eutectic (conglomerate) system.[102]

Solid phase analysis

Also for this system a thorough analytical checks were conducted regarding the solid phase. This was done to ascertain that there is no formation of solvates and/or polymorphs in the chiral systems. Figure 69 illustrates experimental XRPD patterns for the solid phases obtained in solubility measurements for N-methylephedrine in (*S*)-2-(methoxycarbonyl) pyrrolidinium bis (trifluoromethylsulfonyl) amide / MeOH 70/30 v/v at 35 °C. Since N-methylephedrine in [(*S*)-2-Pro-Me][NTF$_2$] / MeOH 70/30 v/v is obviously a conglomerate forming system (see Figure 68) the reflexes of the enantiomers and the racemic mixture must be identical.
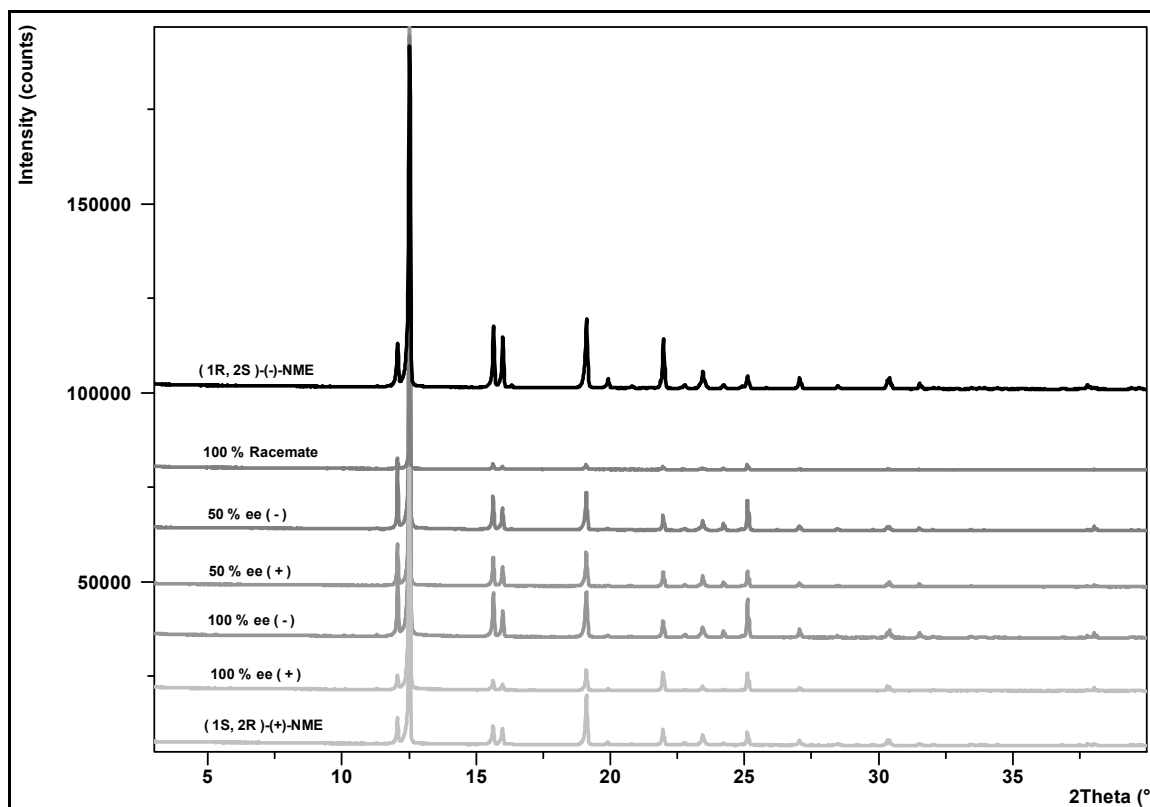
Figure 69 Experimental XRPD patterns for pure enantiomers, the racemate of N-methylephedrine, and the experimental compositions from (*S*)-2-(methoxycarbonyl) pyrrolidinium bis (trifluoromethylsulfonyl) amide / MeOH 70/30 v/v and N-methylephedrine at 35 °C.

No additional or new phases differing from those of the pure enantiomers were identified from the results of the crystal lattice analysis by XRPD. The various compositions really mimic the reference reflexes in the XRPD patterns.

The solubility isotherms in Figure 68 are more curved or bent compared to isotherms of the N-methylephedrine/"classical" chiral solvent system. It has been discussed already in the above section that the shape of the solubility isotherm influences the possible productivity of preferential crystallization strategies. The more bent the solubility isotherm is the smaller the α_{mol} value. The solubility ratio (α_{mol}) which was determined here to be ~1.3 is much lower than 2 (characterizing an ideal solubility case). As it has been discussed extensively in Figure 63 concerning the slope of the solubility isotherms and how they affect the productivity of the preferential crystallization process. So, comparing the case of "classical" chiral solvent, (*2R,3R*)-diethyl tartrate and chiral ionic liquid, (*S*)-2-(methoxycarbonyl) pyrrolidinium bis (trifluoromethylsulfonyl) amide / MeOH 70/30 v/v, it can be deduced that the chiral ionic liquid should be a better solvent for chiral separation of the pair of enantiomers studied since it has the lower α_{mol} value. The subsequent section will also deal with N-methylephedrine in,

(*1R,2S*)-(-)-Dimethylephedrinium bis (trifluoromethylsulfonyl) amide as another chiral ionic liquid.

4.3.2.2 N-methylephedrine in (*1R,2S*)-(-)-Dimethylephedrinium bis (trifluoromethylsulfonyl) amide

First of all a successful HPLC method which was used to determine the concentrations and enantiomeric compositions has been discussed in detailed. The reason for this has already been given in the above section with the chiral ionic liquid, (*S*)-2-(methoxycarbonyl) pyrrolidinium bis (trifluoromethylsulfonyl) amide.

Chiral HPLC separation / analysis

The analytical method prepared and employed for determining concentrations and enantiomeric compositions is described in Figure 70 showing a characteristic chromatogram of a racemate of N-methylephedrine dissolved in (*1R,2S*)-(-)-Dimethylephedrinium bis (trifluoromethylsulfonyl) amide. The separation factor (α) was determined according to Equation 36 which gives a measure of the separation or the selectivity between the enantiomers. The separation factor was determined to be 1.6 and a baseline separation was obtained. The (-)-enantiomer eluted before the (+)-enantiomer.
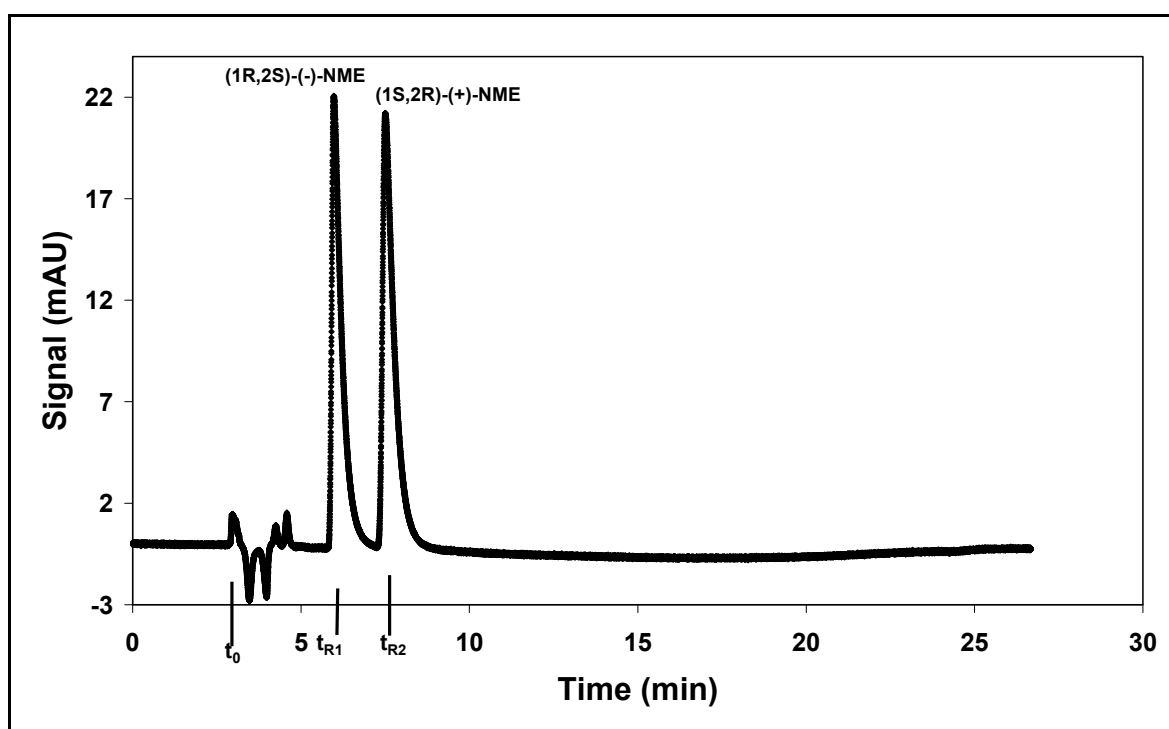
Figure 70: Chromatographic separation of racemic N-methylephedrine (*1R,2S*)-(-)-Dimethylephedrinium bis (trifluoromethylsulfonyl) amide. Injection volume, 5μl; flow rate, 1 ml/min; temperature 25 °C; detection,

UV at 254 nm. Chiral stationary phase, Eurocel OD (Knauer, 5μm, 250x4.6mm); mobile phase, 85% n-Hexane, 15% isopropanol and 0.1% diethylamine.

Though the viscosity of the chiral ionic liquid, (*1R,2S*)-(-)-Dimethylephedrinium bis (trifluoromethylsulfonyl) amide is very high no co-solvent was added. This was done to maintain the structure properties of the solvent which was expected to improve the interactions between the solvent and solute molecules.

Table 24: Mass fraction solubility (w_i) of (*1S,2R*)-(+)-N-methylephedrine (3) and (*1R,2S*)-(-)-N-methylephedrine (4) in (*1R,2S*)-(-)-Dimethylephedrinium bis (trifluoromethylsulfonyl) amide at different enantiomeric excesses (ee) $\left[ee = |w_3 - w_4|/(w_3 + w_4) \right]$.

100 ee	100 ($w_{3+}w_4$)	100 w_3	100 w_4	100 $w_{solvent}$
		t = 35 °C		
100.00	11.21	11.21	0.00	88.79
5.32	19.26	10.14	9.12	80.74
100.00	9.28	0.00	9.28	90.72

A summary of the solubility data in mass fraction (w_i) of both enantiomers of N-methylephedrine in (*1R,2S*)-(-)-Dimethylephedrinium bis (trifluoromethylsulfonyl) amide at 35 °C has been compiled in Table 24. The ternary solubility phase diagram has been constructed based on these data.
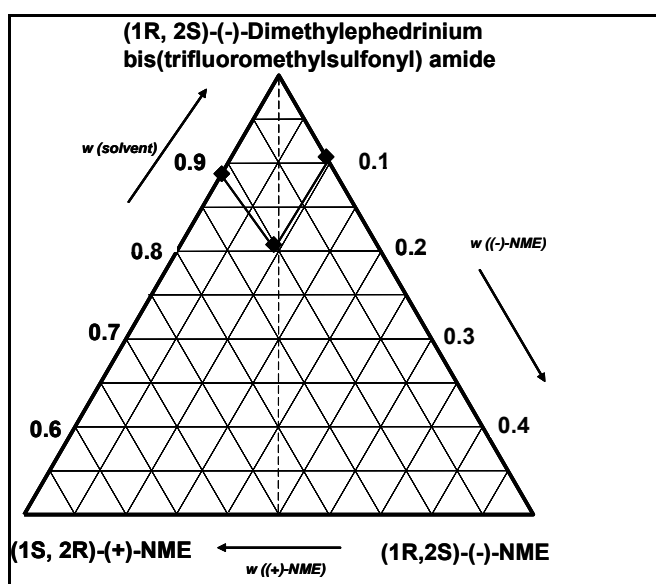
Figure 71: Ternary phase diagram of N-methylephedrine in (*1R,2S*)-(-)-Dimethylephedrinium bis (trifluoromethylsulfonyl) amide at 35 °C. Axes in weight fractions; $w_{(+)-NME}$ and $w_{(-)-NME} \leq 0.5$. The isothermal lines have been added as a visualization aid and only the marked points show measured data.

Solubility experiments were only possible at higher temperatures, because the solvent has a very high viscosity (481.6 mPa s, at 23.10°C). A ternary solubility phase diagram of N-methylephedrine enantiomers in chiral ionic liquid, (*1R,2S*)-(-)-Dimethylephedrinium bis (trifluoromethylsulfonyl) amide at 35 °C is shown in Figure 71. The phase diagram depicts a typical simple eutectic (conglomerate) system. The solubility measurements were repeated twice and the mean values were used for the derivation of the ternary solubility phase diagram. The phase diagram shows an asymmetry, which reveals that the chiral ionic liquid (*1R,2S*)-(-)-Dimethylephedrinium bis (trifluoromethylsulfonyl) amide has a measurable chiral recognition with the N-methylephedrine enantiomers. The shape of the isotherms in the ternary phase diagram for one side is steeper compared to the other. The α_{mol} values ranges between 1.5 to 1.8 for (*1S,2R*)-(+)-N-methylephedrine and (*1R,2S*)-(-)-N-methylephedrine enantiomers, respectively. This is due to the asymmetry behavior of the phase diagram. Nevertheless, in both cases the α_{mol} values are smaller than 2 (ideal case). Thus, the system would be favorable for a preferential crystallization processes, and would provide wide area for entrainment. It should eventually be feasible to enter the two phase region of the phase diagrams via crystallization, which would be more lucrative for obtaining single enantiomers. According to the determined ternary solubility phase diagram it can be deduced that the studied chiral ionic liquids seems to be a promising solvent for the enantioseparation of N-methylephedrine due to the lower α_{mol} values via preferential crystallization.

Solid phase analysis

Figure 72 illustrates experimental XRPD patterns for the solid phases obtained during the solubility measurements for N-methylephedrine in (*1R,2S*)-(-)-Dimethylephedrinium bis (trifluoromethylsulfonyl) amide at 35 °C. Since N-methylephedrine in (*1R,2S*)-(-)-Dimethylephedrinium bis (trifluoromethylsulfonyl) amide is evidently a conglomerate forming system (see Figure 71) so the reflexes of the enantiomers and the racemic mixture must be identical. Indeed, no additional or new phases, differing from those of the pure enantiomers, were identified from the results of the crystal lattice analysis by XRPD. The various compositions really mimicked the reference reflexes in the XRPD patterns.
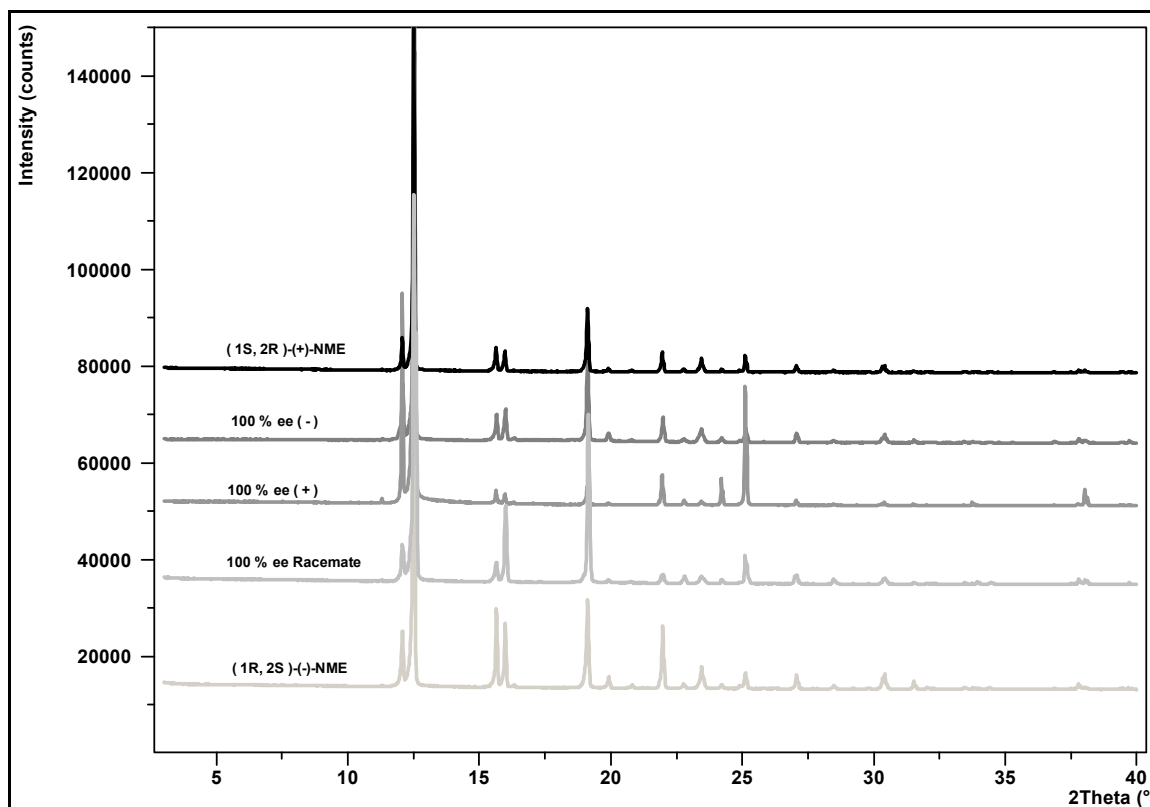
Figure 72: Experimental XRPD patterns for pure enantiomers, the racemate of N-methylephedrine, and the experimental compositions from (*1R,2S*)-(-)-Dimethylephedrinium bis (trifluoromethylsulfonyl) amide and N-methylephedrine at 35 °C.

4.3.3 Mandelic acid in tailor-made chiral solvents

The enantioselective crystallization of conglomerate forming systems by the use of pure enantiomers or tailor-made additives has been well studied by several research groups.[55,143-145] Furthermore, Mughal et al.[48,146] and Leeman et al.[147] have successfully applied tailor-made additives to compound forming substance. Motivation for the use of tailor-made additive comes from the above mentioned examples. Therefore, tailor-made chiral solvents were synthesized with criteria set such that the structure of the solvent resembles the mandelic acid chemical structure stereochemically.

Unfortunately, no HPLC method was available for this system and alternative measuring and analytical techniques were used. Crystal16[TM] (polythermal method) and refractometry have been employed for concentration measurements in preliminary experiments.

4.3.3.1 Mandelic acid in (S)-propyl mandelate

The tailor-made chiral solvent, (S)-propyl mandelate was employed as solvent in solubility measurements of mandelic acid. Here, a polythermal method with the crystal16[TM] was used in as preliminary experiment conducted to verify the potential of the tailor-made chiral solvents

for chiral discrimination. The results obtained from the solubility measurements of (*S*)-mandelic acid and (*R*)-mandelic acid in (*S*)-propyl mandelate are shown in Figure 73.
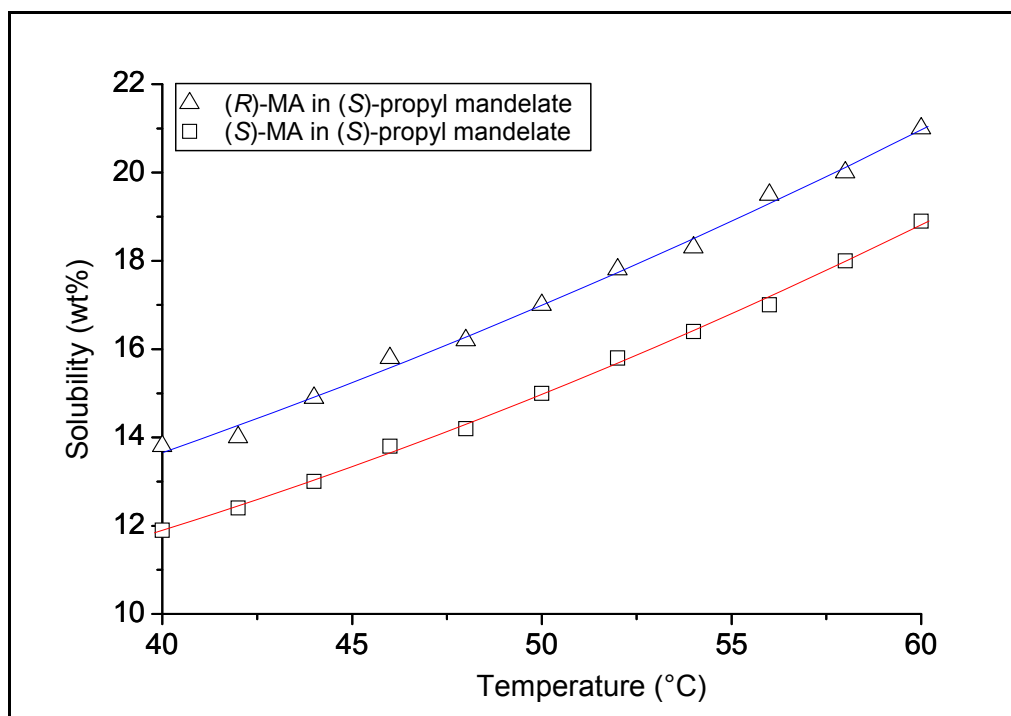
Figure 73: Solubility in wt % of (*S*)-mandelic acid ((*S*)-MA) and (*R*)-mandelic acid ((*R*)-MA) in (*S*)-propyl mandelate as a function of temperature.

Depicts is a plot of concentrations as a function of temperature. There is a clear trend that increase in temperature resulted in solubility increments. The Figure clearly shows differences in the solubility of the (*S*)- and (*R*)-mandelic acid enantiomers. The results indicate the existence of measurable interactions of the chiral molecules and the chiral solvent in the liquid phase. From the results can be deduced, that there is a measurable chiral recognition in the liquid phase provided by the (*S*)-propyl mandelate. Based on these results of preliminary measurements, subsequent solvent was now applied to see the effect of different chain lengths of the tailor-made chiral solvents. Thus, further studies were conducted for (*S*)-isopropyl mandelate. Solubility experiments were performed for the enantiomers and the racemic mandelic acid. Thorough solubility measurements were not possible to be carried out for the single enantiomers, the eutectic and the racemic compositions, because there was no HPLC method available to analyze the enantiomeric compositions.

Molecular modeling studies were also performed to get a deeper understanding of the solvent-solute interactions in the system. Figure 74 shows a schematic representation of optimized molecular structures of the dimer of (a) (*S*)-mandelic acid and (*S*)-propyl mandelate and (b)

(*R*)-mandelic acid and (*S*)-propyl mandelate, respectively, and with connection of hydrogen bonds.
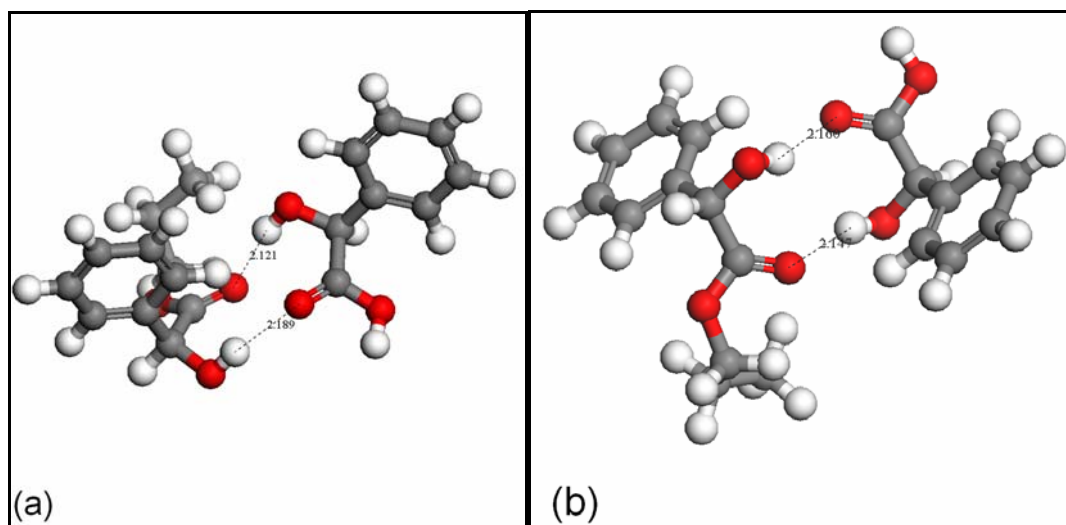
Figure 74: Schematic representation of optimized molecular structures of the dimer of (a) (*S*)-mandelic acid and (*S*)-propyl mandelate and (b) (*R*)-mandelic acid and (*S*)-propyl mandelate, respectively, and the molecules are connected by hydrogen bonds.

The optimized structure of mandelic acid/(S)-isopropyl mandelate system is not being shown, as there are only slight differences in the two.

Table 25: Summary of results of ΔH_{form} of individual molecules and dimers of (*S*)- and (*R*)-MA in (*S*)-propyl mandelate and (*S*)-isopropyl mandelate.

Single molecule energies		Dimer energies		Stabilization enthalpy
Single molecules	$\Delta H_{form}^{Solute/solvent}$ (kcal/mol)	Dimer types	ΔH_{form}^{Dimer} (kcal/mol)	$\Delta H_{form}^{Stabilization}$ [ΔH_{form}^{Dimer} - ($\Delta H_{form}^{Solute} + \Delta H_{form}^{Solvent}$)] (kcal/mol)
(*S*)-MA	-117.56			
(*S*)-PM	-122.97	(*S*)-MA-(*S*)-PM	-243.31	-2.78
(*R*)-MA	-117.56			
(*S*)-PM	-122.97	(*R*)-MA-(*S*)-PM	-246.00	-5.47
(*S*)-MA	-117.56			
(*S*)-IPM	-120.99	(*S*)-MA-(*S*)-IPM	-242.52	-3.97
(*R*)-MA	-117.56			
(*S*)-IPM	-120.99	(*R*)-MA-(*S*)-IPM	-244.42	-5.87

MA, mandelic acid; PM, Propyl mandelate; IPM, isopropyl mandelate.

The optimized structures were used in the calculations of the heat of formation (ΔH_{form}) and their corresponding stabilization energies. The results obtained from the molecular modeling, compiled in Table 25 indicate that the $\Delta H_{form}^{Stabilization}$ of (*R*)-mandelic acid and (*S*)-propyl mandelate dimer is more negative (-5.96 kcal/mol) compared to that of (*S*)-mandelic acid and (*S*)-propyl mandelate which is less negative (-2.78 kcal/mol). Thus, it can be expected that the most stable dimer ((*R*)-mandelic acid and (*S*)-propyl mandelate) should be more soluble compared to the less stable dimer ((*S*)-mandelic acid and (*S*)-propyl mandelate). The observed solubility differences for both enantiomers in (*S*)-propyl mandelate point in the same direction as the molecular modeling results.

4.3.3.2 Mandelic acid in (S)-isopropyl mandelate

A summary of the obtained solubility results of the enantiomers and racemic mandelic acid in the tailor-made chiral solvent, (*S*)-isopropyl mandelate at 50 °C is given in Table 26.

Table 26: Summary of mandelic acid solubilities in the tailor-made synthesized chiral solvent at 50 °C.

Solvent	(*S*)-MA wt %	(*R*)-MA wt %	(racemic)-MA wt %
(*S*)-isopropyl mandelate	18.44	21.82	35.96

Table 26 depicts a distinct solubility difference between the two pure enantiomers of mandelic acid. Additional molecular modeling calculations were performed to explain these differences. The outcome of the calculations is summarized in Table 25. Table 25 indicates that the $\Delta H_{form}^{Stabilization}$ of (*R*)-mandelic acid and (*S*)-isopropyl mandelate dimer is more negative (-5.86 kcal/mol) compared to that of (*S*)-mandelic acid and (*S*)-propyl mandelate (-3.96 kcal/mol). Hence, (*R*)-mandelic acid/(*S*)-isopropyl mandelate should form a rather stable dimer and as a result of this should be more soluble This is contrary to the case of (*S*)-mandelic acid/(*S*)-isopropyl mandelate.

As discussed earlier, thorough solubility measurements were not feasible in this case. A literature search revealed few studies with quantifiable solubility differences between the two pure enantiomers using chiral solvents. For instance, Yamamoto et al.[6] reported pure enantiomer solubilities for a chiral cobalt salt in (*2R,3R*)-(+)-diethyl tartrate and described measurable differences between them. Thus, the observed solubility differences in this present work are in line with previously reported work on chiral solvents. The difference of our work

is that a special synthesized tailor-made chiral solvent was applied for the measurement, which provided appreciable solubility differences. These differences might be employed for resolution purposes. Unfortunately, in this current work no phase diagrams could be determined, due to the fact that no suitable HPLC method was available for enantiomeric compositions determination.

Solid Phase Analysis

Figure 75 depicts experimental XRPD patterns for solid phases obtained during the solubility measurements of mandelic acid in (*S*)-isopropyl mandelate at 50 °C. In each case the reflexes of the racemic compound and/or the mandelic acid enantiomer are clearly distinguishable. Typical reflexes characterizing the different species are indicated by grey to black colors, e.g. reflex at 6.0° is typical for the enantiomer, and reflex at 10.84° is typical for the racemic compound. No additional or new phases were identified (other than the racemic compound and the enantiomers) from the crystal lattice analysis by XRPD.
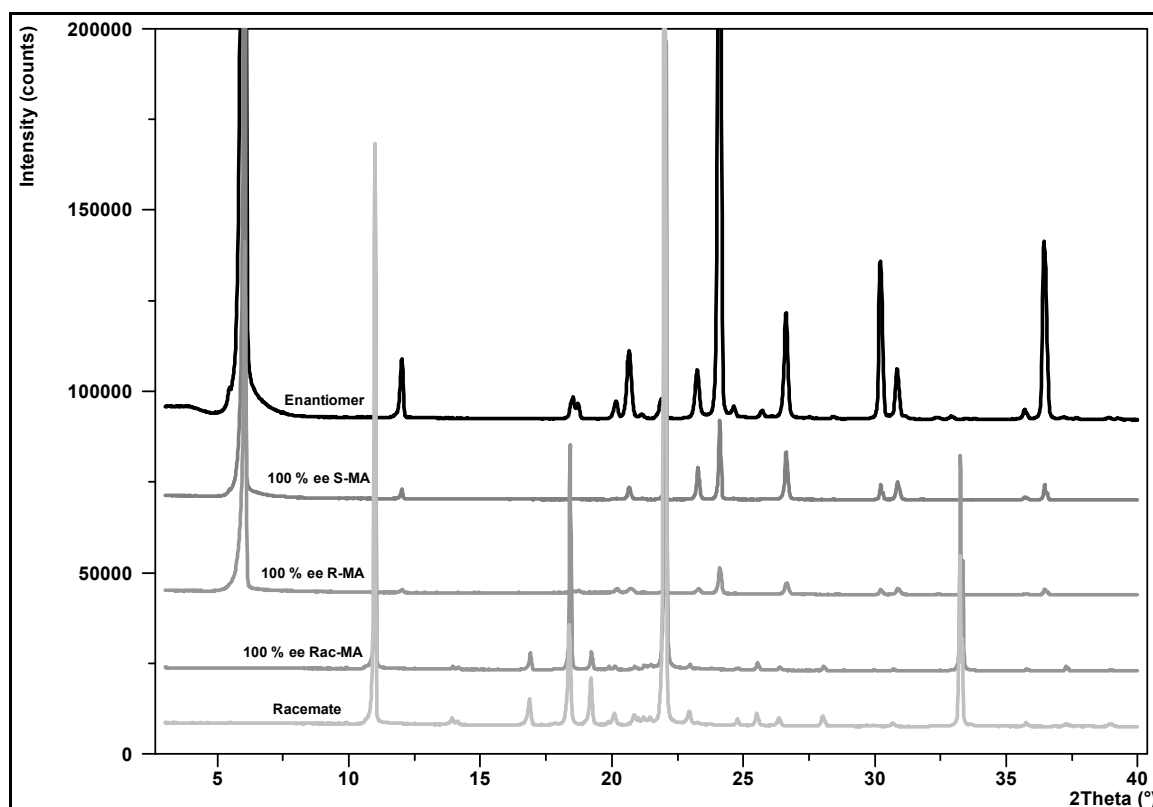
Figure 75: Experimental XRPD patterns for pure enantiomers, the racemate of mandelic acid, and the experimental compositions from (*S*)-isopropyl mandelate and mandelic acid at 50 °C.

Also the solid phases for both pure enantiomers of mandelic acid in (*S*)-propyl mandelate were checked, and there were no additional or new phases formed in the crystal lattice.

The next section will give a discussion on nucleation points and how they affect the design of enantioselective crystallization processes.

4.4 Nucleation points (MSZW and Induction time)

Nucleation point experiments are needed in designing enantioselective crystallization processes. There were two main types of experiments applied to evaluate the nucleation points namely, the metastable zone width with regard to primary nucleation and induction times.

4.4.1 Mandelic acid and N-methylephedrine in "classical" chiral solvents

The solubility results obtained for of mandelic acid and N-methylephedrine in different chiral solvents were employed for the MSZW experiments.

4.4.1.1 Mandelic acid in "classical" chiral solvents

Figures 76 and 77 depict the metastable zone width with respect to primary nucleation for mandelic acid in (2R, 3R)-diethyl tartrate at 55 °C and 60 °C, respectively. The obtained data for all studied temperatures are summarized in Table 27. It can be seen that the metastable zone is most extended for racemic mandelic acid (racemic-MA), followed by (*S*)-mandelic acid ((*S*)-MA) and (*R*)-mandelic acid ((*R*)-MA), respectively. The maximum possible subcooling ΔT_{max} and the maximum possible nucleation-free supersaturation ΔC_{max} of racemic-MA in (*2R,3R*)-diethyl tartrate are rather remarkable and increase significantly when the temperature is increased. In the case of the pure enantiomers there was no clear trend found.
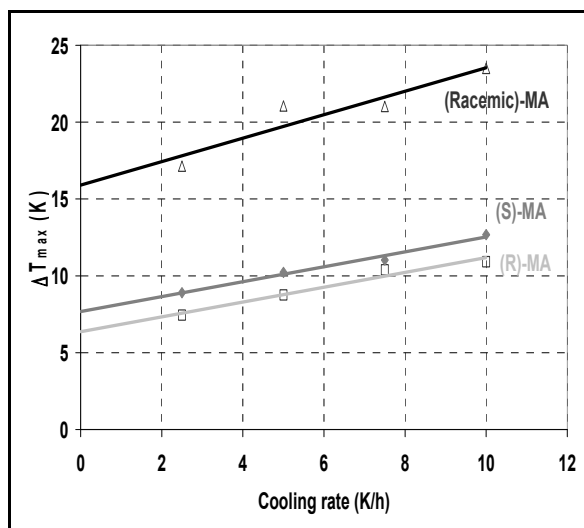
Figure 76: Experimentally determined metastable zone width with respect to primary nucleation for mandelic acid in (*2R,3R*)-diethyl tartrate at T_{sat} = 55 °C.
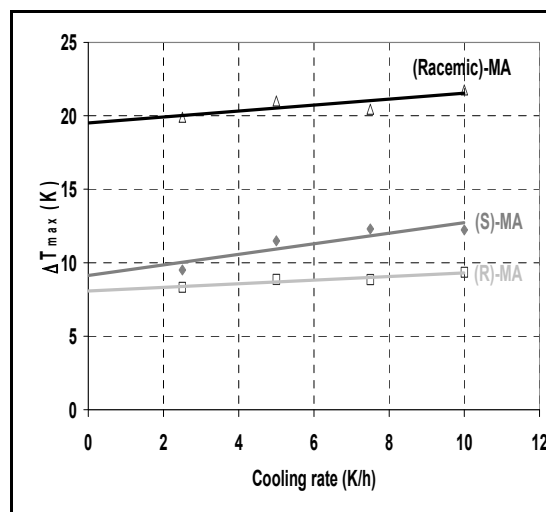
Figure 77: Experimentally determined metastable zone width with respect to primary nucleation for mandelic acid in (*2R,3R*)-diethyl tartrate at T_{sat} = 60 °C.

Table 27: Metastable Zone Width Data for the Mandelic acid / (2R, 3R)-diethyl tartrate System.

T_{sat} (K)	(*S*)-MA		(*R*)-MA		Racemic-MA	
	ΔT_{max} (K)	ΔC_{max} (wt %)	ΔT_{max} (K)	ΔC_{max} (wt %)	ΔT_{max} (K)	ΔC_{max}(wt %)
323.15	8.9	3.67	8.2	3.08	14.3	8.44
328.15	7.7	3.05	6.4	2.65	15.9	9.16
333.15	9.2	3.57	8.1	3.31	19.5	13.46

Since the MSZW of (*R*)-MA is smaller compared to that of (*S*)-MA and in particular to that of racemic-MA, preferential nucleation of (*R*)-MA, and thus kinetically controlled selective production of the (*R*)-MA enantiomer might be feasible from this solvent.

Figure 78 depicts the metastable zone width (primary nucleation) for mandelic acid in (*S*)-ethyl lactate at T_{sat} = 15 °C. It can be clearly seen that the MSZW increases with increasing cooling rate. Racemic-MA nucleates before (*S*)-MA. For (*R*)-MA it is obvious that there exists a specific kinetic inhibition for crystallization from (*S*)-ethyl lactate. No nucleation was observed, independent on the cooling rate used. Due to the experimental limitation in subcooling temperature coupled with a high viscosity of the (*S*)-ethyl lactate measurements could not be carried out below -15 °C.
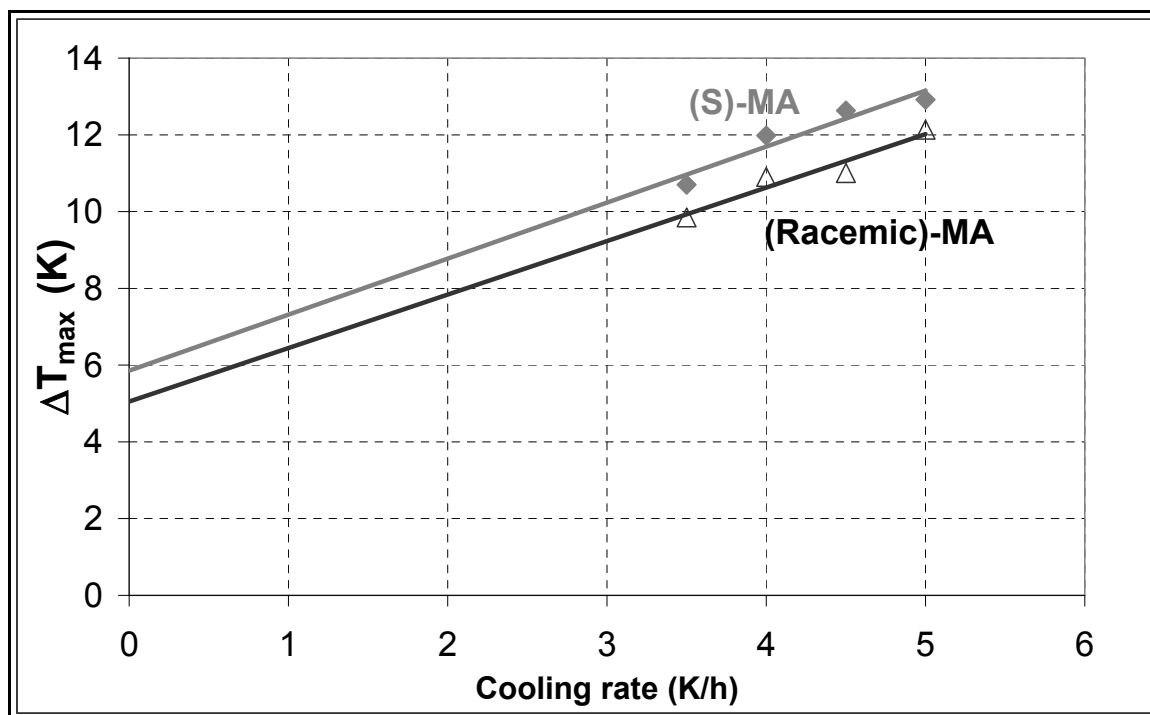
Figure 78: Experimentally determined metastable zone width with respect to primary nucleation for mandelic acid in (S)-ethyl lactate at T_{sat} = 15 °C. ((R)-MA: no nucleation in the range of measurement).

According to Lorenz et al.[47] metastable zone width measurements for mandelic acid in water illustrated that the ΔT_{max} values, both with regard to primary and secondary nucleation, respectively were larger for racemic-MA than for the pure enantiomers. Here the opposite case is observed: racemic-MA nucleates first. This should be due to the effect of the chiral solvent. Thus, preferential nucleation of pure enantiomers is not possible for this system. However, considering the fact that (R)-MA never nucleates, initiating preferential crystallization of (S)-MA by adding seeds of (S)-MA might be an option to selectively produce pure (S)-MA from (S)-ethyl lactate.

Complementary molecular modeling studies were performed again to get deeper understanding of the solvent-solute interactions in the system. A detail explanation how this molecular modeling was conducted was already given in the above section. The same procedure was applied here. The optimized structures of the dimers which were used in the calculations are shown below. Figure 79 illustrates a schematic representation of optimized molecular structures of the dimer of (a) (S)-mandelic acid and (S)-ethyl lactate and (b) (R)-mandelic acid and (S)-ethyl lactate, respectively.
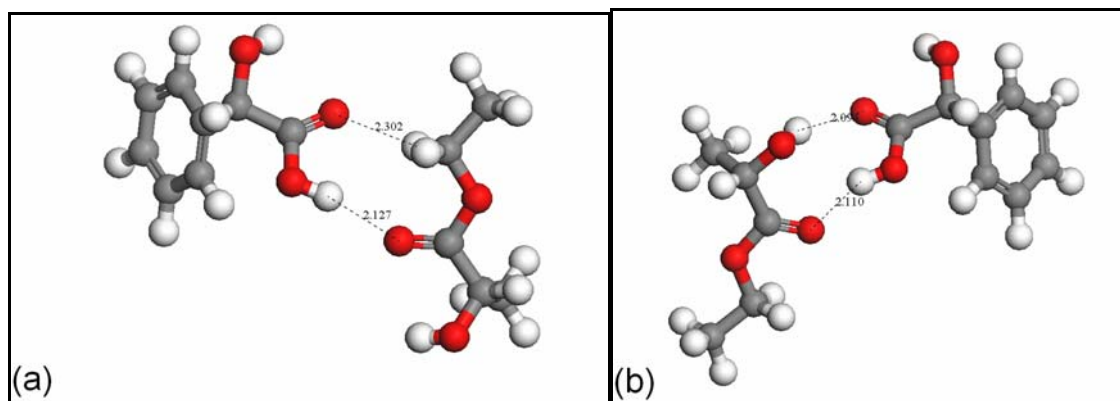
Figure 79: Schematic representation of optimized molecular structure of the dimer of (a) (*S*)-mandelic acid and (*S*)-ethyl lactate and (b) (*R*)-mandelic acid and (*S*)-ethyl lactate, respectively, and showing connected by hydrogen bonds.

The other pair of the schematic representation of the optimized molecular structures of the dimer of (a) (*S*)-mandelic acid and (*2R,3R*)-diethyl tartrate and (b) (*R*)-mandelic acid and (*2R,3R*)-diethyl tartrate, respectively is represented in Figure 80.
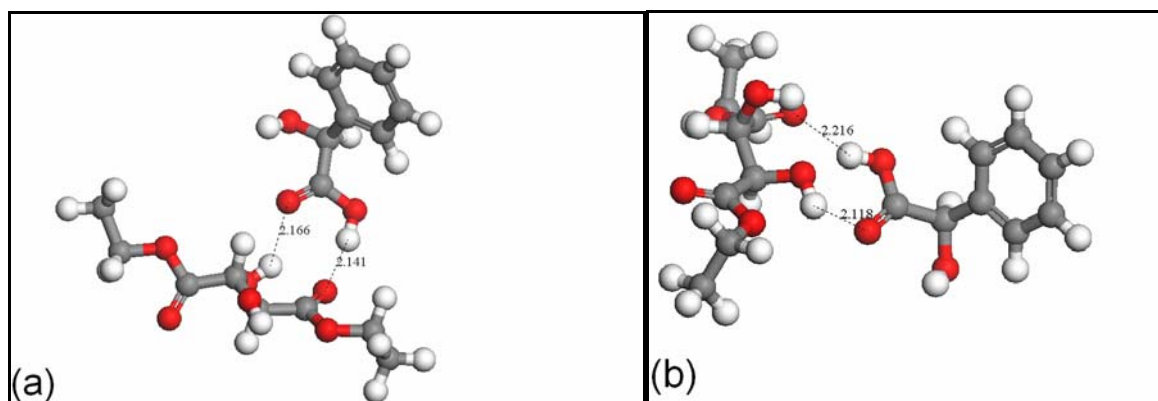
Figure 80: Schematic representation of optimized molecular structures of the dimer of (a) (*S*)-mandelic acid and (*2R,3R*)-diethyl tartrate and (b) (*R*)-mandelic acid and (*2R,3R*)-diethyl tartrate, respectively, and showing connected by hydrogen bonds.

The results derived from the molecular modeling calculations are compiled in Table 28. They also explain the inhibition effects observed during the MSZW measurements. It can be seen that, the stabilization enthalpies $\Delta H_{form}^{Stabilization}$ for (R)-mandelic acid in (*S*)-ethyl lactate and (*S*)-MA in (*2R,3R*)-diethyl tartrate are with -5.96 kcal/mol and -4.39 kcal/mol respectively, more negative than for the counter-enantiomers (-4.29 kcal/mol and -0.63 kcal/mol, respectively). From a thermodynamic point of view the dimer with the most negative $\Delta H_{form}^{Stabilization}$ is the most thermodynamically stable dimer and would remain in solution. The contrary would be the case for the dimer with the less negative $\Delta H_{form}^{Stabilization}$, i.e. thermodynamically less stable would crystallize easily from solution first. The results of these calculations explain the

results obtained in the MSZW experiments, where (*S*)-mandelic acid in (*S*)-ethyl lactate and (*R*)-mandelic acid in (*2R,3R*)-diethyl tartrate crystallized first.

Table 28: Summary of results of ΔH_{form} of individual molecules and dimers of (S)- and (R)-MA in (S)-ethyl lactate and (2R, 3R)-diethyl tartrate.

Single molecule energies		Dimer energies		Stabilization enthalpy
Single molecules	$\Delta H_{form}^{Solute\,/\,Solvent}$ (kcal/mol)	Dimer types	ΔH_{form}^{Dimer} (kcal/mol)	$\Delta H_{form}^{Stabilization}$ $[\,\Delta H_{form}^{Dimer} - (\Delta H_{form}^{Solute} + \Delta H_{form}^{Solvent})\,]$ (kcal/mol)
(*S*)-MA	-117.56			
(*S*)-EL	-152.00	(*S*)-MA-(*S*)-EL	-273.85	-4.29
(*R*)-MA	-117.56			
(*S*)-EL	-152.00	(*R*)-MA-(*S*)-EL	-275.52	-5.96
(*S*)-MA	-117.56			
(*2R,3R*)-DT	-282.46	(*S*)-MA-(*2R,3R*)-DT	-404.41	-4.39
(*R*)-MA	-117.56			
(*2R,3R*)-DT	-282.46	(*R*)-MA-(*2R,3R*)-DT	-400.65	-0.63

MA, mandelic acid; EL, ethyl lactate; DT, diethyl tartrate.

Investigation of different chain lengths of the lactates

Investigations were also carried out to verify how the chain lengths of the lactates, (*S*)-methyl lactate, (*S*)-ethyl lactate, (*S*)-propyl lactate and (*S*)-butyl lactate affects the MSZW measurements. Unfortunately, there were no definite trends observed. Thus, the results are not discussed here but are included in Appendix D.

4.4.1.2 N-methylephedrine in "classical" chiral solvents

Figure 81 depicts the results of the MSZW measurements (primary nucleation) for N-methylephedrine in (S)-ethyl lactate. Contrary to the mandelic acid/(S)-ethyl lactate system, for N-methylephedrine both enantiomers crystallized at higher subcooling compared to the racemate. Thus, the use of preferential nucleation as a resolution method is not expected to be feasible for NME. However, preferential crystallization might be a possible resolution method to be employed here.
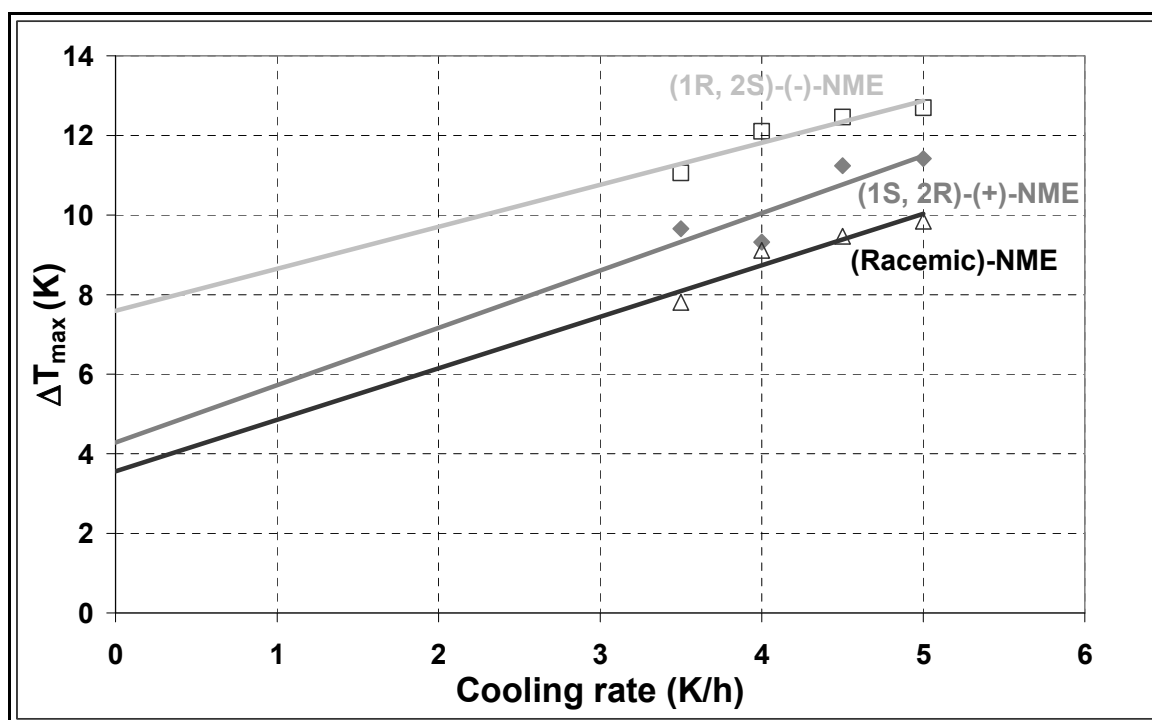
Figure 81: Experimentally determined metastable zone width (primary nucleation) for N-methylephedrine (NME) in (S)-ethyl lactate at $T_{sat} = 15°C$.

Also, in the case of N-methylephedrine in (*2R,3R*)-diethyl tartrate MSZW measurements were not possible, due to the high viscosity of the solvent. Therefore, induction time experiments were carried out instead. Primary nucleation experiments were performed for racemic-N-methylephedrine, (*1S,2R*)-(+)-N-methylephedrine and (*1R,2S*)-(-)-N-methylephedrine in (2R, 3R)-diethyl tartrate at 35 °C. There was a pronounced delay of the appearance of first crystals for racemic-N-methylephedrine observed. The induction time t_{ind} was determined to be around 500 seconds, which was longer time compared to (*1S,2R*)-(+)-N-methylephedrine with 364 seconds and (*1R,2S*)-(-)-N-methylephedrine with 240 seconds, respectively. This nucleation delay behavior of the racemic-N-methylephedrine was expected based on the α_{mol} values determined to be ~1.5 to 1.7 (see section 4.3.1.2) for this system. Wang et al[35] reported that classical nucleation theory can explain this observed phenomenon. According to this theory, the induction time (t_{ind}) of the racemic mixture will depend on the concentrations of the two enantiomers. The solubility of the racemate is larger than that of the enantiomer, but the α_{mol} is smaller than 2. In this situation, though more molecules are in solution, the (*1S,2R*)-(+)-N-methylephedrine-molecules and the (*1R,2S*)-(-)-N-methylephedrine-molecules are required to arrange in equal quantities to form racemic-N-methylephedrine. Consequently, the effective concentration to form nuclei is in reality only half the total concentration. If $\alpha_{mol} < 2$, implies the effective enantiomer concentration ((+)-NME:(-)-NME = 0.5:0.5) is smaller than

that of the pure enantiomer. Hence, the t_{ind} of the racemate should be longer than that of the pure enantiomer. According to the results obtained from the nucleation experiment, the determine induction time (t_{ind}) of the (+)-NME with the less time might selectively crystallize out first (preferential nucleation/crystallization) after cooling a racemic mixture of N-methylephedrine in (*2R,3R*)-diethyl tartrate solution. This is considered as a possible resolution method.

4.4.2 N-methylephedrine and chiral ionic liquid

In this system it was really impossible to perform metastable zone width with regard to primary nucleation because only a limited amount of solvent was available. This was due to the fact that the chiral ionic liquid, (*S*)-2-(methoxycarbonyl) pyrrolidinium bis (trifluoromethylsulfonyl) amide is very expensive. In this case the appropriate experiment for the determination of the nucleation point was the induction time experiments which require a smaller amount.

In primary nucleation tests carried out for racemic-N-methylephedrine, (*1S,2R*)-(+)-N-methylephedrine and (*1R,2S*)-(-)-N-methylephedrine in [(*S*)-2-Pro-Me] [NTF$_2$] / methanol 70/30 v/v at 35 °C it was observed that there was a pronounced delay of the appearance of first crystals for racemic-N-methylephedrine, i.e. the induction time t_{ind} was determined to be 437 seconds, which was long time compared to (*1R,2S*)-(-)-N-methylephedrine with 314 seconds and (*1S,2R*)-(+)-N-methylephedrine with 124 seconds, respectively. The solubility ratio (α_{mol}) has been determined to be ~1.3 (see section 4.3.2.1). This nucleation delay behavior of the racemic-N-methylephedrine was expected based on this α_{mol} values. Thus, the same trend of induction time was found, as discussed in the above section. Therefore the racemic mixture of the N-methylephedrine would have wider MSZW compared to the single enantiomers. According to the results obtained from the nucleation experiment, the determine induction time (t_{ind}) of the (+)-NME might selectively crystallize out first (preferential nucleation/crystallization) after cooling and without/with seeding a racemic mixture of N-methylephedrine in [(*S*)-2-Pro-Me][NTF$_2$] / MeOH 70/30 v/v solution with (+)-NME crystals. This was considered as a possible resolution method.

In the case of the other system, N-methylephedrine/(*1R,2S*)-(-)-Dimethylephedrinium bis (trifluoromethylsulfonyl) amide it was not feasible to determine the nucleation points since the solvent is extremely viscous (481.6 mPa.s at 23.10 °C) and difficult to stir at lower temperatures.

4.4.3 Mandelic acid in "tailor-made" chiral solvent

Figures 82 depicts the metastable zone width with respect to primary nucleation for mandelic acid in (*S*)-propyl mandelate at 50 °C. It can be clearly seen that the MSZW increases with increasing cooling rate. (*S*)-MA nucleates before (*S*)-MA. For (Racemic)-MA it became evident that there exists a particular kinetic inhibition for crystallization from (*S*)-propyl mandelate. Hence no nucleation was observed independent of the cooling rate used. The same type of effect was noticed in the case of mandelic acid/(*S*)-ethyl lactate system, but in contrast here one of the enantiomers did not nucleates.There was an experimental limitation to subcooled the solution below 20.5 °C since the solvent will freeze at this temperature.
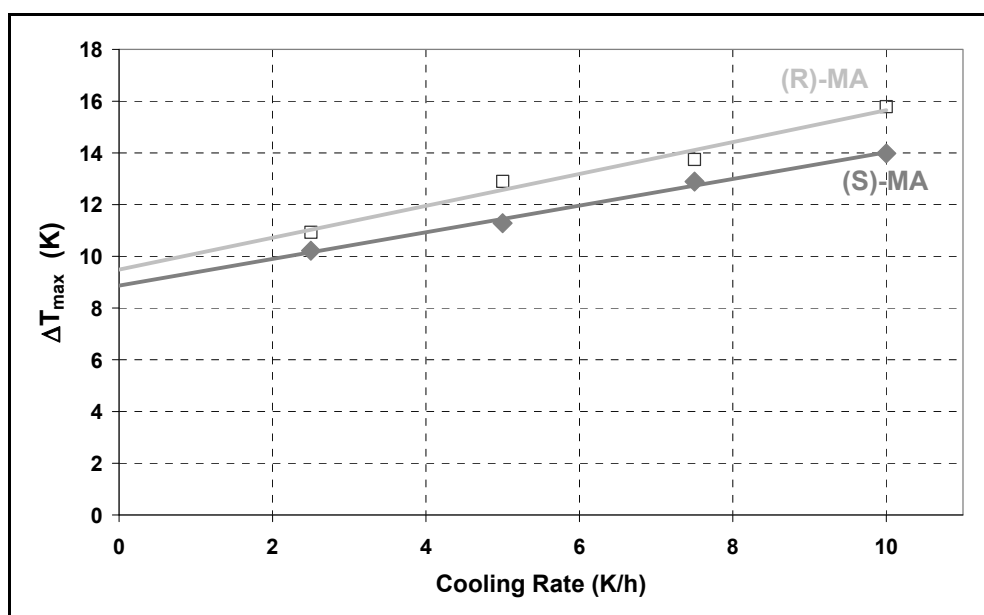
Figure 82: Experimentally determined metastable zone width with respect to primary nucleation for mandelic acid in (*S*)-propyl mandelate at T_{sat} = 50 °C. ((Racemic)-MA: no nucleation in the range of measurement).

It can be seen that the metastable zone is most extended for racemic mandelic acid ((Racemic)-MA), followed by (*R*)-mandelic acid ((*R*)-MA) and (S)-mandelic acid ((*S*)-MA), respectively. Moreover, at higher the cooling rate gives better gap between the MSZW of the (*S*)-MA and the (*R*)-MA. Since the MSZW of (*S*)-MA is smaller compared to that of (*R*)-MA and in particular to that of racemic-MA, preferential nucleation of (*S*)-MA, and thus selective production of the (*S*)-MA enantiomer might be feasible from this tailor-made chiral solvent.

The molecular modeling results summarized in Table 25 also support the MSZW measurements results. The Stabilization enthalpies ($\Delta H_{form}^{Stabilization}$) for (*R*)-MA in (*S*)-propyl mandelate and (*S*)-MA in (*S*)-propyl mandelate are with -5.96 kcal/mol and -2.78kcal/mol respectively. The more negative $\Delta H_{form}^{Stabilization}$ indicates the thermodynamically more stable

dimer which would stay in solution, whilst the less negative case indicates the thermodynamically less stable dimer which would crystallize first. In the course of a resolution process the yield of the less soluble enantiomer ((S)-MA) can be increased by exploiting the wide MSZW of the more soluble counter enantiomer ((R)-MA). The crystallization of the counter-enantiomer can be prevented exclusively by the differences in the solubilities of the two enantiomers.[44] It could be possible to drive the crystallization further, by creating conditions where the more soluble enantiomer is supersaturated but still in the metastable zone, so that it does not crystallize. In the case of the other tailor-made chiral solvent used ((S)-isopropyl mandelate), it was impossible to carry out the metastable zone width measurements due to the high viscosity (solid at room temperature) of the solvent.

The following section will discuss the enthalpy of dissolution results in relation to the observed kinetic effects in the MSZW measurements.

4.5 Enthalpy of dissolution

Generally, dissolution processes involve two different steps. First, there is the breakage of the crystal lattice which is connected to the fusion enthalpy (ΔH_{fus}). As a result the solvent gets in contact with the solute molecules (solvent-solute-interaction). This interaction leads to a particular solvation (second step), which is connected with a certain solvation enthalpy (ΔH_{solv}). From both enthalpies of fusion and dissolution, which are measurable, it is possible to derive the enthalpy of solvation for nonideal systems from the following relation:[148]

$$\Delta H_{solv} = \Delta H_{diss} - \Delta H_{fus}$$

Equation 37

The solvation enthalpy is a relevant thermodynamic measure for the degree of interaction of the solvent and the solute molecules. It has an importance in describing many aspects of crystallization such as growth and nucleation kinetics. The extent of solvent-solute interaction has impact on the solid-liquid interfacial energy, which is a significant physical property influencing nucleation and growth of crystals.[148-151]

Based on the experimentally determined dissolution enthalpies for the MA enantiomers in (S)-ethyl lactate and (2R, 3R)-diethyl tartrate and the enthalpies of fusion of (S)-/(R)-MA (taken from previous work[100]), the subsequent solvation enthalpies (ΔH_{solv}) were derived from Equation 37. The results are summarized in Table 29.

Table 29: Mean enthalpies of dissolution (ΔH_{diss}), and solvation enthalpy (ΔH_{solv}) of mandelic acid in (*S*)-ethyl lactate and (*2R,3R*)-diethyl tartrate. (T = 298.15 K, n_{MA} /$n_{chiral\ solvent}$ = 1: 50, in kJ/mol)

MA species	(S)-ethyl lactate		(2R, 3R)-diethyl tartrate	
	ΔH_{diss}	ΔH_{solv}	ΔH_{diss}	ΔH_{solv}
(*S*)-MA	+7.81 ± 0.35	-16.7	+4.27 ± 0.28	-20.2
(*R*)-MA	+6.41 ± 0.31	-18.1	+7.35 ± 0.26	-17.2

($\Delta H_{fus\ \text{(S)-/(R)-MA}}$ = +24.5 kJ/mol)[100]

As can be seen, the solvation enthalpies for (*R*)-MA in (*S*)-ethyl lactate and (*S*)-MA in (*2R,3R*)-diethyl tartrate are with -18.1 kJ/mol and -20.2 kJ/mol respectively, more negative than for the counter-enantiomers (-16.7 kJ/mol and -17.2 kJ/mol, respectively). Large negative enthalpies of solvation (i.e. higher absolute solvation enthalpy value) indicate strong solvent-solute interactions. Generally, stronger solvent-solute interactions mean that the solute is surrounded by a solvation shell in the liquid phase. So, for the nucleation process to take place the shell needs to be removed. The higher the absolute enthalpy value, the more energy is required[152], which supports the hindrance of the nucleation process. Since for a nucleation process to take place there should be the addition of the solute molecule, which acts as a nuclei or surface for the subsequent solute deposition. Afterwards, the aggregated solute molecule is changed from the liquid to the solid phase. The whole process would be hindered if the solute and solvent in solution forms a strong solvated dimer. Hence, the enantiomer with the more absolute solvation enthalpy value is the one that would create a solute-solvent dimer, which is strongly solvated and would stay in solution, whilst its counter-enantiomer with the less absolute solvation enthalpy would crystallize out first. This explains the results obtained in the MSZW (see Figures 76 and 78) and resolution experiments (see Figures 83 and 85), where (*R*)-mandelic acid in (*2R,3R*)-diethyl tartrate and (*S*)-mandelic acid in (*S*)-ethyl lactate crystallized first. For this reason, the dissolution enthalpy of N-methylephedrine in (*2R,3R*)-diethyl tartrate was measured to understand the reason why resolution was feasible. According to the experimentally determined dissolution enthalpies for the NME enantiomers in (*2R,3R*)-diethyl tartrate and the enthalpy of fusion of (+)-/(-)-NME (taken from literature[102]), solvation enthalpies (ΔH_{solv}) were derived from Equation 37, as described above. The obtained results are summarized in Table 30.

Table 30 Mean enthalpies of dissolution (ΔH_{diss}), and solvation enthalpy (ΔH_{solv}) of N-methylephedrine in (*2R,3R*)-diethyl tartrate. (T = 298.15 K, n_{NME}/$n_{chiral\ solvent}$ = 1: 50, in kJ/mol)

NME species	ΔH_{diss}	ΔH_{solv}
(*1S,2R*)-(+)-NME	+1.208	-29.3
(*1R,2S*)-(-)-NME	+2.162	-28.4

($\Delta H_{fus\ (+)-/(-)-NME}$ = +30.531 kJ/mol)[102]

It can be seen in Table 30 that the solvation enthalpies for (*1S,2R*)-(+)-NME in (*2R,3R*)-diethyl tartrate is with -29.3 kJ/mol more negative than for the counter-enantiomers (-28.4 kJ/mol, respectively). Hence, (*1S,2R*)-(+)-NME stays in solution whilst (*1R,2S*)-(-)-NME would crystallize first. The dissolution enthalpy determination which allowed estimating solvation enthalpies gave an understanding of the observed kinetic effects regarding the induction time and the results of resolution experiments (see Figure 86).

The following section will discuss the results of the feasible enantioselective crystallization experiments which were performed.

4.6 Application of chiral solvents for crystallization-based racemate resolution

Enantioselective crystallization is the implementation of cooling crystallization in such a way that the pure enantiomer can be separated from its respective racemates. The following sections describe how different enantioselective crystallization techniques have been exploited to obtain for selected systems pure enantiomers.

In this thesis investigations have been done to verify the potential of chiral solvents for racemate resolution. With respect to kinetics a chiral solvent can modify the rate of growth of enantiomeric crystals. More precisely, can influence the nucleation/crystal growth rates of the chiral substrates in different ways, depending on the nature, stereospecificity and the effectiveness of solvent-substrate interaction.[5] Hence, this section will deal with how the interactions identified for the chiral solvents were used to perform separation.

4.6.1 Preferential nucleation of mandelic acid in (2R, 3R)-diethyl tartrate

On the basis of the measured solubility and metastable zone width data first resolution experiments of racemic-mandelic acid in (2R, 3R)-diethyl tartrate were designed and conducted. The width of the metastable zone determined at 55 °C is favorable for preferential nucleation. This is due to the fact that the difference between ΔT_{max} values for (S)-mandelic acid and (R)-mandelic acid is wider compared to the other temperatures (Table 27).

Figure 83 depicts a typical result of a preferential nucleation experiment for racemic-mandelic acid in (2R, 3R)-diethyl tartrate at 55 °C. To observe the course of the crystallization process the profiles of the optical rotation and the solution density are presented.
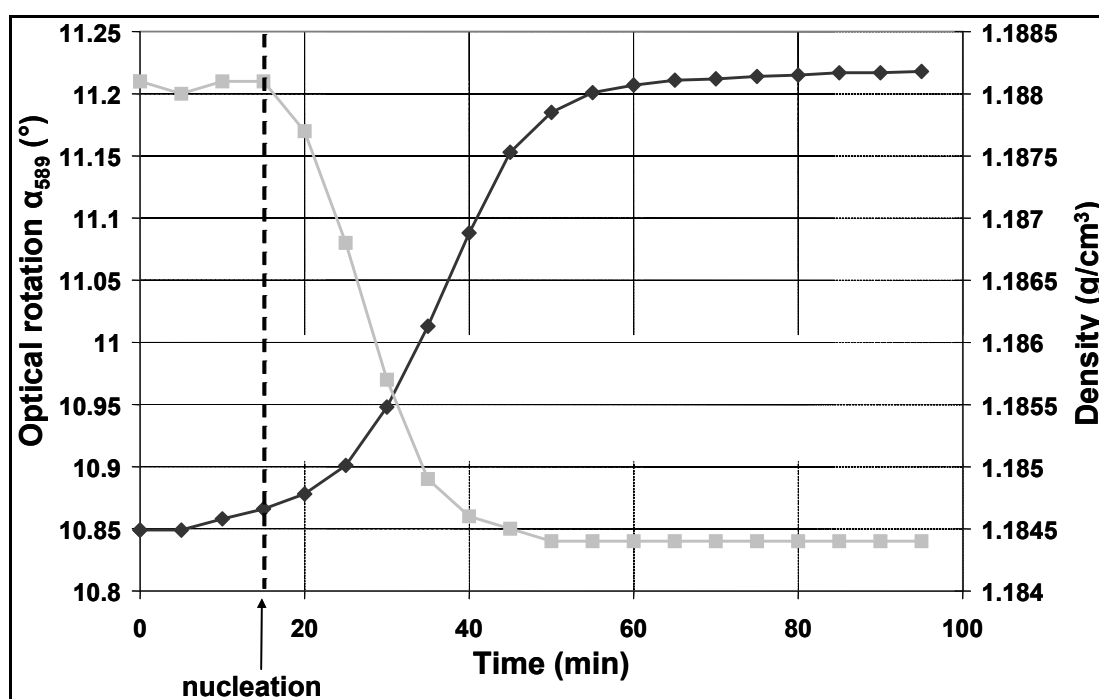
Figure 83: Polarimeter and densitymeter signal for a preferential nucleation experiment starting with racemic-MA in (2R, 3R)-diethyl tartrate at T_{sat} = 55 °C, (Optical rotation in black color and density in gray color).

Before nucleation occurred, both the polarimeter and the densitymeter signals remained roughly constant at 10.849° and 1.1881 g/cm^3, respectively, characterizing the optical rotation of the starting solution of racemic-mandelic acid in (*2R,3R*)-diethyl tartrate (w_{sat} = 31.66 wt %). As nucleation started the trajectory of the polarimeter signal increased continuously for ~ 45 min and remained constant later on. Consistently, the densitymeter signal decreased continuously until it became contant. Since the filter in the sampling line got blocked with very fine crystals the process was stopped after 90 min. The results show that (*S*)-mandelic acid enriches in the liquid phase, which consequently implies that (*R*)-mandelic acid is crystallizing selectively. This course is in agreement with the MSZW measurements. From

the densitymeter and polarimeter signals, the enantiomeric excess reached in the liquid phase was evaluated to be around 55% (*S*)-mandelic acid. In the experiments carried out about 0.98 g of (*R*)-mandelic acid crystallized.

In order to directly compare the results to the situation with water as the solvent, in Figure 84 a similar experiment for racemic-MA in water carried out at 33 °C is shown. The experiments were conducted at the same initial concentration as used for the chiral solvent (w_{sat} = 32 wt %) before.
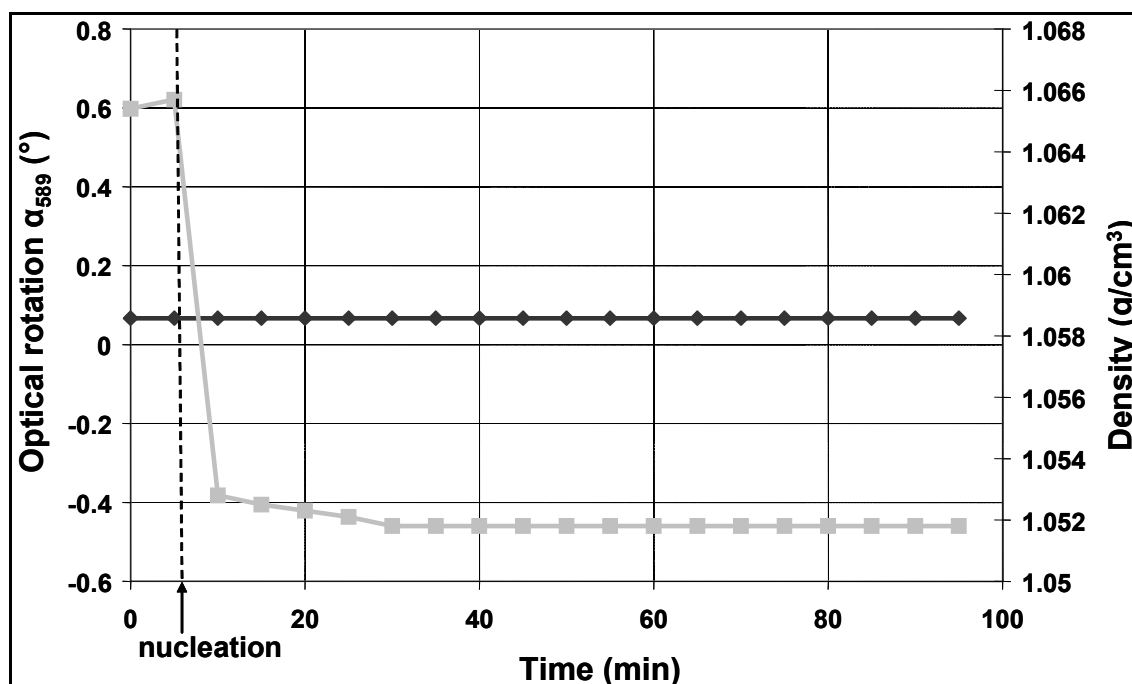
Figure 84: Polarimeter and densitymeter signal for a preferential nucleation experiment starting with racemic-MA in water at T_{sat} = 33 °C, (Optical rotation in black color and density in gray color).

As can be seen, before nucleation the optical rotation and densitymeter signals were at 0.067° and 1.065 g/cm^3, respectively characterizing the starting (racemic) solution. The slight deviation of the optical rotation signal from the zero line is due to a slight initial enrichment in the racemic-MA used. Nucleation is indicated by a sharp decrease in the solution density to about 1.052 g/cm^3. However, the optical rotation remained unchanged, measuring that just racemic-MA has crystallized and, thus, no enantioselective crystallization occurred.

Mughal et al.[48] conducted similar work on primary nucleation in the mandelic acid/water system by starting with eutectic composition of the mandelic acid enantiomers in water ((*S*)-enantiomer in excess) using an additive. The authors could demonstrate an enantiomeric enrichment of the (*S*)-MA in the crystallized material for a certain period of time. This is expected since the MSZW of the mandelic acid enantiomers in water is explicitly lower than that of the racemic compound in the temperature range studied.[47] However, this

enantioselective crystallization process needs to start with a solution containing the enantiomers (more or less) in eutectic composition. In our work the racemate was directly resolved using a chiral solvent.

4.6.2 Preferential crystallization of mandelic acid in (S)-ethyl lactate

According to the results obtained from the metastable zone width measurements for primary nucleation (see Figure 78), (*S*)-mandelic acid should selectively crystallize out after seeding a racemic-mandelic acid in (*S*)-ethyl lactate solution with (*S*)-mandelic acid crystals. This was considered as the starting point for possible resolution method.

Figure 85 illustrates the result of such a seeded experiment presented as course of the enantiomeric excess of (*R*)-mandelic acid in the mother liquor as a function of time after the onset of crystallization.
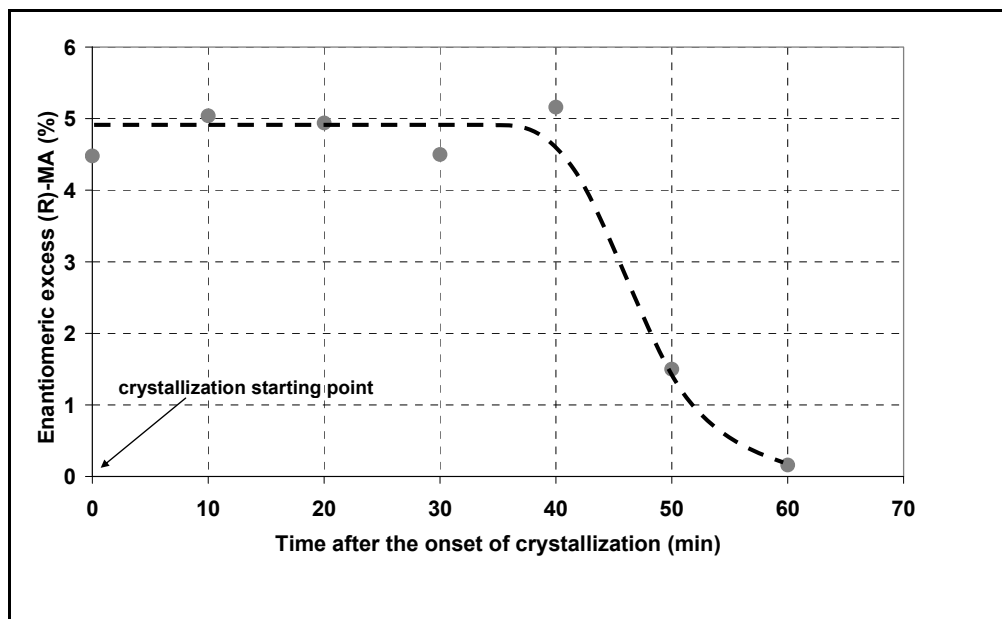
Figure 85: Course of preferential crystallization of (*S*)-mandelic acid over a certain period of time from (S)-ethyl lactate as solvent.

The sudden jump of the enantiomeric excess to almost 5% ee of (*R*)-mandelic acid in the solution indicates a rapid crystallization of (*S*)-mandelic acid after seeding. For further 40 min the enantiomeric excess of (*R*)-mandelic acid in the liquid phase remained at that value. Afterward, the enantiomeric excess decreased since (*R*)-mandelic acid also started to crystallize out. The solution composition then tended towards the racemic composition (i.e. to ee = 0).

Moreover, Hüttenhain and Dickenhof[81] conducted an investigation on asymmetric induction by using same chiral solvents ((*S*)-ethyl lactate) to realize enantioselectivity. The main aim of

their work was to convert acetophenone to phenyl ethanol. Thus, acetophenone was successfully converted to 33% ee of (*R*)-phenyl ethanol in the liquid phase with the aid of the chiral solvent (*S*)-ethyl lactate at 0 °C. The authors could demonstrate an enantiomeric excess of (*R*)-phenyl ethanol (i.e. the (*R*)-form) which is similar to our work where also (*R*)-mandelic acid was enantiomerically in excess in liquid phase. In both investigations (*S*)-ethyl lactate was applied as solvent.

4.6.3 Preferential nucleation of N-methylephedrine in (2R, 3R)-diethyl tartrate

Based on the induction time results this system was a very obvious candidate for a preferential nucleation experiments to might be feasible here. As already discussed in detailed in the above section in this chapter, there was a clear observation about a distinct delay of the appearance of first crystals for racemic-N-methylephedrine the induction time t_{ind} was determined to be 500 seconds, which was longer time compared with the (*1R,2S*)-(-)-N-methylephedrine with 364 seconds and (*1S,2R*)-(+)-N-methylephedrine with 200 seconds, respectively.

In Figure 86 the enantiomeric excess is presented as function of time for a preferential nucleation experiment of (*1R,2S*)-(-)-N-methylephedrine in (*2R,3R*)-diethyl tartrate at 35 °C.
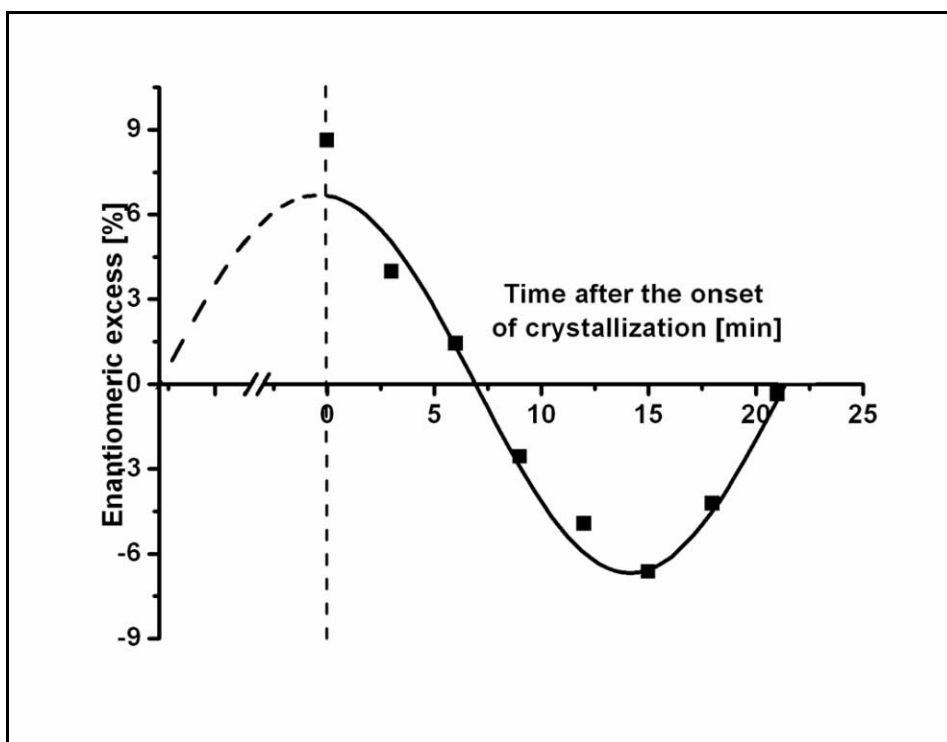
Figure 86: Enantiomeric excess of (*1S,2R*)-(+)-N-methylephedrine in the liquid phase over a certain period of time. Preferential nucleation experiment of (*1R,2S*)-(-)-N-methylephedrine in (*2R,3R*)-diethyl tartrate at 35 °C. Dotted vertical line represents sampling point.

It illustrates the course of the enantiomeric excess of (*1S,2R*)-(+)-N-methylephedrine in the mother liquor as function of time, after onset of nucleation. The sudden jump of the enantiomeric excess to almost 6% ee of (*1S,2R*)-(+)-N-methylephedrine in the solution for some time period indicates a rapid crystallization of (*1R,2S*)-(-)-N-methylephedrine after nucleation. The dashed line designates the onset of nucleation point. Afterward, the counter-enantiomer (*1S,2R*)-(+)-N-methylephedrine started crystallizing, and resulted in enantiomeric excess of (*1R,2S*)-(-)-N-methylephedrine in the liquid phase. Eventually, the enantiomeric excess decreased since the (*1S,2R*)-(+)-N-methylephedrine also started to crystallize out.

The solution composition then tended in the direction of the racemic composition (ee = 0). After the composition reached 0 % ee (racemic mixture), further crystallization of (*1S,2R*)-(+)-N-methylephedrine gave rise to (*1R,2S*)-(-)-N-methylephedrine in the liquid phase to a maximum point. At this maximum point (*1R,2S*)-(-)-N-methylephedrine crystallizes again increasing the trajectory and finally, became equal in amount of enantiomeric excess of both enantiomers. The resolution of N-methylephedrine is cumbersome based on the fact that there is oscillatory behavior of the resolution trajectory, i.e. one phase crystallizes followed by the other phase. This makes the resolution difficult to understand. Further work conducted in our group devoted to characterize the solid phase of N-methylephedrine has shown that two polymorphic forms as proven by both XRPD and DSC. Therefore this behavior could be attributed to the fact that there are that modifications of N-methylephedrine and they could crystallize with different rates.

4.6.4 Preliminary preferential crystallization of mandelic acid in (S)-propyl mandelate

On the basis of the differences in the solubility and metastable zone width of the enantiomers observed, initial resolution experiments of mandelic acid in (*S*)-propyl mandelate were planned and performed. Based on the measurement data from the HPLC analysis for the harvested crystals after crystallization the enantiomeric excess (ee) was derived. The product purity was appreciable with a value of 97.2% ee of (*S*)-MA. A product purity of 100% was not expected since the purity of the seeds was just 99%. The objective of this experiment is to get a first hand knowledge about which phase could crystallize out. The harvested crystals were examined with XRPD and no additional or new phases were formed in the crystal lattice. Also the reflexes identified mimicked the typical enantiomers reflex which implies that the product crystals are 100% ee of enantiomer. The results are in agreement with the solubility and the MSZW measurements.

4.7 Summary

In this chapter the results obtained in the experimental study were comprehensively discussed. First, the binary phase diagrams of the selected model systems mandelic acid and N-methylephedrine from literature data were introduced. Afterward, different forms of racemic mandelic acid (Form I and Form II) were discussed subsequently. Later the fundamental experiments, solid liquid equilibria and nucleation points measurements required for enantioselective crystallization.

In this section also the use of molecular modeling calculations applied to support the derived results was presented. Furthermore, Raman spectra results were described the solvent-solute interaction in the liquid phase were correlated to solid liquid equilibria. Also, the outcome of the FTIR spectroscopy measurements was discussed in the Appendix A. Then enthalpy of dissolution measurements to characterize the solvent-solute interaction has been discussed. Finally, successful resolution experiments designed based on the derived fundamental experiments results are discussed.

Chapter 5. Conclusions and recommendations for future work

Chapter 5

5. Conclusions and Recommendations for Future Work

5.1 Summary and Conclusions

In this PhD thesis, the primary goal was to effect enantioselective crystallization with the aid of chiral solvents by using mandelic acid and N-methylephedrine as model compounds. Three different types of chiral solvents were studied: (a) "classical" chiral solvents, (b) chiral ionic liquids and (c) tailor-made chiral solvents. In this work, initial investigations were carried out to identify appropriate "classical" chiral solvents for the discrimination of enantiomers with the aid of nuclear magnetic resonance (NMR) spectroscopy.[153] The screening of the "classical" chiral solvent was specifically performed with mandelic acid, since this component belongs to the class of compound forming systems which are difficult to be resolved.

^{1}H NMR screening measurements and the corresponding Raman spectra showed that the twelve "classical" chiral solvents that were evaluate had no measurable influence on the chiral system studied. It was found that these solvents had small or no interactions which was not sufficient enough to be exploited for thermodynamically based discrimination of two enantiomers. The ternary solubility phase diagrams for the "classical" chiral solvents and the chosen model systems determined at different temperatures were also found to be symmetrical. In the case of N-methylephedrine in the chiral ionic liquid, (*1R,2S*)-(-)-dimethylephedrinium bis (trifluoromethylsulfonyl) amide there was asymmetry found in the ternary solubility phase diagram. This result shows that there was for this system a stereospecific interaction between the solute and the solvent molecules, resulting in the differentiation of the enantiomers. Furthermore, in the case of mandelic acid and the tailor-made chiral solvents (*S*)-propyl mandelate and (*S*)-isopropyl mandelate systems, there was also an asymmetry in the phase diagram, indicating strong selective interactions between the solute-solvent molecules. This important observation made in this thesis work was supported also by the results of molecular modeling calculations carried out in parallel. These results are a clear indication that, whilst the "classical" chiral solvents studied in this work had less or no influence on solution thermodynamics of the chiral systems mandelic acid and N-methylephedrine, the chiral ionic liquid (*1R,2S*)-(-)-Dimethylephedrinium bis (trifluoromethylsulfonyl) amide and the two tailor-made chiral solvents (S)-propyl mandelate and (*S*)-isopropyl mandelate had a strong selective chiral influence on solution thermodynamics. These results confirm various experimental works on chiral solvents reported in the literature regarding differences in interactions with single enantiomers.[6-8] It was rather unfortunate that for the systems mandelic acid and the tailor-made chiral solvents which showed a significant asymmetry, it was not possible to quantify the eutectic point, as there was no suitable HPLC method available to analyzed the enantiomeric compositions. The

ratio of the enantiomers at the symmetric eutectic compositions remained unchanged with temperature at 0.69 and 0.31 in both solvents as it was also reported for non-chiral solvents.[100] Only two systems in this thesis showed measurable effect on solution thermodynamics, i.e. the two single enantiomers exhibited differences in their solubilities leading to asymmetric solubility phase diagrams, but most of the chiral solvent showed no effect. The literature survey revealed a couple of successful chiral resolutions by employing kinetic effects for enantioselective crystallization with the help of chiral solvents.[46,74,75] However, all the studies apply only to conglomerate systems. In the present work during first nucleation measurements certain observations indicated that selective effects on the rate of nucleation and/or growth of one of the enantiomers by the chiral solvent occur also for compound forming systems. Thus, might be exploited for kinetic resolution of racemic compounds. Therefore detailed nucleation point experiments were performed in order to realize enantioselective crystallization of compound forming systems from chiral solvents.

The resolution of racemic-mandelic acid as a typical compound forming system, which cannot be resolved by convectional crystallization methods without any chiral selector alone, is presented. Lorenz et al.[47] and Mughal et al.[48] illustrated the possibility of enantioselective crystallization in this system starting with a solution having (almost) eutectic composition of the racemic compound and one of the pure enantiomers. In this work chiral solvents have been used in order to facilitate selective nucleation/crystallization directly from the racemic solution.[154]

Though most of the chiral solvents did not show any measurable chiral recognition in terms of solution thermodynamics, regarding kinetics pronounced selective inhibition effects were observed as indicated by differences in MSZW and induction times. The data determined for metastable zone width with regard to primary nucleation illustrated that in (*S*)-ethyl lactate as chiral solvent nucleation of the (*R*)-mandelic acid is significantly inhibited compared to racemic-mandelic acid and the (*S*)-enantiomer. Although resolution of racemic-MA was not feasible by preferential nucleation, so adding (*S*)-mandelic acid seeds, i.e. preferential crystallization allowed for selective crystallization of (*S*)-MA for a certain time period. In the case of the (*2R,3R*)-diethyl tartrate system, the MSZW for the racemic-MA was significantly higher compared to the single enantiomers. Moreover, the MSZW of (*S*)-MA exceeded that of (*R*)-MA enantiomer. Experiments performed on that basis clearly confirmed the feasibility of crystallizing selectively (*R*)-MA from a racemic mixture for a certain time period. Furthermore, a racemic-mixture of N-methylephedrine/(*2R,3R*)-diethyl tartrate was successfully resolved by applying a preferential nucleation method. According to the induction time experiments racemic mixtures of N-methylehpedrine required a long time to

crystallize (inhibited). There were also differences in the induction times of the single enantiomers ((*1R,2S*)-(-)-N-methylephedrine crystallizes first followed by its counter enantiomers).The only problem was the observation of the oscillatory behavior of the resolution trajectory because one phase crystallize at first followed by another phase. This makes the resolution difficult attributed to the fact that there are two modifications of N-methylephedrine as identified during the modification tests using both XRPD and DSC.

Usually, in the presence of a chiral selective additive the so called "rule of reversal"[55,69] holds. This means that the additive is stereoselectively adsorbed at the surface of growing crystals of the enantiomer of the same absolute configuration, resulting in a strong reduction in the growth rate and, thus, allowing for preferential crystallization of the counter-enantiomer. Considering the results of this work and considering the solvent as a chiral selective additive obviously the "rule of reversal" is not obeyed. In our work it was found that in presence of (*S*)-ethyl lactate, (*R*)-MA was inhibited and the (*S*)-MA could grow. Also in the case of (*2R,3R*)-diethyl tartrate, (*S*)-MA was inhibited and promoted (*R*)-MA to grow. The determined solvation enthalpies of (*S*)-MA in (*2R,3R*)-diethyl tartrate, (*R*)-MA in (*S*)-ethyl lactate and (*1S,2R*)-NME in (*2R,3R*)-diethyl tartrate, respectively were more negative than (*R*)-MA in (*2R,3R*)-diethyl tartrate, (*S*)-MA in (*S*)-ethyl lactate and (*1R,2S*)-NME in (*2R,3R*)-diethyl tartrate, respectively, indicating stronger solvent-solute interactions than for the counter-enantiomer. This explains the observed selective inhibition effects and the results of the resolution experiments in the systems. The determination of the solvation enthalpy and molecular modeling calculations could be used as a useful "screening tool" to estimate the degree of interaction between the solvent and the solute molecules and consequently to screen for appropriate chiral solvents.

5.2 Recommendations for future work

In the subsequent sections, some recommendations for future work are given for different fields of research.

5.2.1 Solution thermodynamics

The potential of chiral solvents for enantioselective crystallization has been studied. Further research can be carried out using molecular modeling studies to get a deeper understanding of the solvent-solute interactions in systems with chiral ionic liquids and tailor-made chiral solvents, since these two types of chiral solvents showed clear differences in the solubilities of

the single enantiomers. Molecular modeling calculations coupled with enthalpy of dissolution measurements should serve as a "screening tool" for the chiral solvents that could give better chiral recognitions.

More focus should be directed towards developing HPLC method for the tailor-made chiral solvents to render it possible to analyze the enantiomeric compositions from liquid samples drawn from the solubility measurements. The availability of HPLC method would make it feasible to generate more reliable ternary solubility phase diagrams. This will give more precise eutectic points and solubility isotherms.

5.2.2 Resolution experiments

The induction time experiments were performed for the examples of N-methylephedrine and (*S*)-2-(methoxycarbonyl) pyrrolidinium bis (trifluoromethylsulfonyl) amide. The outcome of further experiments could be very lucrative. There, future work should be carried out to realize for example the resolution of the racemic mixture of N-methylephedrine using the described entrainment process.

Solubility and metastable zone width of mandelic acid and the tailor-made chiral solvent (*S*)-propyl mandelate were studied. Both the solution thermodynamics and kinetics showed chiral discrimination. The racemic mandelic acid did not crystallize in the range covered in the MSZW experiments. This makes it a good candidate for enantioselective crystallization (possibly selective crystallization). Future work should be directed towards the realization of optimized enantioselective crystallization. Further research should be focused also on other tailor-made chiral solvents with different chain length since they already showed chiral recognition in both thermodynamics and kinetic sense.

5.2.3 Areas for future investigations

Further investigation should be performed on chiral solvents by using liquid crystals and chiral ionic liquids for enantioselective crystallization since their structured nature might provide more exploitable chiral interactions. Also, future work should be directed towards characterizing and applying chiral solvents which can provide stronger stereospecific interactions. In principle a classical three-point attachment[155,156] which is up to now not sufficiently investigated should be favourable for improved chiral differentiation.

<u>Appendix</u>

Appendix

A. Appendix A-FTIR measurements

The various peaks observed in the FTIR spectra can be assigned to functional groups. The assignment of the hydroxyl groups is extremely complicated just from applying the bands in the FTIR spectra. Every form has two hydroxyl peaks which require to be assigned; one sharp band at about 3400 cm-1 and a broad peak around 2500 – 3000 cm-1. From literature[106,157] the broad O–H stretching vibrations observed at ~2550 – 3050 cm-1 are characteristic of carboxylic acid hydroxyl groups, while more rigidly bound –OH groups tend to give sharper bands at higher frequency.
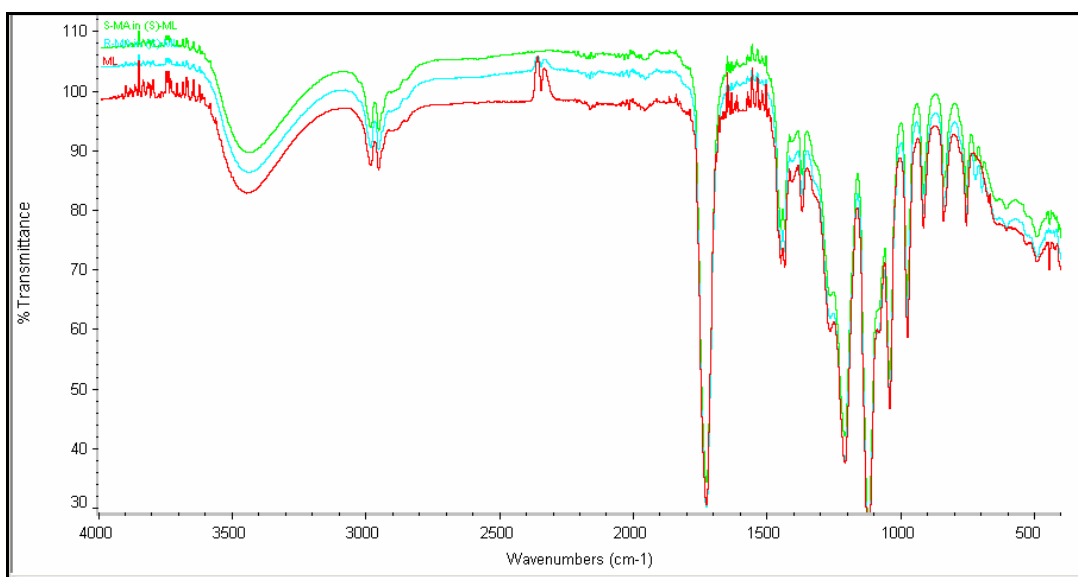
Figure A.87: Overlay of (S)-MA in (S)-ML, (R)-MA in (S)-ML and (S)-ML FTIR spectra.
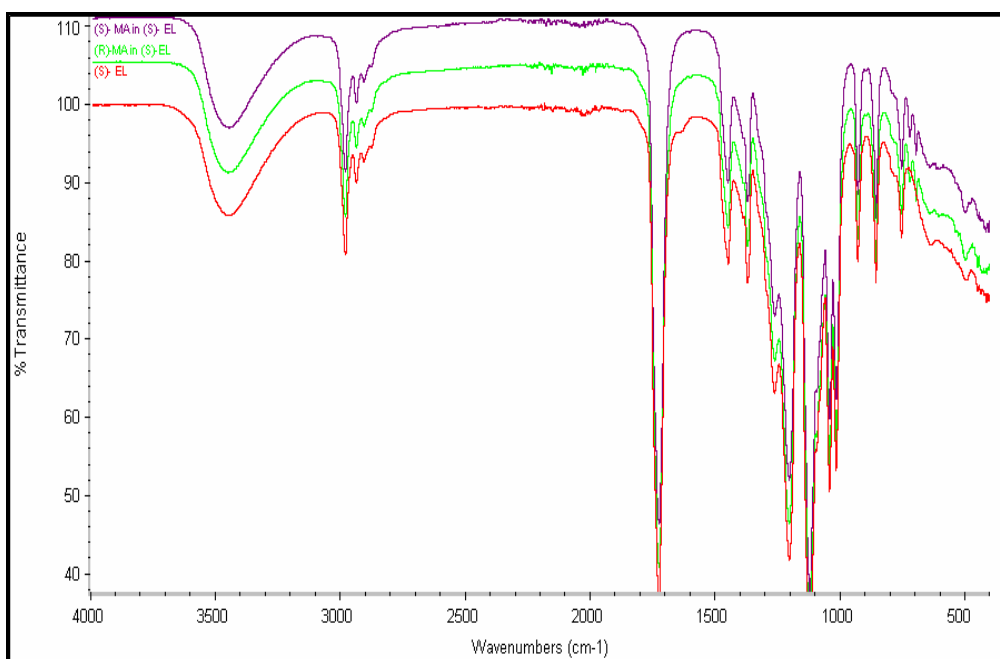
Figure A.88: Overlay of (S)-MA in (S)-EL, (R)-MA in (S)-EL and (S)-EL FTIR spectra.
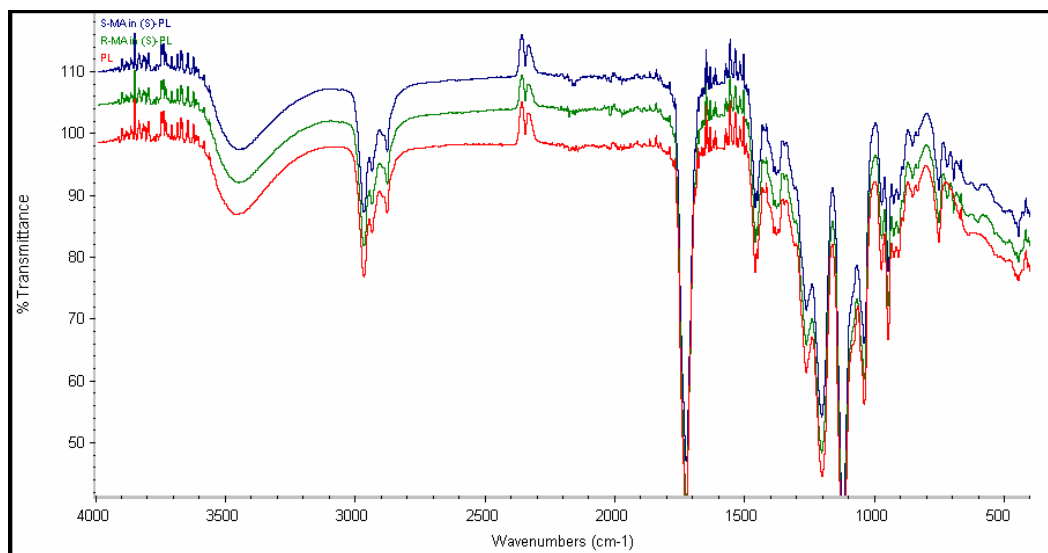
Figure A.89: Overlay of (S)-MA in (S)-PL, (R)-MA in (S)-PL and (S)-PL FTIR spectra.
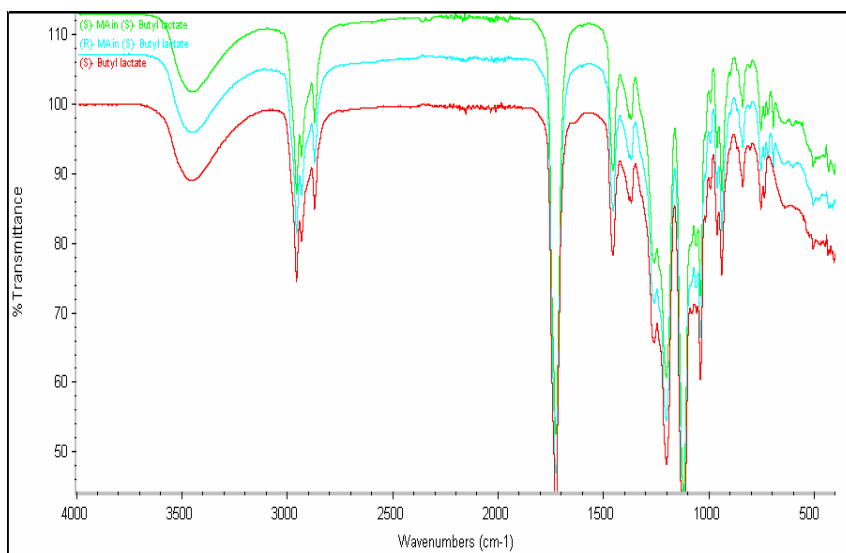
Figure A.90: Overlay of (S)-MA in (S)-BL, (R)-MA in (S)-BL and (S)-BL FTIR spectra.
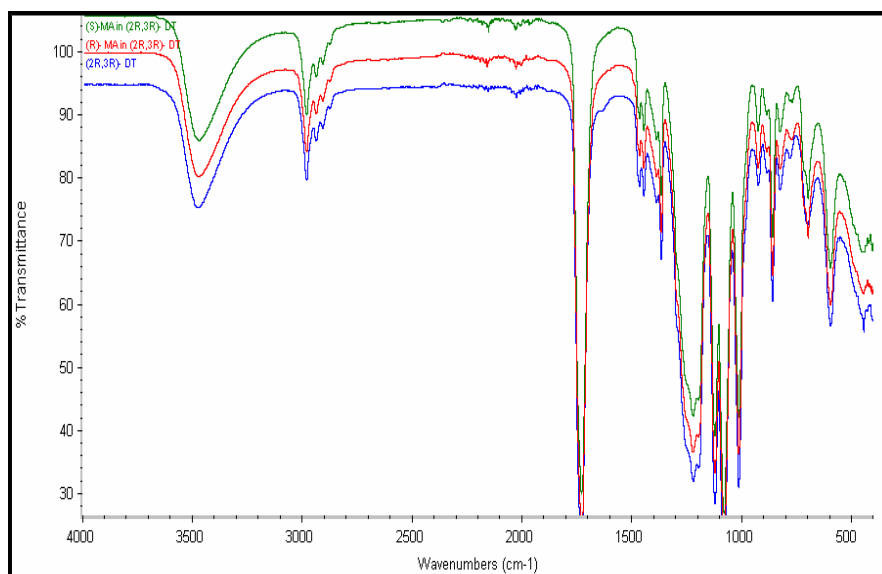
Figure A.91: Overlay of (S)-MA in (2R, 3R)-DT, (R)-MA in (2R, 3R)-DT and (2R, 3R)-DT FTIR spectra.
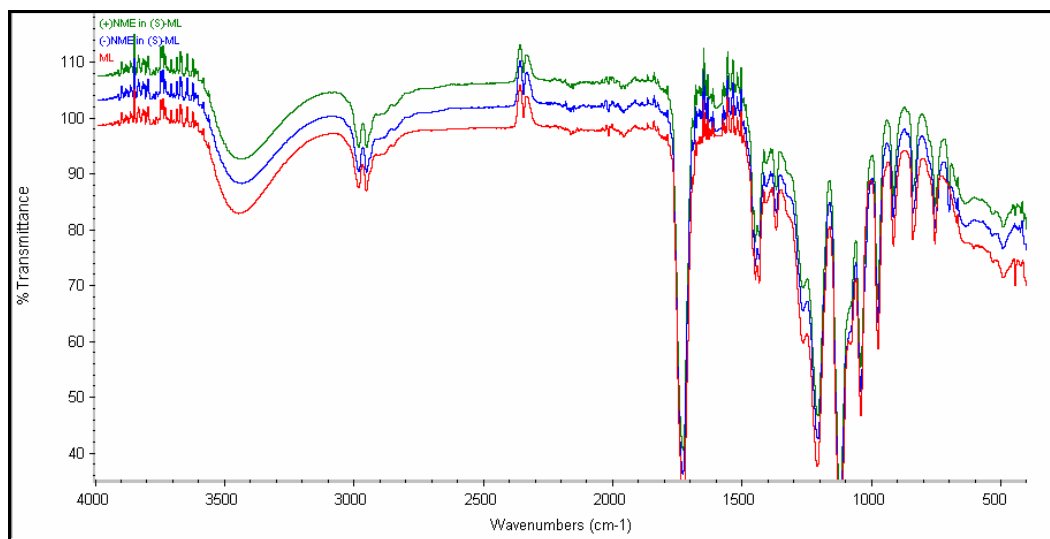
Figure A.92: Overlay of (+)-NME in (S)-ML, (-)-NME in (S)-ML and (S)-ML FTIR spectra.
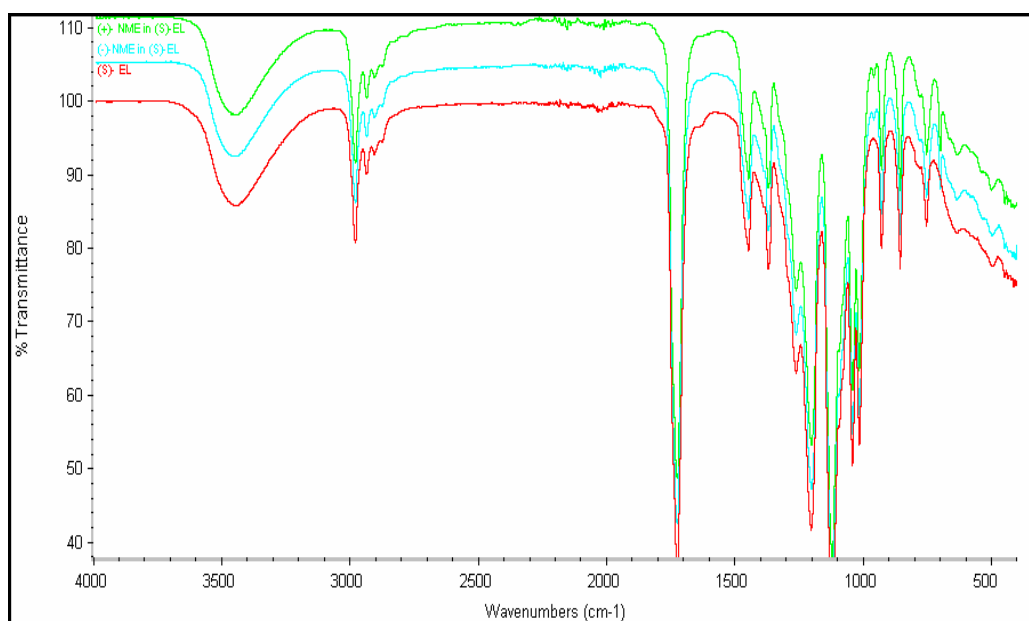
Figure A.93: Overlay of (+)-NME in (S)-EL, (-)-NME in (S)-EL and (S)-EL FTIR spectra.
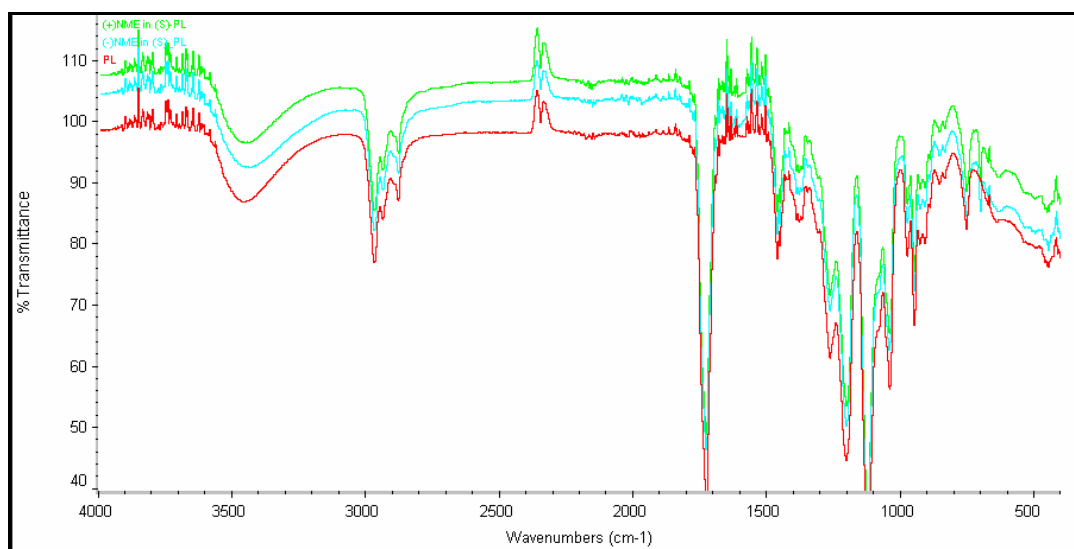
Figure A.94: Overlay of (+)-NME in (S)-PL, (-)-NME in (S)-PL and (S)-PL FTIR spectra.
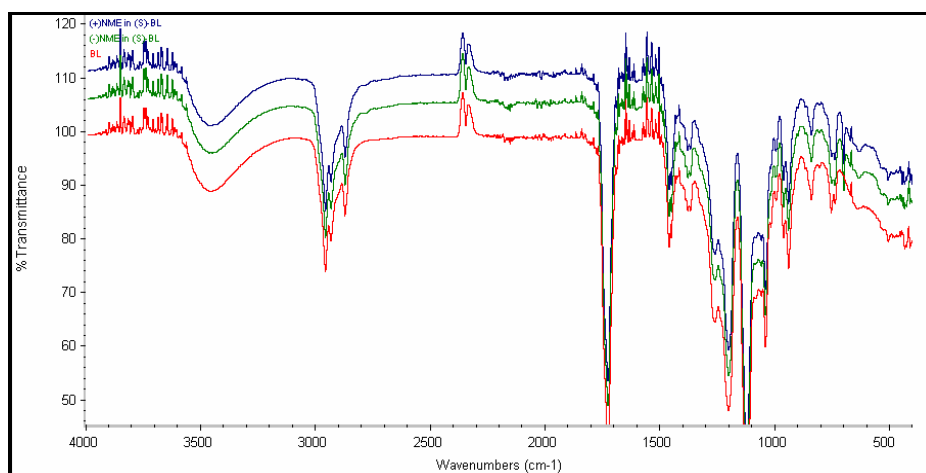
Figure A.95: Overlay of (+)-NME in (S)-BL, (-)-NME in (S)-BL and (S)-BL FTIR spectra.
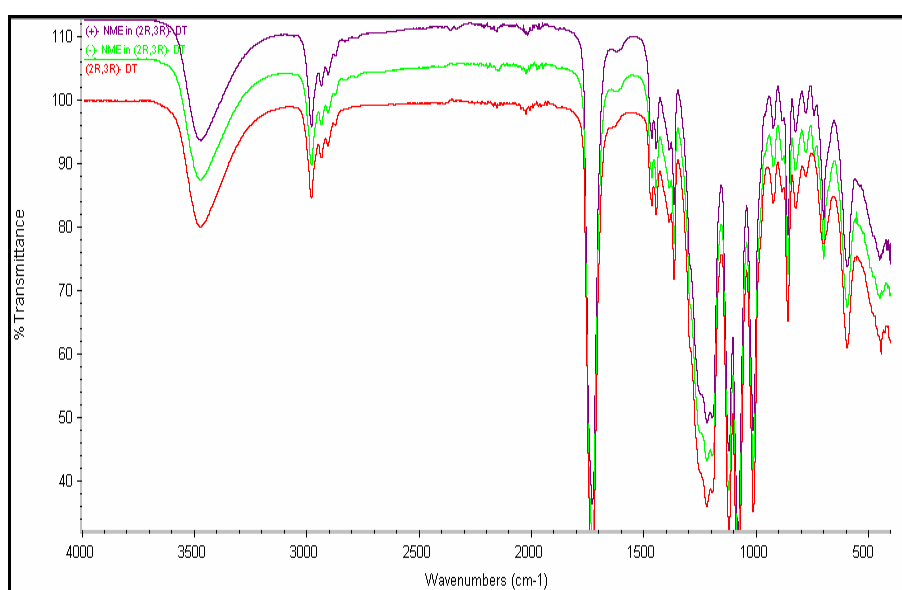
Figure A.96: Overlay of (+)-NME in (2R, 3R)-DT, (-)-NME in (2R, 3R)-DT and (2R, 3R)-DT FTIR spectra.
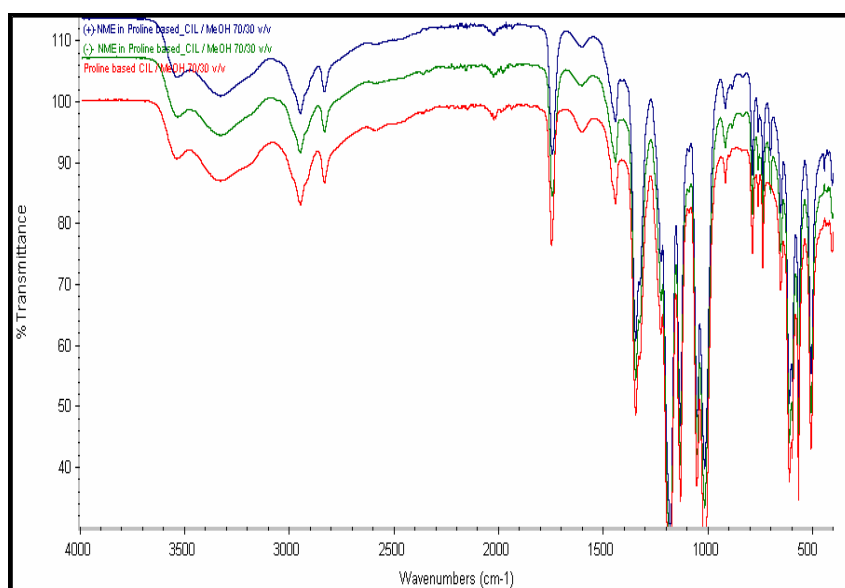
Figure A.97: Overlay of (+)-NME in Proline based CIL/Me0H 70/30 v/v, (-)-NME in Proline based CIL/Me0H 70/30 v/v and Proline based CIL/Me0H 70/30 v/v FTIR spectra.

154
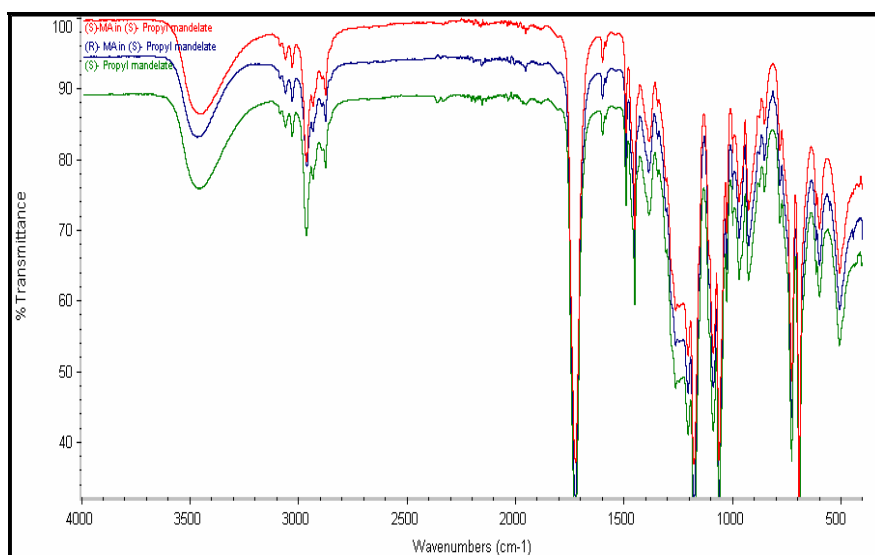
Figure A.98: Overlay of (S)-MA in (S)-PM, (R)-MA in (S)-PM and (S)-PM FTIR spectra.
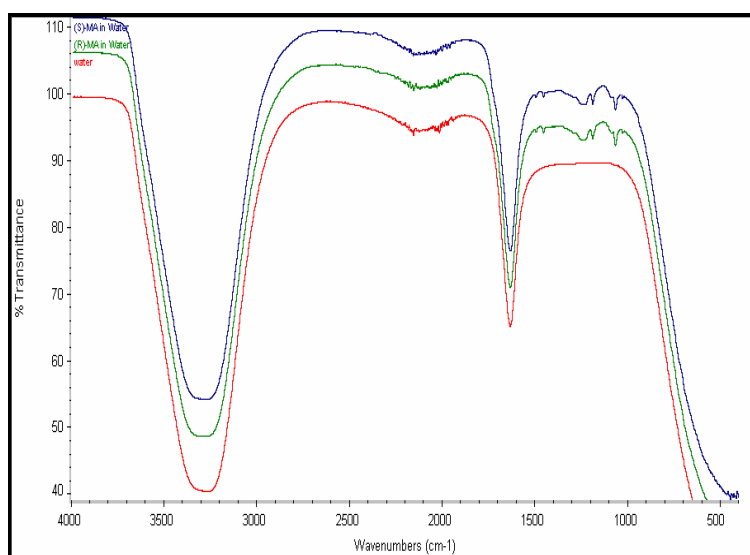
Figure A.99: Overlay of (S)-MA in water, (R)-MA in water and water FTIR spectra.
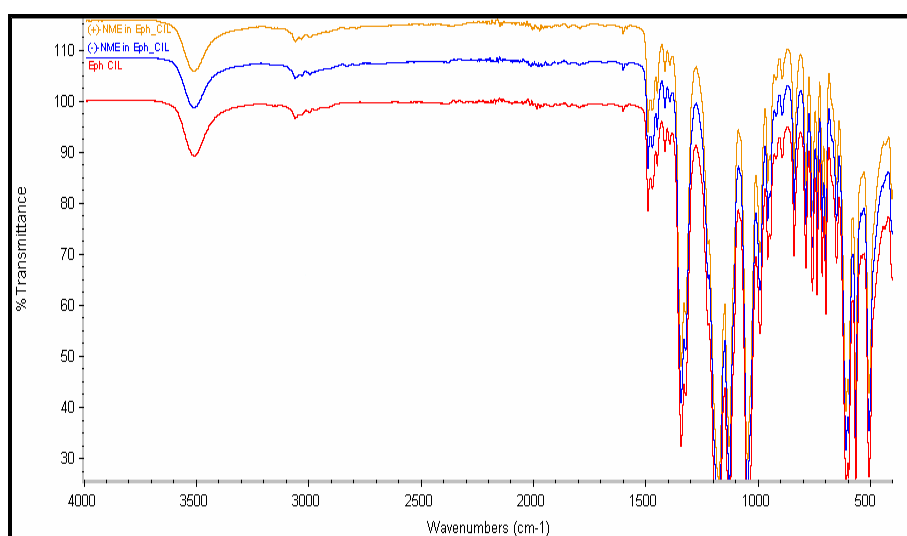
Figure A.100: Overlay of (+)-NME in Eph CIL, (-)-NME in Eph CIL and Eph CIL FTIR spectra.
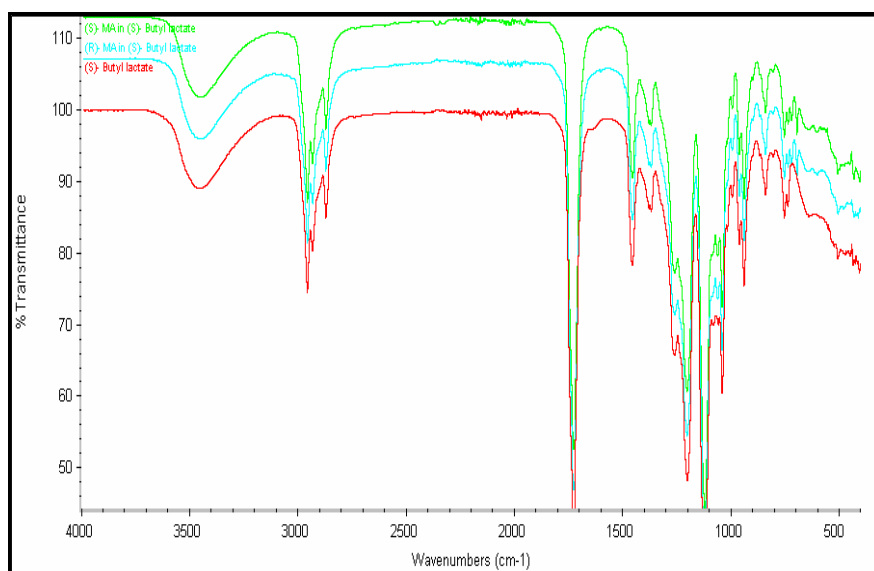
Figure A.101: Overlay of (S)-MA in Butyl lactate, (R)-MA in Butyl lactate and (S)-Butyl lactate FTIR spectra.
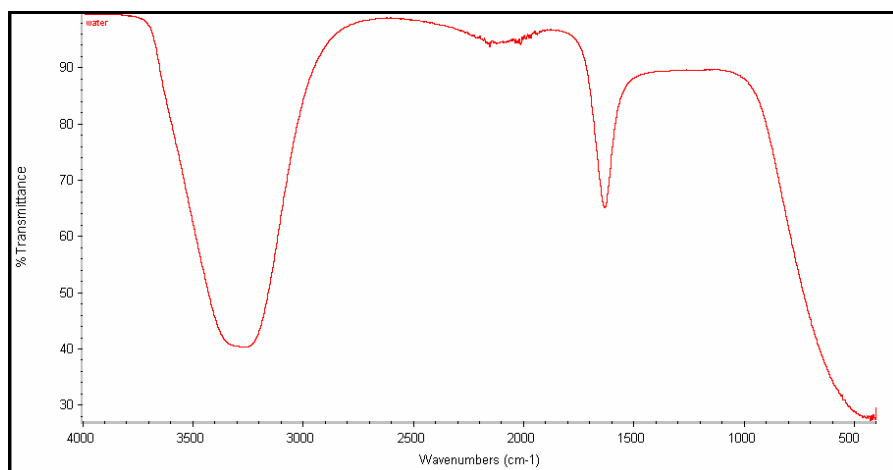
Figure A.102: Water FTIR spectra.
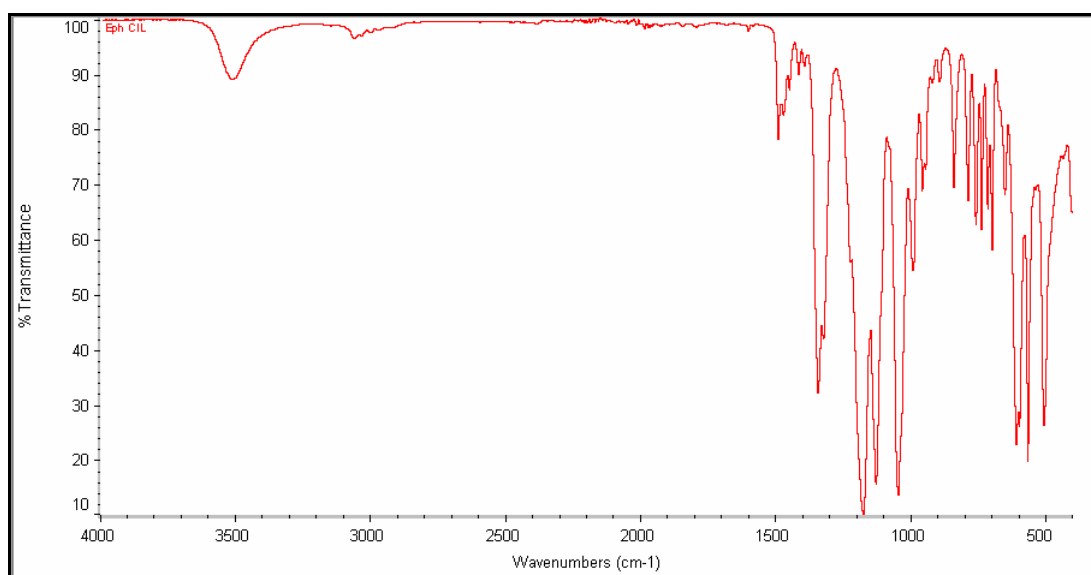
Figure A.103: Eph CIL FTIR spectra.

156
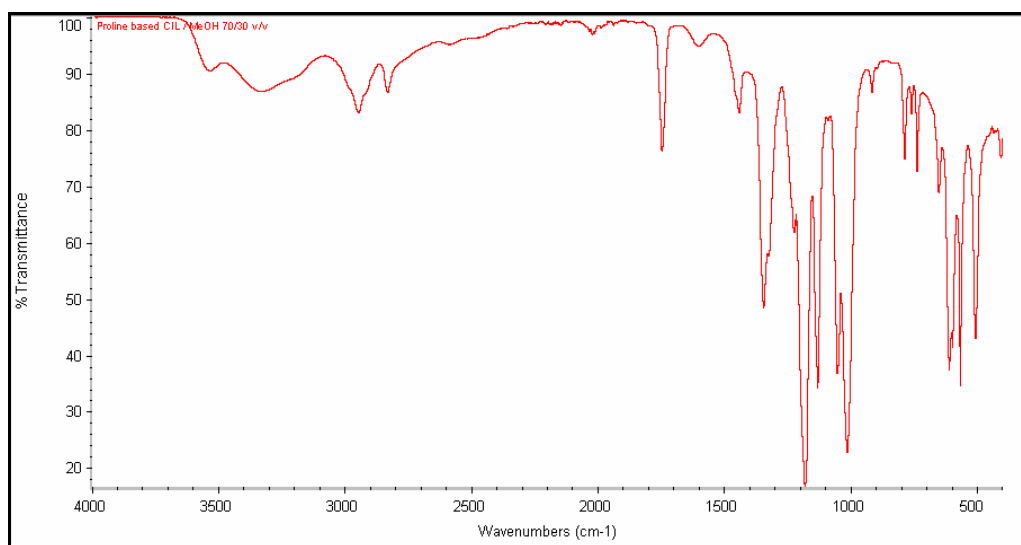
Figure A.104: Proline based CIL/Me0H 70/30 v/v FTIR spectra.
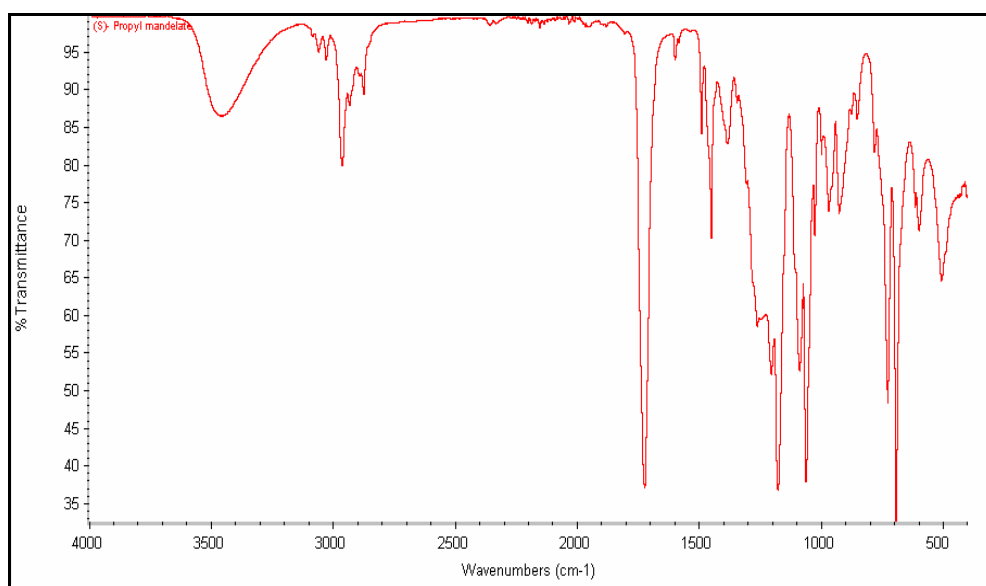
Figure A.105: (S)-propyl mandelate FTIR spectra.
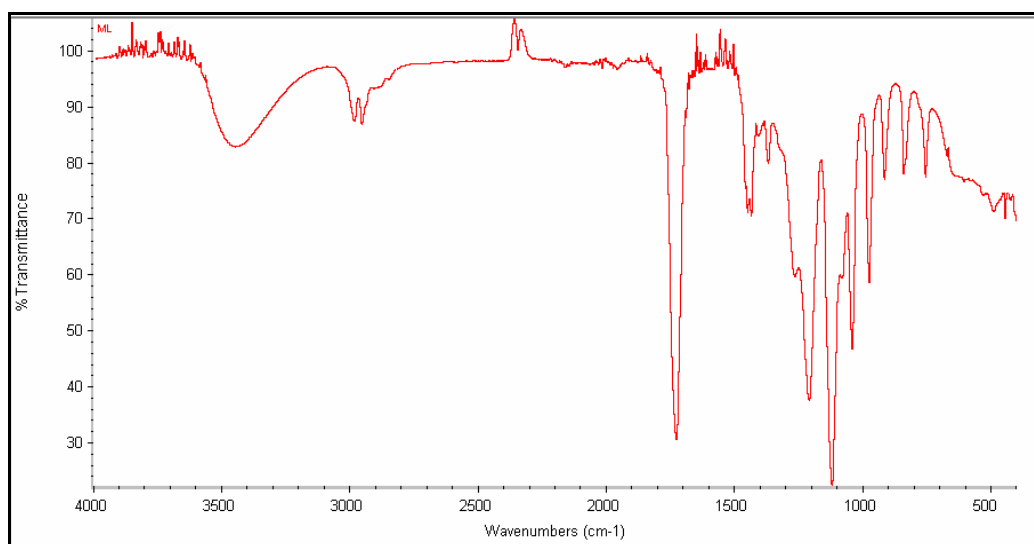
Figure A.106: (S)-methyl lactate FTIR spectra.
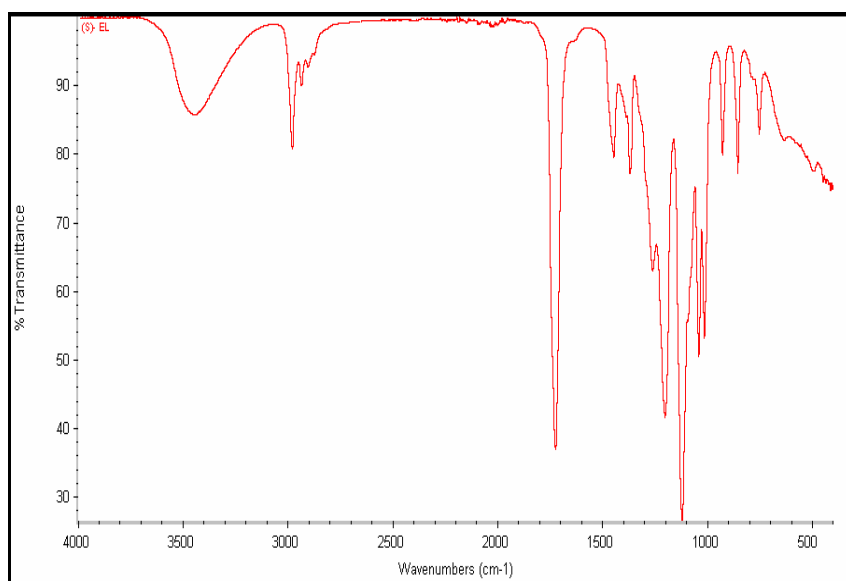
Figure A.107: (S)-ethyl lactate FTIR spectra.
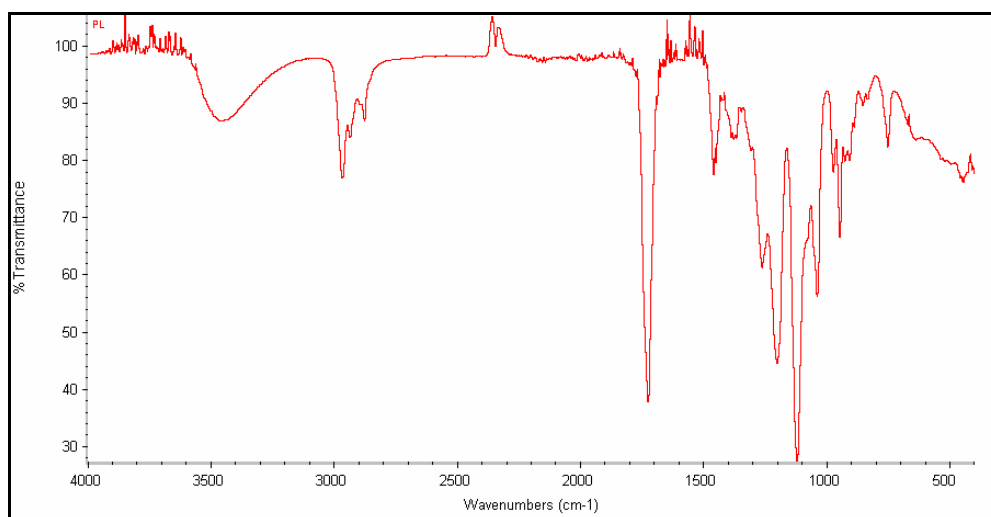
Figure A.108: (S)-propyl lactate FTIR spectra.
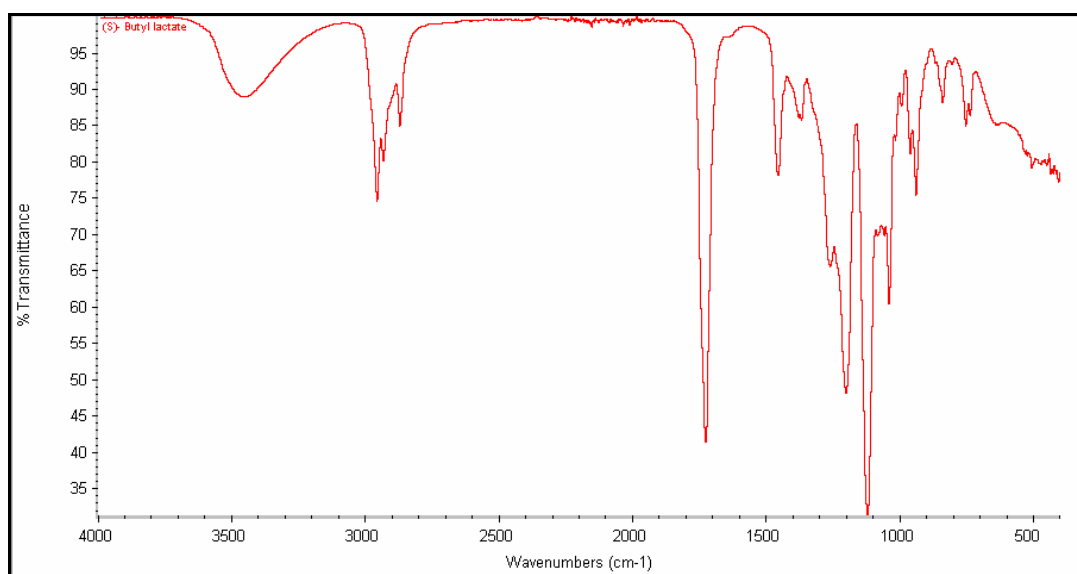
Figure A.109: (S)-butyl lactate FTIR spectra.
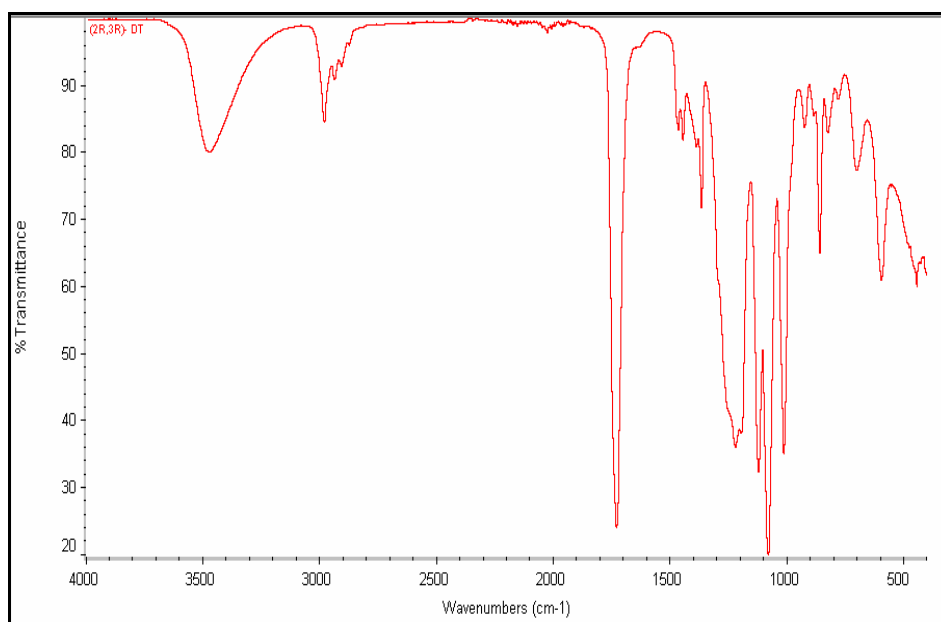
Figure A.110: (2R, 3R)-DT FTIR spectra.

B. Appendix B-Tables with a summary solubility data

B1. Tables of solubility data of mandelic acid in the different "classical" chiral solvent

Table B.31: Mass Fraction Solubility (w_i) of (S)-Mandelic acid (1) and (R)-Mandelic acid (2) in (S)-Methyl Lactate at different Enantiomeric Excesses (ee) $\left[ee = |w_1 - w_2|/(w_1 + w_2)\right]$ and Temperatures.

100 ee	100 ($w_{1+}w_2$)	100 w_1	100 w_2	100 $w_{solvent}$
		t = 0 °C		
100.00	19.83	19.83	0.00	80.17
38.00	27.90	19.25	8.65	72.10
0.00	25.66	12.83	12.83	74.34
38.00	27.97	8.67	19.30	72.03
100.00	19.80	0.00	19.80	80.20
		t = 5 °C		
100.00	22.37	22.37	0.00	77.63
38.08	29.40	20.30	9.10	70.60
0.00	27.08	13.54	13.54	72.92
38.10	29.50	9.13	20.37	70.50
100.00	22.15	0.00	22.15	77.85
		t = 15 °C		
100.00	24.09	24.09	0.00	75.91
38.48	31.03	21.49	9.54	68.97
0.32	29.44	14.67	14.77	70.56
38.10	30.66	9.58	21.08	69.34
100.00	24.00	0.00	24.00	76.00
		t = 25 °C		
100.00	27.57	27.57	0.00	72.43
90.90	28.46	27.17	1.29	71.54
78.42	29.79	26.58	3.21	70.21
71.32	31.34	26.85	4.49	68.66
51.78	33.93	25.75	8.18	66.07
38.08	35.04	24.19	10.85	64.96
28.60	33.93	21.82	12.11	66.07
19.20	33.26	19.82	13.44	66.74
0.00	32.89	16.44	16.44	67.11
21.22	33.21	13.08	20.13	66.79
27.80	33.79	12.20	21.59	66.21
38.10	34.89	10.80	24.09	65.11
49.30	33.80	8.57	25.23	66.20
69.60	31.20	4.74	26.46	68.80
77.80	30.10	3.34	26.76	69.90

Continuation of Table B.31

89.50	27.90	1.46	26.44	72.10
100.00	27.49	0.00	27.49	72.51
		t = 35 °C		
100.00	29.45	29.45	0.00	70.55
38.08	38.46	26.55	11.91	61.54
0.00	35.80	17.90	17.90	64.20
38.10	38.79	12.01	26.78	61.21
100.00	29.15	0.00	29.15	70.85

Table B.32: Mass Fraction Solubility (w_i) of (S)-Mandelic acid (1) and (R)-Mandelic acid (2) in (S)-Propyl Lactate at different Enantiomeric Excesses (ee) $\left[ee = \left| w_1 - w_2 \right| / (w_1 + w_2) \right]$ and Temperatures.

100 ee	100 (w_{1+2})	100 w_1	100 w_2	100 $w_{solvent}$
		t = 5 °C		
100.00	16.10	16.10	0.00	83.90
38.08	21.37	14.75	6.62	78.63
0.00	20.17	10.08	10.08	79.83
38.10	21.21	6.56	14.65	78.79
100.00	15.70	0.00	15.70	84.30
		t = 15 °C		
100.00	18.11	18.11	0.00	81.89
38.32	24.00	16.60	7.40	76.00
0.38	22.41	11.25	11.16	77.59
38.30	23.68	7.31	16.37	76.32
100.00	18.03	0.00	18.03	81.97
		t = 25 °C		
100.00	20.15	20.15	0.00	79.85
90.10	21.83	20.75	1.08	78.17
79.70	23.12	20.77	2.35	76.88
69.94	24.40	20.73	3.67	75.60
49.74	26.87	20.12	6.75	73.13
38.22	27.51	19.01	8.50	72.49
30.40	26.79	17.47	9.32	73.21
19.74	25.99	15.56	10.43	74.01
0.00	25.51	12.76	12.76	74.49
19.98	26.95	10.78	16.17	73.05
38.20	27.35	8.45	18.90	72.65
50.22	27.75	6.91	20.84	72.25
69.94	24.24	3.64	20.60	75.76
80.08	23.28	2.32	20.96	76.72
89.90	22.15	1.12	21.03	77.85
100.00	20.31	0.00	20.31	79.69

Continuation of Table B.32

		t = 35 °C		
100.00	24.64	24.64	0.00	75.36
38.08	32.72	22.59	10.13	67.28
0.00	30.39	15.20	15.20	69.61
38.10	33.36	10.32	23.04	66.64
100.00	24.24	0.00	24.24	75.76

Table B.33: Mass Fraction Solubility (w_i) of (S)-Mandelic acid (1) and (R)-Mandelic acid (2) in (S)-Butyl Lactate at different Enantiomeric Excesses (ee) $\left[ee = |w_1 - w_2|/(w_1 + w_2) \right]$ and Temperatures.

100 ee	100 ($w_{1+}w_2$)	100 w_1	100 w_2	100 $w_{solvent}$
		t = 0 °C		
100.00	12.72	12.72	0.00	87.28
38.00	17.28	11.92	5.36	82.72
0.00	15.05	7.53	7.53	84.95
38.00	17.45	5.41	12.04	82.55
100.00	12.63	0.00	12.63	87.37
		t = 5 °C		
100.00	13.23	13.23	0.00	86.77
38.5	18.83	13.04	5.79	81.17
0.24	16.94	8.45	8.49	83.04
38.44	19.00	5.85	13.15	81.00
100.00	13.23	0.00	13.23	86.77
		t = 15 °C		
100.00	15.28	15.28	0.00	84.72
38.28	21.00	14.52	6.48	79.00
0.00	19.34	9.67	9.67	80.66
38.36	21.23	6.54	14.69	78.77
100.00	15.01	0.00	15.01	84.99
		t = 25 °C		
100.00	16.90	16.90	0.00	83.10
84.00	19.17	17.64	1.53	80.83
74.48	20.43	17.82	2.61	79.57
68.00	21.36	17.94	3.42	78.64
48.00	23.39	17.31	6.08	76.61
46.98	24.06	17.68	6.38	75.94
45.90	23.89	17.43	6.46	76.11
38.08	23.23	16.04	7.19	76.77
24.92	24.47	15.28	9.19	75.53
0.00	21.00	10.50	10.50	79.00
38.10	23.00	7.12	15.88	77.00
45.90	23.35	6.32	17.03	76.65
46.98	23.33	6.18	17.15	76.67

Continuation of Table B.33

48.34	22.71	5.87	16.84	77.29
67.78	20.88	3.36	17.52	79.12
74.48	19.79	2.53	17.26	80.21
83.62	18.85	1.54	17.31	81.15
100.00	16.64	0.00	16.64	83.36
		t = 35 °C		
100.00	20.50	20.50	0.00	79.50
38.58	27.36	18.96	8.40	72.64
0.00	26.31	13.16	13.16	73.69
38.46	27.28	8.39	18.89	72.72
100.00	20.51	0.00	20.51	79.49
		t = 45 °C		
100.00	22.29	22.29	0.00	77.71
37.76	30.90	21.28	9.62	69.10
0.00	28.44	14.22	14.22	71.56
38.10	30.90	9.56	21.34	72.72
100.00	22.29	0.00	22.29	77.71

B2. Tables of solubility data of N-methylephedrine in the different "classical" chiral solvent

Table B.34: Mass Fraction Solubility (w_i) of (+)-N-methylephedrine (3) and (-)-N-methylephdrine (4) in (S)-Methyl Lactate at different Enantiomeric Excesses (ee) $\left[ee = |w_3 - w_4|/(w_3 + w_4)\right]$ and Temperatures.

100 ee	100 ($w_{3+}w_4$)	100 w_3	100 w_4	100 $w_{solvent}$
		t = 0 °C		
100.00	13.32	13.32	0.00	86.68
40.46	18.50	12.99	5.51	81.50
1.19	23.87	12.08	11.79	76.13
42.22	18.80	5.43	13.37	81.20
100.00	12.99	0.00	12.99	87.01
		t = 5 °C		
100.00	16.50	16.50	0.00	83.50
46.40	21.12	15.46	5.66	78.88
0.00	29.03	14.52	14.52	70.97
46.84	21.22	5.64	15.58	78.78
100.00	16.56	0.00	16.56	83.44
		t = 10 °C		
100.00	18.74	18.74	0.00	81.26
46.50	23.45	17.18	6.27	76.55
0.00	31.42	15.71	15.71	68.58

Continuation of Table B.34

47.00	22.98	6.09	16.89	77.02
100.00	18.79	0.00	18.79	71.21
t = 15 °C				
100.00	21.00	21.00	0.00	79.00
46.70	26.60	19.51	7.09	73.40
0.00	36.20	18.10	18.10	63.80
47.70	26.40	6.90	19.50	73.60
100.00	21.15	0.00	21.15	78.85
t = 20 °C				
100.00	23.04	23.04	0.00	76.96
42.88	31.02	22.16	8.86	68.98
0.22	40.36	20.22	20.12	59.64
45.94	30.95	8.37	22.58	69.05
100.00	23.11	0.00	23.11	76.89
t = 25 °C				
100.00	24.41	24.41	0.00	75.59
39.09	35.06	24.38	10.68	64.94
0.97	45.16	22.80	22.36	54.84
39.40	35.06	10.62	24.44	64.94
100.00	24.50	0.00	24.50	75.50

Table B.35: Mass Fraction Solubility (w_i) of (+)-N-methylephedrine (3) and (-)-N-methylephdrine(4) in (S)-Propyl Lactate at different Enantiomeric Excesses (ee) $\left[ee = |w_3 - w_4|/(w_3 + w_4)\right]$ and Temperatures.

100 ee	100 $(w_{3}+w_{4})$	100 w_3	100 w_4	100 $w_{solvent}$
t = 0 °C				
100.00	11.19	11.19	0.00	88.81
46.57	14.68	10.76	3.92	85.32
1.19	22.25	11.26	10.99	77.75
47.01	16.15	4.28	11.87	83.85
100.00	11.25	0.00	11.25	88.75
t = 5 °C				
100.00	14.00	14.00	0.00	86.00
46.50	19.00	13.92	5.08	81.00
0.00	26.00	13.00	13.00	74.00
47.00	19.00	5.04	13.96	81.00
100.00	13.98	0.00	13.98	86.02
t = 10 °C				
100.00	15.25	15.25	0.00	84.75
50.30	19.80	14.88	4.92	80.20
0.00	27.62	13.81	13.81	72.38
51.00	19.70	4.83	14.87	80.30
100.00	15.15	0.00	15.15	84.85

Continuation of Table B.35

t = 15 °C				
100.00	17.51	17.51	0.00	82.49
39.09	23.69	16.47	7.21	76.31
0.97	30.80	15.55	15.25	69.20
38.40	23.75	7.43	16.55	76.25
100.00	16.92	0.00	16.92	83.08
t = 20 °C				
100.00	19.25	19.25	0.00	80.75
39.09	26.00	18.08	7.92	74.00
0.97	34.00	17.16	16.83	66.00
38.40	26.00	8.14	18.12	74.00
100.00	19.30	0.00	19.30	80.70
t = 25 °C				
100.00	20.18	20.18	0.00	79.82
38.85	28.88	20.05	8.83	71.12
0.84	39.34	19.84	19.50	60.66
37.56	29.53	9.22	20.31	70.47
100.00	20.76	0.00	20.76	79.24

Table B.36: Mass Fraction Solubility (w_i) of (+)-N-methylephedrine (3) and (-)-N-methylephdrine (4) in (S)-Butyl Lactate at different Enantiomeric Excesses (ee) $\left[ee = |w_3 - w_4|/(w_3 + w_4)\right]$ and Temperatures.

100 ee	100 ($w_{3+}w_4$)	100 w_3	100 w_4	100 $w_{solvent}$
t = 0 °C				
100.00	10.08	10.08	0.00	89.92
46.19	13.86	10.13	3.73	86.14
0.00	19.42	9.71	9.71	80.58
43.95	14.36	4.02	10.34	85.64
100.00	10.38	0.00	10.38	89.62
t = 5 °C				
100.00	12.61	12.61	0.00	87.39
40.00	16.93	11.85	5.08	83.07
0.00	22.00	11.00	11.00	78.00
42.00	17.26	5.01	14.25	82.74
100.00	12.90	0.00	12.90	87.10
t = 10 °C				
100.00	13.74	13.74	0.00	86.26
52.30	17.40	13.25	4.15	82.60
0.00	25.00	12.50	12.50	75.00
50.00	17.50	4.38	13.12	82.50
100.00	13.60	0.00	13.60	86.40

Continuation of Table B.36

		t = 15 °C		
100.00	15.26	15.26	0.00	84.74
53.70	19.89	15.29	4.60	80.11
0.00	29.26	14.63	14.63	70.74
50.00	20.95	5.24	15.71	79.05
100.00	15.81	0.00	15.81	84.19
		t = 20 °C		
100.00	17.50	17.50	0.00	82.50
46.30	23.90	17.48	6.42	76.10
0.00	32.00	16.00	16.00	68.00
48.30	24.00	6.20	17.80	76.00
100.00	17.40	0.00	17.40	82.60
		t = 25 °C		
100.00	18.60	18.60	0.00	81.40
40.50	27.07	19.02	8.05	72.93
1.43	37.18	18.85	18.33	62.82
37.10	27.85	8.76	19.09	72.15
100.00	18.55	0.00	18.55	81.45

C. Appendix C-Ternary solubility phase diagram

C1. Mandelic acid ternary solubility phase diagrams
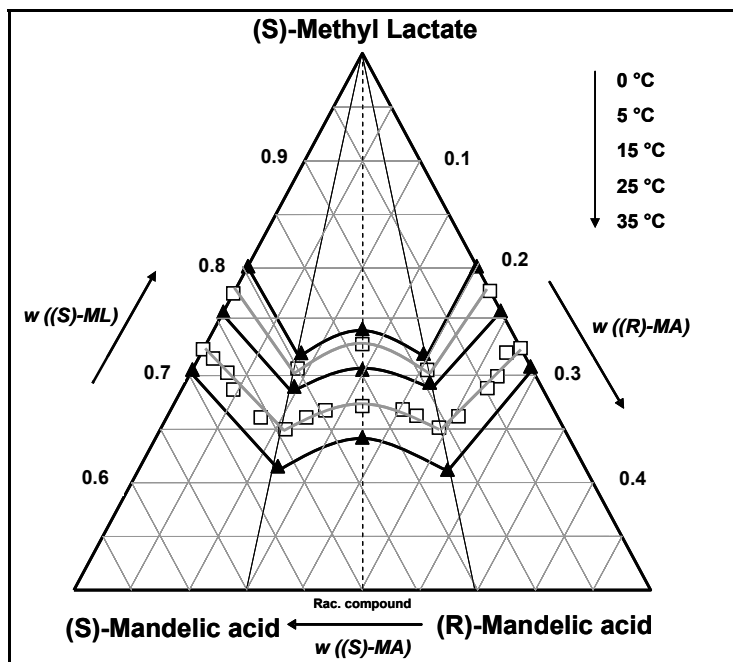
Figure C.111: Ternary phase diagram of mandelic acid in (S)-methyl lactate at different temperatures. Axes in weight fractions; $w_{(S)-MA}$ and $w_{(R)-MA} \leq 0.5$. The isothermal lines have been added as a visualization aid and only the marked points show measured data.
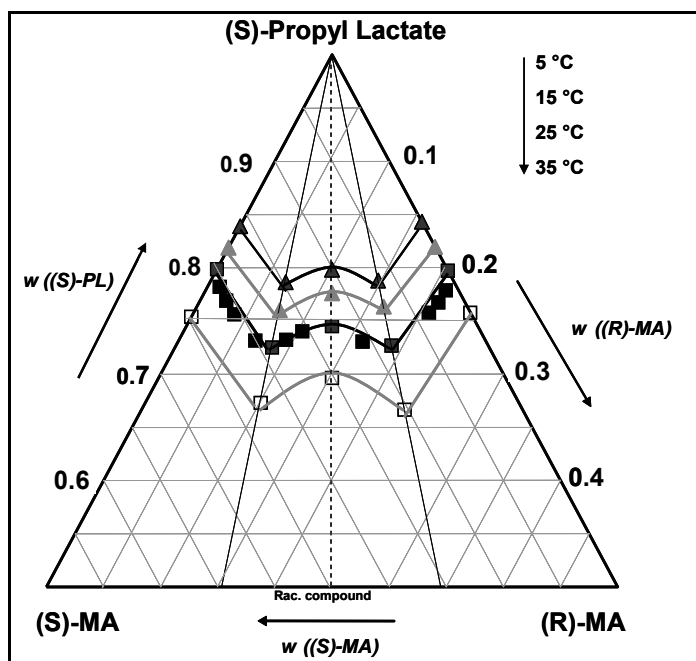
Figure C.112: Ternary phase diagram of mandelic acid in (S)-propyl lactate at different temperatures. Axes in weight fractions; $w_{(S)-MA}$ and $w_{(R)-MA} \leq 0.5$. The isothermal lines have been added as a visualization aid and only the marked points show measured data.
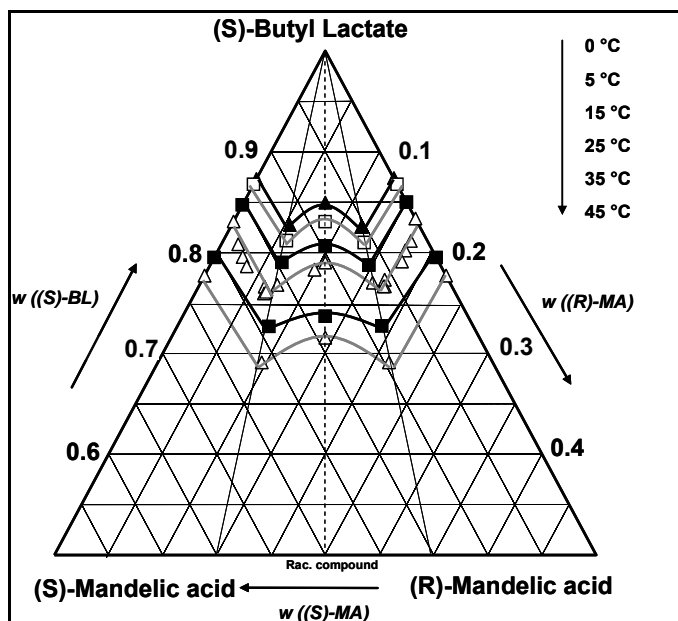
Figure C.113: Ternary phase diagram of mandelic acid in (S)-butyl lactate at different temperatures. Axes in weight fractions; $w_{(S)-MA}$ and $w_{(R)-MA} \leq 0.5$. The isothermal lines have been added as a visualization aid and only the marked points show measured data.

C2. N-methylephedrine ternary solubility phase diagrams
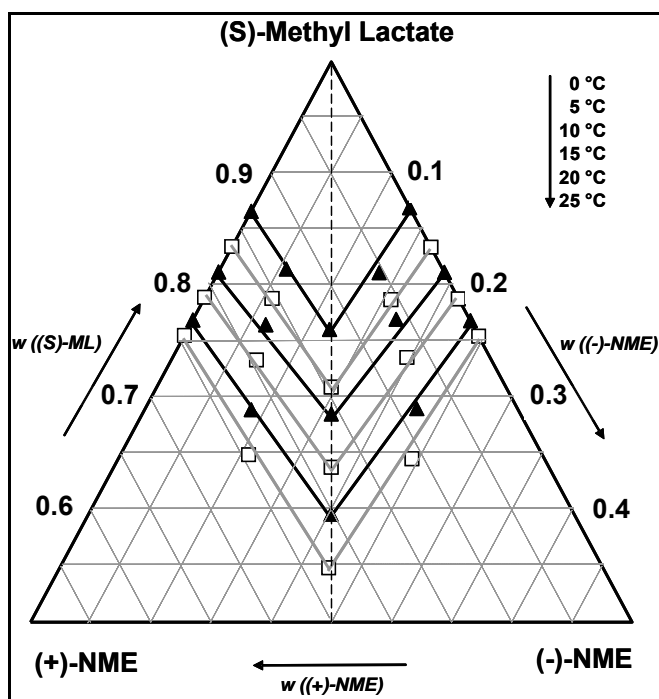
Figure C.114: Ternary phase diagram of N-methylephedrine in (S)-methyl lactate at different temperatures. Axes in weight fractions; $w_{(S)-MA}$ and $w_{(R)-MA} \leq 0.5$. The isothermal lines have been added as a visualization aid and only the marked points show measured data.
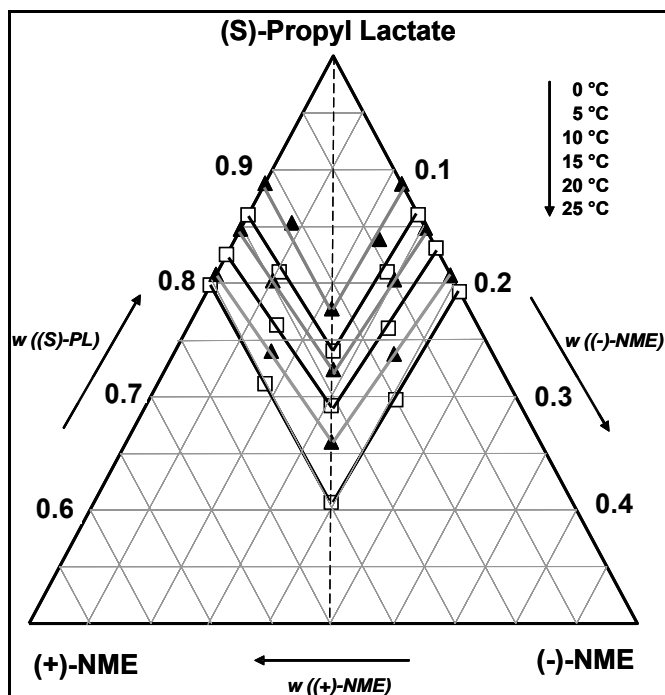
Figure C.115: Ternary phase diagram of N-methylephedrine in (S)-propyl lactate at different temperatures. Axes in weight fractions; $w_{(S)-MA}$ and $w_{(R)-MA} \leq 0.5$. The isothermal lines have been added as a visualization aid and only the marked points show measured data.
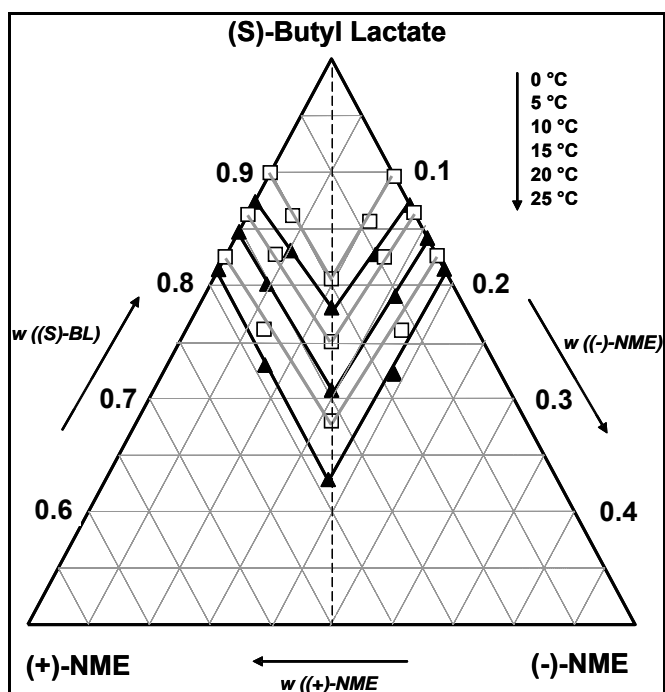
Figure C.116: Ternary phase diagram of N-methylephedrine in (S)-butyl lactate at different temperatures. Axes in weight fractions; $w_{(S)-MA}$ and $w_{(R)-MA} \leq 0.5$. The isothermal lines have been added as a visualization aid and only the marked points show measured data.

D. Appendix D-Nucleation points (MSZW)

D1. MSZW for mandelic acid
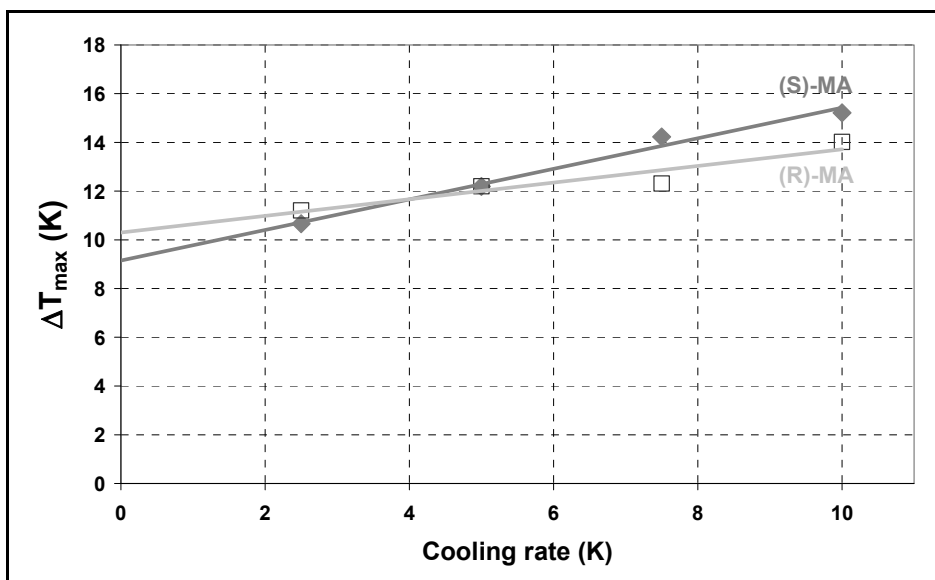
Figure D.117: Experimentally determined metastable zone width with respect to primary nucleation for mandelic acid in (S)-methyl lactate at T_{sat} = 25 °C. ((Racemic)-MA: no nucleation in the range of measurement).
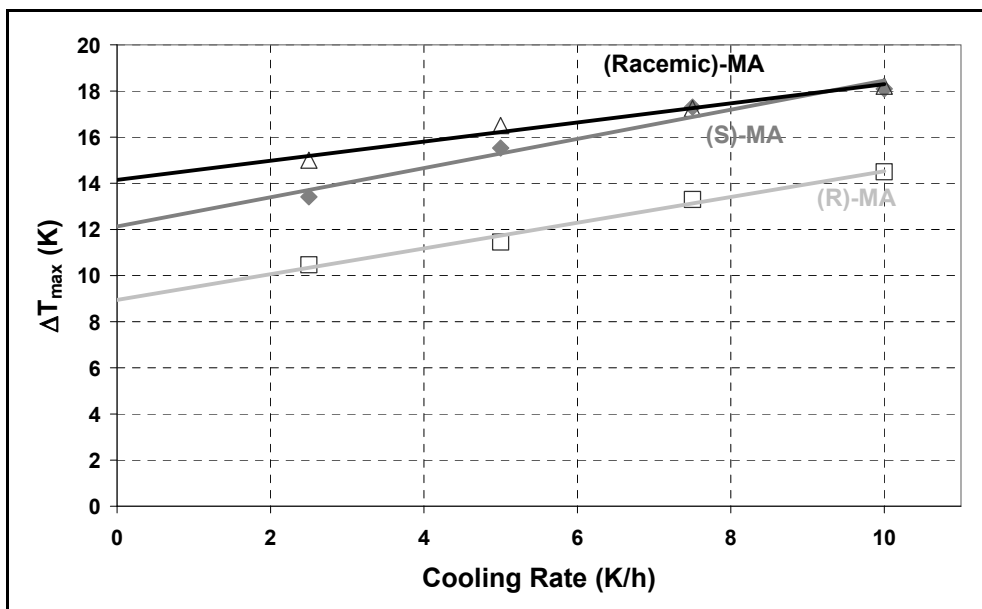
Figure D.118: Experimentally determined metastable zone width with respect to primary nucleation for mandelic acid in (S)-propyl lactate at T_{sat} = 25 °C.
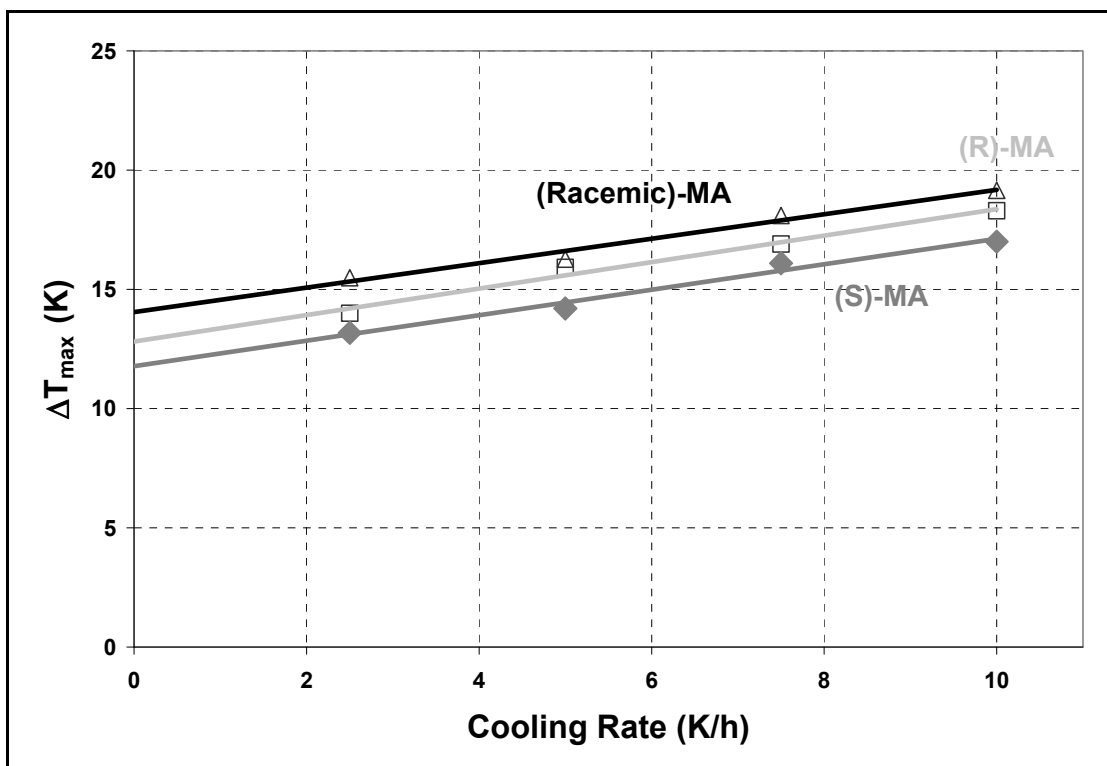
Figure D.119: Experimentally determined metastable zone width with respect to primary nucleation for mandelic acid in (S)-butyl lactate at T_{sat} = 25 °C.

D2. MSZW for N-methylephedrine
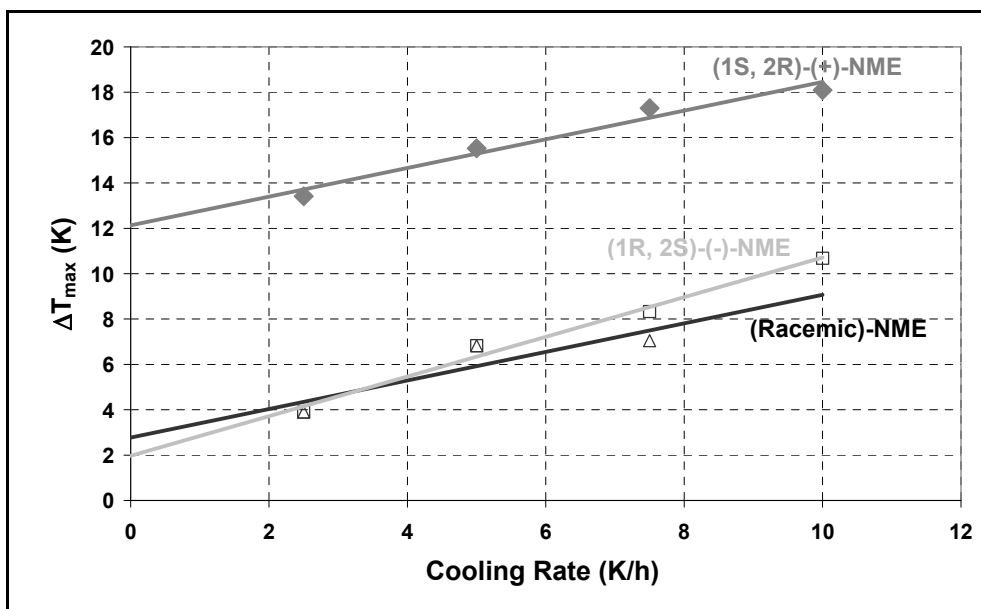
Figure D.120: Experimentally determined metastable zone width with respect to primary nucleation for N-methylephedrine in (S)-methyl lactate at T_{sat} = 25 °C.
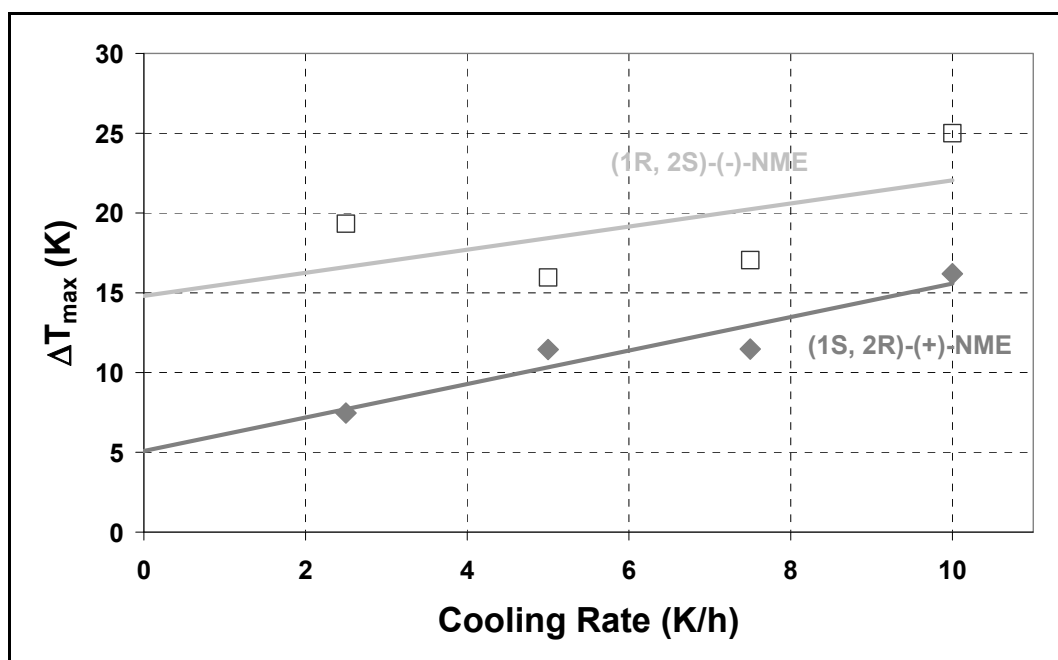
Figure D.121: Experimentally determined metastable zone width with respect to primary nucleation for N-methylephedrine in (S)-propyl lactate at T_{sat} = 25 °C. ((Racemic)-NME: no nucleation in the range of measurement).
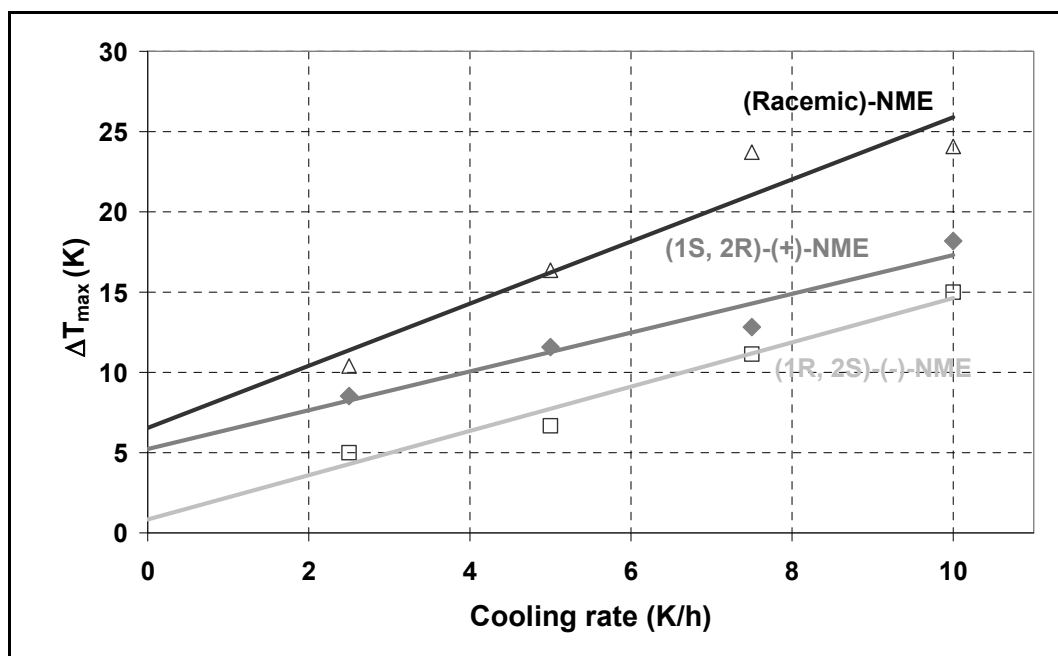
Figure D.122: Experimentally determined metastable zone width with respect to primary nucleation for N-methylephedrine in (S)-butyl lactate at T_{sat} = 25 °C.

E Appendix E Raman spectroscopy
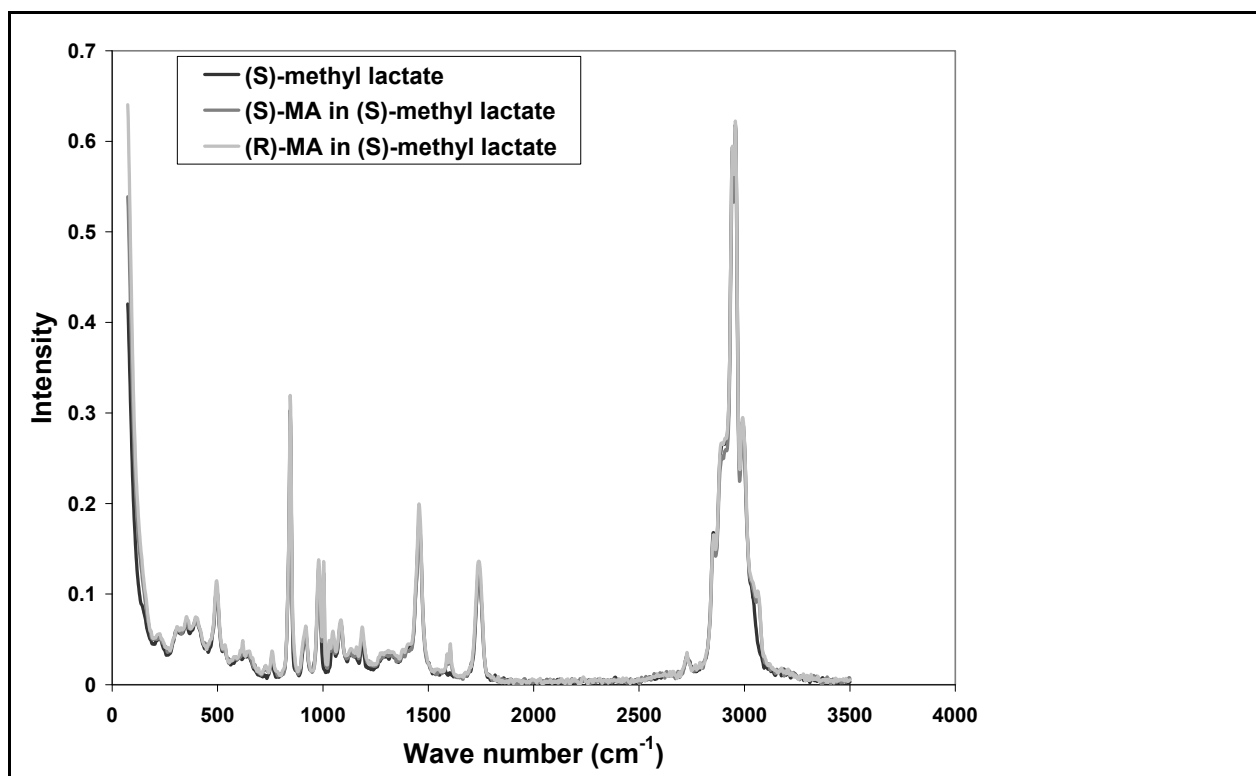
Figure E.123: Raman spectra of (S)- and (R)-mandelic acid in (S)-methyl lactate (liquid phase samples, and concentration of 8 wt %).
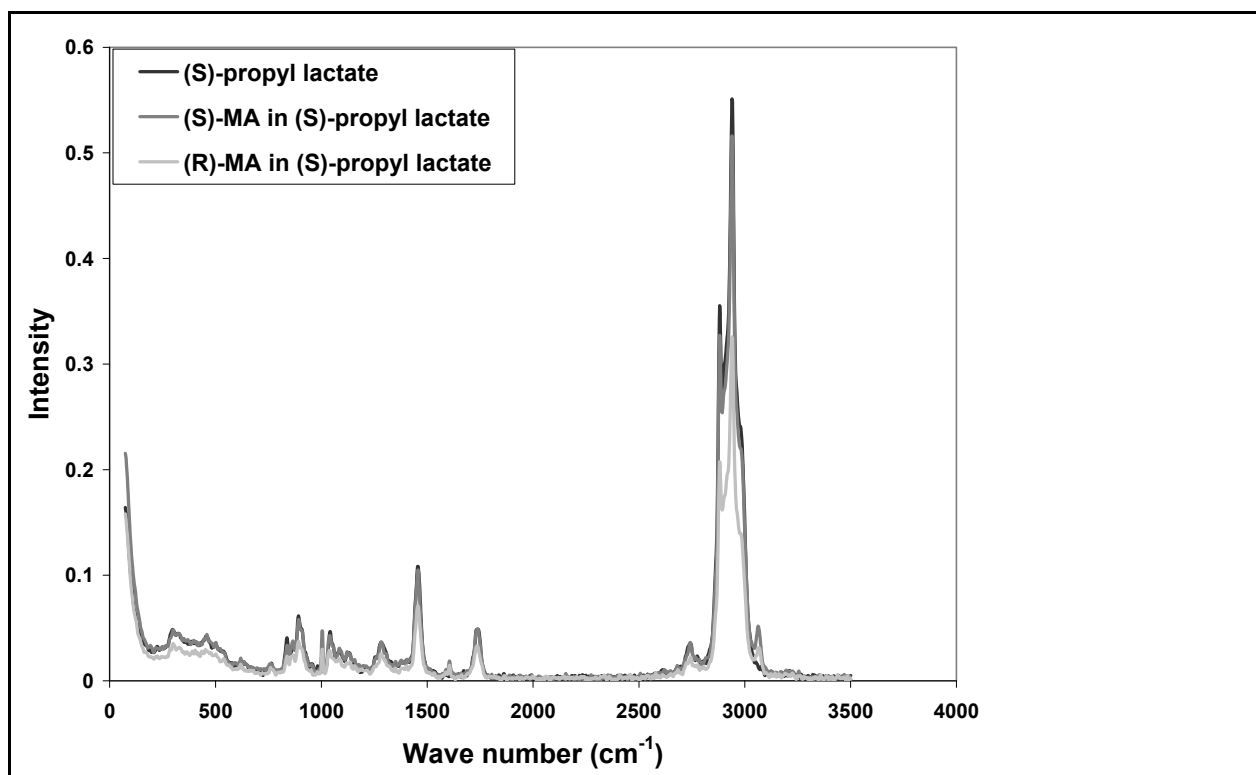
Figure E.124: Raman spectra of (S)- and (R)-mandelic acid in (S)-propyl lactate (liquid phase samples, and concentration of 8 wt %).
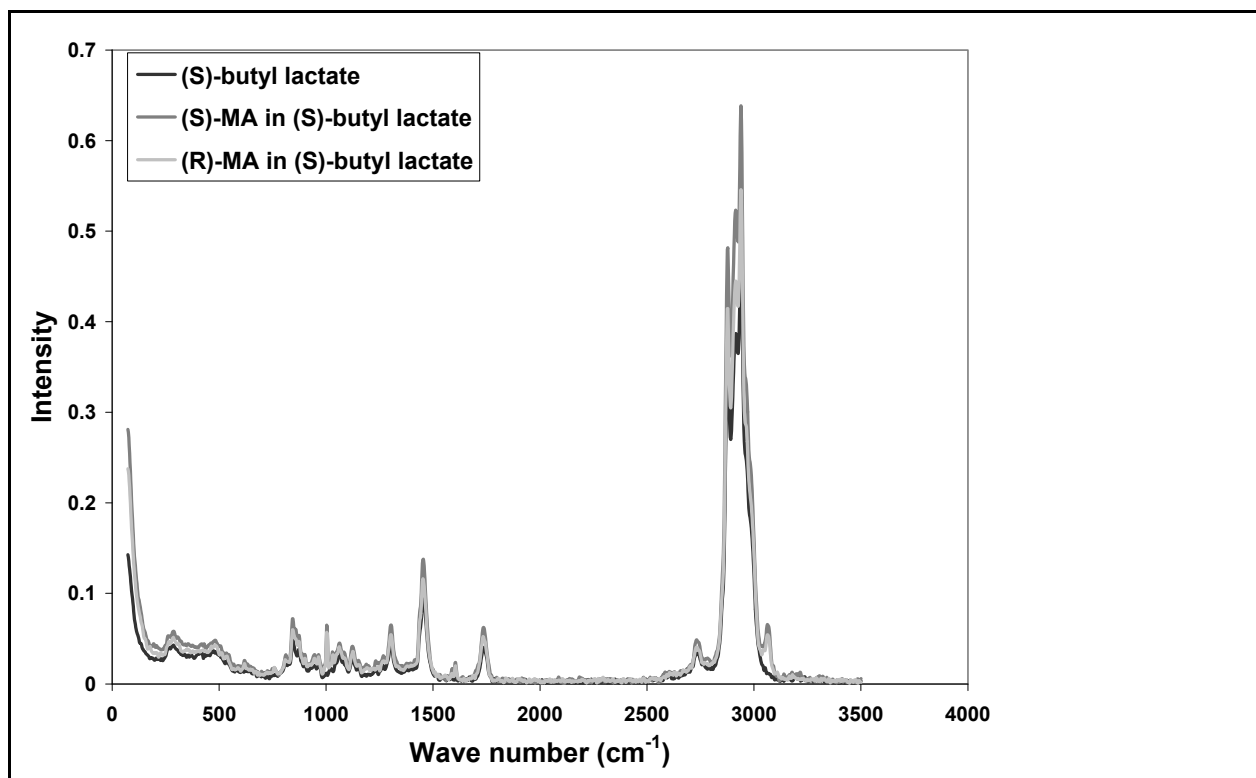
Figure E.125: Raman spectra of (S)- and (R)-mandelic acid in (S)-butyl lactate (liquid phase samples, and concentration of 8 wt %).

<u>References</u>

References

References

1. Collet A. Separation and purification of enantiomers by crystallisation methods. Enantiomer 1999;4(3-4):157-172.
2. Caner H, Groner H, Levy LA, I. Trends in the development of chiral drugs. Drug Discov. Today 2004;9:105-110.
3. Maier NM, Franco P, Lindner W. Separation of enantiomers: needs, challenges, Perspectives. J. Chrom. A. 2001;906:3-33.
4. Reichardt C. Solvents and Solvent Effects in Organic Chemistry: Wiley VCH: Weinheim; 2003.
5. Jacques J, Collet A, Wilen SH. Enantiomers, racemates and resolutions: Malabar, FL:Krieger Publishing Company 1994.
6. Yamamoto M, Yamamoto Y. Stereospecific solute-solvent interaction between Δ-(+)$_D$ or Δ-(-)$_D$ -Co (en) $_3$ $^{3+}$ and L- (+)$_D$ -diethyltartrate appeared in solubility and viscosity. Inorg. Nuclear Chem. Lett. 1975;11:833-836.
7. Bosnich B, Watts DW. Energeties of dissymmetric interactions. Differential solubility d- and l- and dl-cis-[Co(en)$_2$Cl$_2$]Cl0$_4$ and the enantiomerization in (-)-2,3-butanediol. J. Am. Chem. Soc 1968;90:6228-6230.
8. Mizumachi K. The solubility of Optically Active Tris-α-diimine Ruthenium (II) Complexes in l-2-Methyl-1-Butanol. J. Coord. Chem. 1973;3:191-192.
9. Amaya K. Statistical Thermodynamics of Solutions of Optically Active Substances II. Solubility of d- and l-Isomers in Optically Active Solvents. Bull. Chem. Soc. Jpn 1961;34:1803-1806.
10. Jones HO. The Solubility of Stereoisomerides in Optically Active Solvents. Proc. Cambridge Philos. Soc 1907;14:27-29.
11. Kozma D, editor. CRC Handbook of optical resolutions via diastereomeric salt formation. Boca Raton, Florida: CRC Press; 2002.
12. Hoff VJH, editor. La Chimie dans l' Espace, Bazendijk. Rotterdam, The Netherlands; 1875.
13. Hoff VJH. Sur les formules de structure dans l'espace. Néelandaises des Science Exactes et Naturelles 1874;9:445-454.
14. Le Bel JA. Sur les relations qui existent entre les formules atomiques des corps organiques et le pouvoir rotatoire de leurs dissolutions. Bulletin De La Societe Chimique De France 1874;22:337-347.
15. Pasteur L. Recherches sur les relations qui peuvent exister entre la forme cristalline et la composition chimique, et sens de la polarisation rotatoire. Annales de Chimie et de Physique 1848;3:442-459.
16. Eliel EL, Wilen S, Doyle M. Basic Organic Stereochemistry. New York: Wiley-Interscience; 2001.
17. Fischer E. Ueber die Configuration des Traubenzuckers und seiner Isomeren. Berichte der Deutschen Gesellschaft 1891;24:2683-2687.
18. Cahn R, Ingold SC, Prelog V. Spezification der molekularen Chiralität. Angewandte Chemie 1966;78:413-447.
19. Beckett AH. Chirality and Its Importance in Drug Development - What Are the Issues. Biochemical Society Transactions 1991;19(2):443-446.
20. Martin RH. The Helicenes. Angewandte Chemie-International Edition in English;13:649-660.
21. Ariens E. Stereochemistry: A Source of Problems in Medicinal Chemistry. Medicinal Research Reviews 1986;6:451-466.
22. Ariens E. Molecular Pharmacology,. London: Academic Press; 1964.
23. Ohloff G. Chemistry of Odor Stimuli. Experientia 1986;42(3):271-279.
24. Holmstedt B, Frank H, Testa B, editors. Chirality and Biological Activity. New York: Liss; 1990.

25. Ohloff G, Vial C, Wolf HR, Job K, Jegou E, Polonsky J, Lederer E. Stereochemistry-Odor Relationships in Enantiomeric Ambergris Fragrances. Helvetica Chimica Acta 1980;63(7):1932-1946.

26. Russell GF, Hills JI. Odor Differences between Enantiomeric Isomers. Science 1971;172(3987):1043-1044.

27. Emberger R, Hopp R. Synthesis and sensory characterization of menthol enantiomers and their derivatives for the use in nature identical peppermint oils. Spec. Chem. 1987;7:193-201.

28. Caldwell J. Chiral Pharmacology and the Regulation of New Drugs. Chemistry & Industry 1995(5):176-179.

29. Stinson SC. Chiral drug market shows signs of maturity. Chemical & Engineering News 1997;75(42):38-70.

30. Shekunov BY, York P. Crystallization processes in pharmaceutical technology and drug delivery design. Journal of Crystal Growth 2000;211:122-136.

31. Mullin JW. Crystallization. 3rd Edition ed. Oxford: Butterworth-Heinemann; 2000.

32. Mersmann A. Crystallization Technology Handbook. New York: Marcel Dekker, Inc; 2001.

33. Collet A, Brienne M-J, Jacques J. Optical Resolution by Direct Crystallization of Enantiomer Mixtures. Chem. Rev 1980;80:215-230.

34. Myerson AS. Handbook of Industrial Crystallization. Boston: Butterworth-Heinemann; 1993.

35. Wang X, Yang X, Liu Y, Ching CB. Intrinsic MSZW Characteristics of Racemic Species: Implication for Chiral Crystallization. AIChE J. 2008;54:2281-2292.

36. Roozeboom HWB. Löslichkeit und Schmelzpunkt als Kriterien für racemische Verbindungen, pseudoracemische Misch-Krystalle und inaktive Konglomerate. Z. Phys. Chem. 1899;28:494-517.

37. Perlberg A. Untersuchungen zum Einfluss des Gegenenantiomers bei der enantioselektiven Kristallisation aus Lösungen [PhD]. Magdeburg: Otto-von-Guericke Universität Magdeburg; 2007.

38. Meyerhoffer W. Stereochemische Notizen. (Die Pasteur´sche Saltungsmethode mittels activer Verbindungen. - Die Löslichkeit eine Tartrats, verglichen mit der des Racemats. Ber. 1904;37:2604-2610.

39. Prigogine I, Defay R. Chemical Thermodynamics: Longmann: London, UK; 1973.

40. Kaspereit M. Separation of Enantiomers by a Process Combination of Chromatography and Crystallisation [PhD]. Magdeburg: Otto-von-Guericke Universität Magdeburg:Shaker Verlag Aachen:; 2006. 1-140 p.

41. Subramanian G, editor. Chiral Separation Techniques. Weinheim: WILEY-VCH Verlag GmbH; 2001.

42. Rekoske JE. Chiral separations. AIChE J. 2001;47:2-5.

43. Collins AN, Sheldrake GN, Crosby J. Chirality in Industry: The Commercial Manufacture and Applications of Optically Active Compounds. Chichester: John Wiley & Sons; 1992.

44. Collins AN, Sheldrake GN, Crosby J. Chirality in Industry II: Developments in the Manufacture and Applications of Optical Active Compounds. Chichester: John Wiley & Sons; 1997.

45. Seebach A, Grandeury A, Seidel-Morgenstern A. Kontinuierliche Enantiomerenanreicherung mit geprägten Polymermembranen. Chem. Ing. Tech 2005;77:1005- 1006.

46. Buhse T, Kondepudi DK, Hoskins B. Kinetics of chiral resolution in stirred crystallization of D/L-glutamic acid. Chirality 1999;11(4):343-348.

47. Lorenz H, Polenske D, Seidel-Morgenstern A. Application of preferential crystallization to resolve racemic compounds in a hybrid process. Chirality 2006;18(10):828-840.

48. Mughal RK, Davey RJ, Black SN. Application of crystallization inhibitors to chiral separations. 2. Enhancing the chiral purity of mandelic acid by crystallization. Crystal Growth & Design 2007;7(2):225-228.

49. Crosby J. Synthesis of optically active compounds:a large scale perspective. Tetrahedron 1991;47:4789-4846.

50. Harrington PJ, Lodewijk E. Twenty Years of Naproxen Technology. Organic Process Research & Development 1997;1:72-76.

51. Vries T, Wynberg H, van Echten E, Koek J, ten Hoeve W, Kellogg RM, Broxterman QB, Minnaard A, Kaptein B, van der Sluis S, Hulshof, L, Kooistra, J. The Family Approach to the Resolution of Racemates. J. Angewandte Chemie-International Edition 1998;37:2349-2354.

52. Leusen FJJ, Noordik JH, Karfunkel HR. Racemate resolution via crystallization of diastereomeric salts: thermodynamic considerations and molecular mechanics calculations. Tetrahedron 1993;49:5377-5396.

53. Doki N, Yokota M, Sasaki S, Kubota N. Simultaneous crystallization of D- and L-asparagines in the presence of a tailor-made additive by natural cooling combined with pulse heating. Crystal Growth & Design 2004;4(6):1359-1363.

54. Weissbuch I, Addadi L, Lahav M, Leiserowitz L. Molecular Recognition at Crystal Interfaces. Science 1991;253(5020):637-645.

55. Addadi L, Weinstein S, Gati E, Weissbuch I, Lahav M. Resolution of Conglomerates with the Assistance of Tailor-Made Impurities - Generality and Mechanistic Aspects of the Rule of Reversal - a New Method for Assignment of Absolute-Configuration. Journal of the American Chemical Society 1982;104(17):4610-4617.

56. Weissbuch I, Popovitzbiro R, Lahav M, Leiserowitz L. Understanding and Control of Nucleation, Growth, Habit, Dissolution and Structure of 2-Dimensional and 3-Dimensional Crystals Using Tailor-Made Auxiliaries. Acta Crystallographica Section B-Structural Science 1995;51:115-148.

57. Berkovitch-Yellin Z, van Mil J, Addadi L, Idelson M, Lahav M, Leiserowitz L. Crystal Morphology Engineering by "Tailor Made" Inhibitors: A New Probe to Fine Intermolecular Interactions. J. Am. Chem. Soc. 1985;107:3111-3122.

58. Weissbuch I, Lahav M, Leiserowitz L, Meredith GR, Vanherzeele H. Centrosymmetric Crystals as Host Matrices for Second-Order Optical Nonlinear Effects. Cheistry of Materials 1989;1:114-118.

59. Berkovitchyellin Z, Addadi L, Idelson M, Leiserowitz L, Lahav M. Absolute-Configuration of Chiral Polar Crystals. Nature 1982;296(5852):27-34.

60. Weissbuch I, Lahav M, Leiserowitz L. Toward stereochentical control, monitoring, and understanding of crystal nucleation. Crystal Growth & Design 2003;3(2):125-150.

61. Black SN, Williams LJ, Davey RJ, Moffatt F, Jones RVH, Mcewan DM, Sadler DE. The Preparation of Enantiomers of Paclobutrazol - a Crystal-Chemistry Approach. Tetrahedron 1989;45(9):2677-2682.

62. Addadi L, Berkovitchyellin Z, Domb N, Gati E, Lahav M, Leiserowitz L. Resolution of Conglomerates by Stereoselective Habit Modifications. Nature 1982;296(5852):21-26.

63. Addadi L, Berkovitchyellin Z, Weissbuch I, Vanmil J, Shimon LJW, Lahav M, Leiserowitz L. Growth and Dissolution of Organic-Crystals with Tailor-Made Inhibitors - Implications in Stereochemistry and Materials Science. Angewandte Chemie-International Edition in English 1985;24(6):466-485.

64. Houllemare-Druot S, Coquerel G. How far can an unstable racemic compound affect the performances of preferential crystallization? Example with (R) and (S)-alpha-methylbenzylamine chloroacetate. Journal of the Chemical Society-Perkin Transactions 2 1998(10):2211-2220.

65. Li ZJ, Grant DJW. Relationship Between Physical Properties and Crystals Structures of Chiral Drugs. Journal of Pharmaceutical Sciences 1997;86:1073-1078.

66. Ndzié E, Cardinael P, Petit M-N, Coquerel G. Enantiomeric Resolution of (±)-5-Ethyl-5-Methylhydantoin by Means of Preferential Nucleation. Enantiomer 1998;4:97-101.

67. Coquerel G. Preferential crystallization. Novel Optical Resolution Technologies 2007;269:1-51.

68. Addadi L, Vanmil J, Lahav M. Useful Impurities for Optical Resolutions .2. Generality and Mechanism of the Rule of Reversal. Journal of the American Chemical Society 1981;103(5):1249-1251.

69. Zbaida D, Lahav M, Drauz K, Knaup G, Kottenhahn M. A cyclic continuous process for converting conglomerates into optically pure enantiomers by crystallization and dissolution with the assistance of 'tailor-made' polymers. Tetrahedron 2000;56(36):6645-6649.

70. Barton DHR, Kirby GW. Phenol Oxidation and Biosynthesis. Part V.* The Synthesis of Galanthamine. J. Chem. Soc. 1962:806-817.

71. Seebach D. Neue links- und rechtshändige Werkzeuge für den Chemiker. Frankfurt (Main): "25 Jahre Fonds der Chemischen Industrie 1950 - 1975"; 1975.

72. Hoff VJH, editor. Die Lagerung der Atome im Raume. 2 nd ed. Braunschweig: Vieweg; 1894.

73. Kaemmerer H, Heike L, Seidel-Morgenstern A. Theoretical and Experimental Determination of Solid Liquid Equilibria of Chiral Compound Forming Systems in Solution In: Jansens JP, Ulrich J, editors; 2008; Maastricht-Netherlands. p 479-486.

74. Lüttringhaus A, Berrer D. Zur struktur der lösungen - III racemat-spaltung durch ein optisch aktives lösungsmittel. Tetrahedron Letters 1959;10:10-12.

75. Groen MB, Schadenberg H, Wynberg H. Synthesis and Resolution of Some Heterohelicenes. Journal of Organic Chemistry 1971;36(19):2797-2809.

76. Medina DD, Goldshtein J, Margel S, Mastai Y. Enantioselective crystallization on chiral polymeric microspheres. Advanced Functional Materials 2007;17(6):944-950.

77. Gabashvili A, Medina DD, Gedanken A, Mastai Y. Templating mesoporous silica with chiral block copolymers and its application for enantioselective separation. Journal of Physical Chemistry B 2007;111(38):11105-11110.

78. Fireman-Shoresh S, Popov I, Avnir D, Marx S. Enantioselective, chirally templated sol-gel thin films. Journal of the American Chemical Society 2005;127(8):2650-2655.

79. Tang K, Yi J, Huang K, Zhang G. Biphasic Recognition Chiral Extraction: A Novel Method for Separation of Mandelic Acid Enantiomers. CHIRALITY 2009;21:390-395.

80. Dzygiel P, Reeve TB, Piarulli U, Krupicka M, Tvaroska I, Gennari C. Resolution of racemic N-benzyl alpha-amino acids by liquid-liquid extraction: A practical method using a lipophilic chiral cobalt(III) salen complex and mechanistic studies. European Journal of Organic Chemistry 2008(7):1253-1264.

81. Huüttenhain SH, Dickerhof N. Asymmetrische Induktion durch Lösungsmittel. GIT Labor Fachzeitschrift 2009;10:668-672.

82. Hartman P, Perdok WG. On the Relations between Structure and Morphology of Crystals .1. Acta Crystallographica 1955;8(1):49-52.

83. Allen FH. Acta Crystallographica Section B-Structural Science 2002;58.

84. Accelrys Software Inc., Materials Studio Release Notes, Release 4.3. San Diego: Accelrys Software Inc; 2008.

85. Pauling L. The Nature of the Chemical Bond. New York: Cornell University Press; 1960.

86. Etter MC, Macdonald JC, Bernstein J. Graph-Set Analysis of Hydrogen-Bond Patterns in Organic Crystals. Acta Crystallographica Section B-Structural Science 1990;B46.

87. Mughal RK. Chiral crystallisation: Additive induced crystallisation of mandelic acid [Ph. D]. Manchester: The University of Manchester; 2005.

88. Pople JA, Beveridge DL. Approximate Molecular Orbital Theory. New York McGraw-Hill; 1970.

89. Davey RJ, Dent G, Mughal RK, Parveen S. Concerning the relationship between structural and growth synthons in crystal nucleation: Solution and crystal chemistry of carboxylic acids as revealed through IR spectroscopy. Crystal Growth & Design 2006;6(8):1788-1796.

90. Dewar MJS, Zoebisch EG, Healy EF, Stewart JJP. The Development and Use of Quantum-Mechanical Molecular-Models .76. Am1 - a New General-Purpose Quantum-Mechanical Molecular-Model. Journal of the American Chemical Society 1985;107(13):3902-3909.

91. Pople JA, Segal GA. J. Chem. Phys 1965;44:3289-3296

92. Hinchliffe A. Molecular Modelling for Beginners. 2nd ed. Chichester: John Wiley & Sons Ltd; 2008.

93. Frenkel D, Smit B. Understanding molecular simulations from algorithms to applications. San Diego, California: Academic Press; 2002.

94. Acs M, Novotny-Bregger E, Simon K, Argay G. Structural Aspects of Optical Resolutions. Optical Resolution of (R, S)-Mandelic Acid. DSC and X-ray Studies of the Diastereoisomeric Salts. J. Chem. Soc. Perkins Trans. 2 1992:2011-2017.

95. Herráez-Hernández R, Campíns-Falcó P. Chiral separation of ephedrine by liquid chromatography using β-cyclodextrins. Anal Chim. Acta 2001;434:315-324.

96. Wang M, Marriott PJ, Chan W-H, Lee AWM, Huie CW. Enantiomeric separation and quantification of ephedrine-type alkaloids in herbal material by comprehensive two-dimensional gas chromatography. J. Chromatogr. A 2006;1112:361-368.

97. Yamazaki Y, Kajiwara S. Enzymatic synthesis of D-mandelic acid. Bioindustry (Japanese) 1988;5:261-268.

98. Reynolds JEF, editor. The Extra Pharmacopoeia. 30th ed: The Pharmaceutical Press: London; 1993.

99. Elvers B. In: Ullmann`s, editor. Encyclopedia of Industrial Chemistry: Wiley VCH: Weinheim; 1989.

100. Lorenz H, Sapoundjiev D, Seidel-Morgenstern A. Enantiomeric Mandelic Acid System-Melting Point Phase Diagram and Solubility in Water. J. Chem. Eng. Data 2002;47:1280-1284.

101. Wang XJ, Wiehler H, Ching CB. Physicochemical Properties and the Crystallization Thermodynamics of the Pure Enantiomer and the Racemate for N-Methylephedrine. J. Chem. Eng. Data. 2003;48(5):1092-1098.

102. Wang XJ, Wiehler H, Ching CB. Physicochemical Properties and the Crystallization Thermodynamics of the pure Enantiomer and the Racemate for N-Methylephedrine. J. Chem. Eng. Data 2003;48:1092-1098.

103. Gausepohl R, Buskens P, Kleinen J, Bruckmann A, Lehmann CW, Klankermayer J, Leitner W. Highly enantioselective Aza-Baylis-Hillman reaction in a chiral reaction medium. Angewandte Chemie-International Edition 2006;45(22):3689-3692.

104. Reichert WM, Holbrey JD, Vigour KB, Morgan TD, Broker GA, Rogers RD. Approaches to crystallization from ionic liquids: complex solvents-complex results, or, a strategy for controlled formation of new supramolecular architectures? Chemical Communications 2006(46):4767-4779.

105. Basavaiah D, Krishna PR. Synthesis of Chiral Alpha-Aryl-Alpha-Hydroxyacetic Acids - Substituent Effects in Pig-Liver Acetone Powder (Plap) Induced Enantioselective Hydrolysis. Tetrahedron 1995;51(8):2403-2416.

106. Rouessac F, Rouessac A. Chemical Analysis: Modern Instrumentation Methods and Techniques: John Wiley & Sons: Chichester; 2000.

107. Dale JA, Mosher HS. Nuclear Magnetic-Resonance Enantiomer Reagents - Configurational Correlations Via Nuclear Magnetic-Resonance Chemical-Shifts of Diastereomeric Mandelate, O-Methylmandelate, and Alpha-Methoxy-Alpha-Trifluoromethylphenylacetate (Mtpa) Esters. Journal of the American Chemical Society 1973;95(2):512-519.

108. Kobayashi Y, Hayashi N, Tan CH, Kishi Y. Toward the Creation of NMR Databases in Chiral Solvents for Assignments of Relative and Absolute Stereochemistry: Proof of Concept. Org. Lett. 2001;3:2245-2248.

109. Kobayashi Y, N.; H, Kishi Y. Toward the Creation of NMR Databases in Chiral Solvents: Bidentate Chiral NMR Solvents for Assignment of the Absolute Configuration of Acyclic Secondary Alcohols. Org. Lett 2002;4:411-414.

110. Hefter GT, Tomkins RPT, editors. The experimental determination of solubilities. New York: J.Wiley & Sons.Ltd; 2003.

111. Avantium, Technologies. Crystal16 ^{TM} User Manual 1.1, Amsterdam, Netherland, 2008.

112. Nyvlt J, Söhnel O, Matuchova M, Broul M. The kinetics of Industrial Crystallisation. Amsterdam, Netherlands,: Elsevier: ; 1985.

113. Mettler-Toledo, GmbH. Operating Instructions:RE40, Refractometer, Version 4.0 Schwerzenbach,Switzerland; 2001.

114. Mettler-Toledo, GmbH. Operating Instructions:DE40.DE45.DE51, Density Meters, Version 4.0. Schwerzenbach, Switzerland; 2001.

115. Jenkins R, Snyder RL. Introduction to X-ray Powder Diffractometry. New York: John Wiley & Sons; 1996.

116. Britain HG. Physical Characterisation of Pharmaceutical Solids: Marcell Dekker, Inc; 1995.

117. Colthup N, Daly S, Wiberley S, editors. An Introduction to Infrared and Raman Spectroscopy. 2 nd ed. London: Academic Press; 1975.

118. Ferraro JR, Nakamoto K. Introductory Raman Spectroscopy. London: Academic Press; 1994.

119. Centnerszwer M. Ueber Schmelzpunkte von Gemengen optischer Antipoden. Zeitschrift für Physikalische Chemie 1899;29:715-725.

120. Profir VM, Furusjo E, Danielsson LG, Rasmuson AC. Study of the crystallization of mandelic acid in water using in situ ATR-IR spectroscopy. Crystal Growth & Design 2002;2(4):273-279.

121. Mohan R, Lorenz H, Myerson AS. Solubility measurement using differential scanning calorimetry. Industrial & Engineering Chemistry Research 2002;41(19):4854-4862.

122. Lorenz H, Seidel-Morgenstern A. Binary and ternary phase diagrams of two enantiomers in solvent systems. Thermochimica Acta 2002;382(1-2):129-142.

123. Lorenz H, Seidel-Morgenstern A. A contribution to the mandelic acid phase diagram. Thermochimica Acta 2004;415(1-2):55-61.

124. Rose HA. Crystallographic Data .61. Dl-Mandelic Acid. Analytical Chemistry 1952;24(10):1680-1680.

125. Fischer A, Profir VM. A metastable modification of (RS)-mandelic acid. Acta Crystallographica Section E-Structure Reports Online 2003;59:1113-1116.

126. Brandstätter MK, Ulmer R. Beitrag zur thermischen Analyse optischer Antipoden Mandelsäure. Mikrochimica Acta 1974:927-935.

127. Adriani JH. Solidification and conversion occurences in optic antipodes. Zeitschrift Fur Physikalische Chemie--Stochiometrie Und Verwandtschaftslehre 1900;33(4):453-476.

128. Angus WR, Owen RP. The stability of racemates - Mandelic acid and some of its derivatives. Journal of the Chemical Society 1943:227-230.

129. Fujita Y, Fujishir.R, Baba Y, Kagemoto A. Thermal Properties of Optically Active Compounds .1. Study on Thermal Properties of Mandelic Acid Using Differential Thermal-Analysis Method. Nippon Kagaku Kaishi 1972;8(9):1563-1567.

130. Leclercq M, Collet A, Jacques J. Study on Mixtures of Optical-Antipodes .12. Measurement of Stability of True Racemates. Tetrahedron 1976;32(7):821-828.

131. Fouquey C, Leclercq M. Détermination de la pureté optique d'un corps cristallin par calorimétrie—II : Validité de la méthode et précision des résultats. Tetrahedron 1970;26:5637-5651.

132. Nishiguchi N, Moritoki M, Shinohara T, Toyokura K. Separation of L-mandelic acid from asymmetric mixtures by means of high-pressure crystallization. Separation and Purification by Crystallization 1997;667:73-82.

133. Hurd CD, Raterink HR. The pyrolysis of mandelic acid and related compounds. Journal of the American Chemical Society 1933;55:1541-1546.

134. Ross JDM, Morrison TJ. Acid salts of monobasic organic acids Part I. Journal of the Chemical Society 1933:1016-1022.

135. Profir VM, Rasmuson AC. Influence of solvent and the operating conditions on the crystallization of racemic mandelic acid. Crystal Growth & Design 2004;4(2):315-323.

136. Patil AO, Pennington WT, Paul IC, Curtin DY, Dykstra CE. Reactions of Crystalline (R)-(-)-Mandelic and (S)-(+)-Mandelic Acid with Amines - Crystal-Structure and Dipole-Moment of (S)-Mandelic Acid - a Method of Determining Absolute-Configuration of Chiral Crystals. Journal of the American Chemical Society 1987;109(5):1529-1535.

137. Li ZJ, Zell MT, Munson EJ, Grant DJW. Characterization of racemic species of chiral drugs using thermal analysis, thermodynamic calculation, and structural studies. Journal of Pharmaceutical Sciences 1999;88(3):337-346.

138. Lide DR, editor. Handbook of Chemistry and Physics. 82nd ed. Boca Raton, Florida: CRC Press LLC; 2001.

139. Domingo LR, Picher MT, Andres J, Safont VS, Chuchani G. Potential energy surface for the decomposition of mandelic acid. Chemical Physics Letters 1997;274(5-6):422-428.

140. Chuchani G, Martin I. Elimination kinetics of DL-mandelic acid in the gas phase. Journal of Physical Organic Chemistry 1997;10(2):121-124.

141. Levillain G, Tauvel G, G C. How homogeneous equilibria between solvated enantiomers can modify the stable and metastable heterogeneous equilibria. In: Jensens PJ, ter Horst JH, Jiang S, editors; 2006; Delft University of Technology: Delft, The Netherlands. IOS Press. p 244-250.

142. Polenske D, Lorenz H, Seidel-Morgenstern A. Separation of Propranolol Hydrochloride Eantiomers by Preferential Crystallization: Thermodynamic Basis and Experimental Verification. Cryst. Growth Des 2007;7:1628-1634.

143. Weissbuch I, Zbaida D, Addadi L, Leiserowitz L, Lahav M. Design of Polymeric Inhibitors for the Control of Crystal Polymorphism - Induced Enantiomeric Resolution of Racemic Histidine by Crystallization at 25-Degrees-C. Journal of the American Chemical Society 1987;109(6):1869-1871.

144. Mastai Y, Sedlak M, Colfen H, Antonietti M. The separation of racemic crystals into enantiomers by chiral block copolymers. Chemistry-a European Journal 2002;8(11):2430-2437.

145. Lahav M, Weissbuch I, Shavit E, Reiner C, Nicholson GJ, Schurig V. Parity violating energetic difference and enantiomorphous crystalsp-caveats; reinvestigation of tyrosine crystallization. Origins of Life and Evolution of the Biosphere 2006;36(2):151-170.

146. Mughal RK, Davey RJ, Blagden N. Application of crystallization inhibitors to chiral separations. 1. Design of additives to discriminate between the racemic compound and the pure enantiomer of mandelic acid. Crystal Growth & Design 2007;7(2):218-224.

147. Leeman M, Brasile G, Gelens E, Vries T, Kaptein B, Kellogg R. Structural aspects of nucleation inhibitors for diastereomeric resolutions and the relationship to Dutch Resolution. Angewandte Chemie-International Edition 2008;47(7):1287-1290.

148. Omar W, Ulrich J. Solid liquid equilibrium, metastable zone, and nucleation parameters of the oxalic acid-water system. Crystal Growth & Design 2006;6(8):1927-1930.

149. Mersmann A. Crystallization Technology Handbook. New York: Mercel Decker Inc; 1995.

150. Davey RJ. Solvent effects in crystallization processes. In Current Topics in Materials Science. In: Kaldis E, editor. Volume 8. Amsterdam,: North-Holland Publishing Company; 1982.

151. Walton A. Nucleation in Liquids and Solutions. In Nucleation. In: Zettlemeyer AC, editor. New York: Marcel Dekker; 1969. p 225-327.

152. Hosokawa T, Datta S, Sheth AR, Grant DJW. Relationships between crystal structures and thermodynamic properties of phenylbutazone solvates. Crystengcomm 2004;6:243-249.

153. Tulashie SK, Lorenz H, Hilfert L, Edelmann FT, Seidel-Morgenstern A. Potential of chiral solvents for enantioselective crystallization. 1. Evaluation of thermodynamic effects. Crystal Growth & Design 2008;8(9):3408-3414.

154. Tulashie SK, Lorenz H, Seidel-Morgenstern A. Potential of Chiral Solvents for Enantioselective Crystallization. 2. Evaluation of Kinetic Effects. Crystal Growth & Design 2009;9(5):2387-2392.

155. Pispisa B, Venanzi M, Palleschi A. Chiral Discrimination in the Formation of Diastereomeric Pairs - a Thermodynamic and Conformational Investigation. Journal of the Chemical Society-Faraday Transactions 1994;90(3):435-443.

156. Davankov VA. The nature of chiral recognition: Is it a three-point interaction? Chirality 1997;9(2):99-102.

157. Williams HD, Fleming I. Spectroscopic Methods in Organic Chemistry. London: McGraw Hill BookCompany Europe; 1995.

<u>Curriculum vitae</u>

Curriculum vitae

Personal Details:

Family Name: Tulashie

First Names: Samuel Kofi

Date of Birth: 17.01.1971

Gender   Male

Place of Birth   Sekondi, Ghana

Nationality: Ghanaian

Language   English (Fluent), German (Good)

Education:

Ph.D in Chemical and Process Engineering at the **Max Planck Institute for Dynamics of Complex Technical Systems, Magdeburg, Germany** from July 2005 to July 2010.

M.Sc. Chemical and Process Engineering at the **Otto-von-Guericke University, Magdeburg, Germany** from October 2002 – April 2005.

Bachelor of Science (Hons) Chemistry at the **University of Cape Coast, Ghana** from 1997 – 2001.

Degree/Certificate	Field	School/University	Year
B.Sc. (Hons)	Chemistry	University of Cape Coast, Ghana	1997 - 2001
A-Level G.C.E (Abitur)	Science	Nkroful Secondary school, Ghana	1991 - 1993
O level G. C. E	Science	Mim Secondary school, Ghana	1984 - 1989

Project/Internship at Bachelor Degree:

I did a Student Chemist training at the Takoradi thermal power station, Takoradi, Ghana from 04/1998 – 10/1998, where I got practical training in basic chemical analysis. I gained knowledge in Inductively Coupled Plasma, atomic Emission Spectrophotometry, UV Visible Spectrophotometry.

Industrial Experience:

1993 – 1995   Teaching Chemistry, Physics, Mathematics at Adiembra Senior Secondary School, Takoradi-Ghana.

1995 – 1997   Worked as a Quality Control Officer in a Gas Plant "Takoradi Gas Ltd" at Takoradi Ghana. I was checking the quality of the oxygen and the acetylene gas which was produced for industrial use (cutting and welding of metals).

7/2001 – 9/2001   Internship at the Department of Chemistry of the Carl von Ossietzky University Oldenburg, under Prof. Martens. I was involved in preparative organic chemistry and analytical chemistry, which includes NMR Spectroscopy and amino acid synthesis. This training was supported by DAAD-scholarship as part of IAESTE – German National Committee.

6/2003 – 2005   Scientific assistant at the Max-Planck Institute for Dynamics, Magdeburg in the Physical and Chemical Porcess Engineering group. I was working on reaction kinetics of esterification reaction, measuring residue curve maps and also the flux through porous membranes.

7/2005 –7/2010   Research fellow/Ph.D-student at the Max Planck Institute for Dynamics of Complex Technical Systems, Magdeburg, Germany. I am working on crystallization based processes for enantioseparation of pharmaceutical chiral substances by using optically active solvents such as classical chiral solvents, tailor-made chiral solvents and chiral ionic liquids. The work involves the measurement of solid liquid equilibria and nucleation kinetics. My PhD work is supported by the Max Planck Society Scholarship.

12/2008   I was a guest scientist for two weeks in the group of Prof. Roger Davey at the University of Manchester, UK, for a collaborative research work on molecular modeling.

Professional Membership:

27/09/2007-present   Elected as Associate Member of Institution of Chemical Engineers (IChemE), UK.

2010   Member of German Chemical Engineers (Dechema), Germany.

Software used: Accelys Materials Studios (Molecular modeling concerning interactions calculations), Aspen Plus.

Scientific Publications

[1]. Huang, Y. S., Sundmacher, K., Tulashie, S., and Schlünder, E. U., Theoretical and Experimental Study on Residue Curve Maps of Propyl Acetate Synthesis Reaction, *Chem. Eng. Sci.* 60 (2005) 3363-3371.

[2]. Tulashie, S. K., Lorenz, H., Hilfert, L., Edelmann, F. T., Seidel-Morgenstern, A., Potential of Chiral Solvents for Enantioselective Crystallization. 1. Evaluation of Thermodynamic Effects, *Crystal Growth and Design* 8 (2008) 3408-3414.

[3]. Tulashie, S. K., Lorenz, H., Seidel-Morgenstern, A, Potential of Chiral Solvents for Enantioselective Crystallization. 2. Evaluation of Kinetic Effects, *Crystal Growth and Design*. 9 (2009) 2387-2392.

[4]. Tulashie, S. K., Kaemmerer, H., Lorenz, H., Seidel-Morgenstern, A., Solid Liquid Equilibria of Mandelic Acid Enantiomers in Two Chiral Solvents-Experimental Determination and Model Correlation. *J. Chem. Eng. Data*. 55 (2010) 333-340.

[5]. Kaemmerer, H., Tulashie, S. K., Lorenz, H., Seidel-Morgenstern, A., Solid Liquid Phase Equilibria of N-Methylephedrine Enantiomers in Two Chiral Solvents. *J. Chem. Eng Data.* 55 (2010) 1131-1136.

[6]. Tulashie, S. K., Lorenz, H., Malwade, C. R., Seidel-Morgenstern, A, Ternary Solubility Phase Diagrams of Mandelic Acid and N-Methylephedrine in Chiral Solvents with Different Carbon Chain Lengths, *Crystal Growth and Design*. online available.

[7]. Tulashie, S. K., Lorenz, H., Seidel-Morgenstern, A., Solubility of Mandelic Acid Enantiomers and Their Mixtures in Three Chiral Solvents. *J. Chem. Eng. Data*. accepted.

Conference Proceedings

[1]. **Application of chiral solvents for enantioseparation - basic experiments**

Authors: Tulashie, S.; Lorenz, H.; Grandeury, A.; Seidel-Morgenstern, A.

Date of event: 13-09-2006

Place: Delft, Holland.

Name of Conference/Meeting: BIWIC 2006:13th International Workshop on Industrial Crystallization.

[2]. **Crystallization of chiral molecules in optically active solvents**

Authors: Tulashie, S.; Lorenz, H.; Seidel-Morgenstern, A.

Date of events: 28-09-2006

Place: Eli Lilly Hamburg.

Name of Conference/Meeting: Eli Lilly 2006 Analytical Symposium.

[3]. **Potential of chiral solvents in enantioselective crystallization - a case study on two chiral systems**

Authors: Tulashie, S.; Lorenz, H.; Seidel-Morgenstern, A.

Date of event: 29-03-2007

Place: Nürnberg, Germany.

Name of Conference/Meeting: GVC-Fachausschusssitzung "Kristallisation"

[4]. **Potential of chiral solvents for chiral discrimination in crystallization processes**

Authors: Tulashie, S.; Lorenz, H.; Seidel-Morgenstern, A.

Date of event: 09-09-2007

Place: Cape Town, South Africa

Name of Conference/Meeting: BIWIC 2007 - 14th International Workshop on Industrial Crystallization.

[5]. **Enantioseparation by crystallization from chiral solvents**

Authors: Tulashie, S.; Lorenz, H.; Seidel-Morgenstern, A.

Date of event: 06-07-2008

Place: Geneva, Switzerland

Name of conference/Meeting: Chirality 2008-20th International Symposium on Chirality

[6]. **Chiral solvents / chiral ionic liquids for separation of enantiomers – ternary phase diagrams and metastable zone width**

Authors: Tulashie, S.; Lorenz, H.; Klankermayer, J.; Seidel-Morgenstern, A.

Date of event: 03-08-2008

Place: Warsaw, Poland.

Name of conference/Meeting: 20th ICCT-20th International Conference on

Chemical Thermodynamics

[7]. **Enantioselective crystallization using chiral ionic liquids**

Authors: Tulashie, S.; Lorenz, H.; Klankermayer, J.; Seidel-Morgenstern, A.

Place of Publication: Aachen, Germany

Publisher: Shaker Verlag

Date of event: 10-09-2008

Place: Magdeburg, Germany.

Name of Conference/Meeting: BIWIC 2008 - 15th International Workshop on Industrial Crystallization

[8]. **Crystallization from chiral solvents: theoretical an experimental investigations**

Authors: Tulashie, S.; Lorenz, H.; Seidel-Morgenstern, A.

Date of event: 14-09-2008

Place: Maastricht, Holland.

Name of Conference/Meeting: ISIC 17, 17th International Symposium on Industrial Crystallization

[9]. **Chiral tailor-made solvents and their impact on solution thermodynamics and crystallization kinetics of mandelic acid**

Authors: Tulashie, S.; von Langermann, J.; Lorenz, H.; Seidel-Morgenstern, A.

Date of event: 08-09-2010

Place: Halle, Germany.

Name of Conference/Meeting: BIWIC 2010 - 17th International Workshop on Industrial Crystallization.

Magdeburg, 26.08.2010   (Samuel Kofi Tulashie)